



8-1969

Contributions to the Specific Heat Capacity of Nickel, Iron, and the Alloy Ni₃Fe

Thomas Gilman Kollie
University of Tennessee - Knoxville

Follow this and additional works at: https://trace.tennessee.edu/utk_graddiss

 Part of the [Metallurgy Commons](#)

Recommended Citation

Kollie, Thomas Gilman, "Contributions to the Specific Heat Capacity of Nickel, Iron, and the Alloy Ni₃Fe. "
PhD diss., University of Tennessee, 1969.
https://trace.tennessee.edu/utk_graddiss/3536

This Dissertation is brought to you for free and open access by the Graduate School at TRACE: Tennessee Research and Creative Exchange. It has been accepted for inclusion in Doctoral Dissertations by an authorized administrator of TRACE: Tennessee Research and Creative Exchange. For more information, please contact trace@utk.edu.

To the Graduate Council:

I am submitting herewith a dissertation written by Thomas Gilman Kollie entitled "Contributions to the Specific Heat Capacity of Nickel, Iron, and the Alloy Ni₃Fe." I have examined the final electronic copy of this dissertation for form and content and recommend that it be accepted in partial fulfillment of the requirements for the degree of Doctor of Philosophy, with a major in Engineering Science.

C. R. Brooks, Major Professor

We have read this dissertation and recommend its acceptance:

Carl McHayes, B. S. Bowie, E. E. Stansbury, J. E. Spruiell, Lewis Nelson, Harry C. Jacobsen

Accepted for the Council:

Carolyn R. Hodges

Vice Provost and Dean of the Graduate School

(Original signatures are on file with official student records.)

August 1969

To the Graduate Council:

I am submitting herewith a dissertation written by Thomas Gilman Kollie, entitled "Contributions to the Specific Heat Capacity of Nickel, Iron, and the Alloy Ni_3Fe ." I recommend that it be accepted in partial fulfillment of the requirements for the degree of Doctor of Philosophy, with a major in Metallurgical Engineering.

CR Brooks

Major Professor

We have read this dissertation
and recommend its acceptance:

Carl McHughes

B. S. Boyle

E. E. Stansbury

J. E. Spruiell

Lewis Nelson

Harry C. Jacobson

Accepted for the Council:

Hilton A. Smith

Vice Chancellor for
Graduate Studies and Research

CONTRIBUTIONS TO THE SPECIFIC HEAT CAPACITY OF
NICKEL, IRON, AND THE ALLOY Ni_3Fe

A Dissertation
Presented to
the Graduate Council of
The University of Tennessee

In Partial Fulfillment
of the Requirements for the Degree
Doctor of Philosophy

by
Thomas Gilman Kollie

August 1969

ACKNOWLEDGMENTS

The author gratefully acknowledges Dr. C. R. Brooks, his major professor, for his interest, guidance, and cooperation during the author's graduate studies at the University of Tennessee. Dr. Brooks' knowledge and experience in the field of calorimetry were invaluable aids throughout the performance of this research.

To Dr. D. L. McElroy, the author's research group leader at the Oak Ridge National Laboratory for the past ten years and under whose immediate supervision this research was performed, the author extends his gratitude. Without Dr. McElroy's assistance and support, this work would not have been possible. For his advice and encouragement during the author's graduate work, the author is deeply appreciative.

Dr. M. Barisoni assisted in assembling Pulse Calorimeter II and in the performance of the specific heat capacity measurements on iron and Ni_3Fe and the electrical resistivity measurements on Ni_3Fe . This aid greatly accelerated the experimental work. Dr. Barisoni unselfishly performed many menial as well as difficult and tedious tasks during a six-month period. The author is deeply thankful for Dr. Barisoni's fine efforts.

Mr. R. R. Gaddis operated and Mr. J. D. Burke designed and maintained the digital voltmeter circuitry used in the specific heat capacity measurements. Mr. Gaddis' thorough knowledge and experience in electronics proved to be indispensable in the improvements and maintenance of the transient amplification circuitry of the pulse calorimeters during the five years of this research effort. Without the professionalism of

these two gentlemen and the cooperation and advice of Mr. R. K. Adams, their supervisor, the measurement of the transient signals would not have been feasible. Their efforts are worthy of highest praise.

Mr. R. L. Simpson wrote all the FORTRAN programs directly associated with the digital voltmeter data reduction and lent able assistance on many other programs. He also wrote the $\text{Pt}_{70}\text{Rh}_{30}/\text{Pt}_{94}\text{Rh}_6$ thermocouple emf conversion function. For his willing advice, cooperation, and assistance throughout this work, the author is sincerely grateful.

Mr. J. O. Scarbrough performed the heat treatments and low-temperature specific heat capacity measurements on Ni_3Fe . These excellent data greatly reinforced the author's interpretation of the effects of ordering on the specific heat capacity of this alloy. Mr. Scarbrough also encapsulated numerous specimens so that the author might heat treat them. The author thanks him for these efforts.

Mr. J. P. Moore and Mr. R. S. Graves performed the electrical resistivity and thermoelectric power measurements on Ni_3Fe between 77 K and 400 K. These precise measurements confirmed those of the author and added to the completeness of these measurements. Mr. Moore is also thanked for his assistance with the resistance ratio experiments and Mr. Graves for his "helping hand."

Dr. R. W. Williams and Dr. W. Fulkerson are acknowledged for their comments on this lengthy document. Dr. Williams' advice and counsel have been sought on many of the theoretical details of this work. He also wrote the FORTRAN code for the Debye function.

Being the author's office mate for the past year, Dr. P. H. Spindler became involved in many discussions concerning this work. His advice and suggestions have been very helpful to the author. His unselfishness in sharing our office with the voluminous reams of the author's computer output must not go unacknowledged.

Dr. R. K. Williams and Dr. K.-H. Bode are thanked for the advice they have rendered on numerous occasions.

Thanks are extended to all other persons who contributed to this research especially the following: Mrs. Frances Loving for her secretarial assistance; Mrs. Frances Scarboro and Mrs. Pat Viles of the Metals and Ceramics Division Reports Office who prepared this manuscript for reproduction; Mr. J. D. Stohler who prepared the photomicrographs of the specimens; members of the Materials Fabrication Group of the Metals and Ceramics Division, especially Mr. R. E. McDonald, who fabricated the specimens; and members of the Computer Operations Section of the Mathematics Division, especially Mr. C. S. Williams, who provided the many services essential to this work.

The author was privileged to be able to participate in the educational assistance program of the Oak Ridge National Laboratory. The research was sponsored by the United States Atomic Energy Commission under contract with the Union Carbide Corporation.

The final acknowledgements are directed to the author's immediate family, each of whom has contributed in some manner to this work. In particular, the author's mother, Mrs. Thelma A. Kollie, is remembered for the many hours spent in assisting the author in the data compilation.

The author also extends his heartfelt thanks to his wife, Mary, who has persevered through the many trials and tribulations which occurred during the ten years of the author's graduate studies.

ABSTRACT

The specific heat capacity at constant pressure C_p of a ferromagnetic solid is assumed separable into six contributions - that due to the dilation of the lattice C_d , that due to the harmonic oscillations of the atoms C_{vh} , that due to the anharmonic oscillations of the atoms C_{va} , that due to changes in the energy distributions of the electrons C_{ve} , that due to changes in the magnetic coupling among the electrons C_{vm} , and that due to atomic rearrangements C_{vw} . Expressions appearing in the literature for these contributions, which are assumed to be independent, are reviewed and the validity of each is discussed.

Specific heat capacity measurements performed in one of two pulse calorimeters are presented for iron, nickel, and ordered and disordered Ni_3Fe from 300 to 1400 K. Pulse Calorimeter II, having been developed during this research, is described in detail. Primary attributes of this apparatus are accurate and simultaneous measurement of the specific heat capacity ($\pm 1.05\%$) and electrical resistivity ($\pm 0.48\%$) at temperature intervals of 0.2 degree while the specimen is heated 100 to 600 degrees above its initial temperature at rates of 5 to 60 degrees/second. All specimens are in the form of rods (0.3-cm nominal diameter) and are of purity greater than 99.8%, contain no voids, and have a minute trace of second phase - possibly an oxide.

Comparison of the C_p values on nickel and iron with those in the literature indicates two regions of significant disagreement - at high temperatures and near the Curie temperature T_c of each. Both of these discrepancies are attributed to experimental errors in thermometry

and/or methodology. Examples for nickel and iron encountered in this work are given to illustrate these errors.

Expressions for C_{vd} , C_{vh} , C_{va} , and C_{ve} are chosen from the literature and used in conjunction with the C_p data of this investigation to calculate C_{vm} of nickel and iron as a function of temperature T . Some of the parameters requisite to these expressions are taken from the literature and some are obtained from the data treatment. The latter parameters are found to be in reasonable agreement with theory. The C_{vm} values calculated for nickel and iron are within experimental error of literature values based on experimental calculations. Appropriate integrations of the $C_{vm}:T$ relationships yield values of the magnetic energy U_{vm} and entropy S_{vm} which are in agreement with experimental and theoretical treatments of the literature for both materials. Values of the discontinuity ΔC_{vm} in C_{vm} at the Curie temperature T_c agree with theoretical predictions for this second-order transformation. Plots of C_{vm} for nickel and iron versus $\log_{10}|T - T_c|$ do not demonstrate the behavior expected of critical phenomena.

The C_p of Ni_3Fe is found to be a function of the thermal history and temperature of the specimen and of the experimental heating rate for temperatures between 750 and 1050 K. Below 750 K, the C_p decreases as the long-range order of the alloy increases. From theoretical interpretations of C_p data of this investigation for ordered and disordered Ni_3Fe between 1.2 and 4.4 K, this change is attributed to a decrease of the density of electron states and to an increase of the Debye temperature upon ordering. Use of rapid heating rates allows measurements on

ordered structures of Ni_3Fe at temperatures where they are metastable. These measurements reveal that the Curie transformation for a highly ordered metastable structure of Ni_3Fe is 70 degrees above that of the disordered structure and that the order-disorder transformation can be suppressed to temperatures 230 degrees above the equilibrium transformation temperature using heating rates of 60 degrees/second. In spite of this suppression, it is possible to calculate C_{vm} only for the disordered structure of Ni_3Fe because the ordered structures could not be maintained to high enough temperatures for completion of the C_{vm} analysis.

The $C_{\text{vm}}:T$ relationship for the disordered structure is obtained in a manner analogous to that for nickel and iron. Values of U_{vm} and S_{vm} found from these calculations are in excellent agreement with theoretical predictions, whereas the ΔC_{vm} value is not. The energy associated with transforming completely ordered Ni_3Fe to completely disordered Ni_3Fe at the equilibrium temperature is calculated. Only estimates of the entropy of this transformation could be made since the transformation is carried out in an irreversible manner. These values of the energy and entropy are within experimental error of those found in the literature.

Recommendations for further research are listed.

TABLE OF CONTENTS

CHAPTER	PAGE
I. INTRODUCTION AND LITERATURE REVIEW	1
Use and Definition of Specific Heat Capacity	1
Designation of the Order of a Transformation	3
Contributions to the Specific Heat Capacity C_v	5
Contributions to the Specific Heat Capacity C_p	8
Dilation Contribution C_d	8
Harmonic Vibrational Contribution C_{vh}	12
Anharmonic Vibrational Contribution C_{va}	19
Electronic Contribution C_{ve}	22
Magnetic Contribution C_{vm}	26
Contribution of Rearrangement of Atoms C_{vw}	38
The Metals Ni and Fe and the Alloy Ni_3Fe	40
Methods of Measurement of C_p of Solids	59
Thesis Goals	63
II. MEASUREMENT METHODS AND SPECIMENS	65
Electrical Resistivity Measurements	65
Thermoelectric Power Measurements	67
Specific Heat Capacity Measurements	68
Description of Pulse Calorimeter II	72
Specimen Preparation and Characterization	91
III. RESULTS AND DISCUSSION	101
Specific Heat Capacity of Pure Nickel and Iron	101
Measurements of C_p Near the Curie Temperature of Ferromagnets	105

CHAPTER	PAGE
Measurements of C_p of Nickel and Iron Above 1200 K . . .	121
Preliminary Comments on the Calculation of C_{vm} of Nickel and Iron	126
Calculation of C_{vm} of Nickel	128
Calculation of C_{vm} of Iron	138
Discussion of the C_{vm} Values of Nickel and Iron	148
ΔC_{vm} , U_{vm} , and S_{vm} of Nickel and Iron	154
Brief Summary of Results on Nickel and Iron	158
Specific Heat Capacity of Ni_3Fe	161
Interpretation of Low-Temperature C_p Measurements on Ni_3Fe	179
Calculation of C_{vm} of Disordered Ni_3Fe	186
ΔC_{vm} , U_{vm} , and S_{vm} of Disordered Ni_3Fe	190
Calculation of C_{vm} , ΔC_{vm} , U_{vm} , and S_{vm} of Ordered Ni_3Fe	196
Energy of Transformation U_{od} of Ni_3Fe	196
Entropy of Transformation S_{od} of Ni_3Fe	200
IV. SUMMARY AND RECOMMENDATIONS	202
Summary of Chapter I	202
Summary of Chapter II	204
Summary of Chapter III	205
Recommendations	212
BIBLIOGRAPHY	214
APPENDIX	225
VITA	255

LIST OF TABLES

TABLE	PAGE
I. Theoretical Values of Discontinuity in C_{vm}	35
II. Value of (J_e/kT_c) of Various Models	37
III. Comparison of Theoretical and Experimental Values of the Total Magnetic Energy U_{vm} and Entropy S_{vm} of Nickel . .	45
IV. Comparison of Theoretical and Experimental Values of the Total Magnetic Energy U_{vm} and Entropy S_{vm} of Iron . . .	47
V. Chemical Composition in Parts Per Million by Weight of Specimen Stock and Specimens	92
VI. Value of the Constants a, b, A, and B Obtained from the Two Iterations During Calculation of C_{vm} of Iron	145
VII. Errors in the Calculated Values of C_{vm} of Iron Introduced by Errors in Calculating the Values of the Other Contributions to C_p	151
VIII. Results of Fitting the C_{vm} of Nickel and Iron to the Function $a + b \log_{10} T - T_c $ Above and Below the Curie Temperature T_c	155
IX. Magnetic Energy U_{vm} , Entropy S_{vm} , and Discontinuity ΔC_{vm} of C_{vm} at T_c of Nickel and Iron From This Investigation	156
X. Comparison of the Results of This Investigation for Nickel and Iron With Theoretical Values in the Open Literature	157

TABLE	PAGE
XI. Comparison of Results of This Investigation for Nickel and Iron With Literature Values Calculated From Experimental Data	157
XII. Summary of Parameters Used to Calculate Contributions to C_p of Nickel and Iron	159
XIII. Summary of Results on Nickel and Iron	160
XIV. States of Order and Disorder of the Ni_3Fe Specimen for Which C_p Measurements were made in Pulse Calorimeter I	163
XV. Heat Treatments Given the Ni_3Fe Specimen During Formation of Long-Range Order Below the Critical Temperature During Auxiliary Resistivity Measurements .	165
XVI. Correlation of the Heat Treatments Given the C_p Specimens With the Auxiliary Electrical Resistivity Measurements and an Estimate of the Long-Range Order Parameter S for Each State	167
XVII. Least-Squares Parameters from Fits of Low-Temperature C_p Data on Ordered and Disordered Ni_3Fe	182
XVIII. Summary of Results on Disordered Ni_3Fe Alloy	194
XIX. Comparison of the Experimental Results for Disordered Ni_3Fe with Those Predicted from Theory	195
XX. Order-Disorder Enthalpies ΔH_e for Order-States I to VI .	198

TABLE	PAGE
XXI. Specific Heat Capacity, Electrical Resistivity, and Temperature Derivative of Electrical Resistivity of Nickel from 333 K to 1323 K	226
XXII. Specific Heat Capacity, Electrical Resistivity, and Temperature Derivative of Electrical Resistivity of Iron from 318 K to 1178 K	229
XXIII. Specific Heat Capacity of Nickel from 1330 K to 1500 K	232
XXIV. Magnetic Specific Heat Capacity C_{vm} of Nickel from 30 K to 1030 K	232
XXV. Magnetic Specific Heat Capacity C_{vm} of Iron from 15 K to 1673.2 K	233
XXVI. Low-Temperature Specific Heat Capacity Data of Ni_3Fe . .	234
XXVII. Specific Heat Capacity, Electrical Resistivity, and Temperature Derivative of Electrical Resistivity of Vacuum-Quenched Ni_3Fe in Temperature Regions Where Results were Independent of Heating Rates Used in this Work	235
XXVIII. Specific Heat Capacity, Electrical Resistivity, and Temperature Derivative of Electrical Resistivity of Vacuum-Quenched Ni_3Fe Pulsed from Below the Order- Disorder Critical Temperature with Class I Heating Rate in Temperature Region Where Results were Heating Rate Dependent	237

TABLE	PAGE
XXIX. Specific Heat Capacity, Electrical Resistivity, and Temperature Derivative of Electrical Resistivity of Ni_3Fe Pulsed from 75 Degrees Above the Order-Disorder Critical Temperature with Class I Heating Rate	238
XXX. Specific Heat Capacity, Electrical Resistivity, and Temperature Derivative of Electrical Resistivity of Ni_3Fe Pulsed from 106 Degrees Above the Order-Disorder Critical Temperature with Class I Heating Rate	239
XXXI. Specific Heat Capacity, Electrical Resistivity, and Temperature Derivative of Electrical Resistivity of Vacuum-Quenched Ni_3Fe Pulsed from Below the Order- Disorder Critical Temperature with Class II Heating Rate in Temperature Region when Results were Heating Rate Dependent	240
XXXII. Specific Heat Capacity, Electrical Resistivity, and Temperature Derivative of Electrical Resistivity of Ni_3Fe in Order-State I Pulsed from Below the Order- Disorder Critical Temperature with Class I Heating Rate	241
XXXIII. Specific Heat Capacity, Electrical Resistivity, and Temperature Derivative of Electrical Resistivity of Ni_3Fe in Order-State II Pulsed from Below the Order- Disorder Critical Temperature with Class I Heating Rate	243

TABLE	PAGE
XXXIV. Specific Heat Capacity, Electrical Resistivity, and Temperature Derivative of Electrical Resistivity of Ni_3Fe in Order-State III Pulsed from Below the Order- Disorder Critical Temperature with Class II Heating Rate	245
XXXV. Specific Heat Capacity, Electrical Resistivity, and Temperature Derivative of Electrical Resistivity of Ni_3Fe in Order-State IV Pulsed from Below the Order- Disorder Critical Temperature with Class II Heating Rate	246
XXXVI. Specific Heat Capacity, Electrical Resistivity, and Temperature Derivative of Electrical Resistivity of Ni_3Fe in Order-State V Pulsed from Below the Order- Disorder Critical Temperature with Class II Heating Rate	247
XXXVII. Specific Heat Capacity, Electrical Resistivity, and Temperature Derivative of Electrical Resistivity of Ni_3Fe in Order-State VI Pulsed from Below the Order- Disorder Critical Temperature with Class II Heating Rate	248
XXXVIII. Electrical Resistivity of Ni_3Fe in Equilibrium State from 4.2 K to 1361.8 K	250
XXXIX. Thermoelectric Power of Ni_3Fe in Equilibrium State from 80 K to 1362 K	251

TABLE	PAGE
XL. Electrical Resistivity and Thermoelectric Power of Ni ₃ Fe in State at Equilibrium at 767 K	251
XLI. Electrical Resistivity and Thermoelectric Power of Ni ₃ Fe in State at Equilibrium at 755 K	252
XLII. Electrical Resistivity and Thermoelectric Power of Ni ₃ Fe in State at Equilibrium at 735 K	252
XLIII. Electrical Resistivity and Thermoelectric Power of Ni ₃ Fe in State at Equilibrium at 713 K	252
XLIV. Electrical Resistivity and Thermoelectric Power of Ni ₃ Fe Quenched from 1400 K	253
XLV. Magnetic Specific Heat Capacity C_{vm} of Disordered Ni ₃ Fe from 50 K to 1423 K	254

LIST OF FIGURES

FIGURE		PAGE
1.	Discrepancies in the Debye Theory as Explained by the Born-Von Karman Theory. (a) Measured Debye temperature θ_d versus temperature T for indium. (b) Frequency spectrum $g(\nu)$ for tungsten from application of the Born-Von Karman theory to bcc lattice. The Debye spectrum for $\theta_d = 310$ K is that of broken line. (c) θ_d versus T comparing results of the Born-Von Karman theory with experiment for silver (fcc). Note the qualitative similarities between (a) and (c)	17
2.	Energy Distributions of Electrons in a Metal. (a) Total number of electrons per unit volume $N(E)$ as function of energy E for free electrons or parabolic band in metal. (b) Fermi-Dirac distribution function of $f(E)$ for three different temperatures as function of E/ζ , the ratio of energy to thermodynamic potential. (c) $N(E)$ versus E for idealized form of overlapping s- and d-bands in transition metal such as nickel. E_f is the Fermi energy	23
3.	Possible Energy Distribution of Electrons in 3-d Band of Iron. Density of electron states $N(E)$ is plotted as a function of energy for spinup and spindown. The spinup electrons have spins parallel to atom to which they belonged at that instant. Energies connected with the magnetic moment are not presented	28

FIGURE	PAGE
4. Magnetic Specific Heat According to the Constant Coupling Approximation. Ratio of C_{vm} to nk versus reduced temperature for iron and nickel showing the calculated values as solid line and experimental values as dashed line. The quantity n is the effective number of magnetic atoms per mole and k is Boltzmann's constant	32
5. The Equilibrium Phase Diagram for the Nickel-Iron Alloy System	41
6. Harmonic Vibrational C_{vh} , Electronic C_{ve} , Dilation C_d , and Magnetic C_{vm} Contributions to the Specific Heat Capacity C_p as a Function of Temperature T . (a) Nickel and (b) Iron	43
7. Specific Heat Capacity of Ni_3Fe as a Function of Temperature for Three Different Prior Heat Treatments. Curve one was obtained after a water quench from 1000 K. Curve two refers to the alloy as cooled at 1 degree/minute from 925 K. The heat treatment prior to curve three consisted of cooling from 765 K to 643 K over a 150-hour period	50
8. Schematic Diagram of Pulse Calorimeter Which Utilizes Joule Heating to Supply the Required Pulse. The three mechanisms of heat loss from the test section are indicated	70
9. Schematic Diagram of Pulse Calorimeter I Showing the Major Components and Their Interrelationship	73

FIGURE	PAGE
10. Schematic Diagram of the Pulse Calorimeter II Showing the Vacuum Furnace, Sample-Holder Assembly, and the Specimen	74
11. Block Diagram of the Thermometry and Power Circuitry. Steady-state data were input to computer on cards and transient data on magnetic tape	76
12. Schematic Representation of Specimen Power Supply Circuitry. Only two power supplies are depicted	77
13. Schematic Diagram of the Transient Signal Circuitry. (a) The amplification circuitry and (b) the DVM circuits. The circuitry between points X and Y corresponds to that between points X and Y of Figure 12	79
14. Schematic Diagram of the DVM Output During a Pulse Showing the Changes that Occur in the Current (ΔI), Voltage (ΔE), and Temperature (ΔT)	84
15. Photomicrographs of the Nickel Specimen in Etched Condition After Annealing. (a) Transverse section at 100x; (b) transverse section at 500x; (c) longitudinal section at 100x; and (d) longitudinal section at 500x. Etchant composition was 60 cubic centimeters acetic acid, 40 cubic centimeters nitric acid, and 0.5 cubic centimeters hydrochloric acid. Note the second phase in (b) and (d)	95

16. Photomicrographs of the Iron Specimen in Etched Condition. (a) Transverse section at 500 \times after annealing; (b) longitudinal section at 500 \times after annealing; (c) transverse section at 100 \times after C_p measurements in γ -stable region; and (d) same as (c) but at 500 \times . Second phase appears as black dots. Note subgrain structure in (d). Etchant was saturated solution of picric acid in ethyl alcohol 96
17. Photomicrographs of Iron and Ni_3Fe Specimens. (a) Longitudinal section of iron specimen at 100 \times in as-polished condition revealing second phase as black dots; (b) transverse section of disordered Ni_3Fe specimen at 500 \times etched with a solution of 10% nitric acid, 30% hydrochloric acid, and 30% glycerol (by volume); (c) etched transverse section of disordered Ni_3Fe specimen at 500 \times ; and (d) etched transverse section of disordered Ni_3Fe specimen at 200 \times . Etchant for (c) and (d) was saturated solution of ammonium persulfate in water 97
18. Smoothed values of the Specific Heat Capacity of Nickel from 333 to 1323 K Determined by this Investigation. Note the discontinuity of 7.64 joules/gram-atom degree at 633 K, the Curie temperature 102

FIGURE	PAGE
19. Smoothed Values of the Specific Heat Capacity of α -Iron from 318 to 1178 K Determined by this Investigation. Note the discontinuity of 16.64 joules/gram-atom degree at 1043.2 K, the Curie temperature	103
20. Typical Plot of Raw Data Used to Obtain Smoothed Values of C_p as Function of T. Raw data from three pulses are shown as well as the curve from which smoothed values were chosen. .	104
21. A Plot of the Specific Heat Capacity of Nickel of this Investigation Minus that of Five Other Investigations from 333 to 1323 K. The solid curves represent $\pm 2\%$ deviations from the values of this investigation. Numbers in parentheses in legend are reference numbers . .	106
22. Plot of the Specific Heat Capacity of α -Iron of this Investigation Minus that of Seven Other Investigations from 318 to 1178 K. The solid curves represent $\pm 2\%$ deviations from the values of this investigation. Numbers in parentheses are reference numbers	107
23. Effect of a Temperature Gradient in the Specimen of an Adiabatic or Pulse Heating Calorimeter During C_p Measure- ments Near the Curie Temperature T_c of a Ferromagnet. (a) Temperature T of specimen versus time t during measure- ment. (b) Temperature-rate-of-change dT/dt of specimen versus T of specimen. (c) C_p of specimen versus T of speci- men. Both the ideal (no gradient) and smoothed (with gradient) results are shown for a slowly increasing specimen power. .	109

FIGURE

PAGE

24. Effect of Choosing a Break Temperature T_b Which is Above the True Curie Temperature T_c in a Pulse Calorimetric Measurement of the Specific Heat Capacity of a Ferromagnet. (a) Temperature T of specimen versus time t during measurement. (b) Temperature-rate-of-change dT/dt of specimen versus T of specimen. (c) C_p of specimen versus T of specimen. Results for the correct choice (ideal curve) and incorrect choice (smoothed curve) of T_c are shown . . . 111
25. Effect of Choosing a Break Temperature T_b Which is Below the True Curie Temperature T_c in a Pulse Calorimetric Measurement of the Specific Heat Capacity of a Ferromagnet. (a) Temperature T of specimen versus time t during measurement. (b) Temperature-rate-of-change dT/dt of specimen versus T of specimen. (c) C_p of specimen versus T of specimen. Results for the correct choice (ideal curve) and incorrect choice (smoothed curve) of T_c are shown . . . 112
26. Plot of Temperature of Specimen as Function of Time from Data Recorded on DVM During Heating of the Specimen Through Its Curie Transformation. Every fifth temperature point recorded is shown. These points are separated by 0.45 degree in temperature and 45 milliseconds in time. Note the discontinuity of slope at the Curie temperature, 633.2 K 114

FIGURE	PAGE
27. Plot of Voltage Across Test Section of Specimen as a Function of Specimen Temperature from Data Recorded on DVM During Heating of the Specimen Through Its Curie Transformation. Every fifth point recorded is shown. These points are separated by 0.45 degree. Note the discontinuity of slope at the Curie temperature, 632.9 K	115
28. Effects on the Calculated Values of the Specific Heat Capacity Resulting from Five Different Treatments of the Data of a Single Pulse on Nickel Near the Curie Temperature, 633.0 K. Smoothed (reported) curve of Figure 18, page 102, is also shown. See text for discussion	117
29. Effects on the Calculated Values of the Specific Heat Capacity Resulting from Choosing Four Break Temperatures Below the True Curie Temperature. A 65-point group was used for all calculations on the data of a single pulse near T_c of nickel. Smoothed (reported) curve of Figure 18, page 102, is also shown. See text for discussion	119
30. Effects on the Calculated Values of the Specific Heat Capacity Resulting from Choosing Four Break Temperatures Above the True Curie Temperature. A 65-point group was used for all calculations on the data of a single pulse near T_c of nickel. Smoothed (reported) curve of Figure 18, page 102, is also shown. See text for discussion	120

FIGURE

PAGE

31. Illustration of Errors in Measured Values of C_p of Nickel Resulting from Contamination of Thermocouples. Solid curve obtained from pulses with furnace temperatures below 1100 K and the data shown as points were acquired after a furnace temperature of 1220 K had been employed 122
32. Measurements of the C_p of γ -Iron. Note the excellent agreement of pulse one with the C_p values of Dench and Kubaschewski. Numbers in parentheses in legend are reference numbers 125
33. Temperature Dependence of C_x of Nickel Calculated with a γ of 7.028×10^{-3} joules/gram-atom K^2 and a γ_{nl} of 2.624×10^{-6} gram-atom/joule. (a) θ_d equals 471 K, (b) θ_d equals 390 K 130
34. Plot of the Temperature Dependence of C_x of Nickel Calculated with a γ of 7.028×10^{-3} joules/gram-atom K^2 and a γ_{nl} of 2.624×10^{-6} gram-atom/joule. (a) θ_d equals 410 K, (b) θ_d equals 400 K 132
35. Calculated Values of the Dilation Contribution C_d of Nickel as a Function of Temperature. Grüneisen's approximation for C_d is shown as a solid line for a γ_g of 1.88. The Nernst-Lindemann approximation is shown as points for a γ_{nl} of 2.624×10^{-6} gram-atom/joule 134

36. Temperature Dependence of C_{vm} of Nickel Calculated Assuming that the Anharmonic Contribution C_{va} is Negligible. Note that this assumption yields negative values of C_{vm} between 715 and 1500 K 136
37. Contributions to the Specific Heat Capacity of Nickel as a Function of Temperature. ($\theta_d = 400$ K, $\gamma = 7.028 \times 10^{-3}$ joules/gram-atom K^2 , $\gamma_{nl} = 2.624 \times 10^{-6}$ gram-atom/joule, $A = -1.48 \times 10^{-10}$ joules/gram-atom K^4 , and $B = -1.76 \times 10^{-3}$ joules/gram-atom K^2 .) 139
38. Expanded Plot of Figure 37 Showing the Contributions to the Specific Heat Capacity of Nickel as a Function of Temperature. Only C_{ve} , C_d , C_{vm} , and C_{va} are shown 140
39. Temperature Dependence of C_x of Iron Calculated with a γ of 4.741×10^{-3} joules/gram-atom K^2 , a γ_{nl} of 2.349×10^{-6} gram-atom/joule, and a θ_d of 440 K 141
40. Plot of C_x of Iron as a Function of $\log_{10} |T - T_c|$ for Temperatures above the Curie Temperature of 1043.2 K. The straight line was obtained by fitting C_x to the function $a + b \log_{10} |T - T_c|$ between 1057 and 1123 K . . 143
41. Contributions to the Specific Heat Capacity of Iron as a Function of Temperature. ($\theta_d = 440$ K, $\gamma = 4.741 \times 10^{-3}$ joules/gram-atom K^2 , $\gamma_{nl} = 2.349 \times 10^{-6}$ gram-atom/joule, $A = 2.1 \times 10^{-10}$ joules/gram-atom K^4 , and $B = -1.13 \times 10^{-3}$ joules/gram-atom K^2 .) 146

FIGURE	PAGE
42. Expanded Plot of Figure 41 Showing the Contributions to the Specific Heat Capacity of Iron as a Function of Temperature	147
43. Comparison of the Calculated Values of C_{vm} of Nickel and Iron with Those of Other Investigations. (a) Nickel; (b) iron. Numbers in parentheses are reference numbers. Note the discontinuities of 11.13 and 6.66 joules/gram-atom degree in the C_{vm} of nickel and iron, respectively .	149
44. Plot of C_{vm} of Nickel as a Function of $\log_{10} T - T_c $ for Temperatures above and below the Curie Temperature of 633.0 K. The straight lines were obtained by fitting the data between 358 and 622 K and between 637 and 833 K	152
45. Plot of C_{vm} of Iron as a Function of $\log_{10} T - T_c $ for Temperatures above and below the Curie Temperature of 1043.2 K. The straight lines were obtained by fitting the data between 318 and 1028 K and between 1053 and 1673 K	153
46. Electrical Resistivity Measurements on the Ni_3Fe Alloy as a Function of Its State of Order and Temperature	166

FIGURE

PAGE

47. Low-Temperature C_p of Ordered and Disordered Ni_3Fe Plotted as C_p/T Versus T^2 . Disorder produced by quenching specimen from 1400 K into ice water. Order produced by successive one-week anneals at 753, 733, 723, and 683 K. Curves obtained by fitting the data using method of least squares 169
48. The Specific Heat Capacity as a Function of Temperature for Order-States I, II, and VI and for Vacuum-Quench A of the Ni_3Fe Specimen in Temperature Range where Results were Independent of Heating Rate 171
49. The Specific Heat Capacity as a Function of Temperature for Four Locally Ordered States of Ni_3Fe Showing the Effects of Heating Rate 173
50. The Specific Heat Capacity and Electrical Resistivity of Ni_3Fe as a Function of Temperature for States Having Long-Range Order Parameters of 0.66 (Order-State I) and 0.60 (Order-State V), Showing the Effects of Heating Rate. (a) Specific heat, (b) electrical resistivity plus Equilibrium-State curve 175
51. The Specific Heat Capacity and Electrical Resistivity of Ni_3Fe as a Function of Temperature for States Having Long-Range Order Parameters of 0.88 (Order-State II) and 0.78 (Order-State III), Showing the Effects of Heating Rate. (a) Specific heat, (b) electrical resistivity plus Equilibrium-State curve 178

FIGURE	PAGE
52. The Specific Heat Capacity and Electrical Resistivity as a Function of Temperature for a Highly Ordered State. (Order-State VI, $S = 0.96$.) (a) Specific heat, (b) electrical resistivity plus Equilibrium-State curve	180
53. Specific Heat Capacity Calculated from Two-Term and Three-Term Least-Squares Functions Minus the Experimental Values for Ordered Ni_3Fe Alloy between 1.2 and 4.4 K. The solid curves represent $\pm 0.2\%$ deviations from the experimental values	184
54. Specific Heat Capacity Calculated from Two-Term and Three-Term Least-Squares Functions Minus the Experimental Values for Disordered Ni_3Fe Alloy between 1.2 and 4.4 K. The solid curves represent $\pm 0.2\%$ deviations from the experimental values	185
55. Temperature Dependence of C_x of Disordered Ni_3Fe Calculated with a γ of 4.053×10^{-3} joules/gram-atom K^2 , a γ_{nl} of 2.56×10^{-6} gram-atom/joule, and a θ_d of 410 K	188
56. Contributions to the Specific Heat Capacity of Disordered Ni_3Fe as a Function of Temperature. ($\theta_d = 410$ K, $\gamma = 4.053 \times 10^{-3}$ joules/gram-atom K^2 , $\gamma_{nl} = 2.56 \times 10^{-6}$ gram-atom/joule, $A = 1.282 \times 10^{-9}$ joules/gram-atom K^4 , and $B = -1.67 \times 10^{-3}$ joules/gram-atom K^2 .)	191

FIGURE	PAGE
57. Expanded Plot of Figure 56 Showing the Contributions to the Specific Heat Capacity of Disordered Ni_3Fe as a Function of Temperature. Only C_{ve} , C_d , C_{vm} , and C_{va} are shown	192
58. Temperature Dependence of C_{vm} of Disordered Ni_3Fe Calculated from Experimental C_p Values	193
59. Enthalpy ΔH_e of the Order-Disorder Transformation as a Function of the Square of the Long-Range Order Parameter. Solid straight line shows extrapolation to complete order. Dashed lines are estimated maximum and minimum extrapolations	199

CHAPTER I

INTRODUCTION AND LITERATURE REVIEW

Use and Definition of Specific Heat Capacity

According to the first law of thermodynamics, absorption of a quantity of heat dQ by an isolated substance at constant volume V results in an equivalent increase of dU in its internal energy. When this energy change is accompanied by a change dT in the temperature of the substance, the ratio of the heat added per mole of substance to the temperature change is defined as the specific heat capacity at constant volume

$$C_v = \left(\frac{dQ}{dT} \right)_V = \left(\frac{dU}{dT} \right)_V . \quad (1)$$

The quantity C_v is an intensive property of the substance and its determination as a function of temperature is of immense fundamental interest. For example, a change in internal energy of a substance is caused by changes in the translational, rotational, vibrational, electronic, and nuclear energy of its atoms. If one then derives a theoretical expression for the temperature dependence of each of these energy forms as well as their interactions, partial differentiation with respect to temperature of the sum of these expressions yields C_v by Equation (1). Comparison of these calculated values with experimentally determined ones allows a quantitative test of the theories employed. One of the goals of this work was to examine such comparisons on solid ferromagnets, namely nickel, iron, and nickel-iron alloys.

Unfortunately, it is very difficult to measure C_v directly for solids. Normally, the specific heat capacity C_p at constant pressure P is determined. Using the first law and the definition of the specific enthalpy H , C_p is given by

$$C_p = \left(\frac{dQ}{dT} \right)_P = \left(\frac{dU + P dV}{dT} \right)_P = \left(\frac{dU + d(PV)}{dT} \right)_P = \left(\frac{dH}{dT} \right)_P . \quad (2)$$

At the absolute zero of temperature, C_p and C_v are equal to zero. However, as the temperature is raised the solid expands under the condition of constant pressure but does not under the restraint of constant volume. The temperature derivative of the internal energy change associated with this expansion of the solid is called the dilation contribution C_d to the specific heat capacity and is equal to the difference between C_p and C_v ; that is,

$$C_d = C_p - C_v . \quad (3)$$

An expression for C_d in terms of other physical properties of a solid is discussed in detail later.

Besides the example given above, there are many uses, both applied and fundamental, for C_p and C_v data. Many of the applied uses are associated with heat transfer calculations that require temperature-rate-of-change predictions of a transient process. On the other hand, specific heat capacity data are often used to extrapolate various thermodynamic properties, such as enthalpy and entropy, from a temperature at which they are known to some other temperature of interest. Other examples, which are of particular interest in this work, are the use of C_p data to

obtain the energetics of configurational and magnetic ordering transformations. The behavior of the $C_p:T$ and $C_v:T$ relationships near the transformation temperature is considered below.

Designation of the Order of a Transformation

At many transformations, such as allotropic transformations, a solid absorbs heat and raises its internal energy isothermally. Due to the definitions of Equations (1) and (2), C_p and C_v are undefined at the transformation temperature T_0 . In addition, C_p and C_v are discontinuous at T_0 ; that is, the specific heat is different in the limit as T_0 is approached from above and below. There also exists another class of transformations, such as a transition from the ferromagnetic to paramagnetic state, that has a discontinuous specific heat capacity at T_0 but that occurs over an extended temperature interval, instead of isothermally. The former transformations are classified as "first order" and the latter as "second order."

The classification of the order of a transformation is based on the following thermodynamic argument given by Pippard^{1*} and attributed originally to Ehrenfest. The specific Gibbs free energies G of two phases of a pure substance in equilibrium are equal. Therefore, the function $G(T)$ is continuous at any transformation, but the derivatives of G with respect to pressure P and absolute temperature T need not be. These derivatives for either phase can be written as

*Denotes reference. See page 214.

$$\left(\frac{\partial G}{\partial P} \right)_T = V, \quad (4)$$

$$\left(\frac{\partial G}{\partial T} \right)_P = -S, \quad (5)$$

$$\left(\frac{\partial^2 G}{\partial T \partial P} \right)_{P,T} = V\alpha \quad (6)$$

$$\left(\frac{\partial^2 G}{\partial P^2} \right)_T = -V\chi, \quad (7)$$

and

$$\left(\frac{\partial^2 G}{\partial T^2} \right)_P = -\frac{C_p}{T}, \quad (8)$$

where χ is the isothermal compressibility and α is the volumetric coefficient of expansion. If the specific volumes V and specific entropies S are different for the two phases at T_o , then $\left(\frac{\partial G}{\partial T} \right)_P$ and $\left(\frac{\partial G}{\partial P} \right)_T$ are discontinuous at T_o . This is called a first-order transformation.

Note that for this case all higher order derivatives of G are also discontinuous at T_o , and hence C_p must be discontinuous at a first-order transformation. Suppose that V and S are continuous but that $\left(\frac{\partial^2 G}{\partial T^2} \right)_P$, $\left(\frac{\partial^2 G}{\partial P^2} \right)_T$, and $\left(\frac{\partial^2 G}{\partial T \partial P} \right)_{P,T}$ are discontinuous at T_o . Then C_p , α , and χ are discontinuous at T_o , and this is called a second-order transformation.

Consequently, C_p and C_v are discontinuous at both first- and second-order transformations. However, near a first-order transformation, C_p and most other physical properties usually do not change rapidly. That is, the physical properties normally give no hint of the drastic change which is about to occur. On the other hand, C_p and many physical

properties change very rapidly at temperatures above and below a second-order transformation. In fact, the $C_p:T$ relationship for this type transition is normally in the shape of the Greek letter λ with the maximum occurring at T_0 . For this reason, second-order transformations are often called "lambda transformations." Determinations of rapidly varying $C_p:T$ relationships are very demanding on experimental methods. Hence, measurements of C_p near T_0 of first-order transformations are much more accurate and straightforward than those near T_0 of second-order ones. (This is discussed in Chapter III.)

Contributions to the Specific Heat Capacity C_v

Expressions for the specific heat capacity at constant volume C_v can be derived theoretically by considering the atomistic mechanisms associated with internal energy changes of a substance. Since C_v is the sum of the first temperature derivative of the internal energy of each of these mechanisms and their interactions, C_v can be expressed as

$$C_v = C_{vt} + C_{vr} + C_{vn} + C_{vw} + C_{vi} + C_{vv} + C_{ve} , \quad (9)$$

where

- C_{vt} = contribution of translational motion of atoms,
- C_{vr} = contribution of rotational motion of atoms,
- C_{vn} = contribution of nuclear structure changes,
- C_{vw} = contribution of rearrangement of atoms,
- C_{vi} = contribution of interactions of above mechanisms,
- C_{vv} = contribution of vibrational motion of atoms, and
- C_{ve} = contribution of electronic structure changes.

Consider each of these contributions for a solid substance. Since the atoms of a solid are bound together on a relatively rigid lattice, little translational and rotational motion of the atoms occurs. Hence, the first two terms of Equation (9) may be neglected. Likewise, the nuclear contribution C_{vn} is also negligible above about 10 K. (The symbol K stands for degrees kelvin.) However, at temperatures near absolute zero C_{vn} becomes quite large for some solids such as cobalt and is proportional to $1/T^2$.

The term C_{vw} is a "catch-all" quantity and is used here to describe contributions due to transformations such as configurational ordering and vacancy or divacancy formation. Because most of these transformations depend principally on atom diffusion, they are usually unimportant below 400 K. In practice, C_{vw} is also considered to include contributions due to first-order transformations which occur over an interval of temperature during measurement because of the slow kinetics of the transformation and/or because of the rapid temperature change encountered during measurement. Of course to be meaningful, contributions of this type must be converted by thermodynamic reasoning to a change in internal energy ΔU at the transformation temperature T_0 .

The contribution C_{vi} due to the interaction of the various mechanisms is very difficult to assess. Normally, C_{vi} is assumed to be negligible; sometimes, however, changes are made in the expressions for the other mechanisms to validate this assumption. This is particularly true of alloys which possess both configurational and magnetic ordering. For

these alloys, C_v can be accurately predicted by allowing C_{ve} and C_{vv} to be a function of the configurational state of the alloy, as discussed below.

With the assumptions outlined above, Equation (9) reduces to

$$C_v = C_{vv} + C_{ve} + C_{vm} . \quad (10)$$

Consider now the two quantities C_{vv} and C_{ve} which have not been discussed. The term C_{ve} is the electronic contribution and is negligible for almost all insulators and is very small for most metals. For example, C_{ve} for copper at 1000 K is about three percent of C_v . However, for transition metals the electronic contribution is much larger, amounting to about twenty-five percent of the total at the melting point of nickel. An even larger electronic contribution is that due to the Curie transformation — a second-order transformation from the ferromagnetic to paramagnetic state. For iron, C_{ve} is about seventy-five percent of C_v at the Curie temperature T_c . In practice, the magnetic part of the electronic contribution is considered separately and denoted as C_{vm} .

At low temperatures, the normal modes of vibration of the atoms of a solid may be considered to be in harmonic oscillation, and thus have potential energies that vary as the square of their displacements from their equilibrium positions. As the temperature is increased, anharmonic oscillations are introduced whose potential energies vary as the third and fourth power of their displacements. Consequently, the vibrational contribution C_{vv} is considered as the sum of an harmonic C_{vh} and anharmonic C_{va} contribution. In terms of these new quantities, Equation (10) becomes

$$C_v = (C_{vh} + C_{va}) + (C_{ve} + C_{vm}) + C_{vw} . \quad (11)$$

Contributions to the Specific Heat Capacity C_p

The contributions to the specific heat capacity at constant pressure C_p are precisely those given in Equation (11) plus that due to the dilation of the lattice C_d . Thus, an expression for C_p is

$$C_p = C_d + C_{vh} + C_{va} + C_{ve} + C_{vm} + C_{vw} . \quad (12)$$

Sometimes it is convenient to consider C_d as being the sum of several contributions. In particular, the dilation contribution C'_d , which does not include the contribution due to the magnetic transformation, yields another expression for C_p

$$C_p = C'_d + C_{vh} + C_{va} + C_{ve} + C_{pm} + C_{vw} , \quad (13)$$

where C_{pm} is the magnetic contribution at constant pressure. The theoretical expressions for each of the quantities of Equation (12) are considered individually below. In general, these expressions are only approximations based on an assumed model for the particular contribution. Consequently, the expressions are subject to many qualifications, some of which are pointed out explicitly.

Dilation Contribution C_d

The dilation contribution to the specific heat capacity of solids is derived in most texts on thermodynamics and is given by

$$C_d = C_p - C_v = \frac{TV\alpha^2}{\chi} . \quad (14)$$

In this expression, χ is the coefficient of isothermal compressibility

$$\chi = -\frac{1}{V} \left(\frac{dV}{dP} \right)_T , \quad (15)$$

and α is the volumetric coefficient of thermal expansion, which for isotropic solids is related to the linear coefficient of thermal expansion α_ℓ by

$$\alpha = \frac{1}{V} \left(\frac{dV}{dT} \right)_P = 3\alpha_\ell = \frac{3}{\ell} \left(\frac{d\ell}{dT} \right)_P, \quad (16)$$

where ℓ is the length of the solid.

Although the linear coefficient of thermal expansion is known for some pure metals over a wide range of temperature, few values of χ are available except at room temperature and below. For this reason, one of two approximations is normally employed to obtain C_d . The first was proposed by Grüneisen² during his development of an equation of state for solids assuming central-force interactions of atoms. Grüneisen's approximation states that the quantity

$$\gamma_g = \frac{\alpha V}{\chi C_v} \quad (17)$$

should be a constant with temperature, having a mean value of 1.8 for most substances. Thus the dilation contribution may be rewritten as

$$C_d = C_v \gamma_g \alpha T = 3C_v \gamma_g \alpha_\ell T. \quad (18)$$

In the Nernst-Lindemann³ approximation, a similar but empirical ratio has been found to be constant with temperature and is given by

$$\gamma_{nl} = \frac{\alpha^2 V}{\chi (C_p)^2}. \quad (19)$$

The resulting expression for C_d is

$$C_d = \gamma_{nl} (C_p)^2 T. \quad (20)$$

Equations (18) and (20) for C_d are only approximations and hence subject to error. For most metals, this contribution is a maximum at the melting point, where it is of the order of 10% of the total. Consequently, a 10% error in the calculation of C_d results in about a 1% error in C_v .

Blackman⁴ pointed out that Grüneisen's theory is not exact, especially at low temperatures where γ_g is not constant. In particular, he states that this approximation is of dubious value on materials, such as silicon, which have negative coefficients of linear thermal expansion. Frasier and Hallett⁵ have measured α_ℓ for copper, gold, silver, iron, nickel, and aluminum and used literature values of C_p and the adiabatic compressibility χ_s to calculate γ_g as a function of temperature from 4 to 300 K. In terms of χ_s , Grüneisen's constant is

$$\gamma_g = \frac{3\alpha_\ell V}{\chi_s C_p} \quad (21)$$

because

$$\chi_s = -\frac{1}{V} \left(\frac{\partial V}{\partial P} \right)_S = \frac{C_v}{C_p} \chi \quad (22)$$

Their results show that, for temperatures above one-fourth the Debye temperature, γ_g is essentially a constant for the metals investigated. Below this temperature, striking deviations occur from a constant value of γ_g .

The validity of the Nernst-Lindemann approximation has been tested by Chang and Hultgren⁶ for copper and α brass using their measurements of the compressibility from 77 to 800 K and literature values of α and

C_p . Their results show that this approximation is very adequate for these two materials. Using data available in the literature for zinc, indium, aluminum, lead, and tin, they found that the Nernst-Lindemann equation tends to overestimate the dilation contribution near the melting points of these metals. On the other hand, Singh and Verma⁷ found that this approximation underestimates C_d of tungsten from 300 to 2100 K. They relied on literature values for all the required quantities.

In the vicinity of the Curie transformation of ferromagnets, the difficulties in calculating an accurate dilation contribution are compounded due to the rapid variation of all the quantities in Equation (14). Also, the validity of the two approximations is questionable near the Curie temperature T_c . In fact, the Grüneisen expression cannot be applied because a theoretical expression is not available for C_v near T_c . Braun and Kohlhaas⁸ state that ". . . the approximate formula of Nernst and Lindemann yields no reasonable results for ferromagnetic metals." Undoubtedly this rash statement was prompted by the abnormally high values of C_d obtained from Equation (20) because of the large values of C_p near T_c . To test the validity of this statement reconsider the thermodynamic expression for C_d in Equation (14). Expansion data of Nix and MacNair⁹ predict a value of α_L for magnetic nickel which is 20% higher than nonmagnetic nickel at T_c . Consequently, α^2 should be 44% higher. Since the Curie transformation is second-order, Equations (4), (5), and (7), page 4, predict that V should be continuous and χ and α_L discontinuous at T_c . The specific volume V is directly related to α_L and thus should experience an increase near T_c . Therefore, if χ has a maximum near T_c , it will

tend to counteract the maximum in α_l . If on the other hand, χ has a minimum at T_c , the dilation contribution would have a large maximum as predicted by the Nernst-Lindemann as well as the Grüneisen approximations. Unfortunately, reliable values of χ are not available for most high temperature ferromagnets such as nickel and iron, the materials of interest in this work.

These difficulties near the Curie transformation have led some investigators to ignore the dilation due to magnetic transformation and to obtain C_{pm} instead of C_{vm} , as shown in Equation (13). For example Tauer and Weiss¹⁰ state that the expression

$$C_d = AC_{vh}T \quad (23)$$

is adequate to account for the lattice dilation of a number of magnetic materials, where A had the constant value 1.0×10^{-4} per degree.

Kaufman, Clougherty, and Weiss¹¹ used this expression in their investigation of the lattice stability of iron and similar expressions have been used by a number of different investigators in analysis of the specific heat capacity of ferromagnets.

Harmonic Vibrational Contribution C_{vh}

In 1907, Einstein¹² proposed the first relatively successful theory for the harmonic vibrational contribution C_{vh} to the specific heat capacity of solids. He assumed that all atoms of a solid vibrate harmonically with the same characteristic frequency ν_e and that their energy is quantized and given by the expression

$$U = \frac{h\nu_e}{\exp(h\nu_e/kT) - 1} \quad , \quad (24)$$

where h and k are Planck's and Boltzmann's constants. For an isotropic three-dimensional lattice consisting of one mole of atoms,

Einstein's expression for C_{vh} is¹³

$$C_{vh} = \left(\frac{dU}{dT} \right)_V = 3R \left[\frac{\exp(h\nu_e/kT)}{\{\exp(h\nu_e/kT) - 1\}^2} \left(\frac{h\nu_e}{kT} \right)^2 \right], \quad (25)$$

where R is the universal gas constant. As T becomes large the term in brackets in Equation (25) approaches one, yielding the Dulong and Petit value of $3R$ for C_{vh} at high temperatures. However, as T approaches zero Einstein's theory predicts a C_{vh} which approaches zero too rapidly. This inadequacy is due to the assumption that all atoms vibrate at the same frequency. Nernst and Lindemann³ improved Einstein's theory at low temperature by modifying it to include two frequencies, $\nu_e/2$ and ν_e , which were assumed to be equally distributed among the atoms.

To put this theory on firmer theoretical ground, Debye¹⁴ replaced the single Einstein frequency and the empirically assumed dual frequencies of Nernst and Lindemann with a spectrum of frequencies. The vibrational spectrum Debye chose was the parabolic one of an isotropic elastic continuum because the more realistic spectrum which is obtained when each atom is allowed to vibrate independently necessitated detailed assumptions concerning the coupling between atoms in the solid. However, the frequencies of an elastic continuum range from zero to infinity, whereas in a solid frequencies which correspond to wavelengths shorter than an interatomic distance are not realistic. Hence it was necessary for Debye to introduce an upper limit to the spectrum. He accomplished this by showing that the

number of normal modes $g(\nu)d\nu$ whose frequencies range from ν to $\nu + d\nu$ is¹³

$$g(\nu)d\nu = BV\nu^2d\nu, \quad (26)$$

where B is a function of the longitudinal and transverse wave velocities in the continuum. Then he assumed that above a characteristic frequency ν_d the density of modes $g(\nu)$ falls abruptly to zero. Since each atom has at most three degrees of freedom, there can be only $3N_a$ normal modes of vibration per mole of solid, where N_a is Avogadro's number. Thus, integration over all the allowed modes of Equation (26) yields

$$3N_a = \int_0^{\nu_d} g(\nu)d\nu = \int_0^{\nu_d} BV\nu^2d\nu = \frac{BV}{3} \nu_d^3. \quad (27)$$

Eliminating B by combining Equations (26) and (27), Debye found that

$$g(\nu)d\nu = \frac{9N_a \nu^2}{\nu_d^3} d\nu. \quad (28)$$

Based on Einstein's quantization assumption and Equation (24), the energy of a mole of such oscillators is

$$U = \int_0^{\nu_d} \frac{g(\nu)h\nu d\nu}{\exp(h\nu/kT) - 1} = \frac{9N_a h}{\nu_d^3} \int_0^{\nu_d} \frac{\nu^3 d\nu}{\exp(h\nu/kT) - 1}. \quad (29)$$

Differentiation of this expression with respect to T yields Debye's expression for the contribution of the harmonic vibration of the normal modes of the atoms of a solid to the specific heat capacity, namely

$$C_{vh} = \left(\frac{\partial U}{\partial T} \right)_V = \frac{9N_a h^2}{\nu_d^3 k T^2} \int_0^{\nu_d} \frac{\nu^4 \exp(h\nu/kT)}{\{\exp(h\nu/kT) - 1\}^2} d\nu. \quad (30)$$

The more familiar form of Debye's law is obtained using the parameter

$$X = h\nu/kT \quad (31)$$

and the Debye characteristic temperature

$$\theta_d = h\nu_d/k \quad (32)$$

in Equation (30), yielding

$$C_{vh} = 9R \frac{T^3}{\theta_d^3} \int_0^{\theta_d/T} \frac{X^4 \exp(X)}{\{\exp(X) - 1\}^2} dX \quad (33)$$

At low temperatures Equation (33) reduces to the famous "Debye T^3 Law"

$$C_{vh} = \frac{12 R \pi^5}{5} \left(\frac{T^3}{\theta_d^3} \right) = \beta T^3, \quad (34)$$

where β is $(124.83/\theta_d)^3$ when C_{vh} is in millijoules/gram-atom degree. At high temperatures a power series expansion of Equation (33) yields⁴

$$C_{vh} = 3R \left(1 - \frac{X_d^2}{20} + \frac{X_d^4}{560} - \frac{X_d^6}{18144} + \dots \right), \quad (35)$$

and becomes the Dulong and Petit value at very high temperatures.

Normally the integral and coefficient $3(T/\theta_d)^3$ of Equation (33) are called the Debye function, and the value of this function

$$\frac{C_{vh}}{3R} = F_d(T/\theta_d) = 3 \left(\frac{T}{\theta_d} \right)^3 \int_0^{\theta_d/T} \frac{X^4 \exp(X) dX}{\{\exp(X) - 1\}^2} \quad (36)$$

is tabulated to six place accuracy in Reference 15.

Regarding the validity of Debye's theory, Blackman⁴ states "Most, if not all, of the difficulties which have arisen in the comparison of Debye theory and experiment disappear when once it is conceded that the properties of the crystal, as distinct from those of the continuum, should be used. The vibrational spectra of crystals show such marked

differences from a Debye spectrum, that it is not surprising that deviations from Debye theory are found. On the contrary, what is surprising is that the Debye theory should be such a good approximation."

In detail, Blackman finds two major discrepancies with the Debye theory. The first, and less serious, concerns the inability to represent the whole of the results using one Debye characteristic temperature. For example, Figure 1(a) is a reproduction of a figure from Clement's¹⁶ work in which his specific heat capacity measurements on indium were used to derive the temperature dependence of θ_d . Similar results are given by Blackman for a number of different solids, and the general trend is toward a constant value of θ_d at temperatures of about the Debye temperature and above.

The second and major discrepancy between Debye's theory and experiment which Blackman points out is the difference in θ_d values calculated from specific heat capacities at low temperatures and those values calculated from low-temperature elastic measurements. Almost without exception the specific heat capacity Debye temperatures are lower. (Since Blackman published his fine review of Debye's theory in 1955, better agreement has been obtained between C_p and elastic property measurements of θ_d by considering additional contributions, such as spin-waves, when analyzing the low-temperature C_p data for θ_d .) Both of these discrepancies are qualitatively explained by the various modifications of the Born-Von Karman theory.

In order to obtain a more realistic frequency spectrum than the parabolic one of Debye, Equation (28), Born and Von Karman¹⁷ visualized the

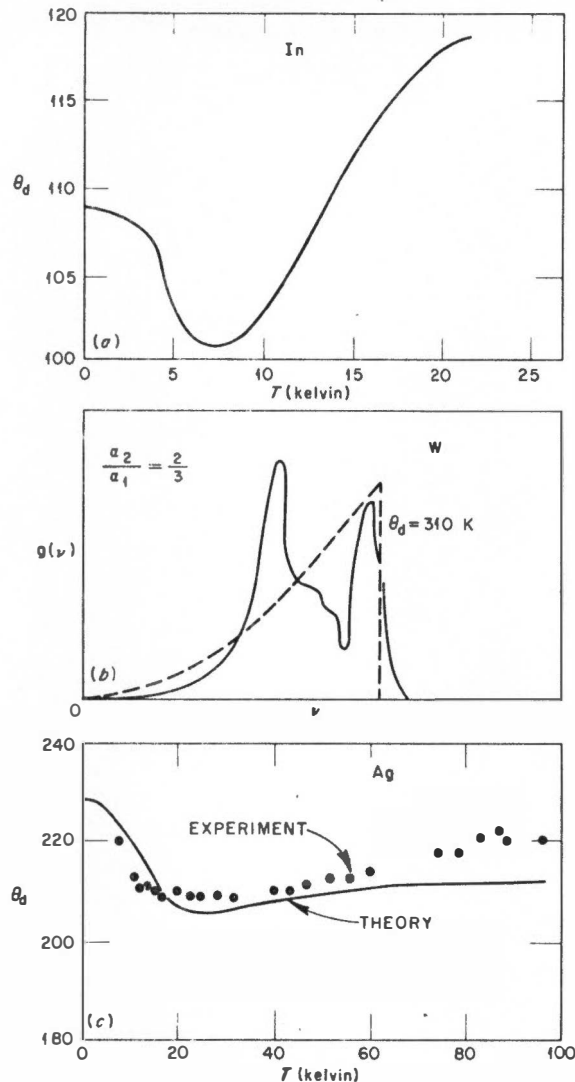


Figure 1. Discrepancies in the Debye Theory as Explained by the Born-Von Karman Theory. (a) Measured Debye temperature θ_d versus temperature T for indium. (b) Frequency spectrum $g(\nu)$ for tungsten from application of the Born-Von Karman theory to bcc lattice. The Debye spectrum for $\theta_d = 310$ K is that of broken line. (c) θ_d versus T comparing results of the Born-Von Karman theory with experiment for silver (fcc). Note the qualitative similarities between (a) and (c).

Source: (a) Clement, J. R., "Atomic Heat of Indium Below 20°K," Physical Review, 92: 258-267, October 1953. (b) Fine, P. C., "The Normal Modes of Vibration of a Body-Centered Cubic Lattice," Physical Review, 56: 355-359, August 1939. (c) Leighton, R. B., "The Vibrational Spectrum and Specific Heat of a Face-Centered Cubic Crystal," Reviews of Modern Physics, 20: 165-174, January 1948.

atoms of a solid to be bound together by elastic forces which could be treated as though created by springs. This theory has been applied to the body-centered cubic (bcc) lattice by Fine¹⁸ and to the face-centered cubic (fcc) lattice by Leighton.¹⁹ Their models assume central force interactions only between nearest and next-nearest neighbors, which they describe by the force constants α_1 and α_2 , respectively. Figure 1(b) shows the frequency spectrum for bcc tungsten according to Fine for α_2/α_1 equal to two-thirds. Also depicted is the Debye spectrum for θ_d equal to 310 K, the low-temperature specific heat capacity value. Note that the spectrum is below the Debye curve near the origin so that the specific heat capacity near the absolute zero of temperature is lower than that of the Debye model for θ_d equal 310 K. Hence the effective θ_d must be greater than 310 K, which accounts for the second of Blackman's discrepancies.

As the temperature is raised and higher frequencies are excited, the frequencies near the first peak of Figure 1(b) are activated, followed by those of the valley, then by those of the next peak. Thus, the resulting functional form of θ_d versus T should decrease initially, pass through a minimum, and then rise again with increasing temperature. Figure 1(c) shows the θ_d versus T plot for fcc silver derived by Leighton¹⁹ from a frequency spectrum similar to that of Figure 1(b). Comparing Figure 1(a) and Figure 1(c), it is seen that this theory explains, at least qualitatively, the first discrepancy noted by Blackman.

Of course, the Born-Von Karman theory, which is quite cumbersome to use, is only a highly sophisticated approximation to the spectrum of a

solid. Its reliance on elastic constant data to determine α_1 and α_2 precludes its use at high temperatures at the present time. In the final analysis, what really is needed is an experimental determination of the vibrational spectrum of the atoms of a solid as a function of temperature. Such determinations can be made in principle by x-ray and neutron diffraction and scattering techniques, but due to many experimental complexities, this has not been done for iron and nickel at high temperatures.

The lack of a completely satisfactory theory at all temperatures for the harmonic vibration contribution C_{vh} to the specific heat capacity seriously limits the quantitative interpretation of specific heat capacity data. This is true because for most solids C_{vh} is the dominant contribution from 10 K to the melting point.

Anharmonic Vibrational Contribution C_{va}

The Taylor series expansion of the potential energy $V(x)$ of a one-dimensional oscillator about its equilibrium position is

$$V(x) = V_0 + \left(\frac{\partial V}{\partial x} \right)_0 x + \frac{1}{2!} \left(\frac{\partial^2 V}{\partial x^2} \right)_0 x^2 + \frac{1}{3!} \left(\frac{\partial^3 V}{\partial x^3} \right)_0 x^3 + \frac{1}{4!} \left(\frac{\partial^4 V}{\partial x^4} \right)_0 x^4 + \dots, \quad (37)$$

where all the partial derivatives with respect to position x are evaluated at the equilibrium position (that is, x equal to zero). Since the force $\left(\frac{\partial V}{\partial x} \right)_0$ on the oscillator must be zero at the equilibrium position and since V_0 can be chosen arbitrarily to be zero, the first two terms in Equation (37) vanish. The third term is the harmonic contribution, and

the subsequent terms are usually called the anharmonic contributions to the potential energy.

For a crystal, each oscillator, or atom, has three degrees of freedom. By Equation (37), each of the three normal modes that result have potential energies of the form

$$V(x) = ax^2 + bx^3 + cx^4 + \dots, \quad (38)$$

where 'a, b, and c are constants. Below about $\theta_d/3$, the oscillations of the atoms are small enough to be represented adequately by the first term in Equation (38). This term was considered above in detail. At temperatures above $\theta_d/3$, the oscillations of the atoms increase in magnitude, requiring more terms of the Taylor expansion to express the potential energy accurately.²⁰ Exactly what contribution these anharmonic oscillations make to the specific heat capacity is subject to question. Indeed, even the sign of this contribution is not agreed upon as shown in the following two treatments.

Foreman²¹ has evaluated the specific heat capacity arising from the anharmonic terms on the basis of the elastic continuum approximation. For iron, Foreman derives the expression

$$C_{va} = 1.41 \times 10^{-4} RT, \quad (39)$$

where R is the universal gas constant. He also quotes results of several other theories which yield similar results, except for the value of the coefficient in Equation (39). For example, the linear chain — a one dimensional Born-Von Karman approach — yields a constant of 3×10^{-4} . A bcc lattice model based on the Born-Von Karman approach and similar to that of Fine¹⁸ for the harmonic oscillator gives the coefficient as 1.11×10^{-4} .

Thus these models for C_{va} give a positive contribution proportional to T . For iron, this contribution is about five percent of C_v at 1000 K.

Keller and Wallace²² investigated the anharmonic specific heat capacity for bcc and fcc crystals with one atom per unit cell using central Lenard-Jones forces. In their treatment, they considered nearest and next-nearest neighbor interactions as well as an approximation for dispersion, which was not done by Foreman. Keller and Wallace state that the cubic and quartic terms of Equation (38) contribute to C_{va} with opposite sign, with the negative quartic term dominating. Their expression for the anharmonic term is

$$C_{va} = -A(kT/ma^2w_0^2) , \quad (40)$$

where m is the mass of the atom and a the lattice parameter of the crystal. The constant A has the value of 4289 joules/gram-atom degree for fcc crystals and 2155 joules/gram-atom degree for bcc crystals. Keller and Wallace relate the frequency w_0 to the Debye temperature by the expression

$$\hbar w_0 = (2/\pi)k\theta_d , \quad (41)$$

where \hbar is Planck's constant over 2π . Using a literature value for θ_d , w_0 is found to be 4.22×10^{13} vibrations per second for iron, yielding a C_{va} of iron of

$$C_{va} = -2.57 \times 10^{-4} RT . \quad (42)$$

This expression of Keller and Wallace is of the same magnitude as that of Foreman but of opposite sign. Thus, these theories predict that C_{va}

is directly proportional to the temperature, that C_{va} contributes about five percent to C_v at 1000 K for iron, but the theories differ as to whether the contribution is positive or negative.

Electronic Contribution C_{ve}

The electronic contribution C_{ve} to the specific heat capacity of a solid is due to the change in the energy distribution of the electrons with temperature. The total internal energy of the electrons per unit volume is given by²³

$$U = 2 \int_0^{\infty} N(E)f(E)EdE = 2 \int_0^{\infty} \frac{N(E)EdE}{\exp\{(E - \zeta)/kT\} + 1}, \quad (43)$$

where $N(E)dE$ is the number of electronic states per unit volume having energies between E and $E + dE$. In this equation, the quantity ζ is the thermodynamic potential per electron and is thus a function of temperature. As in the quite analogous expression for the internal energy of the harmonic oscillators [Equation (29), page 14], the main task in calculating U and thus C_{ve} is to determine the distribution $N(E)$ for the electrons. Again in analogy to the determination of $g(\nu)$ for the oscillators, various approximations for $N(E)$ are made to render Equation (43) amenable to solution.

Perhaps the most often quoted approximation is to assume that $N(E)$ has the parabolic form of free electrons as shown in Figure 2(a). This approximation is quite sufficient for some metals, such as the alkali metals,²⁴ and leads to the expression²⁵

$$C_{ve} = \left\{ \frac{\pi^2}{2} \frac{nk}{T_0} \right\} T \left\{ 1 - \frac{3\pi^2}{10} \left(\frac{T}{T_0} \right)^2 \right\} = \gamma T \left\{ 1 - \frac{3\pi^2}{10} \left(\frac{T}{T_0} \right)^2 \right\}, \quad (44)$$

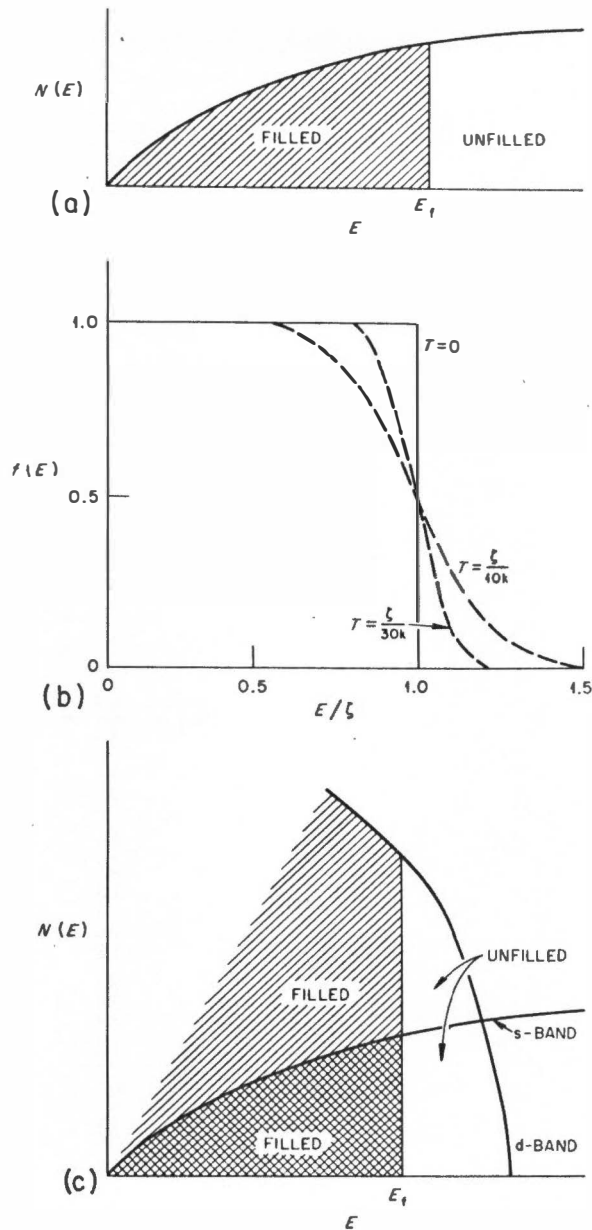


Figure 2. Energy Distributions of Electrons in a Metal. (a) Total number of electrons per unit volume $N(E)$ as function of energy E for free electrons or parabolic band in metal. (b) Fermi-Dirac distribution function $f(E)$ for three different temperatures as function of E/ζ , the ratio of energy to thermodynamic potential. (c) $N(E)$ versus E for idealized form of overlapping s- and d-bands in transition metal such as nickel. E_f is the Fermi energy.

Source: (c) Stoner, E. C., "The Magnetic Susceptibility and Electronic Specific Heat of Transition Metals in Relation to their Electronic Structure," Acta Metallurgica, 2: 259-273, 1954.

which is valid at low temperatures or temperatures above the Curie temperature. In Equation (44), the quantity n is the effective number of electrons or holes, and T_0 is the degeneracy or Fermi temperature of the electron gas and is related to the Fermi energy E_f by

$$T_0 = E_f/k , \quad (45)$$

where k is Boltzmann's constant. The Fermi energy is the maximum energy of any electron in the solid at absolute zero.

Before considering other approximations, it is important to point out that only those electrons having energies near ζ contribute to C_{ve} . This can be seen by considering the Fermi-Dirac distribution function $f(E)$ of Equation (43), namely

$$f(E) = \frac{1}{\exp\{(E - \zeta)/kT\} + 1} . \quad (46)$$

As shown in Figure 2(b), when T is increased only those states having energies immediately below ζ decrease in probability of occupancy while the few above ζ increase in probability of occupancy. This concept is important in understanding the abnormally high C_{ve} of transition metals.

For transition metals such as nickel and iron, the simple parabolic distribution of Figure 2(a) must be discarded²⁶ for one similar to that of Figure 2(c). This configuration arises because the d- and s-bands of transition metals are not filled. Since electrons at the top of these bands have energies near ζ , electrons of both bands contribute to C_{ve} . As is noted by Seitz²⁷ and depicted in Figure 2(c), the density of states of the d-band electrons is much larger than that of the s-band or that of the free electron distribution. Consequently, a larger number of electrons

are excited when the temperature of a transition metal is raised and results in the abnormally large value of C_{ve} for these metals.

Stoner²⁶ points out that the distribution of the electrons at the top of the d-band is somewhat parabolic for nickel and other transition metals. Consequently, Equation (44) may be approximately correct for these metals. On the other hand, Mott²⁴ states that a distribution such as that of Figure 2(c) is a gross oversimplification of the true distribution in a transition metal. In particular, Mott finds that hybridization of the bands will normally occur when they overlap, adding to the complexity of finding $N(E)$. Such complexities are outside the scope of this work. However, Shimizu, Takahashi, and Katsuki²⁸ have attempted to circumvent these difficulties by experimental means. Their method consists of determining the electronic state density from low-temperature specific heat data and from these data calculate the temperature variation of C_{ve} at high temperatures. At low temperatures, Equation (44) becomes

$$C_{ve} = \gamma T, \quad (47)$$

where γ is a constant and is thus the temperature coefficient of C_{ve} .

Shimizu, Takahashi, and Katsuki found that at high temperatures the γ obtained from low-temperature data was too high for some transition metals and too low for others. That is, if C_{ve} is written for all temperatures as

$$C_{ve} = \gamma^* T, \quad (48)$$

they found that $d\gamma^*/dT$ is positive for some and negative for other transition metals. In particular, $d\gamma^*/dT$ for iron is positive and for nickel is negative. Note that a negative $d\gamma^*/dT$ is predicted by

Equation (44). Such a treatment suggests that C_{ve} should be given by

$$C_{ve} = \gamma_0 T \{1 + F(T)\} , \quad (49)$$

where γ_0 is the low-temperature γ . The quantity $F(T)$ is a positive or negative function of temperature. For a nondegenerate gas, $F(T)$ is proportional to T^2 . Of course, $F(T)$ for free electrons or metals having parabolic bands is

$$F(T) = -\frac{3\pi^2}{10} \left(\frac{T}{T_0} \right)^2 . \quad (50)$$

Thus, the simple γT relation for C_{ve} given in Equation (47) is not applicable to transition metals at high temperatures.

The validity of the arguments of Shimizu, Takahashi, and Katsuki has been proven by Miller and Brockhouse²⁹ for the case of palladium. The former authors predicted that $d\gamma^*/dT$ should be negative for palladium. Using triple-axis spectrometers to measure the frequency-wave-vector dispersion relation for the lattice of palladium, Miller and Brockhouse were able to calculate C_{vh} and C_{va} and thus deduce C_{ve} from experimental measurements of C_p . They found that at 800 K the experimental value of C_{ve} was a factor of four below that predicted by Equation (47) using the low-temperature γ .

Magnetic Contribution C_{vm}

Different electronic configurations within solids produce several distinguishable forms of magnetism. Classically speaking, the electrons of a solid are envisioned as orbiting about their parent atoms and hence possess orbital angular momentum. When the atoms are placed in an external magnetic field, an interaction occurs between the electrons and the field, inducing a magnetic moment upon the atoms. This phenomenon

is called diamagnetism. Since all matter contains electrons moving in orbits, diamagnetism occurs to some extent in all substances. All other forms of magnetism arise because of permanent moments resulting from the intrinsic spin of the electrons. These moments are present in the absence of an external field. In paramagnetic substances, the spin moments of the different atoms are not coupled strongly whereas in ferromagnetic materials the moments are aligned parallel and in antiferromagnets they are antiparallel.

The form of magnetism to be considered herein is ferromagnetism. For the ferromagnets iron, nickel, and cobalt, the 3-d and 4-s bands are not filled as seen in Figure 2(c), page 23. In the rare earths, the 4-f and 5-s bands are not filled. Since the electrons in a filled band compensate each others' spin, there must be more electrons of one spin direction than the other in the unfilled bands. Such an electronic distribution is suggested in Figure 3 for the 3-d band of iron.³⁰

Two schools of thought on ferromagnetism in solids are currently in vogue. One, expounded originally by Heisenberg,³¹ assumes the unpaired spins to be localized at the atom and is more reasonably applied to the rare earth metals. The other school associates the unpaired spins with the solid as a whole as sort of an electron gas. This is the itinerant or collective electron theory and is more applicable to ferromagnets such as iron, nickel, and cobalt. Both theories revolve about the energy change upon parallel alignment of the spins. If this alignment lowers the total energy, ferromagnetism results. This coupling of the electron spins is often termed the "exchange interaction" and bears no

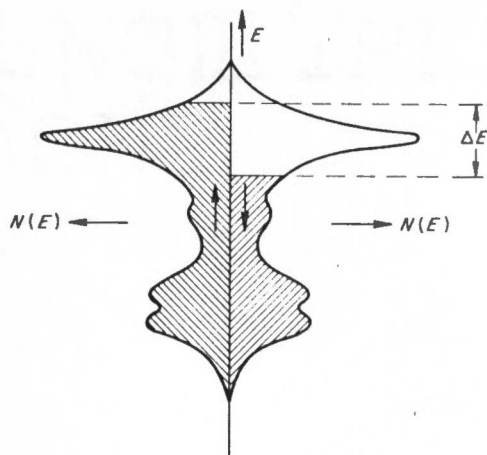


Figure 3. Possible Energy Distribution of Electrons in 3-d Band of Iron. Density of electron states $N(E)$ is plotted as a function of energy for spinup and spindown. The spinup electrons have spins parallel to atom to which they belonged at that instant. Energies connected with the magnetic moment are not presented.

Source: Gersdorf, R., "Ferromagnetic Properties of Fe and Ni in Relation to Their Band Structure," Journal de Physique et le Radium, 23: 726-729, October 1962.

classical analogue. The interested reader is referred to Mott's²⁴ review for further discussion of this point.

Localized Electron Models. At zero kelvin, the third law of thermodynamics requires zero entropy (that is, complete order of the electron spins). As the temperature is raised slightly, enough thermal energy is available to reverse one electron spin. Due to the exchange interaction, this reversed spin will propagate through the lattice. This phenomenon is termed a spin-wave or magnon. The generation of spin-waves requires energy, and the resultant contribution to the specific heat at low temperatures is given by^{32,33}

$$C_{vm} = \alpha_m T^{3/2} (1 - 0.39 T_g/T + 0.04 T_g^2/T^2) \approx \alpha_m T^{3/2}, \quad (51)$$

where T_g is the energy gap temperature. The quantity α_m is a constant given by^{32,33}

$$\alpha_m = 0.113 \xi N_a \left\{ \frac{k}{2JS} \right\}^{3/2}, \quad (52)$$

where ξ is a geometric factor equal to one-half for bcc and one-fourth for fcc crystals. The term $2JS$ is a measure of the exchange interaction between neighboring spins, and its value may be deduced from spin-wave resonance, magnetization, and neutron scattering experiments.³³

Equation (51) for C_{vm} is applicable only at temperatures near the boiling point of helium and has been used with limited success to interpret C_p data of iron, nickel, and cobalt by Dixon, Hoare, Holden, and Moody³³ and of nickel-based iron and copper alloys by Dixon, Hoare, and Holden.³⁴ The major difficulty in testing the validity of this expression is that C_{vm} is less than three percent of C_v for these metals between one and four kelvin, the temperature span of most low-temperature calorimeters.

In the derivation of the spin-wave and most of the other localized electron models, the Hamiltonian, commonly called the Heisenberg exchange Hamiltonian, that is applicable has the general form³⁵

$$H = -2J_e \sum'_{ij} \underline{S}_i \cdot \underline{S}_j, \quad (53)$$

where J_e is the isotropic exchange integral. The quantity \underline{S}_i is the total spin of the electrons of the i th atom, and the quantity \underline{S}_j is the total spin of the electrons of the j nearest neighbors of the i th atom. The summation of Equation (53) is over all atoms i of the crystal and for all j of their nearest neighbors. The prime on the summation implies i not equal j .

Few attempts have been made to use this general form for H but rather various simplifications have been developed. Probably the most widely used approximation is that of Ising,³⁶ who assumed that the instantaneous values of the neighboring spins may be replaced by their time averages

\bar{S}_j . For z nearest neighbors, the Ising model Hamiltonian is³⁵

$$H_I = -2zJ_e \bar{S}_j \sum_i S_i . \quad (54)$$

Such a Hamiltonian is equivalent to assigning a spin coordinate, either $+1$ or -1 , to each atom of the crystal.³⁷ Hence, ferromagnetism in the Ising model is a cooperative phenomenon because it results when adjacent atoms have the same spin coordinate.

As for most other cooperative theory, the Ising model has been solved in closed form for one- and two-dimensional lattices³⁸ but not for three-dimensional lattices. In his excellent review of cooperative phenomena, Domb³⁹ states that the majority of the work done on the Ising model has been concerned with predictions of the temperature of the Curie transformation and of magnetic properties rather than thermodynamic properties. However, the existing models do demonstrate logarithmic singularities in C_{vm} at T_c and exponential decreases of C_{vm} near absolute zero.

The analytic expressions for C_{vm} obtained with the Ising model are quite complex and, although in closed form, are very difficult to manipulate. For example, the expression for C_{vm} obtained by Newell and Montroll³⁷ for a two-dimensional square lattice is

$$C_{vm} = \frac{\partial}{\partial T} \left[-J_e \coth \left\{ 2K \left[1 + \frac{2}{\pi} (2 \tanh^2 2K - 1) K_1(k_1) \right] \right\} \right]_V , \quad (55)$$

where

$$K = J_e (kT)^{-1} , \quad (56)$$

$$k_1 = \sinh(2K) \cosh^{-2}(2K) , \quad (57)$$

$$K_1(k_1) = \int_0^{\pi/2} (1 - k_1^2 \sin^2 \varphi)^{-\frac{1}{2}} d\varphi . \quad (58)$$

Another simplification of Equation (53) is the constant coupling approximation of Kasteleijn and Van Kranendonk⁴⁰ in which an effective Hamiltonian for a pair of nearest neighbor atoms with a net spin of one-half is derived. The coupling between these two spins is Heisenberg type, $\underline{S}_i \cdot \underline{S}_j$, and the coupling constant is assumed to be J_e and invariant. Coupling of the spins of the i th and j th atoms with other atoms is represented by the effective field which all atoms produce at the i th and j th atoms. This effect is incorporated in the theory by an additional term in the Hamiltonian. Wagner⁴¹ extended the constant coupling method to higher half-integral spins. As in the case of the Ising models, Wagner's constant coupling expressions for C_{vm} are very complex and are not included herein. However, Ballensiefen and Wagner⁴² used a computer to solve these expressions for several special cases, and their results for iron and nickel are presented in Figure 4. Note that for both iron and nickel, the theoretical value of C_{vm} is too high at temperatures below T_c and is too low near and above T_c . The latter discrepancy is normally attributed to second-nearest neighbor interactions which were not considered in detail in this approximation. Smart⁴³ and Weiss⁴⁴ have developed theories which take better account of these short-range forces.

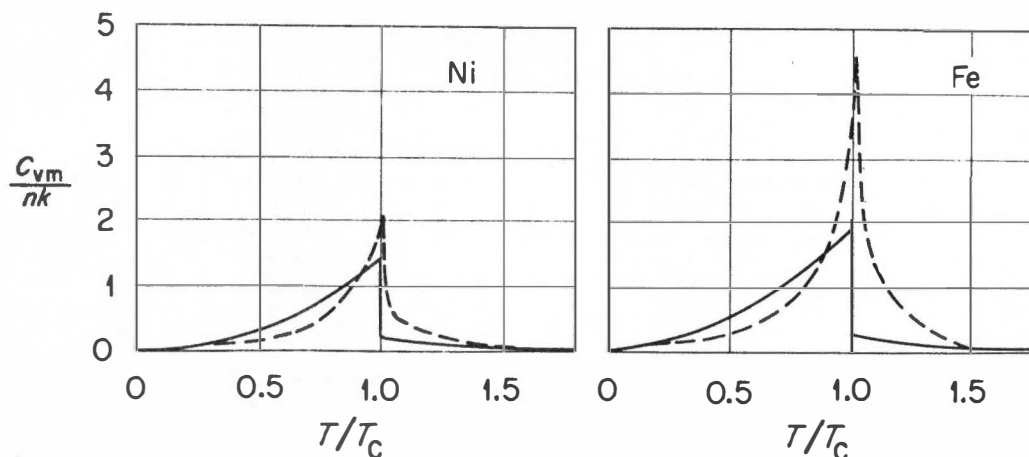


Figure 4. Magnetic Specific Heat According to the Constant Coupling Approximation. Ratio of C_{vm} to nk versus reduced temperature for iron and nickel showing the calculated values as solid line and experimental values as dashed line. The quantity n is the effective number of magnetic atoms per mole and k is Boltzmann's constant.

Source: Ballensiefen, G. and D. Wagner, "Specific Heat In Constant-Coupling Approximation," Physica, 30: 1543-1544, 1964.

The results of Smart are applicable only above T_c and consider the second-nearest neighbor interactions directly by means of a modified constant coupling approximation. To the author's knowledge, no numerical calculations have been made for iron or nickel using the extremely complex expression for C_{vm} derived by Smart.

Weiss's treatment is a modification of the Bethe-Peierls short-range configurational order theory and considers clusters of atoms consisting of a central atom and its z nearest neighbors. The interaction of the neighbor atoms with each other is computed by an Ising-type model. In order to incorporate the short-range forces, the interactions of the atoms outside the cluster are represented by an effective field which acts on the z nearest neighbors of the central atom. Since this method

is principally concerned with local order within a cluster, it neglects the long-range and spin-wave effects that are important at low temperatures.³⁵ This theory is thus applicable only near T_c as discussed later.

There exist several other localized electron models, such as the series expansion method, as well as many modifications of the above theories which will not be considered.

Itinerant Electron Models. Regarding the itinerant electron theories Mattis⁴⁵ states, "Outstanding problems still to be resolved include the thermodynamics of magnetism in the band theory, particularly near and above the Curie temperature." To this author's knowledge, no band theory calculations of C_{vm} exist for iron and nickel over the temperature interval of interest to this work. This is indeed unfortunate because only the itinerant models of ferromagnetism should be strictly applicable to these metals.

Stoner,²⁵ however, has derived an expression for C_{vm} based on a parabolic or free electron density of states for the electrons. In the limit that the ratio of T_c to the degeneracy temperature T_0 approaches zero, Stoner's relation for C_{vm} [that is, the electronic specific heat capacity in excess of that of Equation (44), page 22] is

$$C_{vm} = \frac{\pi^2}{4} \gamma \left(\frac{T}{T_0} \right)^3, \quad (59)$$

where γ is the temperature coefficient of C_{ve} . For iron and nickel the ratio T_c/T_0 is less than 0.1, therefore Equation (59) should be applicable to these metals. The major criticism of this theory is that it predicts

that C_{vm} vanishes above the Curie transformation, which is contradictory to experimental evidence.

In his paper, Stoner points out that his expression for C_{vm} approaches that of the classical molecular field theory as T_O/T_C approaches zero. For a spin per atom J , the molecular field theory value of C_{vm} is³⁵

$$C_{vm} = - \frac{3Jnk}{2(J+1)} \frac{d[M(T)/M(0)]^2}{d(T/T_C)}, \quad (60)$$

where $M(T)$ is the spontaneous magnetization at T . The value of the relative magnetization $M(T)/M(0)$ can be obtained experimentally.

Discontinuity in C_{vm} . Since the ferromagnetic to paramagnetic transformation is second-order, C_{vm} for ferromagnets should be discontinuous at T_C . The value of this discontinuity ΔC_{vm} is predicted by several of the theories presented above and is listed in Table I for each.

The one- and two-dimensional Ising models demonstrate logarithmic singularities in C_{vm} at T_C . Such a discontinuity is also predicted for the second order transformation of a two-phase liquid-vapor system to a homogeneous phase system, the critical transformation. From criticality theory, C_v in the vicinity of the critical temperature T_R is^{46,47}

$$C_v = a + b \log|T - T_R|, \quad (61)$$

where the slope b is the same for temperatures above and below T_R . The constant a is different for temperatures above and below T_R and is equal to C_v at T_R plus one degree and C_v at T_R minus one degree, respectively.

Landau and Lifshitz⁴⁸ consider the Curie transformation as a type of critical phenomenon, and hence several investigators have employed

TABLE I
THEORETICAL VALUES OF DISCONTINUITY IN C_{vm}

Theory	$\Delta C_{vm}/nk$	Structure	Spin	References*
Weiss (Bethe-Peierls)	2.05 3.40	bcc	1/2 1	44
Weiss (Ising)	1.71 1.63	bcc fcc	1/2 1/2	44
Constant coupling	1.10 1.76 2.05 1.29 1.88 2.13	bcc fcc	1/2 1 3/2 1/2 1 3/2	41
Free electron	$12.2 \left(\frac{T_c}{T_0} \right)^3$	Any	Any	25
Molecular field	1.5 2.0 2.21	Any	1/2 1 3/2	35

*See page 214.

Equation (61) in interpreting the heat capacity of ferromagnets. For example, Miedema, Wielinga, and Huiskamp⁴⁹ obtained excellent agreement for the exotic Heisenberg-ferromagnet $\text{CuK}_2\text{Cl}_4 \cdot 2\text{H}_2\text{O}$, whereas the results of Voronel, Garber, Simkina, and Charkina⁵⁰ on gadolinium do not appear to follow this relationship.

Kraftmakher plotted C_p versus $\log |T - T_c|$ for nickel⁵¹ and iron⁵² and found fair agreement with Equation (61) within about 150 K of T_c . Obviously C_{vm} , not C_p , should be the ordinate of this plot because the

other contributions to C_p of nickel and iron do not have a logarithmic temperature dependence.

Total Energy and Entropy of Magnetization. Lacking a completely reliable theory to predict the shape and magnitude of C_{vm} , many investigators have considered instead the total energy U_{vm} and entropy S_{vm} associated with the transition from complete magnetic order at zero kelvin to complete magnetic disorder at $T \gg T_c$. These quantities are obtained from experimentally determined values of C_{vm} by

$$U_{vm} = \int_0^{\infty} C_{vm} dT \quad (62)$$

and

$$S_{vm} = \int_0^{\infty} \frac{C_{vm}}{T} dT . \quad (63)$$

In the localized electron model, S_{vm} may be calculated from the expression for the entropy S of a distribution of objects, which is

$$S = k \ln W , \quad (64)$$

where W is the number of possible configurations of the system under a given condition of restraint. For a system of n "magnetic atoms" having spin J , the maximum number of configurations is the maximum number of ways of arranging these spins on the $2J + 1$ spin sublevels, namely $(2J + 1)^n$. Such an arrangement, called W_{∞} , is energetically possible at very high temperatures. Since at zero kelvin the entropy must be zero by the third law of thermodynamics, W must be one by Equation (64) and hence

$$S_{vm} = S_{\infty} - S_0 = k[\ln(2J + 1)^n - \ln(1)] = nk \ln(2J + 1) . \quad (65)$$

Considering only interactions of the z nearest neighbors, the energy U_{vm} for a system of localized spins having a Hamiltonian of the form of Equation (53), page 29, is

$$U_{vm} = nkT_c z J^2 (J_e/kT_c) . \quad (66)$$

The quantity (J_e/kT_c) is usually obtained in theoretical calculations of T_c in applications of the various models discussed above. Unfortunately, the value of (J_e/kT_c) cannot be expressed in closed form for most of these models but approximate expressions have been obtained and some are listed in Table II.

TABLE II
VALUE OF (J_e/kT_c) OF VARIOUS MODELS

Theory	(J_e/kT_c)	Structure	Spin	References*
Weiss (Bethe-Peierls)	0.344	bcc	1/2	44, 53
	0.115		1	
	0.0598		3/2	53
Ising (Kramers-Opechowski)	0.419	bcc	1/2	53
	0.128		1	
	0.0649		3/2	
	0.236	fcc	1/2	
	0.0785		1	
	0.0405		3/2	
Constant coupling	0.203	fcc	1/2	42
	0.115	bcc	1	

*See page 214.

Stoner²⁵ has evaluated the magnetic energy as a function of temperature based on a parabolic or free-electron density of states for the electrons. In the limit that the ratio of T_c to the degeneracy temperature T_0 approaches zero, Stoner's expression for U_{vm} is

$$U_{vm} = \frac{3}{4} \gamma \frac{T_c^2}{T_0} \left\{ 1 + \frac{23\pi^2}{240} \left(\frac{T_c}{T_0} \right)^2 + \dots \right\}, \quad (67)$$

where γ is the temperature coefficient of C_{ve} . Stoner has also evaluated U_{vm} for other values of T_c/T_0 but these expressions are not in closed form and are not included herein.

Contribution of Rearrangement of Atoms C_{vw}

As used in Equation (9), page 5, the term C_{vw} is a "catch-all" quantity that encompasses all contributions to C_v not heretofore discussed. Of principal concern to this work is that part of C_{vw} due to configurational order-disorder transformations in binary alloys. This type of transformation is normally assumed to occur by atomic diffusion and is therefore dependent on the vacancy concentration and the atomic mobility within the alloy.^{54,55} Since both the vacancy concentration and atomic mobility vary exponentially with temperature,⁵⁶ the kinetics of the order-disorder transformation are strongly temperature dependent.

If it is assumed that the order-disorder transformation occurs under equilibrium conditions, C_{vw} is

$$C_{vw} = \frac{d}{dT} [U_{od}(T)N(T)] = N(T) \frac{dU_{od}(T)}{dT} + U_{od}(T) \frac{dN(T)}{dT}, \quad (68)$$

where $U_{od}(T)$ is the energy of formation of one mole of ordered alloy at constant volume at T and $N(T)$ is the equilibrium mole fraction of ordered

atoms at T . To a first approximation, $U_{od}(T)$ is temperature independent and thus the first term of Equation (68) vanishes leaving

$$C_{vw} = U_{od} \frac{dN(T)}{dT} . \quad (69)$$

Values of U_{od} and $N(T)$ may be obtained from several theories, such as the Bragg-Williams approximation.^{57,58} Unfortunately, these theories as well as Equation (69) are applicable only at equilibrium. Due to the slow kinetics of the order-disorder transformation, especially at lower temperatures, and due to the finite heating rates necessary for most experimental methods, C_{vw} obtained from experiments is not an equilibrium value. Therefore, in general, Equation (69) and the various theories cannot be applied to interpret the experimental results.

As in the case of the magnetic transformation, the total energy U_{od} is the quantity normally calculated from experimental results. From Equation (68) and assuming U_{od} to be temperature independent, one finds

$$U_{od} = \left(\int_{T_i}^{T_f} C_{vw} dT \right) \left(N(T_f) - N(T_i) \right)^{-1} , \quad (70)$$

where T_f is the experimental temperature above which C_{vw} vanishes, and T_i is the experimental starting temperature. If perfect order exists at T_i , $N(T_i)$ is one. The value of $N(T_f)$, which corresponds to N of the random structure, is normally taken as zero. Under these conditions, Equation (70) becomes

$$U_{od} = - \int_{T_i}^{T_f} C_{vw} dT . \quad (71)$$

The Metals Ni and Fe and the Alloy Ni₃Fe

The solids of interest in this research are nickel, iron, and the alloy of composition 75 atomic percent Ni + 25 atomic percent Fe, called Ni₃Fe. The purpose of this section is to discuss the existing knowledge of the specific heat capacity of these solids in light of the previous sections of this chapter. In particular, the experimental and theoretical values of C_{vm} , U_{vm} , and S_{vm} are discussed, and the effect of the order-disorder transformation on these quantities is considered for the alloy.

Structure. The equilibrium phase diagram for the nickel-iron system given by Hansen⁵⁹ is shown in Figure 5. This diagram predicts that between 1715 and 871 K, the alloy Ni₃Fe is single phased, fcc, paramagnetic, and disordered in its equilibrium state. Between 871 and 773 K, Ni₃Fe has a structure which is single phased, fcc, ferromagnetic, and disordered. At 773 K, this alloy undergoes a first-order transformation to an ordered structure which is fcc and ferromagnetic.

Also from Figure 5, the pure metal nickel is seen to be fcc at all temperatures but is paramagnetic above and ferromagnetic below 627 K. Pure iron has a somewhat more complex structure. From its melting point, 1807 K, to 1663 K iron is bcc and paramagnetic, and this phase is called δ -iron. At 1663 K, δ -iron transforms to γ -iron, which is fcc and paramagnetic, and which in turn transforms to α -iron at 1183 K. The phase α -iron is bcc and is paramagnetic above and ferromagnetic below 1043 K.

Nickel. Probably the most complete review of the specific heat capacity measurements of pure metals is the recent compilations of Touloukian.⁶⁰ For nickel, Touloukian has listed and plotted the C_p

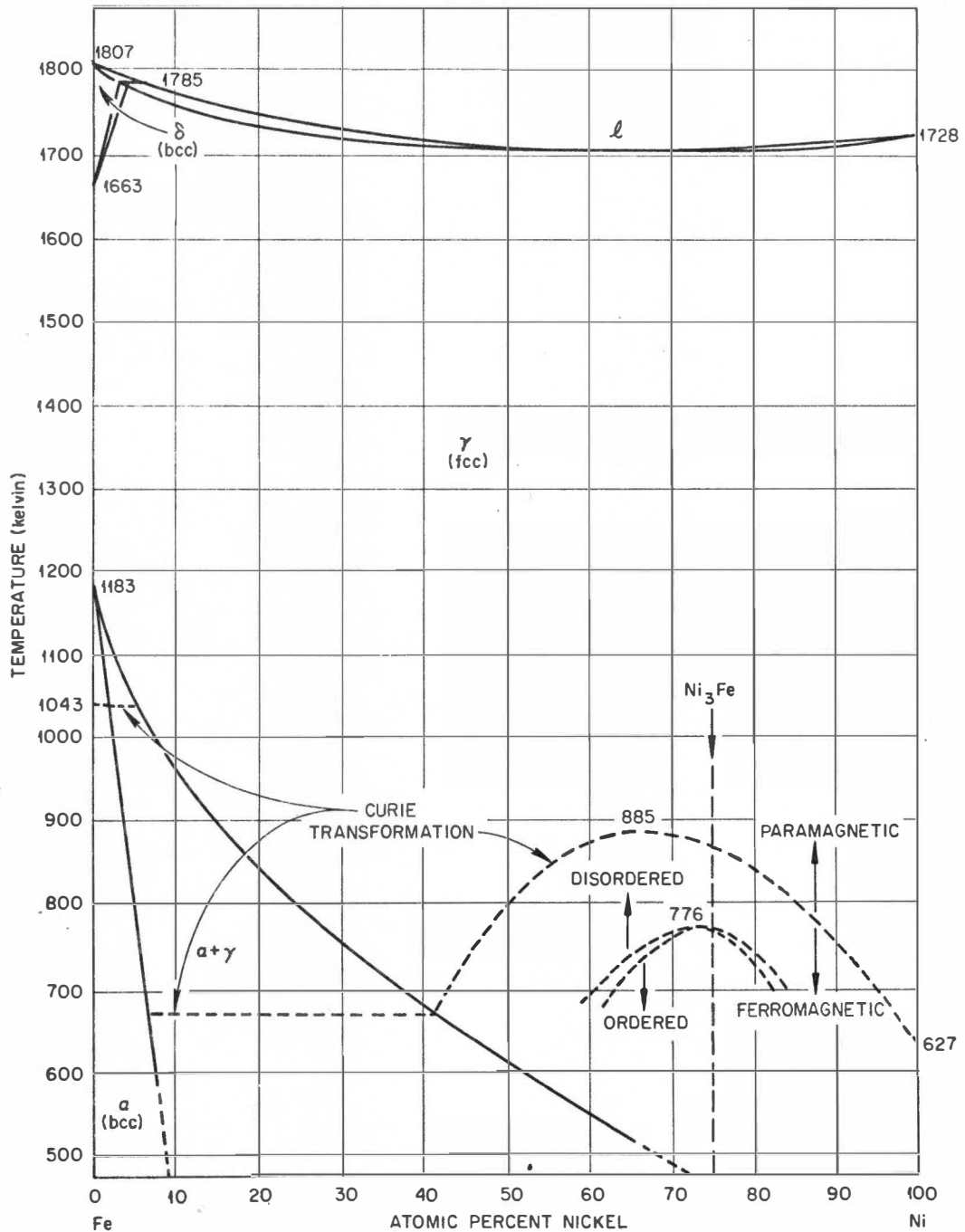


Figure 5. The Equilibrium Phase Diagram for the Nickel-Iron Alloy System.

Source: Hansen, M., Constitution of Binary Alloys. New York: McGraw-Hill, 1958.

results of twelve investigators whose data span the temperature interval 12 K to 1584 K. What is most striking about this plot is that below the Curie temperature T_c , the C_p 's agree to about $\pm 2\%$ but near and above T_c the values diverge radically. Since impurities are known to affect T_c , these deviations are often supposed due to specimen differences. While admitting to small impurity effects, it is the author's opinion that this lack of agreement in C_p near and above T_c is due mainly to experimental errors, such as in temperature measurements, in heat loss corrections, or in improper experimental procedures. This allegation is substantiated in Chapter III.

Because of the differences in the measured values of C_p , similar differences occur in the values of C_{vm} calculated from them. Another cause for the differences in the C_{vm} 's is the use of different theories and approximations when subtracting the other contributions from C_p ; that is, from Equation (12), page 8,

$$C_{vm} = C_p - C_{vh} - C_{va} - C_{ve} - C_{vw} - C_d . \quad (72)$$

If for example two investigators use the Debye theory for C_{vh} , Stoner's theory for C_{ve} , and Grüneisen's approximation for C_d but different values of θ_d , γ , and γ_g , their values for C_{vm} as a function of temperature will in general not agree.

At least seven open-literature publications^{8, 61-66} report values of C_{vm} of nickel calculated using a relationship of the form of Equation (72). In general these results do not agree, but their detailed comparison is deferred until Chapter III. However, Figure 6(a) depicts the results of Braun and Kohlhaas⁸ in which C_p , C_{vh} , C_{ve} , C_d , and C_{vm} of nickel are

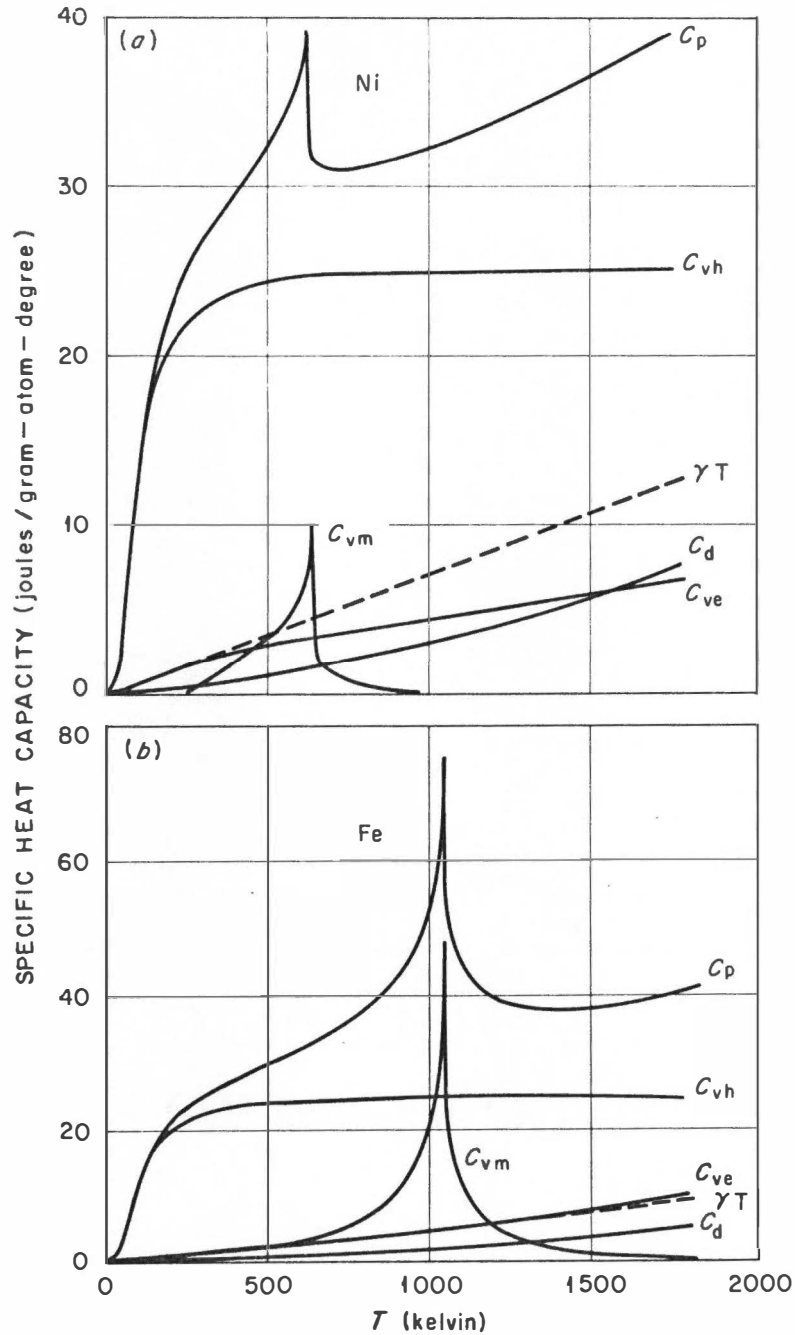


Figure 6. Harmonic Vibrational $C_{v,h}$, Electronic $C_{v,e}$, Dilation C_d , and Magnetic $C_{v,m}$ Contributions to the Specific Heat Capacity C_p as a Function of Temperature T . (a) Nickel and (b) iron.

Source: Braun, M. and R. Kohlhaas, "Die spezifische Wärme von Eisen, Kobalt, und Nickel im Bereich hoher Temperaturen," Physica Status Solidi, 12: 429-444, 1965.

shown as a function of temperature. Also, the values of U_{vm} and S_{vm} of some of these investigators as well as those of several theories are given in Table III for nickel. This table offers a quick summary of the discrepancies in values of C_{vm} of nickel as well as the differences between theory and experiment.

To the author's knowledge, no measurements of ΔC_{vm} of nickel at the Curie temperature have been made since Lapp⁶³ in 1929. However, the $C_p:T$ relationship determined by Lapp does not agree in general with more recent measurements, so that her value of ΔC_{vm} is questionable. Also, the majority of measurements of C_p of nickel do not show a discontinuity at T_c and hence predict that the Curie transformation is third-order or higher. These measurements near T_c are repudiated in Chapter III.

Iron. As for nickel, the existing experimental measurements of the C_p of pure iron are in marked disagreement near and above T_c . In fact, the discrepancies are even larger for iron because the Curie transformation of iron occurs 415 degrees above that of nickel and C_{vm} of iron is a factor of 2.5 higher than that of nickel. For example, Touloukian's tabulations show differences of 30% in experimental C_p 's ten degrees above T_c .

In addition to these experimental difficulties, the occurrence of the α - γ transformation at 1183 K, a temperature at which the magnetic contribution to C_p is not negligible, greatly compounds the errors in the calculation of C_{vm} above 1183 K. Since C_{vm} of γ -iron is zero, part of the energy of the α - γ transformation is associated with magnetic disordering of the α -iron. To circumvent this difficulty, the specific heat

TABLE III

COMPARISON OF THEORETICAL AND EXPERIMENTAL VALUES OF THE
TOTAL MAGNETIC ENERGY U_{vm} AND ENTROPY S_{vm} OF NICKEL

	Reference ^{*t}	U_{vm} (Joules/gram- atom)	S_{vm} (Joules/gram- atom-degree)
<u>Experimental</u>			
Hofmann, Paskin, Tauer, Weiss	62	1758	3.39
Pawel and Stansbury	61	1193	2.51
Lytton	66	1318	3.89
Braun and Kohlhaas	8	1791	Not stated
Grew	65	Not stated	3.36
<u>Theoretical</u>			
$(J = \frac{1}{2}, n = 0.6, T_c = 627 \text{ K})$			
Ising (Kramers-Opechowski)	53	2214	
Constant coupling	42	1907	
Heisenberg approximation $(J_e/kT_c) = 3(J+1)/(2zS)$	62	1566	
Equation (65) (page 36)			3.47

* See page 214.

capacity of α -iron in the γ -stable temperature region must be calculated by thermodynamic reasoning. Such calculations have been performed by Darken and Smith⁶⁷ and more recently by Weiss and Tauer.⁶⁸ Besides the γ -phase C_p , these analyses require the enthalpies of the α - γ and γ - δ transformations. Uncertainties in these quantities contribute to errors in the calculated C_{vm} of α -iron above the α - γ transformation temperature. Obviously, U_{vm} and S_{vm} of iron are also affected.

Figure 6(b) depicts the results of Braun and Kohlhaas for C_p , C_{vh} , C_{ve} , C_d , and C_{vm} of iron as a function of temperature. Only two other calculations of C_{vm} for iron were found in the literature,^{62,66} and the agreement among these may be implied from the values of U_{vm} and S_{vm} in Table IV. The theoretical values of these two quantities are also listed in this table and show that Lytton's⁶⁶ values are probably incorrect.

More recent measurements of the specific heat of iron do not indicate a discontinuity ΔC_{vm} at T_c . However, in the 1920's there was considerable interest in this quantity. For example, Stoner⁶⁹ references three measurements of ΔC_{vm} for iron but notes, "For ferromagnets other than nickel, data for the specific heat near the Curie point are relatively scanty and lacking in precision." Thus, these measurements may be disregarded.

Ni₃Fe, C_p Measurements in General. During the search of the literature, only ten references concerning measurements of the specific heat capacity of nickel-based Ni-Fe alloys were found. Of these, only two involved measurements on pure stoichiometric Ni₃Fe, namely those of Kaya and Nakayama⁷⁰ and Leech and Sykes.⁷¹ Kaya's⁷² earlier work was on

TABLE IV

COMPARISON OF THEORETICAL AND EXPERIMENTAL VALUES OF THE
TOTAL MAGNETIC ENERGY U_{vm} AND ENTROPY S_{vm} OF IRON

	Reference ^{*†}	U_{vm} (Joules/gram- atom)	S_{vm} (Joules/gram- atom-degree)
<u>Experimental</u>			
Hofmann, Paskin, Tauer, and Weiss	62	8079	9.00
Lytton	66	4060	5.86
Braun and Kohlhaas	8	8836	Not stated
<u>Theoretical</u>			
$(J = 1, n = 1.1, T_c = 1043 \text{ K})$			
Ising (Kramers-Opechowski)	53	9766	
Constant coupling	42	8870	
Weiss	44	8844	
Heisenberg $(J_e/kT_c) = 3(J+1)/(2zS)$	62	7070	
Equation (65). (page 36)			10.05

* See page 214.

a 24.1% Fe alloy. Of the others, Zuithoff,⁷³ Keesom and Kurrelmeyer,⁷⁴ Dixon, Hoare, and Holden,³⁴ and Gupta, Cheng, and Beck⁷⁵ performed experiments on pure binary alloys of several nickel compositions, but none were within 5% of the Ni_3Fe composition. Unfortunately, Iida's⁷⁶⁻⁷⁸ three excellent investigations were conducted on the alloy 24.2% Fe + 75.8% Ni + 1% Mn. By Iida's own admission, the presence of this amount of manganese markedly changed the properties of the alloy as compared with pure Ni_3Fe .

Ni_3Fe , C_p at Low Temperatures. The measurements of Keesom and Kurrelmeyer,⁷⁴ Dixon, Hoare, and Holden,³⁴ and Gupta, Cheng, and Beck⁷⁵ were performed between 1 K and 20 K on a series of off-composition, disordered alloys. Such research, while adequate to predict θ_d , γ , and α_m of disordered Ni_3Fe , avoided the very interesting effects of ordering on the C_p of Ni_3Fe . For example, measurements of Bowen⁷⁹ and Rayne⁸⁰ demonstrate an increase of the Debye temperature θ_d and a decrease in the electronic coefficient γ on ordering Cu_3Au . Martin's⁸¹ measurements, which extended down to 0.4 K, also show a decrease in the nuclear contribution to the specific heat capacity when Cu_3Au is ordered. The effects of ordering on θ_d , γ , and α_m of Ni_3Fe are investigated in this work and are presented in Chapter III.

Ni_3Fe , C_p at High Temperatures. Due to the configurational and magnetic ordering transformations, with critical temperatures of 773 K and 871 K, the form of the $C_p:T$ relationship of Ni_3Fe above about 600 K is a function of the prior thermal history of the alloy. Also, the extreme sluggishness of the configurational ordering transformation

adds to the complexity of the measurement of C_p . For example, times of up to two months have been employed by several investigators to insure complete order of the alloy prior to measurement. Consequently, the values of C_{vw} obtained below 773 K are not equilibrium values and are dependent on the heating rates employed during C_p measurements as well as the prior thermal history of the alloy. In addition, the configurational order-disorder transformation of Ni_3Fe is first-order; hence, a highly ordered alloy should display a very large isothermal energy release when heated slightly above 773 K. Due to the slow kinetics of disordering, this energy is not released isothermally during C_p measurements but rather over a large temperature interval. Thus, the C_{vw} values obtained for an ordered alloy above 773 K are even further from equilibrium than those below this temperature. An example is now presented.

Consider Figure 7 which depicts the C_p results of Leech and Sykes⁷¹ for three different heat treatments of stoichiometric Ni_3Fe . All measurements were made with a heating rate of 2 degrees/minute. Curve one was obtained after quenching into water from 1000 K and demonstrates a steady rise in C_p to about 650 K, then a drop to a minimum at 700 K. At higher temperatures two maxima in curve one are observed, one at 800 K and the other at 865 K. Curve two refers to the alloy as cooled at 1 degree/minute from 925 K. Only a slight depression in curve two is noted at 725 K, and the two maxima of curve one appear again. Curve three also demonstrates these two maxima, but the lower temperature maximum is much more pronounced. The heat treatment prior to curve three consisted of cooling from 765 K to 643 K over a 150-hour period.

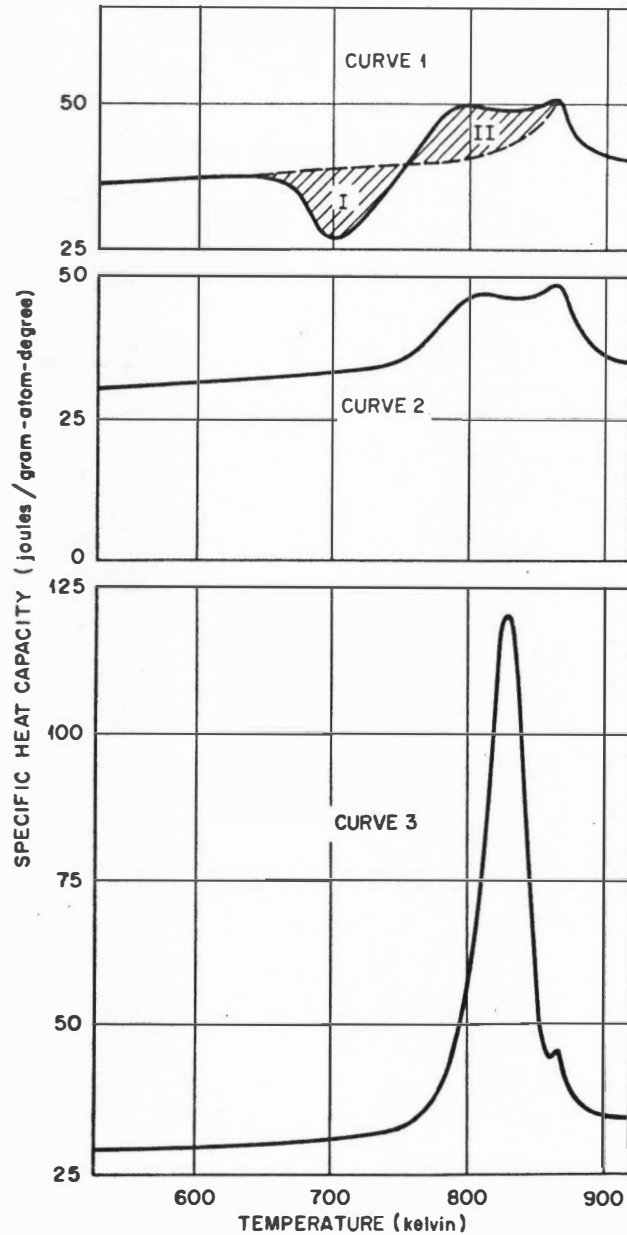


Figure 7. Specific Heat Capacity of Ni_3Fe as a Function of Temperature for Three Different Prior Heat Treatments. Curve one was obtained after a water quench from 1000 K. Curve two refers to the alloy as cooled at 1 degree/minute from 925 K. The heat treatment prior to curve three consisted of cooling from 765 K to 643 K over a 150-hour period.

Source: Leech, P., and C. Sykes, "The Evidence for a Superlattice in the Nickel-Iron Alloy Ni_3Fe ," Philosophical Magazine, Series 7, 27: 742-753, 1939.

The atomistic mechanisms associated with the maxima and minima in these curves are as follows. For curve one, the minimum at 700 K is due to the formation of local configurational order. Because of the very long relaxation time for the formation of long-range order in Ni_3Fe , no long-range order could have been formed during the short time period provided by the 2 degrees/minute heating rate of this measurement. Likewise, the depression near 725 K in curve two is associated with local order formation which had not been completed during the prior heat treatment.

For all three curves, the first maxima are due to the destruction of order, local in curve one and two and long-range in the third, and the second maxima are induced by the Curie transformation. Leech and Sykes note that the shaded areas I and II of curve one are approximately equal because the two processes occurring are essentially reversible. Note that the magnitude of the first maximum in curve three is much larger than that of curve two which in turn is greater than that of curve one, a ramification of the differences in the degree of order of the alloy at the time of measurement.

In their compilation of the C_p data of nickel-iron alloys, Hultgren, Orr, Anderson, and Kelley⁸² disregarded the data of Zuithoff⁷³ because "expected discontinuities (in heat content) due to martensite and ordering transitions do not appear." They also report that the measurements of Kaya and Nakayama⁷⁰ "at temperatures below the anomaly (order-disorder) are higher by 10% than those of Leech and Sykes." In all, these reviewers appear highly skeptical of the validity of any of the C_p measurements on Ni_3Fe appearing in the literature.

On the other hand, the C_p data of Kaya and Nakayama,⁷⁰ of Kaya,⁷⁴ and of Iida⁷⁶⁻⁷⁸ do confirm the general form of those of Leech and Sykes given in Figure 7. However, Iida's principal interest was not the value of C_p per se but rather the use of the $C_p:T$ relationship to interpret the kinetics and mechanisms of the ordering process. Some of Iida's observations pertinent to the present study are now outlined.

Ni₃Fe, Kinetics of Configurational Ordering. Near 875 K, about one hundred degrees above the critical configurational ordering temperature T_{od} , Iida found that local order was formed with a relaxation time of the order of minutes. No critical temperature existed for the local ordering phenomenon but instead, the amount of local order was observed to increase significantly as T_{od} was approached.

For an alloy quenched from 875 K to ten degrees below T_{od} , Iida's measurements show that the ordering process occurs in four overlapping stages. The first stage lasts only about twenty minutes and is associated with the removal of quenched-in imperfections and the inception of local ordering. In the second stage, local order is established, starting with a rapid rate but decreasing monotonically thereafter. This stage is complete ten hours after quenching. Not until the fifth hour does long-range ordering occur, proceeding slowly at first and reaching a maximum after twenty hours. This stage, the third, disappears after sixty hours at which time the fourth stage begins. In this last stage, the antiphase boundaries are removed, yielding the perfectly ordered structure. Due to the "long-range diffusion" involved, the fourth stage proceeds for at least one month.

Ni₃Fe, Energy U_{od} and Entropy S_{od} of Configurational Ordering.

Iida calculated a total decrease of internal energy on perfect ordering U_{od} of 3716 joules/gram-atom. Of this, about one-fourth occurred during the first and second, one-half during the third, and the remainder during the fourth stage of ordering. Iida gave no entropy value.

Leech and Sykes measured a U_{od} of 3350 joules/gram-atom and a S_{od} of 4.78 joules/gram-atom degree for an alloy which had been slow-cooled for twenty-one days from 763 K to 643 K. Iida's treatment was similar but lasted forty-seven days. Kaya's treatment, eight days at 763 K then cool to 723 K at a rate of 10 degrees/day, resulted in a value of 3034 joules/gram-atom for U_{od} . Obviously, Iida's treatment achieved the highest degree of order.

Ni₃Fe, the Magnetic Quantities C_{vm} , U_{vm} , S_{vm} , ΔC_{vm} . To the author's knowledge, no values for C_{vm} , U_{vm} , S_{vm} , or ΔC_{vm} have appeared in the literature for either disordered or ordered Ni₃Fe. Determinations of these magnetically induced quantities of Ni₃Fe are complicated by the close proximity of the magnetic and configurational ordering critical temperatures, about one hundred degrees in the equilibrium state. Also, the energy associated with the magnetic transformation is smaller and is distributed over a larger temperature interval, which further diminishes the magnetic contribution to C_p .

Below 773 K, the ordered state of Ni₃Fe is the stable state. However, the metastable disordered state can be produced by rapid cooling from above 773 K and can be maintained during C_p measurements if very

rapid heating rates, such as are possible with pulse calorimetry, are employed (see Chapter II). Therefore, C_{vm} of the disordered state can be obtained at all temperatures. Collins, Jones, and Lowde⁸³ note that although rapid cooling yields a highly disordered structure for Ni_3Fe , a small but measurable amount of local ordering does exist. This implies that C_{vm} values cannot be determined for completely random Ni_3Fe .

On the other hand, the disordered state of Ni_3Fe is the stable state above 773 K. Because of the sluggishness of the disordering transformation of Ni_3Fe , pulse calorimetric methods permit measurements of C_p of the metastable ordered state to temperatures above 773 K. Using the rule-of-thumb that the kinetics of a reaction increases by a factor of two for every ten degrees above the critical temperature, disordering mechanisms that require an hour near 773 K will occur in seconds at 873 K. Consequently, there exists a practical limit on the maximum temperature to which C_{vm} of a completely or even partially ordered Ni_3Fe can be obtained. Thus, from purely kinetic reasoning, it appears impossible to calculate C_{vm} at all temperatures for the ordered state as is possible for the disordered state. In addition, the Curie temperature of the metastable ordered state is not 871 K, as for disordered Ni_3Fe , but lies somewhere between^{84,85} 954 K and 983 K. This raises by about one hundred degrees the temperatures to which the metastable ordered state must be maintained to measure ΔC_{vm} .

Although C_{vm} , U_{vm} , S_{vm} , and ΔC_{vm} have not been determined for ordered and disordered Ni_3Fe , measurements do exist for several magnetic properties which, when used in conjunction with pertinent theories, yield some

insight into the values to be anticipated for these four quantities. For example, Crangle and Hallam⁸⁶ found that the magnetic moment per atom for disordered Ni_3Fe is 1.16 Bohr magnetons as compared to 0.6 Bohr magnetons for nickel. Assuming that the spin per atom J for disordered Ni_3Fe is the same as that of nickel, Equation (65), page 36, and Equation (66), page 37, predict that S_{vm} and U_{vm} of disordered Ni_3Fe should be 1.9 times that of nickel.

Grabbe's⁸⁷ saturation magnetization measurements indicate a 5.8% increase when Ni_3Fe is ordered. This implies that about a 6% increase in the magnetic moment occurs upon ordering. Hence, similar increases of U_{vm} and S_{vm} are to be expected for the ordered state of Ni_3Fe .

The molecular field theory value of C_{vm} is directly proportional to the product of the magnetic moment, relative magnetization, and the rate of change of the relative magnetization with respect to the reduced temperature T/T_c . [See Equation (60), page 34]. The measurements of Crangle and Hallam⁸⁶ for the relative magnetization show little difference between that of nickel and disordered Ni_3Fe . This indicates that C_{vm} of disordered Ni_3Fe should be about twice that of nickel at any T/T_c .

Above the critical temperature, measurements of the relative magnetization or any other property of ordered Ni_3Fe are limited by the kinetics of disordering as already discussed. Below the critical temperature, Taoka and Ohtsuka's⁸⁵ measurements of the relative magnetization of ordered Ni_3Fe indicate that the C_{vm} of the ordered alloy is significantly lower than that of the disordered alloy.

Ni₃Fe, the Electrical Resistivity ρ . The electrical resistivity ρ of Ni₃Fe is sensitive to changes in both configurational and magnetic order. As discussed in Chapter II, the pulse calorimeter employed to measure C_p affords simultaneous measurement of ρ and C_p . Therefore, the state of order of the alloy is ascertained throughout the C_p measurements by monitoring ρ . This is particularly significant because measurements of the state of order by x-ray or neutron scattering techniques are very difficult, due to the similarity in the scattering properties of nickel and iron atoms. Because of its importance herein, the various contributions to the electrical resistivity are discussed briefly.

The electrical resistivity of a solid possessing both magnetic and configurational order may be expressed as^{88,89}

$$\rho = \rho_i + \rho_t + \rho_m, \quad (73)$$

where ρ_i , ρ_t , and ρ_m are the electron scattering due to alloy atoms, phonons, and electron spin disorder, respectively.

Beal⁹⁰ has developed the following expression for ρ_i at a fixed temperature

$$\rho_i = \rho_o + (1 - S^2) \left[1 + \frac{(1 - S)(3 + S)(1 + 2S)}{(1 + S)} \frac{W}{kT} A(K_F D) \right], \quad (74)$$

where

$$\frac{(1 + 3S)(3 + S)}{3(1 - S)^2} = \exp \left(\frac{4SW}{kT} \right), \quad (75)$$

$$A(K_F D) = \frac{1}{(K_F D)^2} \left[\cos 2K_F D - \frac{\sin 2K_F D}{K_F D} + \frac{1 - \cos 2K_F D}{2(K_F D)^2} \right]. \quad (76)$$

The first term in Equation (74) is the electron scattering by perfectly ordered alloy atoms and the second term is the additional scattering induced by a disordered structure. In the second term, the quantity $(1 - S^2)$ is the contribution to the electron scattering due to the breakdown of perfect long-range order, where S is the long-range order parameter; the quantity in brackets is that stemming from a decrease in local order, which yields a weak but not negligible contribution to ρ_i .

Equation (75) is the Bragg-Williams approximation, which relates the long range order parameter to the interaction energy W and absolute temperature T . In Equation (76), the quantity D is the nearest neighbor distance, and K_F is the wave vector at the Fermi surface of the ordered alloy.

The precise expressions for the temperature dependence of ρ_i , ρ_t , and ρ_m are not known. Normally one assumes ρ_i , which in effect is an "impurity" type scattering, to be temperature independent. Thus ρ_o is equal to the residual resistivity of the perfectly ordered alloy at zero kelvin. At temperatures near and above the Debye temperature θ_d , the Bloch-Grüneisen formula is an approximation for ρ_t and is

$$\rho_t = B \left(\frac{T}{\theta_d} \right)^5 J \left(\frac{\theta_d}{T} \right), \quad (77)$$

where B is a constant. The quantity $J(\theta_d/T)$ is a Debye type function given by

$$J \left(\frac{\theta_d}{T} \right) = \int_0^{\theta_d/T} \frac{x^5 dx}{(\exp x - 1)[1 - \exp(-x)]} \quad (78)$$

When T is greater than $1.5 \theta_d$, the function $J(\theta_d/T)$ may be approximated by

$$J\left(\frac{\theta_d}{T}\right) = \frac{1}{4} \left(\frac{\theta_d}{T}\right)^4. \quad (79)$$

Above the Curie temperature, ρ_m is constant to a first approximation, and Weiss⁸⁸ finds the expression

$$\rho_m \approx 3 \times 10^{-5} J(J+1) \quad (80)$$

to be valid for the 3-d transition metals when ρ_m is expressed in ohm-cm. Since the Curie temperature of Ni_3Fe is about twice θ_d , the electrical resistivity above T_c is

$$\rho = \rho_i + \rho_m + BT/(4\theta_d) = A + \{B/(4\theta_d)\}T, \quad (81)$$

where A is a constant. The constant $B/(4\theta_d)$ is therefore the slope of the linear $\rho:T$ relationship above the Curie temperature.

Below the Curie temperature, the precise functional relationship between ρ_m and T is not known. From Equations (73), (74), and (77),

ρ_m can be determined from experimental values of ρ by

$$\rho_m = \rho - \rho_i - B \left(\frac{T}{\theta_d}\right)^5 J\left(\frac{\theta_d}{T}\right), \quad (82)$$

where ρ_i is assumed to be temperature independent.

In recent literature,⁹¹⁻⁹⁵ there has been considerable interest in the experimentally determined values of ρ_m near T_c . The theory of Craig, Goldburg, Kitchens, and Budnick,⁹¹ for example, yields an expression for $d\rho/dT$ that is a complicated function of $\ln|T - T_c|$ but which does not agree too well with experimental data. Instead, they suggest

$$\frac{d^2\rho}{dT^2} = -a \left(\frac{|T - T_c|}{T}\right)^{-(\lambda+1)}, \quad (83)$$

where a and λ are constants, and have obtained reasonable agreement with experimental measurements above T_c using this expression. For temperatures near T_c , Kraftmakher⁹² found a linear relationship between dp/dT of nickel and $\ln|T - T_c|$, which had the same slopes above and below T_c . Kraftmakher and Romashina⁹³ established a similar temperature dependence for dp/dT of iron. Recall that Kraftmakher found the identical dependence of C_p on T for nickel⁵¹ and iron.⁵² This suggests that C_{vm} and dp_m/dT should be directly proportional.

Moore, Fulkerson, and McElroy⁹⁵ suggest that since ρ_m is a measure of the spin disorder of a solid, ρ_m should be related to the magnetic entropy S_{vm} . If ρ_m is assumed to be directly proportional to S_{vm} with a constant of proportionality α_ρ , these authors find that

$$C_{vm} = \frac{T}{\alpha_\rho} \frac{d\rho_m}{dT}, \quad (84)$$

which is contradictory to Kraftmakher's results.

Methods of Measurement of C_p of Solids

The literature contains a multiplicity of methods for measuring the specific heat capacity C_p of solids. These methods are normally classified as either dropping, adiabatic, or pulse calorimeters.

In drop calorimetry, a specimen is heated to a prescribed temperature T_1 and allowed to equilibrate. The specimen is then rapidly dropped into a calorimeter at temperature T_2 , and the energy released by the specimen while equilibrating with the calorimeter is measured. This heat energy is equal to the relative enthalpy H of the specimen at T_1 with respect to T_2 , called ΔH_1 . Repeating this process at different

temperatures T_1 yields the $\Delta H:T$ relationship. By definition, C_p is the slope $d\Delta H/dT$ of this relationship.

The accuracy of determining C_p by drop calorimetry depends on the accuracy of the ΔH and T_1 measurements, the proximity in temperature of these data, and the functional dependence of ΔH on T assumed in the data fitting procedure. Normally ΔH and T_1 can be measured to within a few tenths of a percent, but due to the labor and time involved, data points are usually taken every fifty degrees. This increases the importance of choosing the proper form for ΔH as a function of temperature $\Delta H(T)$. In theory, the most precise expression for $\Delta H(T)$ is obtained if Equation (12), page 8, is integrated over the temperature interval of interest, namely

$$\Delta H(T) = \int_{T_2}^T C_p dT' = \int_{T_2}^T (C_{vh} + C_{va} + C_{ve} + C_{vm} + C_{vw} + C_d) dT', \quad (85)$$

where the appropriate temperature dependent expressions for C_{vh} , C_{va} , C_{ve} , C_{vm} , C_{vw} , and C_d are employed. Normally, such a complicated relationship as this is impractical, and ΔH is assumed equal to a second or third order polynomial in temperature. This is a good approximation if the temperature interval is not too large, sufficient data are available, and C_p is not a rapidly varying function of temperature. Therefore, in the vicinity of the Curie transformation of iron and nickel, drop calorimetry C_p data are apt to be erroneous.

Most adiabatic calorimeters consist of an isothermal vacuum chamber in which a specimen, having a power resistor enclosed within it, is suspended. When a current is passed through the power resistor, the specimen experiences an increase in temperature. Instrumentation is provided

to maintain the chamber at the same temperature as the specimen and thus provides an adiabatic shield for the specimen. The specific heat capacity of the specimen of mass m is calculated by

$$C_p = \frac{P}{m(dT/dt)} \quad , \quad (86)$$

where P is the electrical power dissipated in the resistor. In most techniques, the time Δt required for the specimen temperature to change ΔT degrees is measured. If the heating rate over this temperature interval is approximately constant, then dT/dt is equal to $\Delta T/\Delta t$. Using a constant power P and small temperature intervals, this approximation is valid except when C_p is varying very rapidly with temperature. Thus near T_c , C_p measurements obtained with this technique may be in error, especially if ΔT encompasses T_c .

In the majority of pulse calorimeters, the specimen is directly heated by passing a current through it, and the power dissipated in the specimen and temperature of the specimen is recorded as a function of time. The specific heat capacity calculation involves an expression of the form

$$C_p = \frac{P - P_L}{m(dT/dt)} \quad . \quad (87)$$

To reduce the power loss P_L , the specimen is heated within a vacuum chamber. In addition, some techniques enclose the specimen in a furnace and, depending on several experimental variables, pulse heat anywhere from one to several hundred degrees above the ambient temperature of the furnace. Other techniques employ input powers of a magnitude large

enough to render P_L negligibly small. These methods usually pulse heat from room temperature.

The accuracy of pulse calorimetry is dependent mainly on the accuracy of calculating dT/dt . Some methods also require accurate evaluation of P_L . The comments made regarding the calculation of dT/dt in adiabatic calorimetry are applicable to pulse calorimetry as well, and this point is discussed in more detail in Chapters II and III.

Of the three methods discussed, only the adiabatic and pulse calorimeters directly measure C_p . Each of these methods has its inherent advantages and disadvantages. In theory, the specific application should determine which method is used to determine C_p , but all too often the method chosen is the one available!

History of ORNL Calorimeters. In August of 1964, the Physical Properties Group of the Metals and Ceramics Division of the Oak Ridge National Laboratory began development of a pulse calorimeter which was to have the capability of 99% accuracy from 77 K to 2200 K. The initial efforts of this endeavor are reported in the author's Master of Science thesis at the University of Tennessee.⁹⁶ This calorimeter, called Pulse Calorimeter I, consisted of a 60-cm-long, 0.25-cm-diameter specimen suspended in a blackbody vacuum chamber held at room temperature. The sample was self-heated by a stepwise pulse of direct current, and a digital voltmeter was employed to measure the transient power and temperature signals. At 1200 K, the power loss was about 25% of the maximum available input power. An accuracy of only 98% was achieved in the estimate of the power loss, and thus this error alone resulted in a $\pm 0.5\%$ error in the

specific heat. Since the power loss increased as T^4 and a temperature capability of 2200 K was desired, it was decided to construct a new calorimeter in which the specimen was placed in an isothermal enclosure within a vacuum furnace. This enclosure was to be maintained at a constant temperature while the specimen was pulsed one hundred to three hundred degrees above the enclosure temperature at rates from 10 degrees/second to 50 degrees/second. In this manner, the power loss was kept within acceptable limits and was measured by allowing the sample to free-cool after the pulse. Part of the research of this thesis was devoted to the construction and development of this calorimeter, called Pulse Calorimeter II. A complete description of this technique and method is given in Chapter II.

Thesis Goals

The efforts of this research were directed toward accomplishing the following goals:

1. To construct a new pulse calorimeter capable of 99% accuracy from 300 K to 1700 K.
2. To measure the specific heat capacity of nickel and iron to 99% accuracy from 300 K to 1700 K and to:
 - a. calculate the magnetic specific heat capacity C_{vm} , energy U_{vm} , and entropy S_{vm} associated with the ferromagnetic state;
 - b. measure the discontinuity ΔC_{vm} in the specific heat capacity at the Curie temperature;
 - c. compare a and b above with theory and other investigations.

3. To measure the specific heat capacity of disordered Ni_3Fe to 99% accuracy from 300 K to 1700 K and to perform steps 2a, 2b, and 2c for this state of order.

4. To measure the specific heat capacity of partially and highly ordered Ni_3Fe to 99% accuracy from 300 K to as high a temperature as possible and to:

- a. perform steps 2a, 2b, and 2c for both states,
- b. calculate the energy U_{od} and entropy S_{od} of ordering at the equilibrium critical temperature,
- c. measure the change on the Curie temperature with ordering.

5. To measure the specific heat capacity of disordered and highly ordered Ni_3Fe to 99.5% accuracy from 1.2 K to 4 K in order to determine the effect of ordering on the Debye temperature θ_d , the temperature coefficient γ of the electronic specific heat capacity, and the temperature coefficient α_m of the magnetic specific heat capacity.

6. To perform auxiliary electrical resistivity measurements on Ni_3Fe to 99.7% accuracy from 4.2 K to 1700 K. These measurements were to be made with various heat treatments of the alloy so that the electrical resistivity might be used to monitor the state of configurational order during specific heat capacity measurements.

7. To measure the thermoelectric power of Ni_3Fe to 99% accuracy from 77 K to 1700 K. These measurements were to be made with various heat treatment of the alloy and were to be acquired as an indirect aid in the interpretation of the specific heat capacity and electrical resistivity data.

CHAPTER II

MEASUREMENT METHODS AND SPECIMENS

During the course of this research, six different apparatuses were used. All but one of these pieces of equipment as well as the methodology employed were developed independent of this work and have been described in sufficient detail in the literature. Therefore, only the one, namely ORNL Pulse Calorimeter II, will be described herein.

Three physical properties were measured — specific heat capacity, electrical resistivity, and thermoelectric power. Of these, the specific heat capacity measurements were of prime importance. The principal use of the electrical resistivity data was as a quantitative indication of the state of configurational order of the nickel-iron alloy during heat capacity measurements. Measurements of the thermoelectric power were obtained in conjunction with the steady-state electrical resistivity measurements described below.

Electrical Resistivity Measurements

Electrical resistivity measurements were made by three steady-state techniques and during the pulse calorimetric measurements of the heat capacity. Of the steady-state methods, two were designed for measurements near room temperature and below and the other for measurements from room temperature to 1700 K.

One of the low-temperature devices⁹⁷ consisted of a long thin-walled tube to which the specimen, normally 7.5 cm in length and 0.3 cm in diameter, was attached by means of two electrodes and two voltage probes.

Since these measurements were made below room temperature, the electrodes and probes were affixed to the specimen by means of adhesive tape and were placed at the ends and 0.5 cm from the ends of the specimen, respectively. This assembly was submerged successively in baths of distilled water, liquid nitrogen and liquid helium and a direct current passed through the specimen. Measurements of the potential E_p across the probes and the potential E_i across a 0.01 ohm standard resistor in series with the specimen allowed a calculation of the electrical resistivity ρ by

$$\rho = \frac{E_p}{100 E_i} \frac{A_c}{l} , \quad (88)$$

where A_c was the cross sectional area of the specimen. The quantity l was the length of the specimen between voltage probes and was ascertained by a comparative electrical technique.⁹⁶ The temperature of the specimen was assumed to be that of the bath. The accuracy of the device is 99%, ± 0.5 degree, and the ρ values were repeatable to within $\pm 0.5\%$.

In both of the other steady-state techniques, two thermocouples were spot-welded to the specimen and the positive thermoelement of each served as the voltage probes. Measurements with the second low-temperature technique⁹⁸ were accomplished by attaching the sample to electrodes within a furnace which was housed in a vacuum chamber. After submerging the vacuum chamber in either a liquid nitrogen or ice-water bath, the furnace was heated to any desired temperature between 77 K and 400 K and the electrical resistivity of the specimen determined. Calculation of ρ was by means of Equation (88), yielding an accuracy of 99.4%, ± 0.1 degree with a repeatability of $\pm 0.1\%$.

For the high-temperature measurements,⁹⁷ the sample was attached to two electrodes and placed in an alumina tube which was an integral part of a vacuum system capable of achieving 10^{-7} mm of mercury. This tube was housed in a furnace which could be controlled at temperatures between 298 K and 1700 K. As above, the electrical resistivity was calculated by means of Equation (88), yielding an accuracy of 99.7%, ± 2.0 degrees with a repeatability of $\pm 0.03\%$.

Measurements of ρ during pulse calorimetry are discussed later, but in essence were achieved by determination of the quantities requisite to Equation (88). All electrical resistivity measurements reported herein have not been corrected for thermal expansion of the specimen.

Thermoelectric Power Measurements

The thermoelectric power was determined using the last two steady-state electrical resistivity devices^{97,98} outlined above. In both, the direct current used in the electrical resistivity measurements was turned off and a thermal gradient applied to the specimen. Measurement of the potential V_+ or V_- between either the positive or negative thermoelements of the two thermocouples as well as their temperatures T_2 and T_1 allowed a calculation of the thermoelectric power of the specimen relative to the thermoelement

$$E_{\pm} = V_{\pm} / (T_2 - T_1) . \quad (89)$$

The absolute thermoelectric power of the specimen was determined by subtracting the absolute thermoelectric power⁹⁹ of the thermoelement from E_+ or E_- , as the case may be.

The accuracy of determining the thermoelectric power with the low-temperature device⁹⁸ was 99.5%, ± 0.1 degree to a repeatability of $\pm 0.1\%$. For the high-temperature device,⁹⁷ the accuracy was $\pm 95.4\%$, ± 3 degrees with a repeatability of $\pm 0.2\%$.

Specific Heat Capacity Measurements

Two methods were used for measurements of the specific heat capacity. At temperatures between 1 K and 4 K, the method utilized¹⁰⁰ employed a 2.0-cm-diameter and 2.5-cm-long specimen which was instrumented with a carbon resistance thermometer and upon which a heater was wound. This specimen was suspended by means of nylon threads in an adiabatic, vacuum chamber. After submerging the vacuum chamber in a liquid helium bath, the pressure over the bath was varied to produce the desired temperature of the specimen. When thermal equilibrium was obtained between bath, chamber, and specimen, a direct current I was passed through the specimen heater and the time required Δt to change the specimen temperature by an amount ΔT was measured. The specific heat capacity of a specimen of mass m was

$$C_p = \frac{1}{m} \left(\frac{EI\Delta T}{\Delta t} - C_a \right), \quad (90)$$

where E was the potential drop across the specimen heater and C_a was the heat capacity of the thermometer and heater. Normally, the temperature change was about thirty millidegrees and thus no correction was necessary for heat losses from the specimen. The resistance thermometer was calibrated in subsequent measurements against the helium bath temperature, which is a well established function of the vapor pressure of helium. The accuracy of this device was 99.5%, ± 0.002 degree with a repeatability of $\pm 0.25\%$.

The second method of measurement of the specific heat capacity was pulse calorimetry. Since Pulse Calorimeter II was developed during the course of this work, this method is outlined in more detail than the resistivity and thermoelectric power techniques.

The determination of specific heat capacity by pulse calorimetry requires measurements of the time dependence of the temperature and the electrical power dissipation within the test section of a specimen during a heat pulse. A heat balance on the test section during a pulse yields

$$\text{Power In} = \text{Power Absorbed} + \text{Power Loss} . \quad (91)$$

For methods which employ joule heating of the specimen by a direct current, the Power In is a product of the current I flowing through the specimen and the voltage drop E across the test section. If it is assumed that the entire mass m of the test section increases in temperature at rate dT/dt , the Power Absorbed by the test section is $mC_p dT/dt$. Here C_p is the specific heat capacity at the average temperature of the test section.

As shown in Figure 8, the Power Loss from the test section is due to three mechanisms - radiation, conduction, and convection. These power losses may be assessed by calculations and/or auxiliary experiments. At high temperatures, the dominant method of heat loss is radiation, which is relatively simple to calculate by the familiar T^4 law. To perform this calculation, a knowledge of the geometry of the specimen and its surroundings as well as their thermal radiative properties is required.

Conduction losses may occur both through the thermocouple or voltage probes attached to the test section and through the specimen

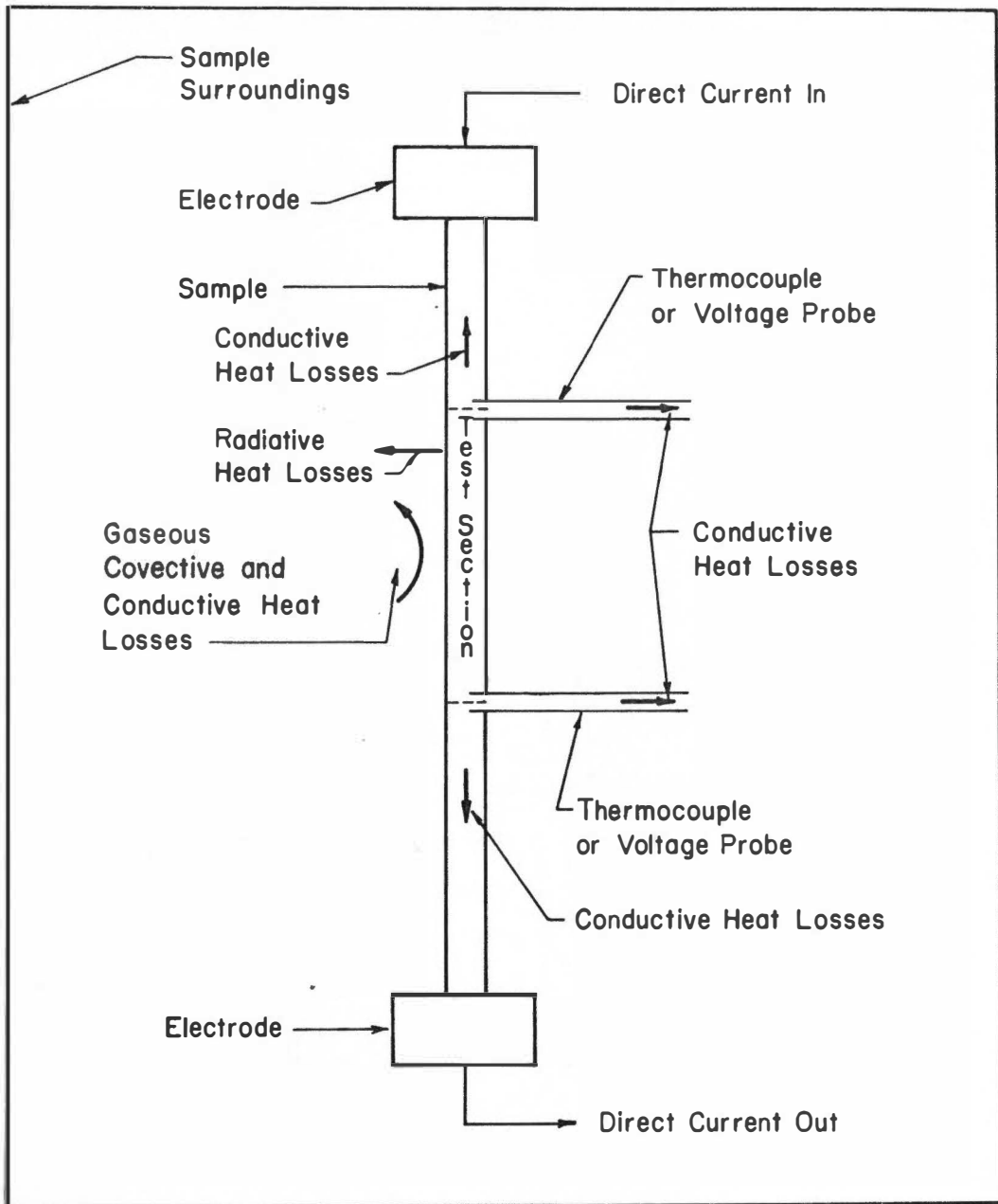


Figure 8. Schematic Diagram of Pulse Calorimeter Which Utilizes Joule Heating to Supply the Required Pulse. The three mechanisms of heat loss from the test section are indicated.

itself to the electrodes. The latter loss is a product of the cross-sectional area and thermal conductivity of the specimen and the instantaneous longitudinal temperature gradient at the extremities of the test section. Similarly, the losses through the thermocouples or voltage probes are a product of their cross-sectional area, thermal conductivity, and the transient temperature gradient at their interface with the test section. Unfortunately, it is very difficult to ascertain these temperature gradients during the pulse; therefore, it is necessary to design the experiment so that the conduction loss term is negligible with respect to the absorption term. This can be achieved by employing very small wires for the thermocouples or voltage probes and by using long, small-diameter specimens. In a vacuum of 10^{-6} mm of mercury or better, gaseous convection and conduction losses are negligible with respect to the power absorbed.

If it is assumed that the heat losses at a given temperature are the same during heating as when the power is turned off and the specimen allowed to free-cool, the total Power Loss may be determined experimentally and is equal to $mC_p(dT/dt)_c$, where $(dT/dt)_c$ is the free-cooling rate. Thus, the expression for C_p is

$$C_p = \left| \frac{EI}{m[dT/dt - (dT/dt)_c]} \right|_{T_i}, \quad (92)$$

where all terms are evaluated at a particular temperature T_i .

As discussed in Chapter I, two pulse calorimeters have been developed at the Oak Ridge National Laboratory in which data were acquired that were amenable to treatment by Equation (92). Pulse

Calorimeter I, shown schematically in Figure 9, consisted of a long, cylindrical specimen suspended in a blackbody vacuum chamber held at room temperature. The specimen was self-heated by a stepwise pulse of direct current, and a digital voltmeter was employed to measure the transient power and temperature signals. Above about 1200 K, the errors introduced by the inaccuracies in the evaluation of the heat losses led to the development of Pulse Calorimeter II. In this calorimeter, the specimen was placed in an essentially isothermal enclosure within a vacuum furnace. This enclosure was maintained at a selected constant temperature while the specimen was pulsed one hundred to three hundred degrees above the enclosure temperature. In this manner, the heat losses were kept within acceptable limits.

Other than the enclosure, the instrumentation and methodology employed in the operation of Calorimeters I and II were practically the same. In the following discussion of Calorimeter II, the differences between the two methods are pointed out. However, the intricate details, such as make and model of commercially available equipment, have been deleted. The reader interested in these details is referred to References 96, 101, and 102.

Description of Pulse Calorimeter II

The vacuum furnace and sample-holder assembly of Calorimeter II are shown schematically in Figure 10. The purpose of this equipment was to provide for the specimen an isothermal enclosure having a sufficiently large mass so that its temperature would remain essentially constant when the specimen was pulsed one hundred to three hundred degrees. The details

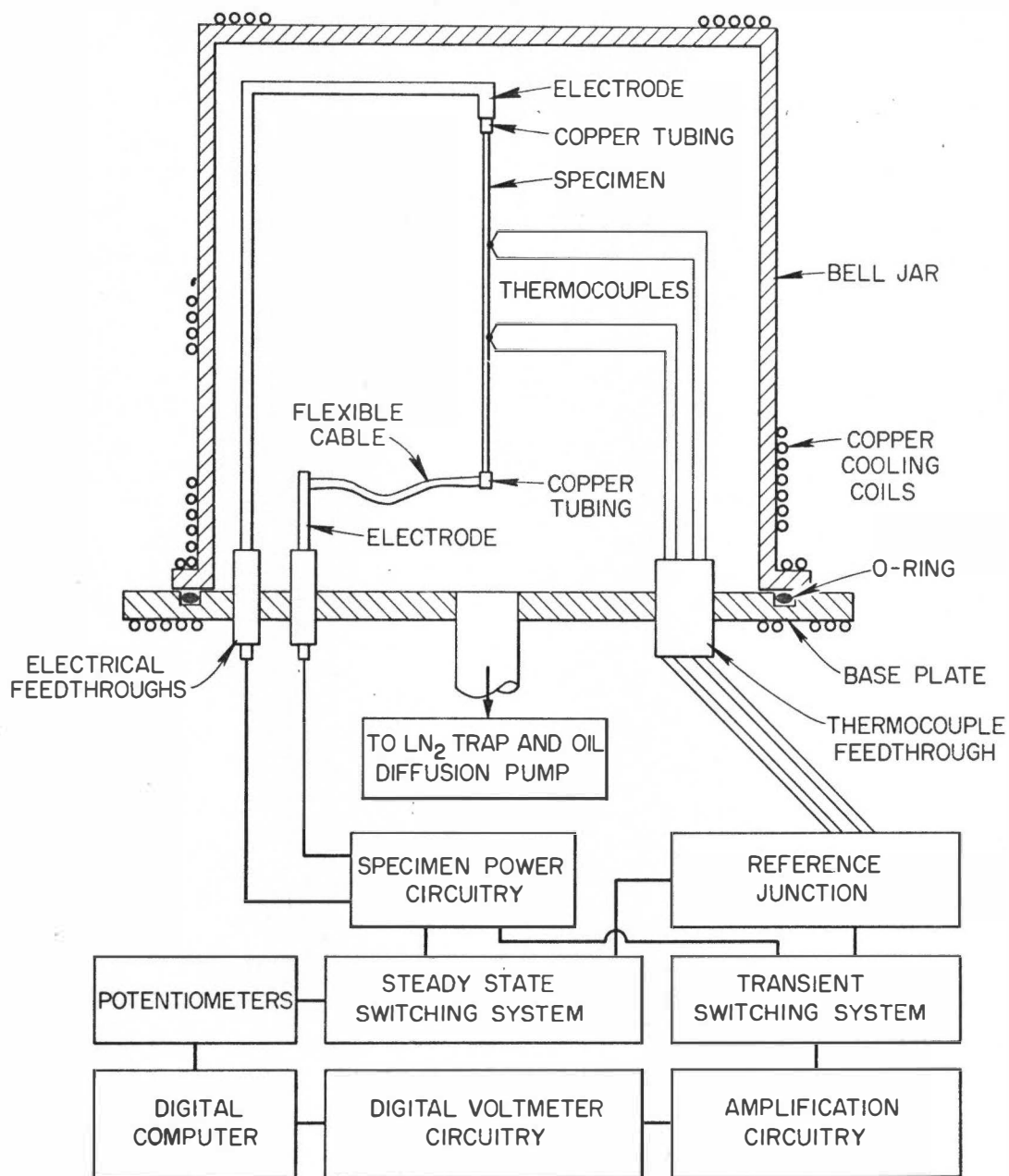


Figure 9. Schematic Diagram of Pulse Calorimeter I Showing the Major Components and Their Interrelationship.

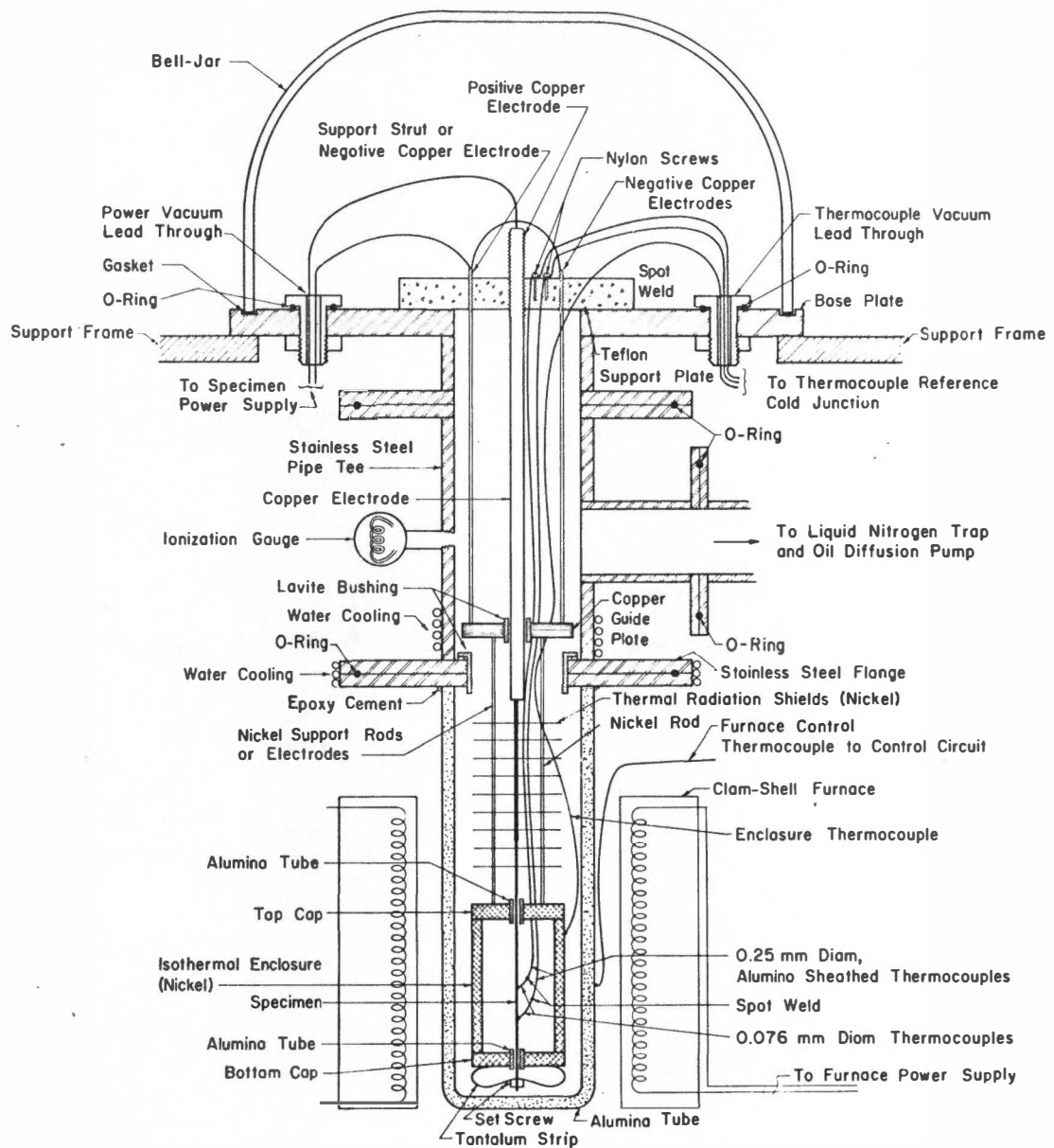


Figure 10. Schematic Diagram of the Pulse Calorimeter II Showing the Vacuum Furnace, Sample-Holder Assembly, and the Specimen.

of this equipment are presented in Reference 102 and are not repeated herein. (The details of the blackbody enclosure of Calorimeter I are presented in Reference 101.)

The Specimen. The specimen was nominally 35 cm in length, 0.25 cm in diameter, and was threaded on the upper end for attachment to the positive electrode of the sample-holder assembly. It was lapped to a diametral tolerance of ± 0.00025 cm to allow an accurate calculation of the test section mass and to produce a mirror surface finish to reduce thermal radiation. (The specimen for Calorimeter I was 60 cm in length.)

Four 0.0076-cm-diameter thermocouples, each 2 cm in length, were tweezer welded to the specimen's surface at 2.5 cm intervals centered about a point which would be in the middle of the enclosure. By observing the welding through a stereomicroscope, the thermocouples were positioned precisely so that each thermoelement was exactly opposite and parallel to its counterpart and so that the hot junction was made through the specimen. This was done to minimize the voltage pickup from the pulse current and to yield more accurate surface temperature measurements. Proper placement was also important because the positive thermoelements served as the voltage taps for the power measurement. Thus, three test sections were available for cross-check measurements of specific heat capacity.

Thermometry and Power Circuitry. As shown in Figure 10, the specimen thermocouples were joined to the permanently mounted 0.025-cm-diameter thermocouple wires of the specimen-holder assembly. These thermocouple wires exited the base plate through epoxy resin seals and extended to

their reference junctions where the required voltage drop and thermal emf connections were made to two multistranded copper cables. As shown in Figure 11, each cable fed separate switching systems – one to select signals for steady state potentiometric measurements and the other for the transient signal measurement circuitry. Use of two switching systems avoided ground loops and interaction between the potentiometric and transient signal circuitry.

The specimen power source consisted of up to three voltage-regulated, direct-current power supplies, which were connected in parallel and which were operated in their constant-current mode. The regulation circuits of the supplies were modified to provide a step-jump in the current. At steady state the total output current was about 3 amperes, and the pulse

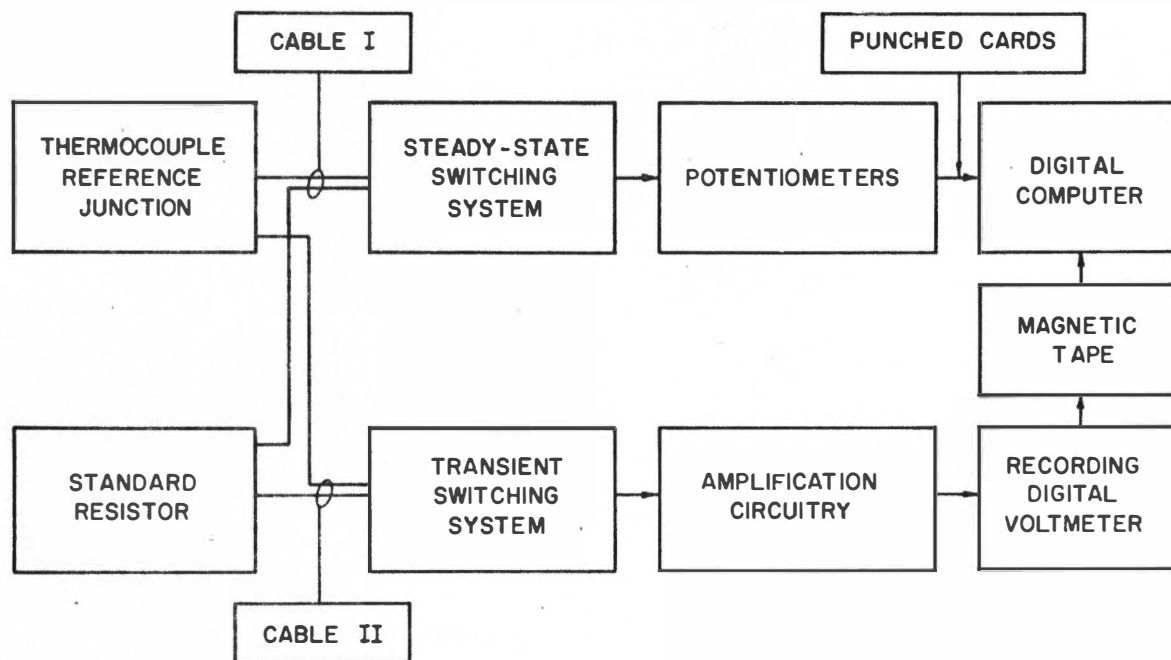


Figure 11. Block Diagram of the Thermometry and Power Circuitry. Steady-state data were input to computer on cards and transient data on magnetic tape.

current was adjustable from 1 to 147 amperes, 150 amperes being the maximum output of the combined supplies. (For Calorimeter I, higher steady-state currents were required to heat the sample to the temperature from which the pulse was applied.)

As depicted in Figure 12, the power circuitry also included two current-reversing relays, a shunt, and a standard resistor. The purpose of the relays was to allow potentiometric measurements to be made with the current flowing in either direction through the specimen. This provided data for calculating the voltage pickup by the test section thermocouples from the pulse current because of misalignment of the thermoelement junctions on the specimen. Also, these data were used to correct the measured test section voltage drops for Seebeck-effect induced voltages.

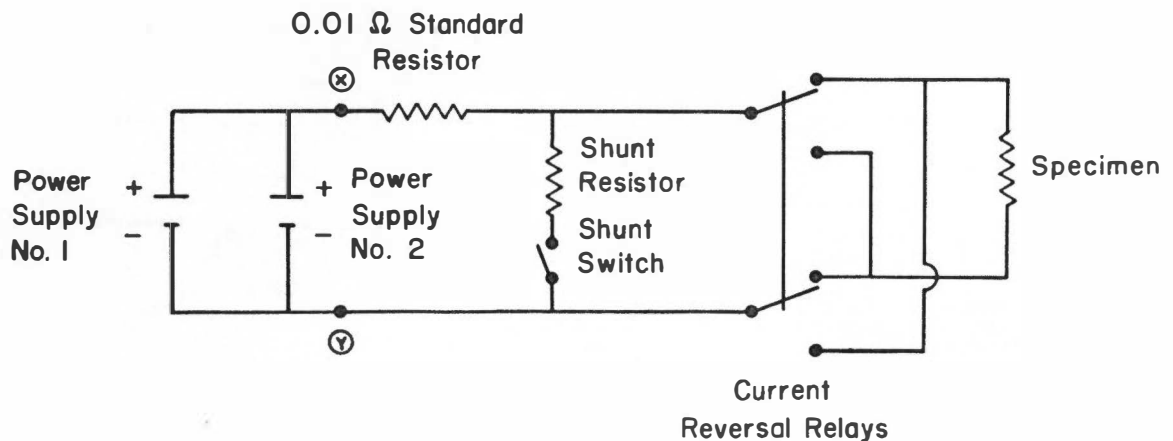


Figure 12. Schematic Representation of Specimen Power Supply Circuitry. Only two power supplies are depicted.

The shunt was wired in parallel with the specimen to prevent a short circuit of the power supply through the relays during reversal and to provide more stable power supply operation by preventing an open circuit during reversal. To accomplish this, the shunt switch was closed before and was opened after the current-reversal relays were activated. By placing the 0.01-ohm standard resistor in series with the specimen, the voltage drop across it was directly proportional to the current flowing through the specimen. Such a transducer was necessary since current could not be measured directly on the digital voltmeter and potentiometers.

The Transient Signal Circuitry. Measurement of the test section voltage, current, and temperature during the heat pulse was accomplished using three separate amplification circuits coupled to a recording digital voltmeter, DVM. As shown in Figure 13, the signals from the transient switching system were placed in series opposition with a bias voltage, and the resulting differential signals connected to the amplifiers. Since the DVM was not portable and was located in a different building than the amplification equipment, tie-in of the three amplification circuits to the DVM was accomplished by means of telecommunication lines. Due to the 60 hertz noise induced on these lines, it was necessary to employ amplifier gains of a magnitude so that the transmitted signals changed from 0.5 to 10 volts, yielding a large signal-to-noise ratio. To further diminish the noise, each signal was passed through a parallel-T rejection filter network tuned for 60 hertz rejection. Experiments indicated that the DVM was not as susceptible to the effects of

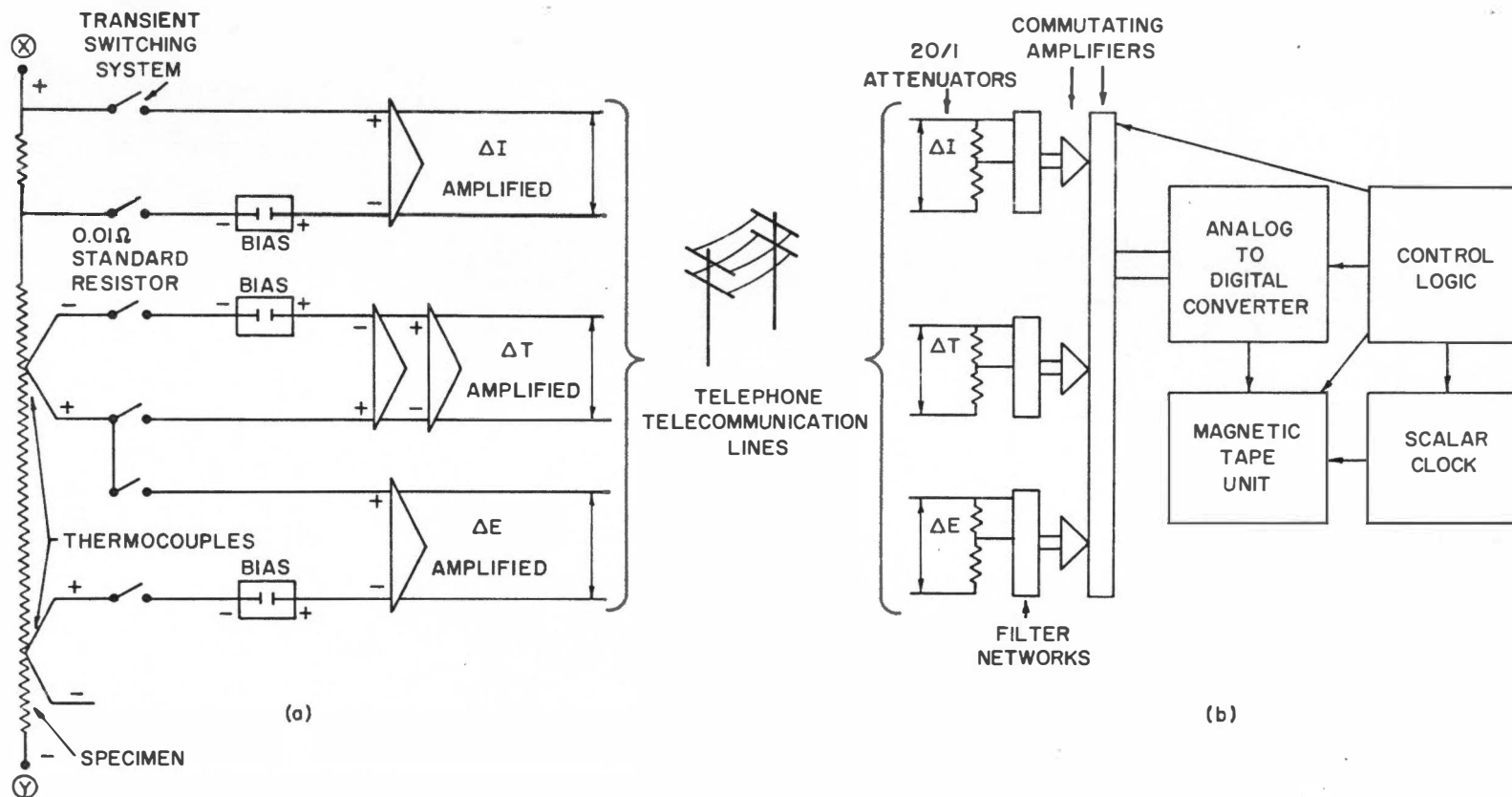


Figure 13. Schematic Diagram of the Transient Signal Circuitry. (a) The amplification circuitry and (b) the DVM circuits. The circuitry between points X and Y corresponds to that between points X and Y of Figure 12.

these noises if the commutating amplifiers of the DVM were operated at a gain of ten. Since the output of the commutating amplifiers had to be 0 to ± 5 volts, a twenty-to-one attenuator was inserted before each filter network. Also, the high-frequency roll-off band pass of the commutating amplifiers was set at 45 hertz.

The heart of the DVM was the Control Logic which had a 10 kilohertz crystal clock for a time base. This logic circuitry channeled the outputs of the commutating amplifiers to an analog-to-digital (A/D) converter in the sequence temperature, voltage, current at the rate of 2000 readings per second. The A/D converter subsequently changed each of these analog signals into a form consisting of a sign plus four digits, yielding a readability of 0.01% for a full-scale deflection of the DVM. From the A/D converter, the Control Logic fed the digitized signals to a magnetic tape unit where they were recorded in a BCD format.

During the free-cooling cycle of the experiment, the logic was modified so that the temperature signal was recorded once per second along with the time elapsed from the start of cooling. The time was calculated from the time base frequency of 10.0013 kilohertz, yielding an accuracy of the time during heating and cooling of fifty parts per million.

Calibration Procedure. Calibration data for the three amplifier-DVM circuits were acquired by feeding five sets of potentiometrically determined voltages from the bias units to each amplifier and reading each set of amplified signals on the DVM for about 3 seconds (6000 readings). Experience demonstrated that one daily calibration was sufficient, but that separate calibrations for each gain employed for a particular

amplifier were necessary. Normally, the calibration data were acquired prior to all other measurements in a given day.

Preliminary Data Measurement Procedure. After instrumenting the specimen and determining the test section lengths and diameters, the specimen was screwed into the positive electrode of the specimen-holder assembly; and the four 0.0076-cm-diameter thermocouples on the specimen were welded to the permanently mounted 0.025-cm-diameter thermocouples of the assembly. The nickel cylinder and cap of the isothermal enclosure were positioned about the specimen, and the assembly was lowered into the vacuum furnace. After connecting the thermocouple and power lines to the vacuum leadthroughs, the bell jar was placed on the base plate and the chamber was evacuated. (For Pulse Calorimeter I, the specimen was mounted directly in the vacuum chamber by clamping to the electrodes.)

When the chamber pressure was 10^{-6} mm of mercury or less, the power supply regulation circuitry was set to yield the desired specimen heating rate, and the amplifier gains and bias voltage outputs were chosen so that the maximum possible deflections of the DVM occurred during recording of the transient signals. Finally, the furnace was heated to the temperature from which the first heat pulse was to be applied, and a small steady-state current of about two amperes was passed through the specimen. (Since Pulse Calorimeter I had no furnace, the specimen was directly heated to the temperature from which the first heat pulse was to be applied by proper selection of the steady-state current.)

Steady-State Data Measurement Procedure. When the specimen had achieved thermal equilibrium, the four specimen thermocouple emf's, the three test section voltages, and the current were measured potentiometrically. The direction of the current through the specimen was reversed and these eight steady-state measurements were repeated.

Transient Data Measurement Procedure. Normally, the temperature and power signals of the central test section were recorded during the transient data measurements. Consequently, these signals were fed to the amplification circuits after the steady-state data measurements had been completed. Since the transient data measurements were differential, the DVM was started four seconds prior to the pulse to permit correlation of these data with the steady-state potentiometric measurements. To initiate the heat pulse, a switch in the regulation circuitry of the specimen power supply was thrown, and the step jump in current which occurred produced a specimen heating rate of between 5 degrees/second and 60 degrees/second. The transient signals which ensued were recorded by the DVM at the rate of 2000 readings/second for the duration of the pulse which varied from 10 to 35 seconds in length, depending on the specific heat capacity of the specimen, the temperature interval of the pulse, and the current pulse size. When a full-scale deflection of the temperature signal had been achieved on the DVM, all power to the specimen was turned off by opening both pairs of current-reversal relays. As the specimen freely cooled, the temperature-time response of the test section was recorded once per second until the initial steady-state temperature was reached. Cooling times varied from 1 to 60 minutes, depending primarily on the

specimen temperature and the differential temperature between the specimen and enclosure. Upon completion of cooling, the DVM was turned off, one set of current-reversal relays was closed, and the specimen was either allowed to come to thermal equilibrium for a repeat run or the furnace temperature was changed to permit measurements over a different temperature interval. Figure 14 is a schematic illustration of the data obtained on the DVM during a typical pulse.

Preliminary Raw Data Calculations. Due to the large quantity of data collected with the DVM, all calculations were FORTRAN coded for a digital computer. The computer placed the data from the DVM magnetic tape into arrays of temperature, voltage, and current. Since about 60,000 values were recorded for a 30-second pulse, the next step was to condense these DVM data as much as possible by either averaging the constant signals or by systematically eliminating data redundancy. Because the calibration signals as well as the signals before the pulse were constant, each of these sets of signals was arithmetically averaged and every point was checked to ensure that it was within ± 1000 DVM units, called counts, of this average. Any point that did not fall within this tolerance limit was discarded and another average calculated. This screening technique was repeated with tolerances of ± 200 , ± 100 , and ± 10 counts.

A large data redundancy existed for the signals during the pulse. For example, 667 temperature readings/second were recorded at a heating rate of 20 degrees/second, yielding a data point every 0.03 degree. Such close proximity of points was indeed redundant for most applications,

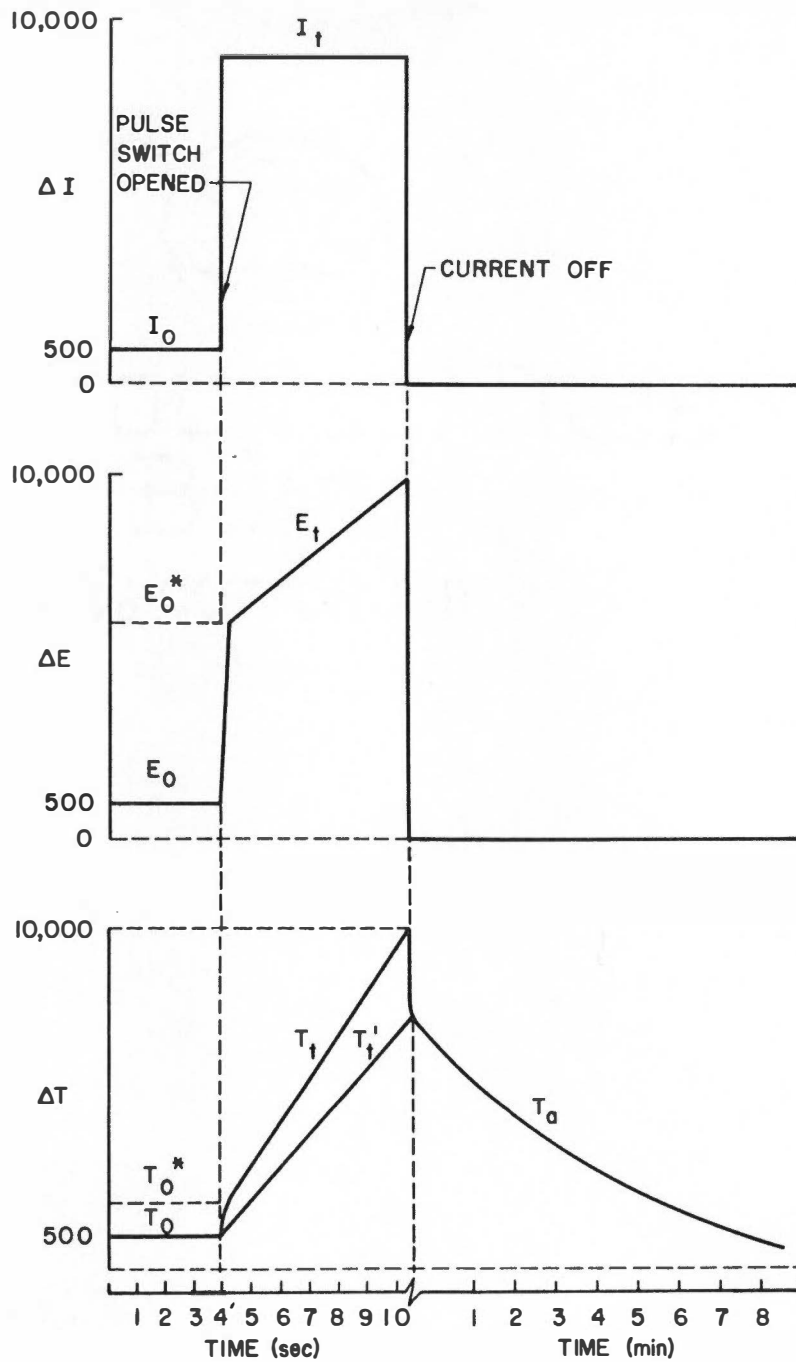


Figure 14. Schematic Diagram of the DVM Output During a Pulse Showing the Changes that Occur in the Current (ΔI), Voltage (ΔE), and Temperature (ΔT).

and consequently the reading rate was effectively reduced to 0.2 degree intervals by arithmetically averaging these data in groups of six points, using the screening technique described above. Since the ultimate use of the temperature-time signal was the calculation of the heating rate dT/dt , the averaged data were smoothed by a least-square technique¹⁰³ — called the convolute method — in groups of 125 points (25 degrees) to a second-order polynomial in time.

Amplifier and DVM Calibration Calculation. To allow accurate conversion of the DVM signals into voltages equal to the amplifier inputs, the averaged readings of the temperature, voltage, and current of the DVM taken during the calibration procedure were fitted to a straight line by the method of least-squares. This resulted in expressions of the form

$$V_i = A_i M_i + B_i , \quad (93)$$

where V_i is the value of the input voltage in microvolts and M_i is the average DVM reading in counts. The quantities A_i and B_i were the least-squares parameters for a particular gain setting of an amplifier. All calibration data fit these equations to better than $\pm 0.1\%$.

Calculation of the Temperature, Voltage, and Current During the Pulse. The temperature, voltage, and current at any time during the pulse were calculated by adding the transient DVM signals to the averaged values of the steady-state potentiometric measurements. As shown in Figure 14, the current was constant before and essentially constant during the pulse; therefore, the total current was given by

$$I = 100[I_p + A_I(I_t - I_o)] , \quad (94)$$

where I_p was the average value of the two steady-state potentiometric current readings. The quantity I_t was the averaged DVM current reading at time t during the pulse, and I_o was the average of all the DVM current readings before the pulse. The factor of 100 was the proportionality constant to convert these voltage readings, which were measured across the 0.01-ohm-standard resistor, into amperes. The quantity A_I was the least-squares parameter obtained from Equation (93) for the particular current amplifier gain employed. Since the DVM measurements were differential, B_i of Equation (93) cancelled during this conversion of the DVM signals into voltages.

In a similar manner, the voltage across the test section was

$$E = E_p + A_E(E_t - E_o) , \quad (95)$$

where quantities E_p , A_E , E_t , and E_o were the voltage circuitry equivalent to the similar terms of Equation (94).

The thermal emf T_e of the specimen thermocouple during the pulse was

$$\begin{aligned} T_e &= T_p + A_T[T_t - (E_t - E_o)(T_o^* - T_o)/(E_o^* - E_o) - T_o] \\ &= T_p + A_T[T_t' - T_o] , \end{aligned} \quad (96)$$

where the quantities T_p , A_T , T_t , and T_o were the temperature circuitry equivalents of the similar terms of Equation (94). The term

$(E_t - E_o)(T_o^* - T_o)/(E_o^* - E_o)$ corrected the thermocouple signal for voltage picked up from the current flowing through the specimen; hence, T_t' would

have been the signal recorded in the absence of pickup. As shown in Figure 14, the quantities T_o^* and E_o^* were obtained by extrapolating the T_t and E_t curves to the time corresponding to the pulse start.

The thermal emfs T_e were converted to temperatures by means of FORTRAN functions. For the Pt-10% Rh versus Pt thermocouple emfs, a function written by D. R. Flynn¹⁰⁴ of the National Bureau of Standards was used. R. L. Simpson¹⁰⁵ of the Oak Ridge National Laboratory wrote the function for the Pt-30% Rh versus Pt-6% Rh thermocouple emfs. Both functions yielded temperatures within one degree of the values recommended by Adams and Davisson¹⁰⁶ for temperatures between 300 K and 1700 K.

Calculation of the Heating Rate During the Pulse. The heating rate dT/dt was proportional to the rate of change of the thermocouple emf dT_e/dt and was given by

$$dT/dt = S dT_e/dt, \quad (97)$$

where S was the reciprocal of the thermocouple sensitivity for the thermal emf T_e . A least-squares technique,¹⁰³ commonly called the "convolute" method, was employed to calculate dT_e/dt for every T_e data point obtained with the DVM. In particular, a quadratic convolute with a 125 point group was normally employed.

Calculation of the Cooling Rate After the Pulse. In order to calculate the cooling rate $(dT/dt)_c$, it was necessary to calculate first the thermal emf T'_e of the specimen thermocouple during the cooling cycle using the expression

$$T'_e = T_R + A_T [T_a - T_o], \quad (98)$$

where A_T and T_O are the same as in Equation (96). Here, T_a was the DVM reading of the thermocouples during free-cooling of the specimen, and T_R was the steady-state potentiometric reading of the thermocouple with the current flowing in the same direction through the specimen as during the heat pulse. The temperature T_c corresponding to each value of T'_e was then calculated using the appropriate FORTRAN function.

At this point in the calculation, these data had not been checked for spurious values. To do this, the method of least-squares was employed to fit the data in temperature intervals of 50 degrees or less to an equation of the form

$$T_c = a + bt + ct^2 \quad (99)$$

where a , b , and c were the parameters obtained from the fit. Every point was checked to ensure that it was within ± 30 degrees of this curve. If it was not, its value was replaced in computer memory by the least-squares point and the fit performed again. This screening procedure was repeated with tolerances of five and one degrees. The parameters obtained after the last tolerance check were used to calculate the cooling rate by

$$(dT/dt)_c = b + 2ct \quad (100)$$

and was applicable only in the temperature interval of the fit.

Calculation of the Test Section Mass. For the cylindrical specimen of density ρ' , the test section mass m was calculated from room temperature measurements by

$$m = \frac{\pi d^2 \rho' l}{4} . \quad (101)$$

The test section length l was the distance between positive thermoelements

of adjacent thermocouples and was determined by a comparative electrical technique before placing the specimen in the isothermal enclosure. At least sixteen measurements of the diameter d of each test section were made using a light-beam micrometer, and the value of d used in Equation (101) was the average of these measurements.

Calculation of the Specific Heat Capacity. Combining Equation (92), on page 71, with Equations (94), (95), (97), (100), and (101), the expression for the specific heat capacity was

$$C_p = \frac{EI}{m[dT/dt - (dT/dt)_c]} \quad (102)$$

$$= \frac{400[E_p + A_E(E_t - E_o)][I_p + A_I(I_t - I_o)]}{\pi d^2 \rho' l [S dT_e/dt - (b + 2ct)_{T'_e}],_{T_e=T'_e}},$$

where all quantities are taken at the same temperature. From this differential equation, the specific heat capacity was obtained for every value of T_e which had been calculated from the DVM data.

Calculation of the Electrical Resistivity ρ and its Temperature-Rate-of-Change $d\rho/dT$. By combining Equation (88), on page 66, with Equations (94) and (95), the following expression for the electrical resistivity ρ was obtained

$$\rho = \frac{E A_c}{I l} = \frac{\pi d^2}{400 l} \frac{[E_p + A_E(E_t - E_o)]}{[I_p + A_I(I_t - I_o)]} \quad (103)$$

In this equation, the quantities E_t and I_t are function of time t during the pulse. Hence, calculation of ρ for each E_t and I_t recorded during heating yielded ρ as a function of time during the pulse. This then allowed calculation of the time-rate-of-change $d\rho/dt$ of the electrical

resistivity by a method analogous to that used to compute dT/dt from the temperature-time relationship. The temperature-rate-of-change $d\rho/dT$ of the electrical resistivity was found by

$$\left(\frac{d\rho}{dT} \right)_{T_1} = \left(\frac{d\rho}{dt} \right)_{t_1} \left(\frac{dT}{dt} \right)_{t_1}^{-1}, \quad (104)$$

where T_1 is the temperature at time t_1 .

Accuracy of Pulse Calorimeter II. The accuracy of an experimental technique may be evaluated by either determining the total error of all the quantities which are measured or by measuring on a standard. In the first method and for C_p , the errors of measurement of all the quantities in Equation (102) must be assessed. This was done previously^{101,102} and was found to be $\pm 1.05\%$ when the power loss was less than 10% of the input power. The errors of measurement of the absolute temperature T during a pulse yield an uncertainty of ± 3.0 degrees in T .

Regarding the method using a standard, no electrically conducting material is widely accepted as a standard for specific heat capacity above 300 K. In fact the question, "What characteristics should a high-temperature specific heat standard possess?" is indeed moot. However, a number of pure elements have been measured by numerous investigators using quite different techniques. In particular, the specific heat capacity of pure iron has been investigated extensively. Previous measurements¹⁰² of C_p of pure iron have confirmed the calculated accuracy to 1200 K.

One other point can be made in regard to the accuracy of this method for C_p . In any experimental measurement, if the results are repeatable, the accuracy of the technique is usually very good, and conversely.

Throughout all measurements, the repeatability of C_p measurements was at least $\pm 0.5\%$ even when large changes were made in the procedural variables such as furnace temperature and cooling rate.

Since all of the terms in Equation (103) for ρ appear in Equation (102) for C_p , the errors of measurement of ρ were evaluated from the error analysis made previously¹⁰¹ for C_p . The error in ρ was found to be $\pm 0.48\%$. Calculation of the errors in $d\rho/dT$ was much more difficult, but these errors were estimated to be less than $\pm 1.5\%$. The repeatabilities of ρ and $d\rho/dT$ measurements were $\pm 0.25\%$ and $\pm 1.0\%$, respectively.

Specimen Preparation and Characterization

All specimens utilized in this research were prepared from stock by the Materials Fabrication Group of the Metals and Ceramics Division of the Oak Ridge National Laboratory. The nickel and iron stock material was purchased commercially as "electrolytically pure," and a typical chemical analysis is shown in Table V. The total contaminants present in these materials were less than 500 ppm (parts per million) for the nickel stock and less than 1000 ppm for the iron stock.

Melting and fabrication of the stock into specimens were accomplished under rigid laboratory control in order that contamination be minimized. The nickel bar-stock and iron plate-stock were cut into small pieces and thoroughly cleaned. For the Ni_3Fe alloy, the appropriate proportions of nickel and iron were weighed and mixed. The stock for each specimen was placed in turn on a water-cooled copper hearth within a "beehive" melting chamber. After evacuating the melting chamber, it was back-filled with a partial pressure of pure argon gas. A tungsten electrode was used to

TABLE V

CHEMICAL COMPOSITION IN PARTS PER MILLION BY WEIGHT
OF SPECIMEN STOCK AND SPECIMENS

Element	Contents in Parts Per Million by Weight				
	Nickel Stock	Iron Stock	Nickel Specimen	Iron Specimen	Ni ₃ Fe Specimen
Ni				100	75.4×10^4
Fe	40		800		24.2×10^4
Al	6	< 200	20	< 300	< 500
B	0.2	< 0.1	0.2	0.6	
C	70	50	35	60	20
Ca	1		1	7	
Cb				2	< 500
Co	30	10	50	30	< 200
Cr	1.5	100	90	160	< 200
Cu	5	500	5	500	200
H ₂	3		1	< 1	2
K			< 0.7	< 0.7	
Mg					~ 100
Mn	1	10	25	370	< 200
Mo	< 2		< 2	70	< 100
N ₂	5	9	1	31	23
O ₂	130	120	10	540	88
P	5	5		20	
Pb	< 0.1				< 200
Pt				3	
S	< 0.4	40			
Sb				10	
Si	< 150	2	< 150	100	< 100
Sn				60	
Sr			15		
T					< 500
Ti	0.3	0.3	1	30	< 100
V	0.3		0.3	1	< 200
Zr				0.3	

strike an arc, and the resulting melt was held in the liquid state for about three minutes to facilitate its homogenization. As a further aid to homogenization, the arc was collapsed, resulting in the solidification of a pancake-shaped billet. This billet was inverted, arc-melted, held liquid, and solidified five more times. Finally, the billet was remelted and drop cast into a 2.5-cm-diameter, water-cooled, copper mold.

These castings were machined to remove surface imperfections and then swaged to 0.32-cm diameter to eliminate casting voids. The final diameter of the low-temperature specific heat capacity specimen was about 1 cm. Due to the added strength in the cold-worked condition, the rods were machined and lapped before annealing. After annealing the iron and nickel specimens at 1100 K and the alloy at 1300 K for 24 hours in vacuums of about 10^{-7} mm of mercury, the specimens were ready for instrumentation.

Chemical analyses of the specimens taken after annealing are shown in Table V. Comparing these analyses with those of the stock materials, it is seen that some contamination occurred during fabrication. In particular, the iron specimen contained 540 ppm oxygen and 370 ppm manganese, whereas the stock material had only 120 ppm oxygen and 10 ppm manganese. The increase in the oxygen content was probably a result of an impure atmosphere in the melting chamber, but the source causing the manganese increase is unknown. Also, the nickel specimen contained 800 ppm iron, though the stock had only 40 ppm. Since the iron specimen was prepared first, it was concluded that the hearth, or mold, was not properly cleaned before fabrication of the nickel specimen. The analysis for the impurities of the Ni_3Fe alloy was by semiquantitative techniques, except

quantitative methods were employed for elements which could have been "picked up" during fabrication — such as oxygen and nitrogen.

These analyses indicate that the nickel specimen was at least 99.89% pure and that the iron specimen was at least 99.79% pure. The alloy was estimated to contain 0.13% impurities by weight and to be 74.77 atomic percent nickel and 25.23 atomic percent iron.

Photomicrographs of the specimens after annealing are displayed in Figures 15, 16, and 17. In Figure 15, both the transverse section and longitudinal section of the nickel specimen are shown in an etched condition at 100x and 500x. (The term 100x refers to a magnification of 100 in the original photomicrograph. Some reduction has occurred in production of these figures. The scale shown in the figure gives the correct magnification.) Little preferred orientation of the grains, resulting from swaging, is noted in the longitudinal sections of Figure 15(c) and 15(d). However, a second phase, presumably an oxide, appears as minute specks in both sections at 500x.

In Figure 16(a) and 16(b), photomicrographs at 500x of the longitudinal and transverse sections of the iron specimen in an etched condition illustrate the extremely fine, striated, preferentially oriented structure present after annealing. In contrast, Figure 16(c), which is for an etched condition and is at 100x, depicts the large, uniform grain structure of the iron specimen after the C_p measurements in the γ region. These measurements required four hours at 1250 K and three 30-second pulses to about 1700 K. Note the subgrain structure of the large grain in the center of Figure 16(d), which was taken at 500x. Also prevalent

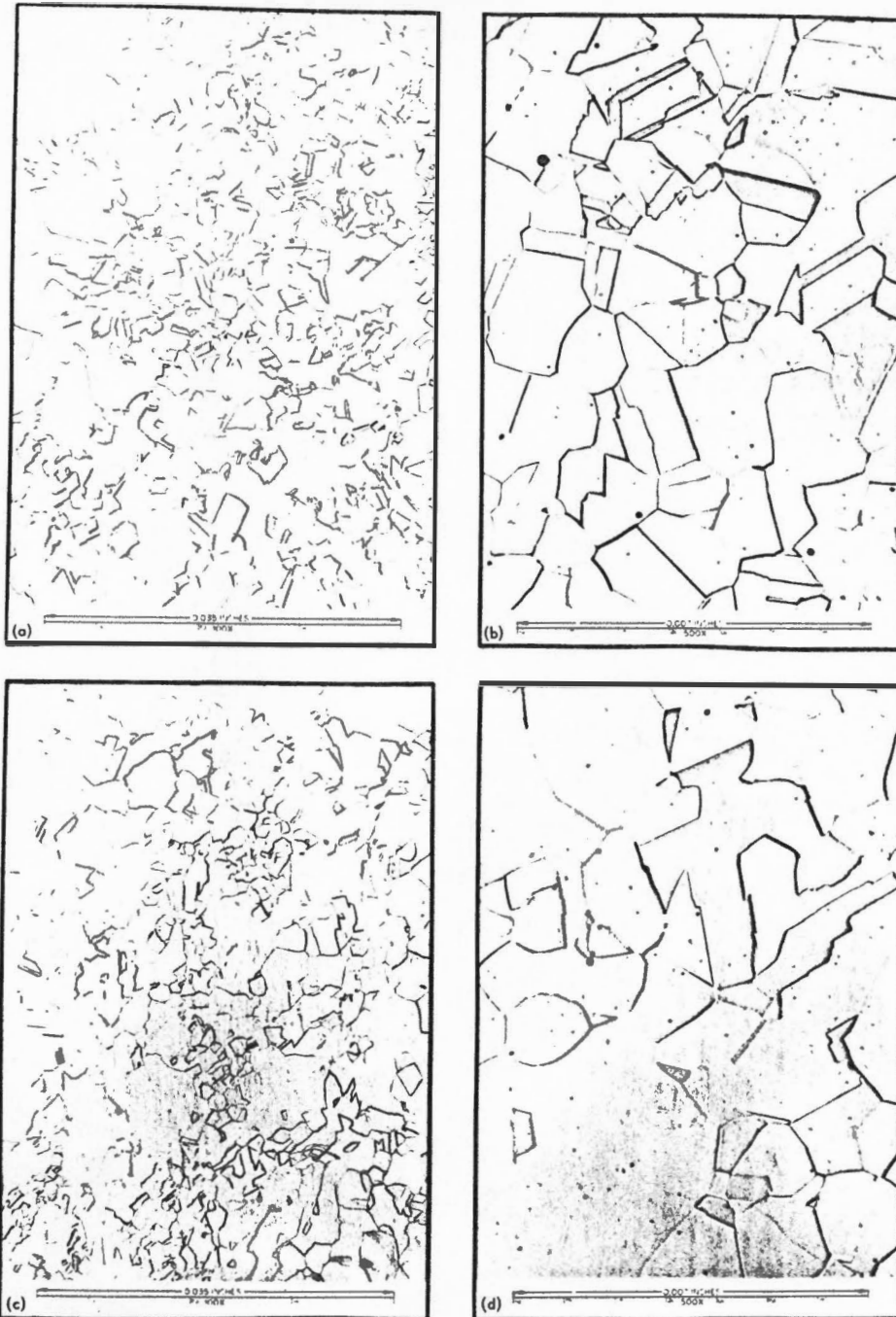


Figure 15. Photomicrographs of the Nickel Specimen in Etched Condition After Annealing. (a) Transverse section at 100x; (b) transverse section at 500x; (c) longitudinal section at 100x; and (d) longitudinal section at 500x. Etchant composition was 60 cubic centimeters acetic acid, 40 cubic centimeters nitric acid, and 0.5 cubic centimeters hydrochloric acid. Note the second phase in (b) and (d).

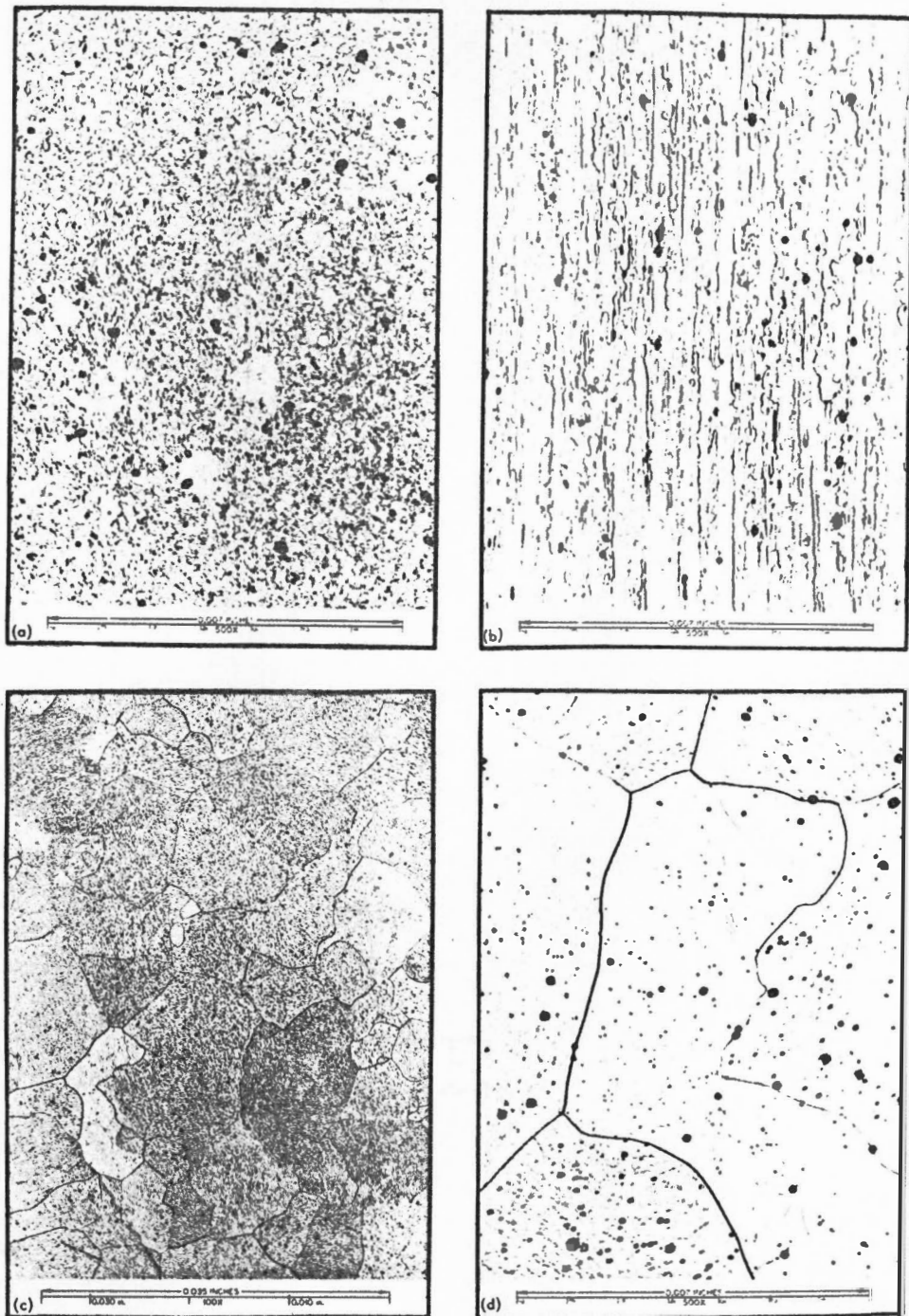


Figure 16. Photomicrographs of the Iron Specimen in Etched Condition. (a) Transverse section at 500x after annealing; (b) longitudinal section at 500x after annealing; (c) transverse section at 100x after C_p measurements in γ -stable region; and (d) same as (c) but at 500x. $Sec-P$ second phase appears as black dots. Note subgrain structure in (d). Etchant was saturated solution of picric acid in ethyl alcohol.

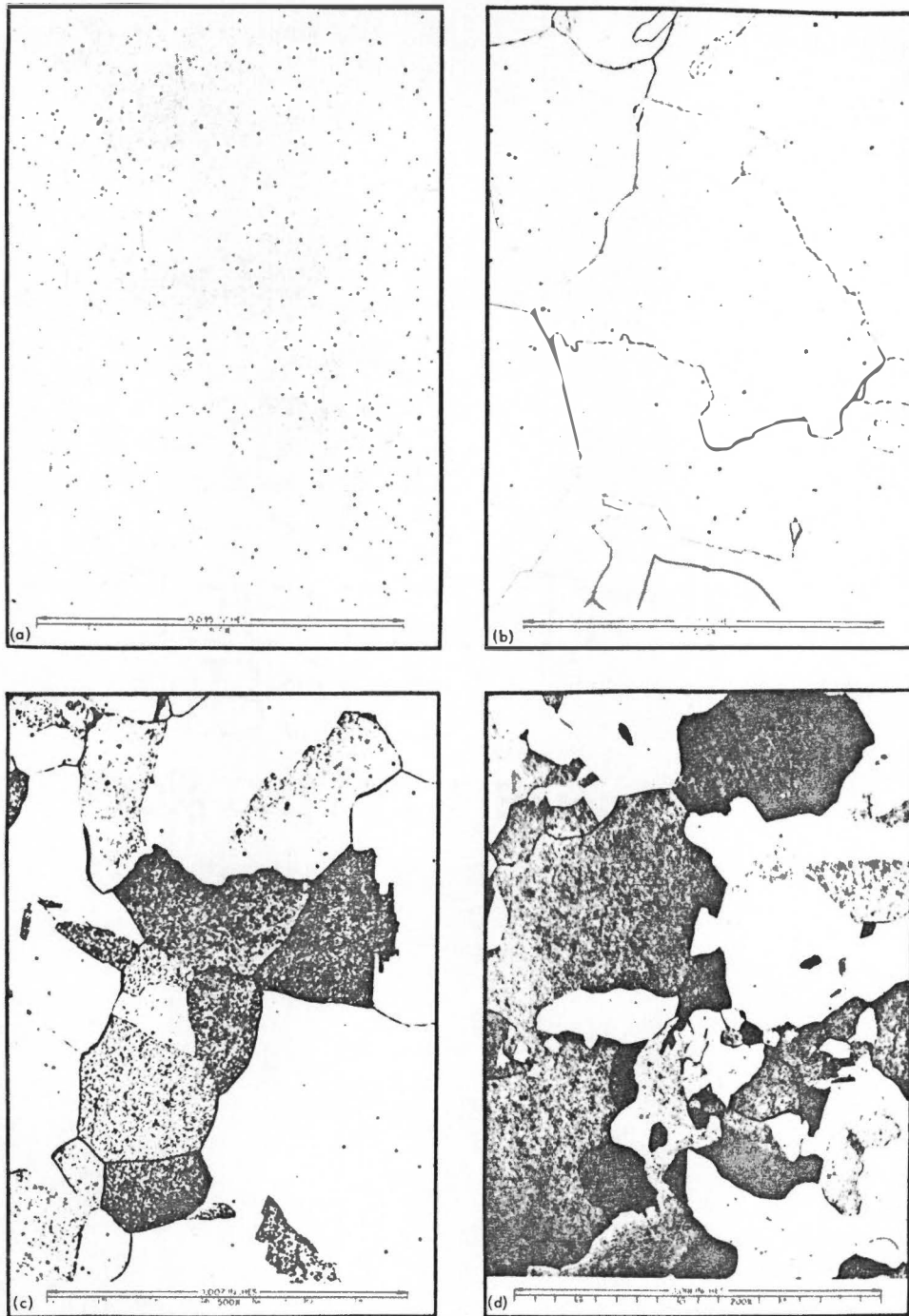


Figure 17. Photomicrographs of Iron and Ni_3Fe Specimens. (a) Longitudinal section of iron specimen at 100X in as-polished condition revealing second phase as black dots; (b) transverse section of disordered Ni_3Fe specimen at 500X etched with a solution of 10% nitric acid, 30% hydrochloric acid, and 30% glycerol (by volume); (c) etched transverse section of disordered Ni_3Fe specimen at 500X; and (d) etched transverse section of disordered Ni_3Fe specimen at 200X. Etchant for (c) and (d) was saturated solution of ammonium persulfate in water.

in this figure is a second phase. This phase is probably an oxide because the iron specimen contained 540 ppm oxygen. From Figure 17(a), the amount of the second phase was estimated to be about 1% by volume.

The microstructure of the Ni_3Fe alloy specimen was similar to that of the nickel specimen except the grain size of the alloy was larger, as can be seen by comparing Figures 17(b) and 15(b). Viting¹⁰⁷ reported that an etch of the alloy with a saturated solution of ammonium persulfate revealed a structure in which the ordered phase appeared white and the disordered phase appeared dark. This etchant was used on the specimen before annealing — a highly disordered state — and on a specimen which had been cooled in a furnace at a rate of 7.5 degrees/minute — a state possessing a small amount of local order. The microstructure of both of these treatments showed a large amount of light and dark areas, and diamond-pyramid hardness tests indicated little difference in the hardness between the light and dark areas of a given treatment. Photomicrographs of the furnace-cooled specimen are shown in Figure 17(c) and 17(d). It is the author's opinion that the difference in brightness of the grains is due only to orientation differences.

Note that a small amount of second phase was present in the alloy. This phase, probably an oxide, is more obvious in Figure 17(c) in which it appears as small black dots.

In recent literature, the ratio of the resistance of a specimen at 298 K to that at 4.2 K has been used as a semiquantitative test of the purity of a specimen. However, this test is not as conclusive for ferromagnetic materials unless the specimen is placed in a magnetic

field large enough to saturate it magnetically. That is, the in-field ratios of a given specimen may be as much as an order of magnitude higher because of the absence of magnetoresistance effects at 4.2 K. On the other hand, out-of-field measurements are helpful. For example, Fulkerson, Moore, and McElroy⁹⁷ report a ratio of 11.5 for a 99.06% pure iron and a ratio of 26.2 for a 99.93% pure iron. These values compare favorably with the value of 25.8 obtained on the 99.79% pure iron specimen of this investigation.

For nickel, Powell, Tye, and Hickman¹⁰⁸ report a ratio of 108 for a "spectrographically pure" (presumably 99.99% pure) nickel specimen. The 99.89% pure nickel specimen of this investigation had a ratio of 38.0.

Voids were not observed in any of the metallographic examinations of samples from the three specimens. Previous experience⁹⁶ has demonstrated that a specimen prepared as described above may be assumed to be 100% dense in the absence of metallographically detectable voids. As further proof of the validity of this assumption, numerous electrical resistivity measurements at room temperature were made along the length of the three specimens using two knife blades separated by a known distance as voltage probes. Variations of $\pm 0.1\%$, the reproducibility of the method, were noted in the resistivity. Also, the absolute value of the resistivity of the iron and nickel specimens was within the experimental error ($\pm 0.3\%$) of literature values of specimens of comparable purity. Consequently, the density of iron (7.874 grams/cubic cm) and nickel (8.902 grams/cubic cm) reported in the Metals Handbook¹⁰⁹ was employed in calculations of the mass of the specimen by Equation (101), page 88.

The theoretical density of the disordered Ni_3Fe alloy was calculated from the lattice parameter data of Wakelin and Yates⁸⁴ and found to be 8.5745 grams/cubic cm. Density measurements by a water immersion technique yielded a value of 8.6065 grams/cubic cm. The average of these two values 8.59 grams/cubic cm was used in Equation (101) to calculate the mass of the alloy.

CHAPTER III

RESULTS AND DISCUSSION

In this chapter, the experimental results on nickel, iron, and Ni_3Fe are presented and compared with values from the open literature. Calculations of the quantities C_{vm} , ΔC_{vm} , U_{vm} , and S_{vm} - which are associated with the ferromagnetic state of these solids - are given and are discussed with respect to the theories presented in Chapter I. The energy and entropy of the order-disorder transformation of Ni_3Fe are calculated, and the effects of this transformation on the various measured and calculated quantities are presented and discussed.

Specific Heat Capacity of Pure Nickel and Iron

Smoothed values of the specific heat capacities of pure nickel and iron are presented as a function of temperature in Figures 18 and 19, respectively. These values were obtained from plots of the data acquired using Pulse Calorimeter II. The scales of these plots were chosen to maintain four significant digits in C_p and the nearest half degree in T . A smooth curve was drawn through these plotted data in a manner such that the 99% accuracy of the method was not affected. Figure 20 is typical of these plots and depicts the C_p of nickel between 700 and 850 K. In this figure, data from three separate pulses are plotted at increments of two and one-half degrees. Note that pulse one has about a one percent oscillation from the smooth curve between 725 and 750 K. A similar oscillation also appeared in the calculated value of dT/dt of pulse one and was attributed to a series of small spikes in the temperature signal which were not completely removed by the data screening or data smoothing techniques.

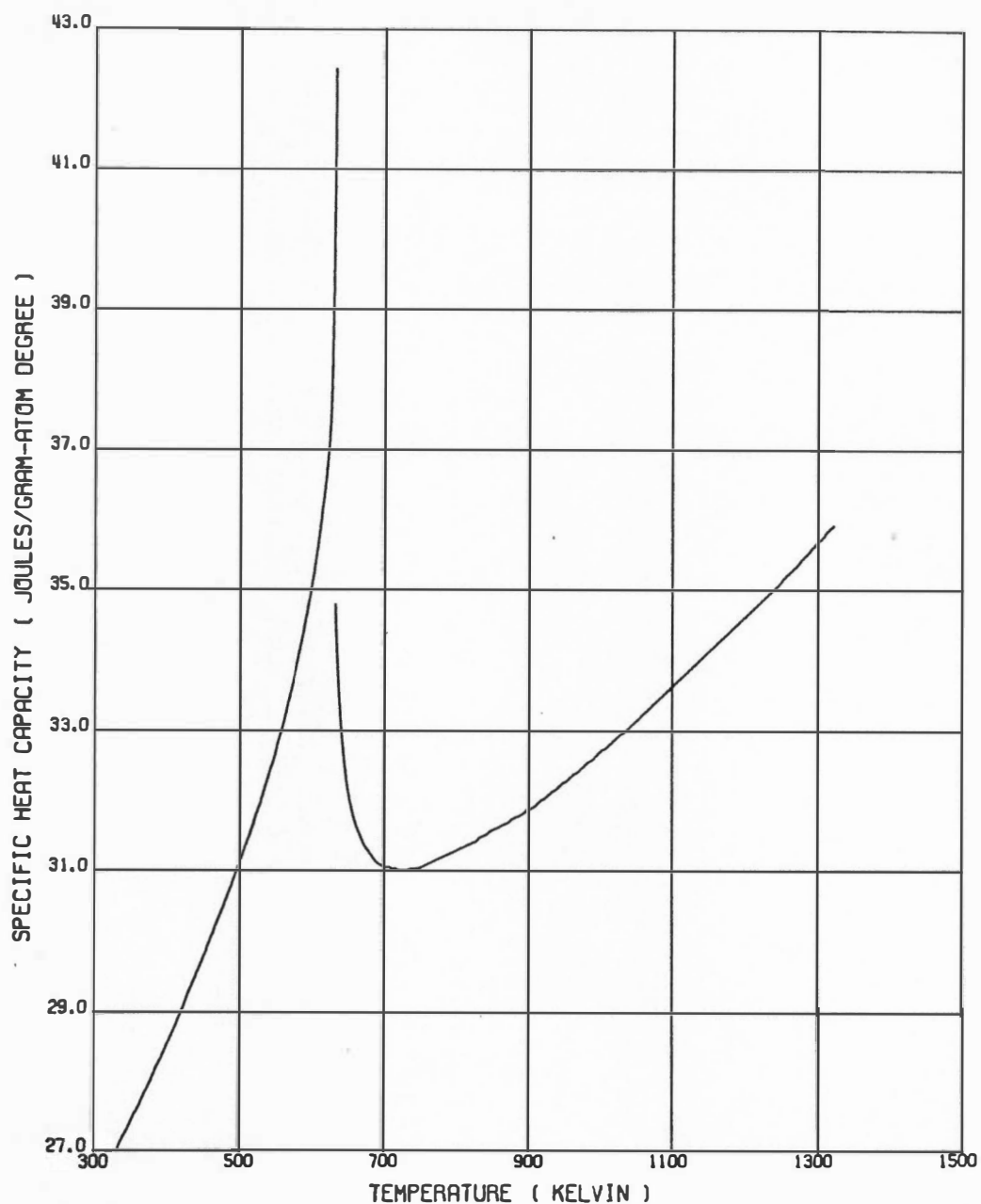


Figure 18. Smoothed Values of the Specific Heat Capacity of Nickel from 333 to 1323 K Determined by This Investigation. Note the discontinuity of 7.64 joules/gram-atom degree at 633 K, the Curie temperature.

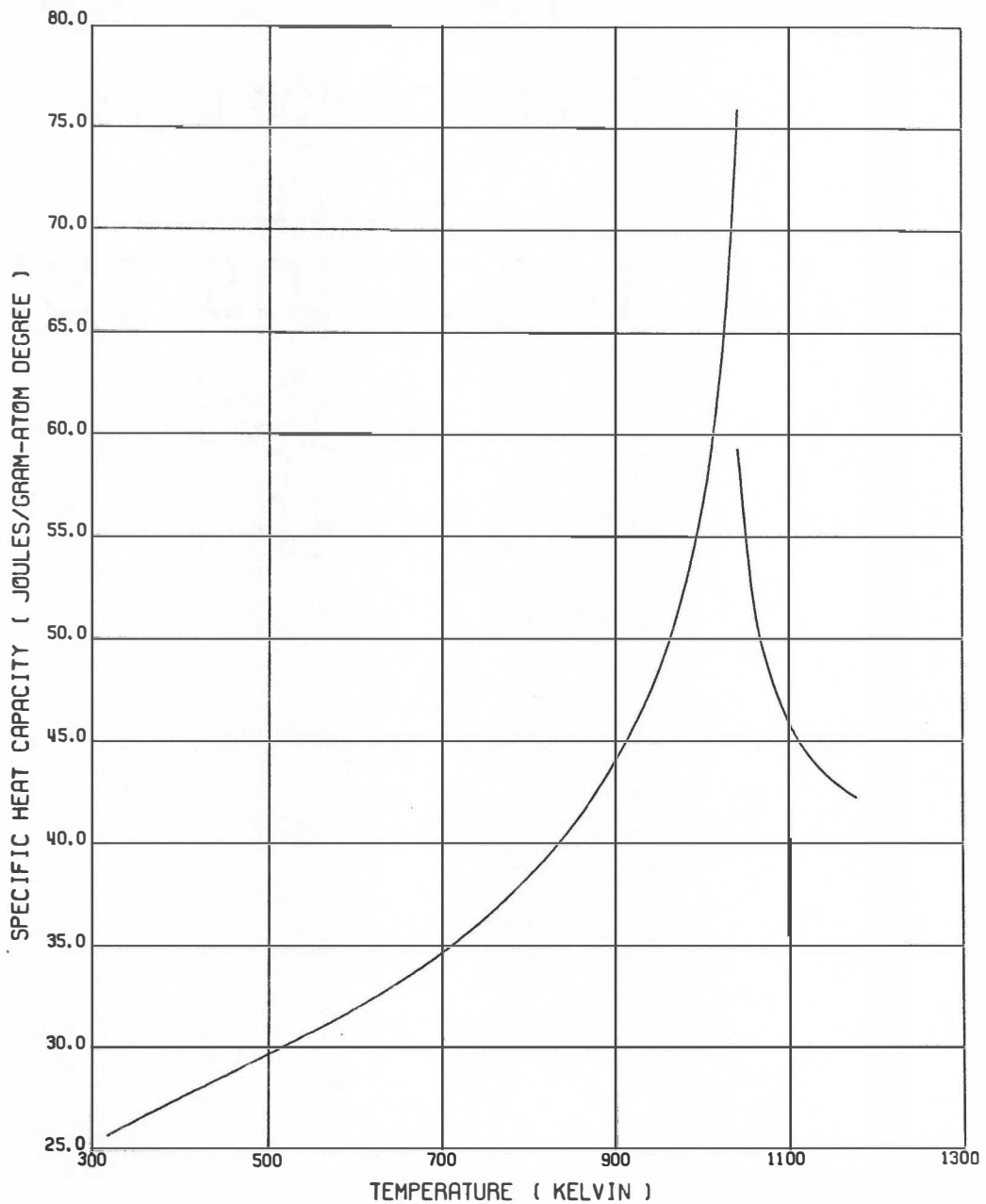


Figure 19. Smoothed Values of the Specific Heat Capacity of α -Iron from 318 to 1178 K Determined by This Investigation. Note the discontinuity of 16.64 joules/gram-atom degree at 1043.2 K, the Curie temperature.

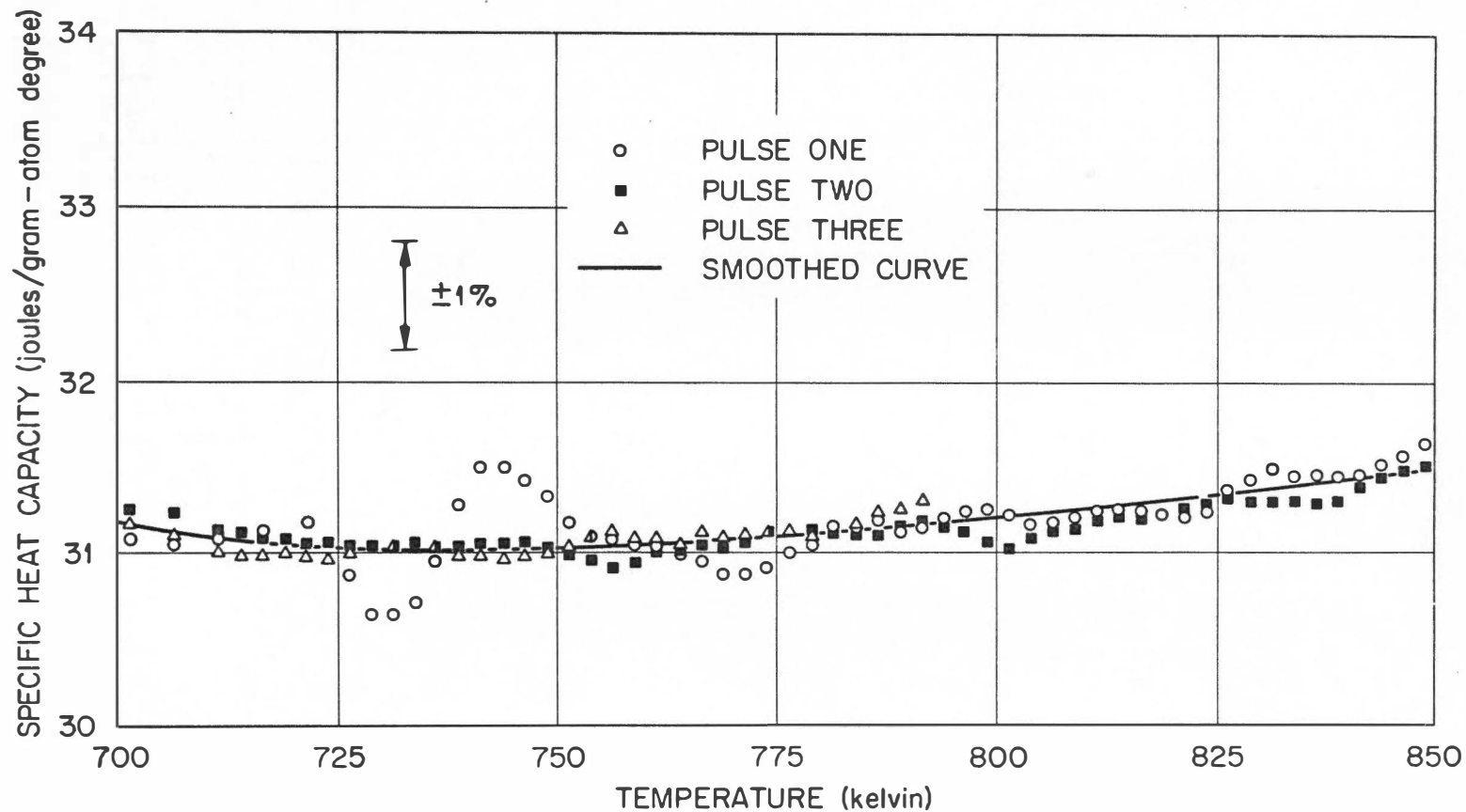


Figure 20. Typical Plot of Raw Data Used to Obtain Smoothed Values of C_p as Function of T . Raw data from three pulses are shown as well as the curve from which smoothed values were chosen.

The cause of the spikes - a dirty contact in the oscillator of the temperature circuit amplifier - was discovered after most of the data on nickel and iron were obtained. However, the effects were not significant enough to warrant repetition of these measurements. Fortunately, the measurements on the Ni_3Fe alloy were made either before the oscillator became faulty or after it was repaired. Consequently, the data on the alloy were not smoothed. For completeness, the smoothed values of C_p of nickel and iron are listed as a function of temperature in Tables XXI and XXII in the Appendix.

For the sake of comparison, the measurements of the specific heat capacity of nickel and iron of several other investigators are presented in Figures 21 and 22 as difference plots based on the measurements of the author. Most of these measurements are within $\pm 2\%$ of the author's. Since $\pm 2\%$ represents the combined errors of the author and the other investigators, these measurements are essentially in agreement. However, two regions of significant disagreement are evident from these figures, namely in the vicinity of the Curie transformations and at high temperatures. It is the author's opinion that these differences are due to experimental difficulties in these two regions, and cannot, for example, be attributed to impurity effects.

Measurements of C_p Near the Curie Temperature of Ferromagnets

Due to the definition of the specific heat capacity, it can be measured only by techniques in which the temperature of the specimen is changed. Most methods of direct measurement produce this temperature

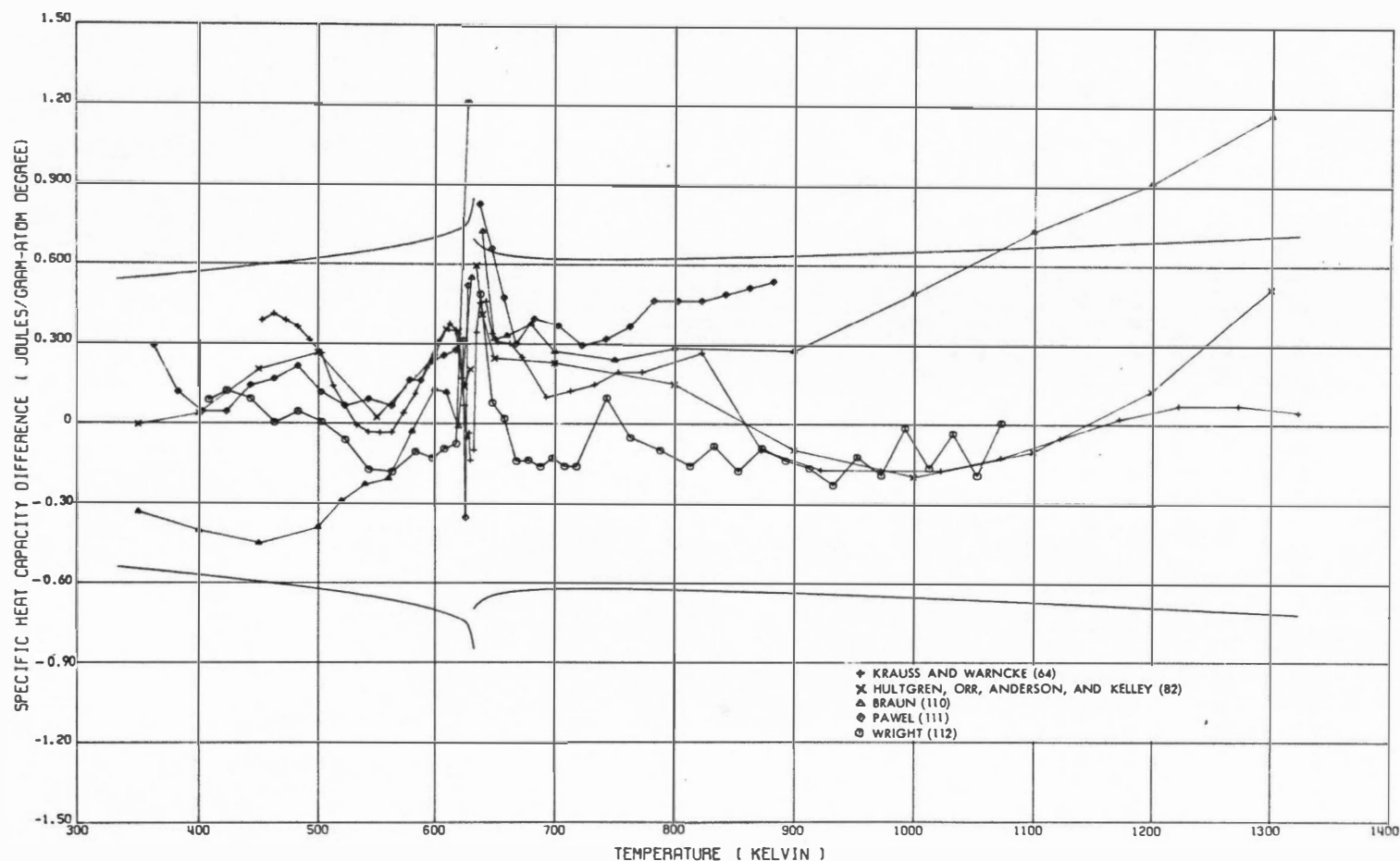


Figure 21. A plot of the Specific Heat Capacity of Nickel of this Investigation Minus that of Five Other Investigations from 333 to 1323 K. The solid curves represent $\pm 2\%$ deviations from the values of this investigation. Numbers in parentheses in legend are reference numbers.

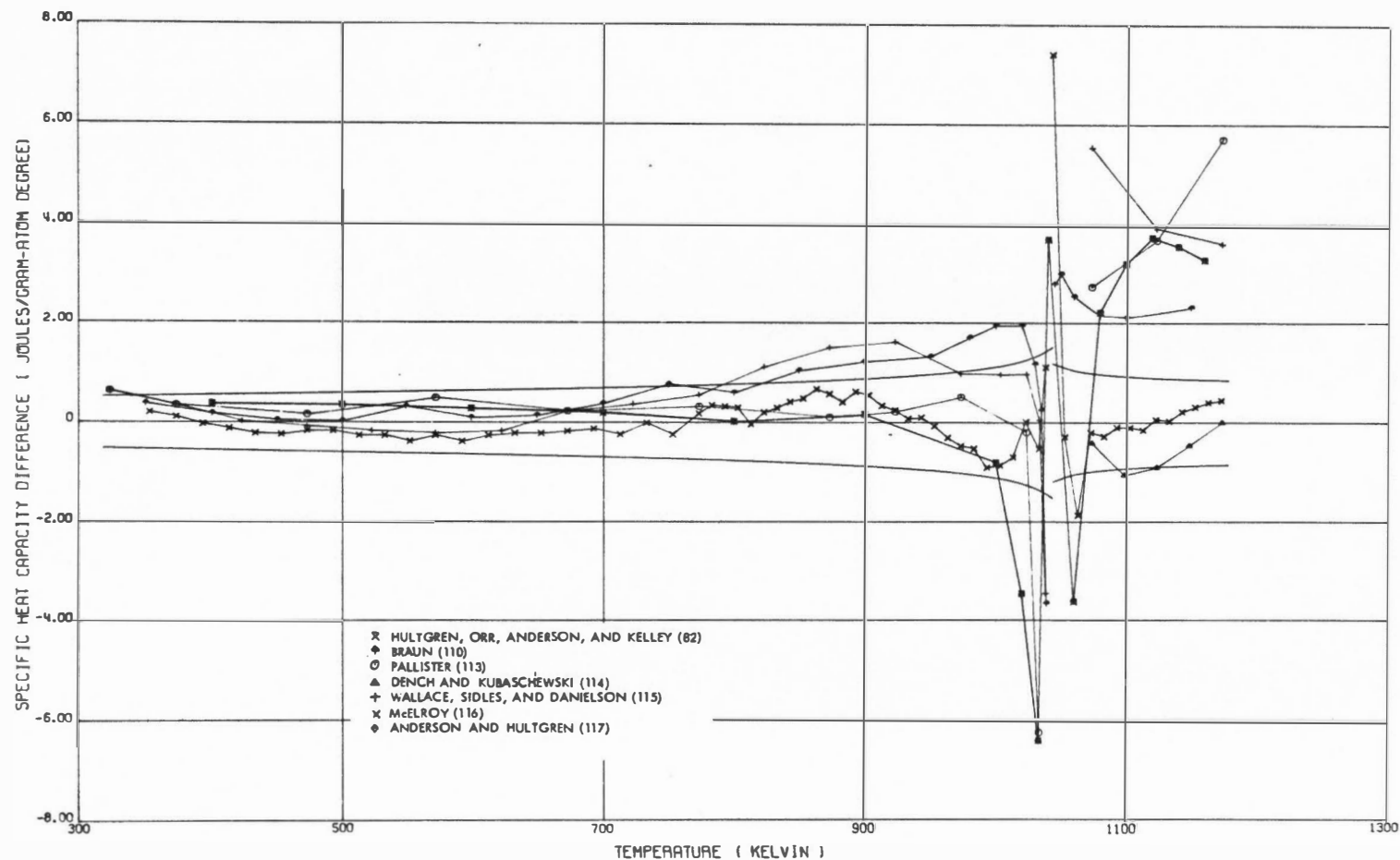


Figure 22. Plot of the Specific Heat Capacity of α -Iron of this Investigation Minus that of Seven Other Investigations from 318 to 1178 K. The solid curves represent $\pm 2\%$ deviations from the values of this investigation. Numbers in parentheses are reference numbers.

change by means of electrical power, which necessitates the measurement of the temperature of the specimen as a function of time. The requirement of a transient specimen temperature leads to extreme difficulties in C_p measurements at the critical temperature of a second-order transformation. It is the author's opinion that this is the reason for the large discrepancies between the various measurements of the specific heat capacity of nickel and iron near their Curie transformations. The following detailed argument is given to support this hypothesis.

Near the Curie temperature T_c , the temperature-time relationship of the specimen of an adiabatic or pulse calorimeter operating with a slowly increasing power is shown in Figure 23(a). (The case for a decreasing power is similar but is not presented.) If the specimen is completely isothermal, the temperature-time relationship will be that of the ideal curve of this figure. However, when the specimen has a temperature gradient within it, the temperature-time relationship will be smoothed as shown. The temperature-rate-of-change dT/dt and C_p obtained using these relationships are depicted in Figure 23(b) and 23(c). Note that the C_p values below T_c are too low and those above T_c are too high for the smoothed relationship. Also, the maximum C_p occurs below the true Curie temperature for the smoothed case and the maximum value of C_p is much lower than that for the true relationship.

Suppose, on the other hand, that the temperature-time relationship is ideal or that the temperature gradient in the specimen is small (the order of a tenth of a degree). Using an adiabatic calorimeter, the

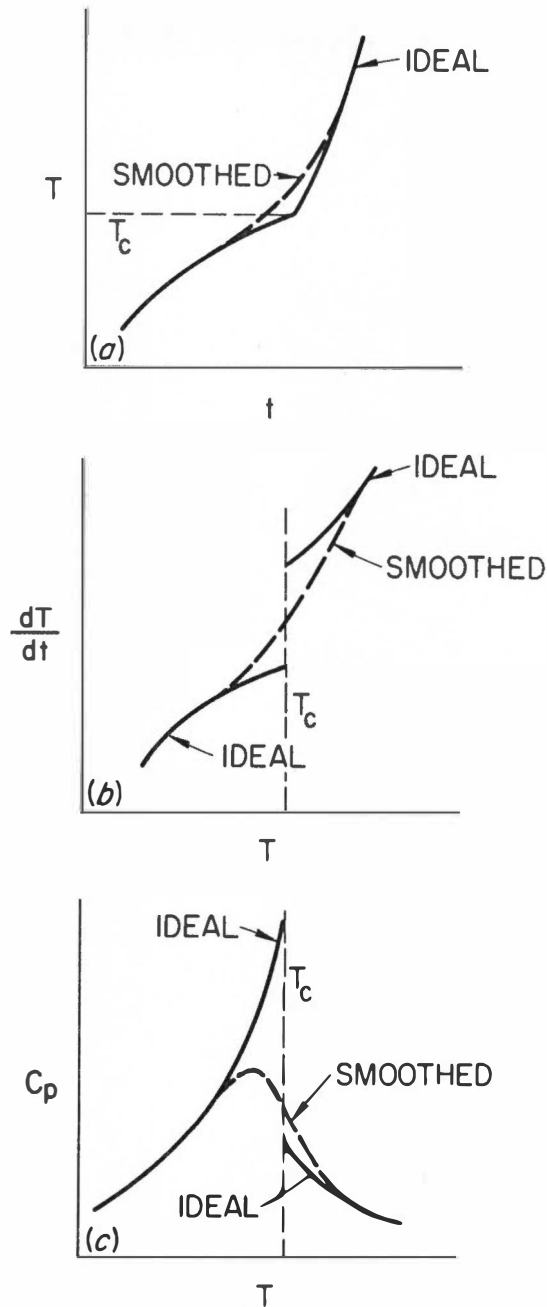


Figure 23. Effect of a Temperature Gradient in the Specimen of an Adiabatic or Pulse Heating Calorimeter During C_p Measurements Near the Curie Temperature T_c of a Ferromagnet. (a) Temperature T of specimen versus time t during measurement. (b) Temperature-rate-of-change dT/dt of specimen versus T of specimen. (c) C_p of specimen versus T of specimen. Both the ideal (no gradient) and smoothed (with gradient) results are shown for a slowly increasing specimen power.

temperature interval used in calculating $\Delta T/\Delta t$ must be small (less than about a degree) and must not span the Curie temperature in order to yield accurate values of C_p . With the pulse calorimeter used in this work, it is necessary to treat the data above and below T_c separately in order to obtain accurate C_p values. To accomplish this, the exact value of T_c must be known. How then does choosing the wrong Curie temperature affect the values of C_p derived with this technique? Consider Figure 24 and remember that the data are smoothed twice using a second-order polynomial in time before dT/dt is calculated. This figure shows the effect on T , dT/dt , and C_p if the temperature T_b is chosen above T_c . Note that below T_c , the C_p values are too low, but between T_c and T_b the C_p values are too high. Above T_b , the calculated values of C_p are correct.

In Figure 25, an example for which too low a Curie temperature has been selected is presented. For this choice, the C_p values below T_b are correct, the C_p values between T_b and T_c are too low, and the values above T_c are too high. Obviously, treating the data above and below T_c as an entity, that is without selecting a T_b , yields the results shown in Figure 23.

The qualitative argument discussed above is now made quantitative by presentation of a particular example of various treatments of data taken near T_c of nickel in Pulse Calorimeter II. The data used in this example are very representative of that acquired on nickel and iron. For example, the furnace temperature was about 570 K, and the heating and cooling rates of the specimen at this temperature were 8.0 and 0.09 degrees/second, respectively. A maximum specimen temperature of 870 K was achieved at the end of the pulse, where the heating and cooling rates of the

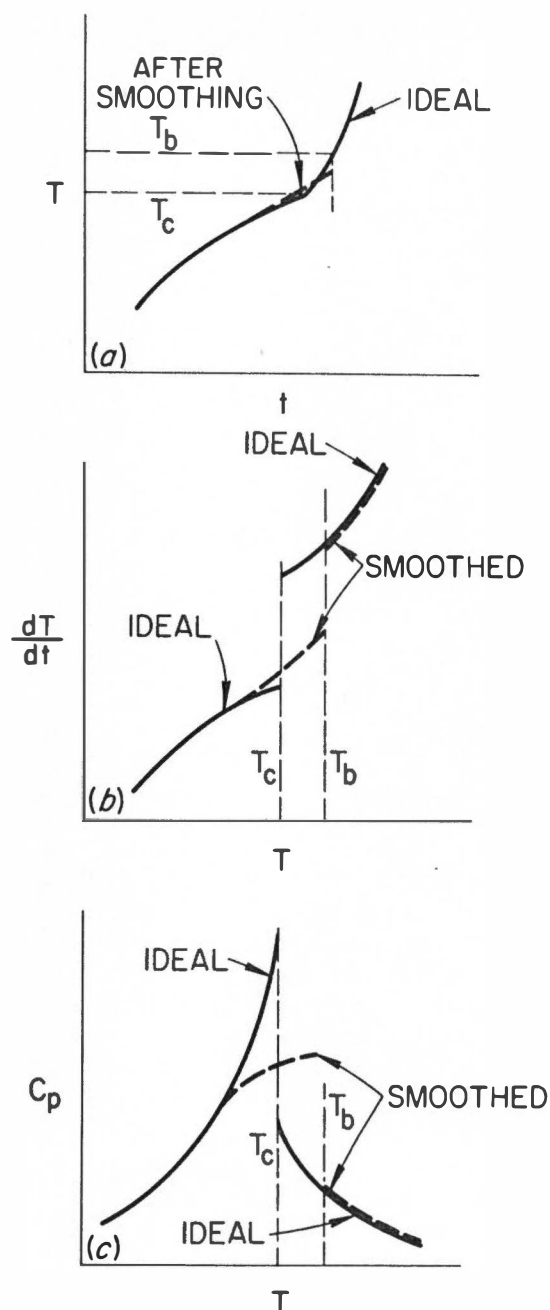


Figure 24. Effect of Choosing a Break Temperature T_b Which is Above the True Curie Temperature T_c in a Pulse Calorimetric Measurement of the Specific Heat Capacity of a Ferromagnet. (a) Temperature T of specimen versus time t during measurement. (b) Temperature-rate-of-change dT/dt of specimen versus T of specimen. (c) C_p of specimen versus T of specimen. Results for the correct choice (ideal curve) and incorrect choice (smoothed curve) of T_c are shown.

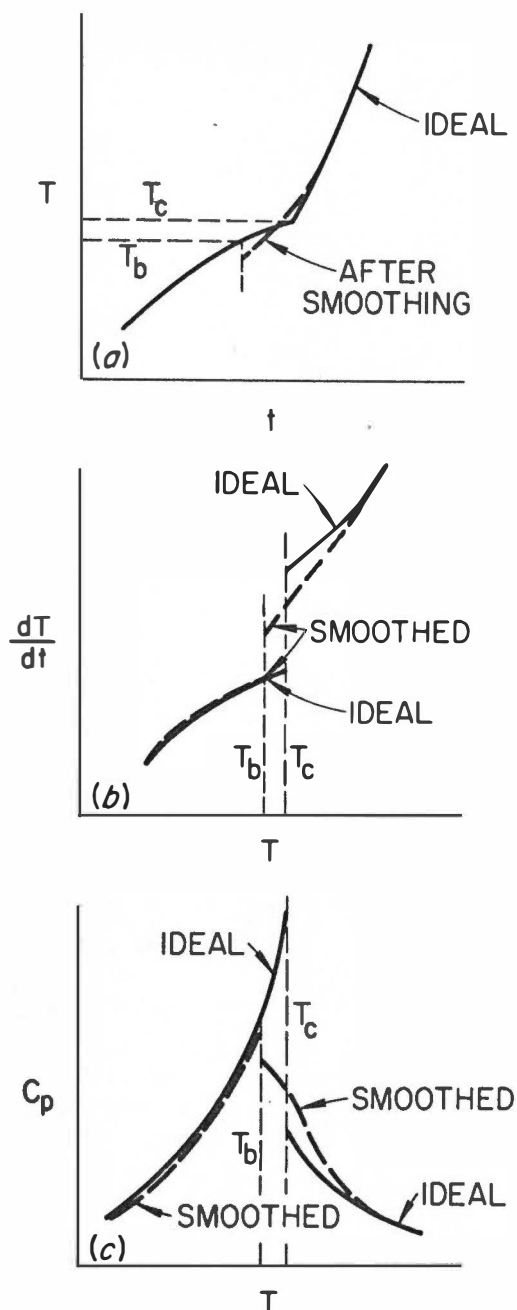


Figure 25. Effect of Choosing a Break Temperature T_b Which is Below the True Curie Temperature T_c in a Pulse Calorimetric Measurement of the Specific Heat Capacity of a Ferromagnet. (a) Temperature T of specimen versus time t during measurement. (b) Temperature-rate-of-change dT/dt of specimen versus T of specimen. (c) C_p of specimen versus T of specimen. Results for the correct choice (ideal curve) and incorrect choice (smoothed curve) of T_c are shown.

specimen were 12.3 and 0.90 degrees/second, respectively. At the Curie temperature, 633.0 K, the heating rate was about 10 degrees/second and the cooling rate was about 0.1 degree/second. Also, from the steady-state temperature measurements, the longitudinal temperature gradient on the test section of the specimen was estimated to be 0.5 degree/cm. From qualitative heat transfer arguments, it was estimated that the measuring thermocouple was affected by specimen material which varied in temperature by as much as one degree. Hence, C_p values obtained within ± 1.0 degree of T_c cannot be expected to be correct because some of the specimen will have transformed and some will not have transformed.

In order to select T_c , every fifth point of the temperature signal recorded on the DVM was plotted as shown in Figure 26. These points were approximately 45 milliseconds apart in time and 0.45 degree apart in temperature. Note that the straight line drawn between points 20 and 105, a temperature span of 7.3 degrees, fits these data to within $\pm 0.1\%$. Likewise the straight line between points 100 and 170, a temperature span of 6.3 degrees, describes these data to within $\pm 0.1\%$. These two lines are not parallel and intersect at a point corresponding to 633.2 K. This plot, per se, is ample proof that the Curie transformation is second order because even though a temperature gradient existed within the sample, the slope of the temperature-time relationship is obviously discontinuous at T_c . Therefore, C_p is discontinuous at T_c , the criterion for a second-order transformation.

Another plot which is extremely useful in choosing T_c is shown in Figure 27. Here every fifth voltage signal of the test section recorded

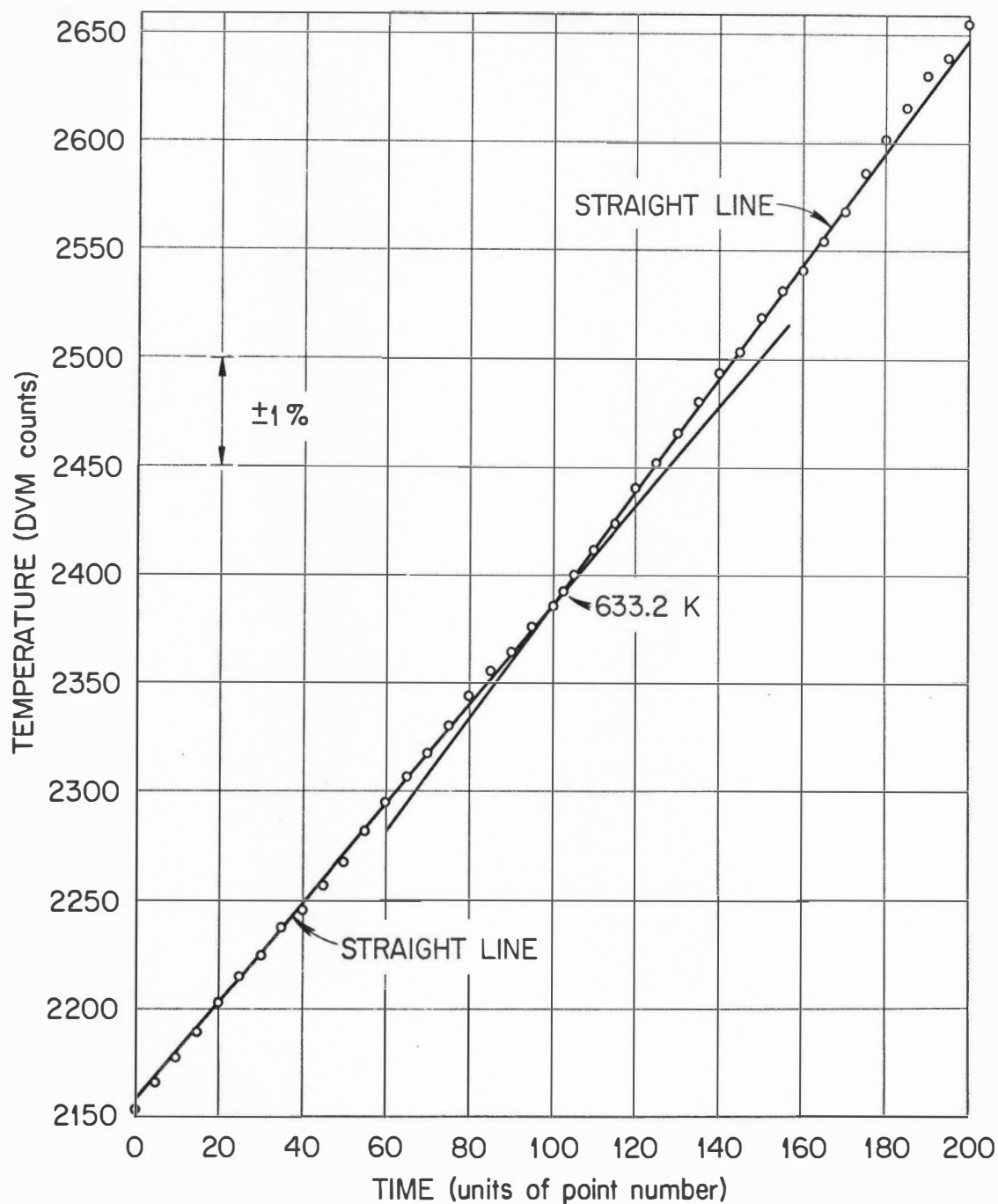


Figure 26. Plot of Temperature of Specimen as Function of Time from Data Recorded on DVM During Heating of the Specimen Through its Curie Transformation. Every fifth temperature point recorded is shown. These points are separated by 0.45 degree in temperature and 45 milliseconds in time. Note the discontinuity of slope at the Curie temperature, 633.2 K.

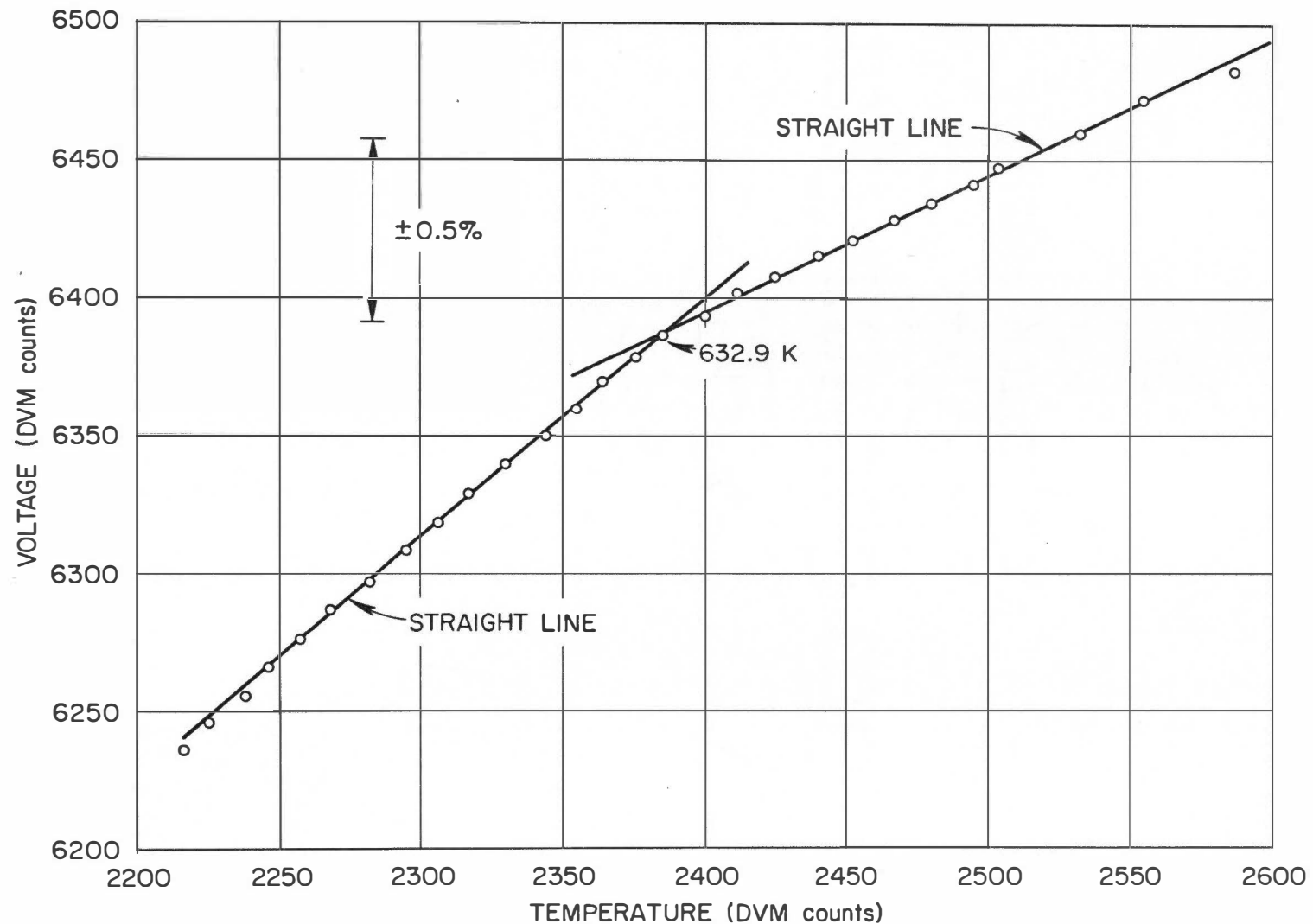


Figure 27. Plot of Voltage Across Test Section of Specimen as a Function of Specimen Temperature from Data Recorded on DVM During Heating of the Specimen Through Its Curie Transformation. Every fifth point recorded is shown. These points are separated by 0.45 degree. Note the discontinuity of slope at the Curie temperature, 632.9 K.

on the DVM is plotted versus the temperature signal. The difference in slope of the two straight lines drawn through these data is more obvious than the previous example. This is due, of course, to the compounding of the discontinuities of C_p and dp/dT at T_c , the voltage being directly proportional to the electrical resistivity ρ with a constant current through the sample. This method yielded a T_c of 632.9 K. Since this method of determining T_c is more reliable due to the sharper discontinuity of the slopes, a Curie temperature of 633.0 K was selected as the true Curie temperature of pure nickel.

Figure 28 shows the results of five different treatments of the data of a single pulse on nickel near T_c as well as the smoothed values shown in Figure 18, page 102. Note that smoothing the data twice as an entity with a 151 point group (hereafter referred to as PG), produces the "smoothed" results of Figure 23, page 109. With the heating rate employed in obtaining these data, a 151 PG corresponds to a 13.5 degree temperature interval. It is significant that the maximum value of 37.4 joules/gram-atom degree occurs at 627 K for this treatment. Approximately this C_p value and temperature are reported as the maximum C_p and Curie temperature by several of the investigators mentioned previously, suggesting that their measurements were made without proper regard to the Curie transformation effects.

Of the four other treatments shown in Figure 28, two are for selected Curie or "break" temperatures above the true T_c and two are for below the true T_c . These are included to show the differences obtained with two sizes of the temperature-time smoothing group in calculating

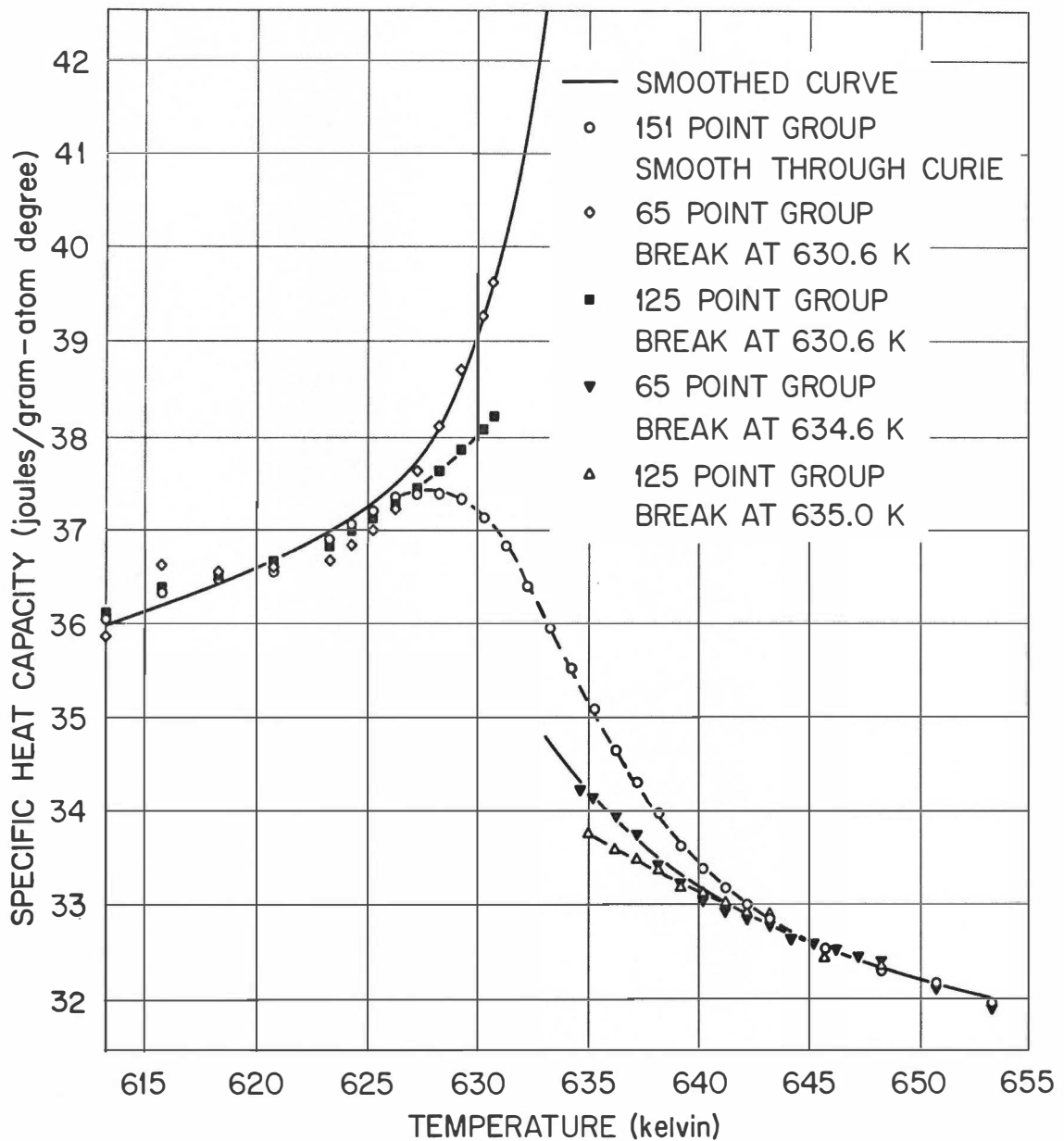


Figure 28. Effects on the Calculated Values of the Specific Heat Capacity Resulting from Five Different Treatments of the Data of a Single Pulse on Nickel Near the Curie Temperature, 633.0 K. Smoothed (reported) curve of Figure 18, page 102, is also shown. See text for discussion.

dT/dt , namely a 65 PG and a 125 PG corresponding to temperature intervals of 5.9 and 11.3 degrees.

With a selected break temperature of 630.6 K, which is 2.4 degrees below the true T_c , the values obtained below T_c with a 125 PG smooth are too low. This is because a second-order polynomial in time did not properly describe the temperature-time relationship over a 11.3 degree interval immediately below T_c . However, below 625 K the second-order polynomial in time is sufficient because the values obtained with the 125 PG and 65 PG are essentially the same. Although not shown in this figure, a 45 PG — a 4.0 degree interval — was used and yielded essentially the same values as the 65 PG. Use of this smaller PG size was not desirable due to the larger oscillations in C_p that are obtained. This effect can be seen between 613 K and 623 K in Figure 28 when the results of the 65 PG and 125 PG treatments are compared.

The results obtained with the break temperatures selected above the true T_c are completely analogous. That is, the 125 PG is too large for treatments in the immediate vicinity of T_c .

Figure 29 depicts results obtained when temperatures 2.8, 2.4, 2.0, and 0.5 degrees below the true T_c were selected as the break temperatures. All computations were made using a 65 PG. Note that the values obtained using a Curie point of 632.5 K are too low below T_c because of the temperature gradient in the sample. Using the Curie temperatures of 630.2, 630.6, and 631.0 K, only the data above these temperatures are in error as predicted in Figure 25, page 112.

Figure 30 is completely analogous to Figure 29, except that break temperatures 0.1, 0.9, and 1.6 degree above the true T_c were used. Only

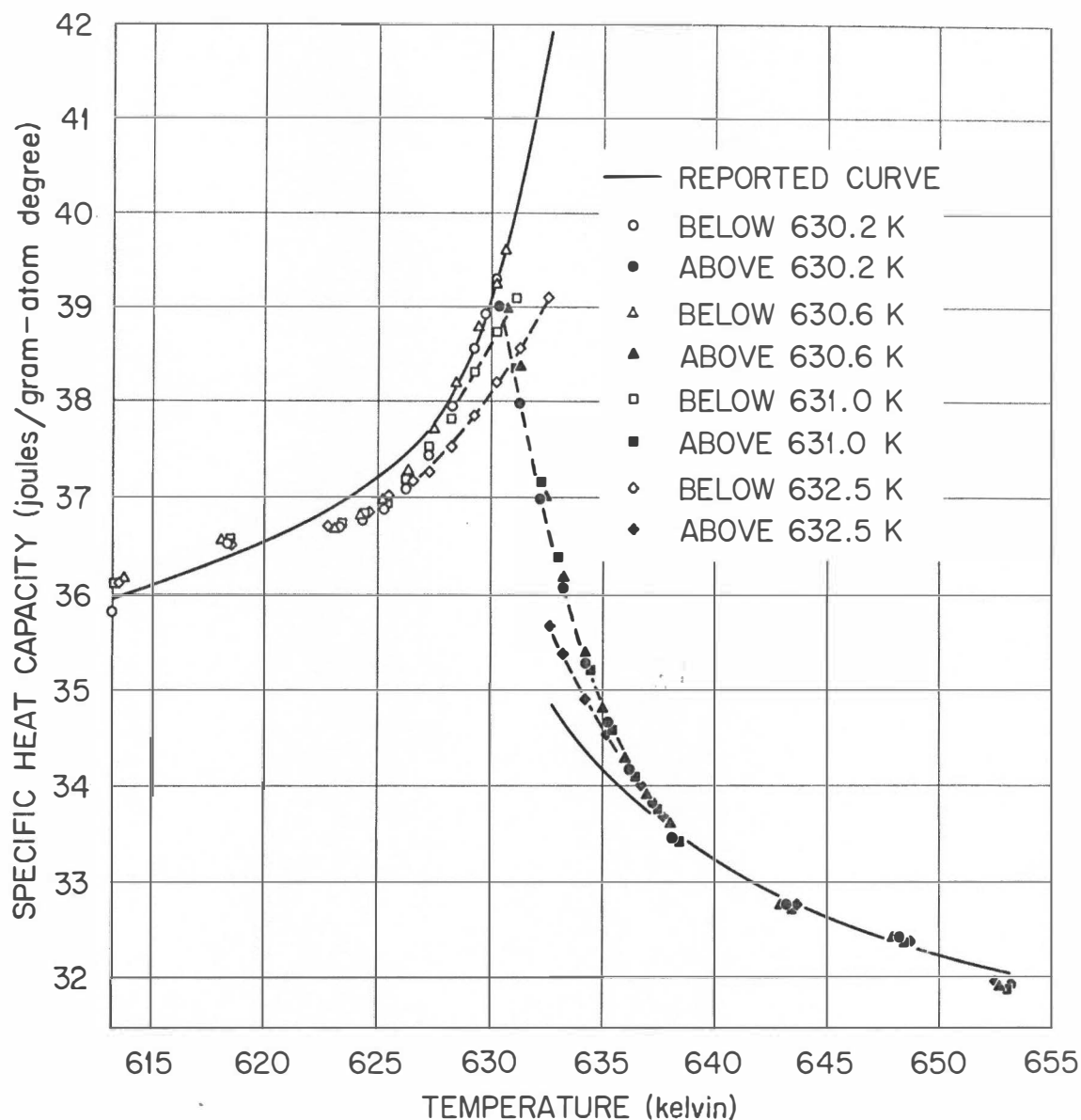


Figure 29. Effects on the Calculated Values of the Specific Heat Capacity Resulting from Choosing Four Break Temperatures Below the True Curie Temperature. A 65 point group was used for all calculations on the data of a single pulse near T_c of Nickel. Smoothed (reported) curve of Figure 18, page 102, is also shown. See text for discussion.

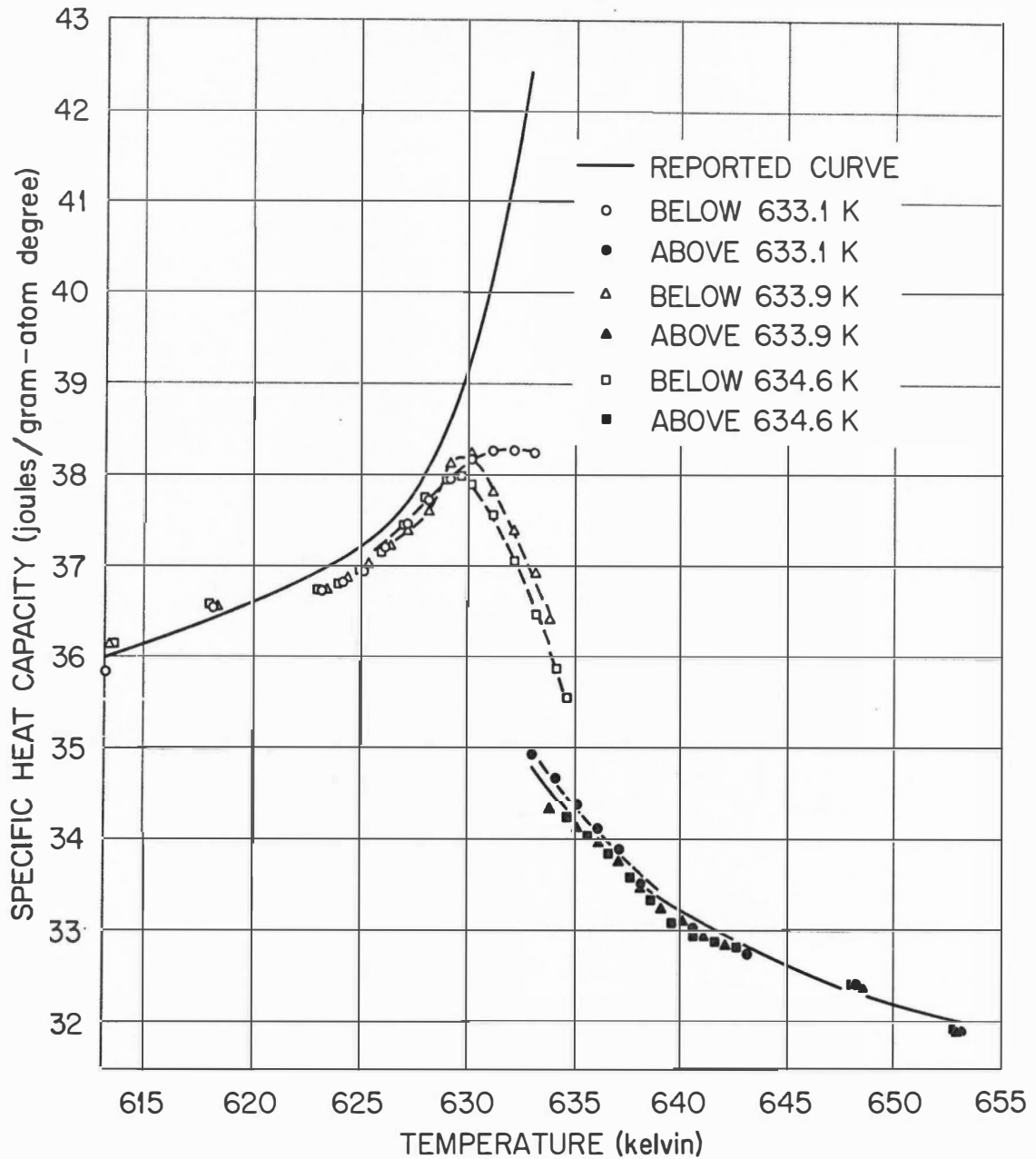


Figure 30. Effects on the Calculated Values of the Specific Heat Capacity Resulting from Choosing Four Break Temperatures Above the True Curie Temperature. A 65 point group was used for all calculations on the data of a single pulse near T_c of nickel. Smoothed (reported) curve of Figure 18, page 102, is also shown. See text for discussion.

the values below the T_c are in error as predicted in Figure 24, page 111. Notice that missing T_c by only 0.1 degree seriously affects the C_p values below T_c .

To recapitulate, great care must be exercised in measuring the specific heat capacity near the Curie temperature of ferromagnets. In particular, temperature gradients in the sample must be eliminated as much as possible; the functional form assumed for the temperature-time relationship used in calculating dT/dt must be correct; and calculations must not span the true Curie temperature. Use of a recording digital voltmeter is extremely advantageous in these measurements because the data can be treated in many different ways to obtain meaningful results as shown in Figures 28, 29, and 30.

Measurements of C_p of Nickel and Iron Above 1200 K

At temperatures above 1000 K, accurate specific heat capacity determinations become increasingly difficult. In particular, thermocouple thermometry errors occur because of the breakdown of the electrical insulation material in which the thermocouples are sheathed and because of contamination of the thermocouples by their environment. The latter was the principal complication encountered in the measurements of C_p of iron and nickel above 1200 K.

The solid $C_p:T$ curve of Figure 31 was obtained on the nickel specimen in Calorimeter II using pulses from furnace temperatures of less than 1100 K. When the furnace temperature was raised to 1220 K and pulses to 1500 K were performed, the C_p values calculated with the thermocouples

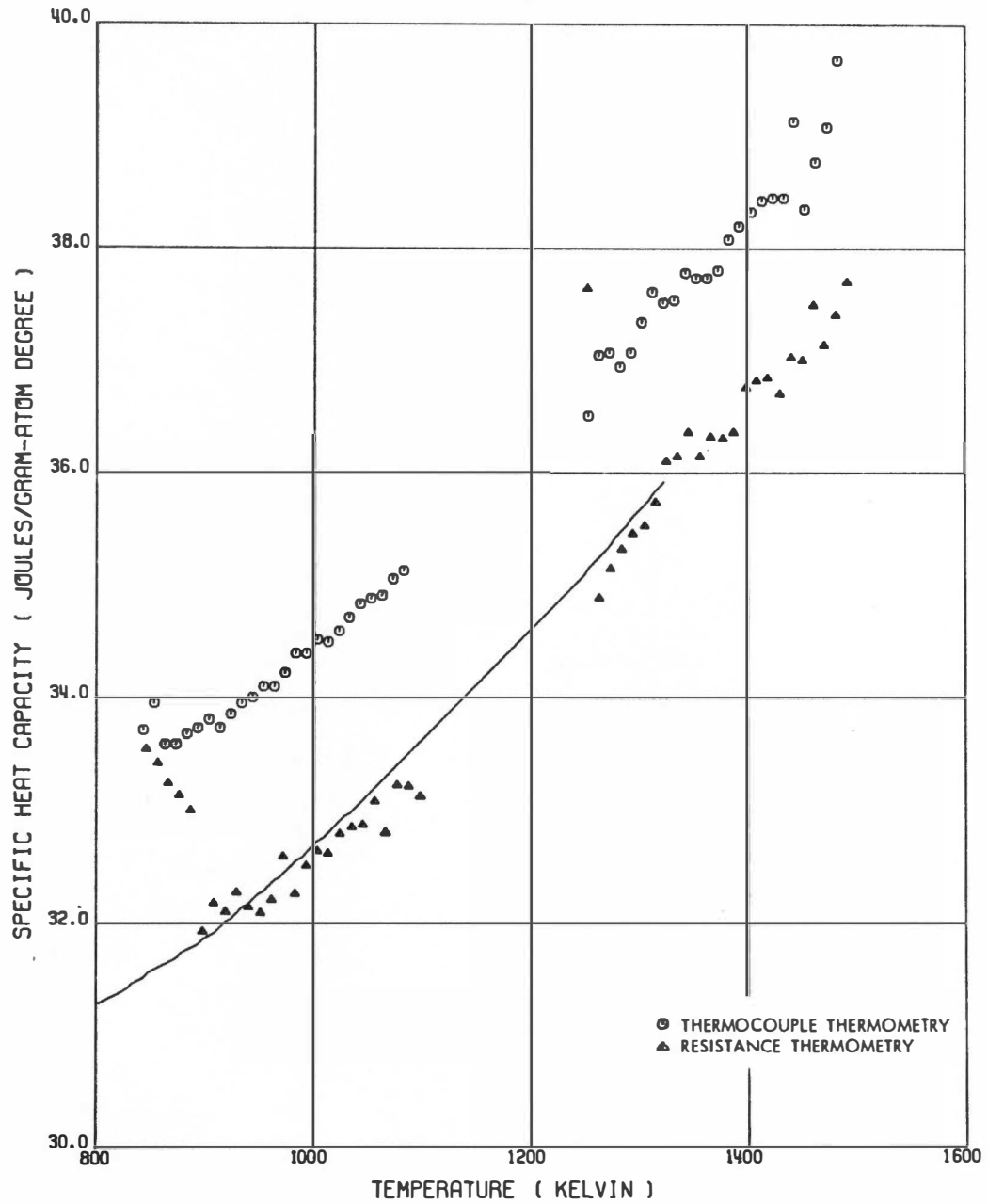


Figure 31. Illustration of Errors in Measured Values of C_p of Nickel Resulting from Contamination of Thermocouples. Solid curve obtained from pulses with furnace temperatures below 1100 K and the data shown as points were acquired after a furnace temperature of 1220 K had been employed.

as temperature sensors were about 5% too high, as shown in Figure 31. Subsequently, the furnace temperature was lowered to 840 K, and the C_p values obtained from a pulse to 1080 K were about 6% high. However, when the data from these two pulses were recalculated using the specimen as its own resistance thermometer, the C_p values were found to be within the experimental error of those obtained previously. This confirmed that the thermocouples had been contaminated after the furnace temperature was raised to 1220 K.

Examination of the specimen thermocouples after these measurements revealed that they had been coated with nickel. This is understandable because at 1220 K the vapor pressure of nickel is within an order of magnitude of the pressure which was maintained in the furnace (10^{-7} millimeters of mercury). In addition, it is believed that during a pulse, large temperature gradients occur within the thermocouples near their junction with the specimen. This gradient would greatly amplify the error producing effects of inhomogeneities in the thermocouples caused by their contamination with nickel.

Similar results were observed during the measurements of the C_p of γ -iron. Due to the slow kinetics of the α - γ transformation, C_p measurements on γ -iron could not be made with pulses from the lower temperature α -stable region. This necessitated heating the furnace to about 1200 K and allowing the transformation to occur before C_p measurements. Values of C_p acquired in subsequent pulses were 10 to 20% too high and did not have the correct temperature dependence. However, when these data were recalculated using the specimen as its own resistance thermometer, the

C_p values computed between 1200 and 1500 K substantiated those of Dench and Kubaschewski,¹¹⁴ as shown in Figure 32.

The results on iron and nickel discussed above were obtained using Pt-10% Rh versus Pt thermocouples. Reasoning that a small amount of contamination might grossly affect the absolute thermoelectric power of the pure platinum thermoelement, but not of the alloy thermoelement, Pt-70% Rh versus Pt-6% Rh thermocouples were employed during remeasurements of iron. The C_p values obtained on α -iron with the latter thermocouples were within the experimental error of those obtained with the former thermocouples, but the C_p values of α -iron were as much as 20% too high. Again, use of resistance thermometry confirmed that contamination had occurred.

In retrospect, the large discrepancies at high temperatures among the various measurements of iron and nickel which appear in the literature are, in the opinion of this author, due to thermometry errors. These thermometry errors are influential in two ways. First, errors in the absolute temperature can change where the C_p value is to be placed in the $C_p:T$ relationship. This is very important near the Curie points of iron and nickel where a five degree error produces a 3% error in C_p . Secondly, contamination causes serious errors in the computed values of ΔT used in the calculation of C_p . The total error induced into the measurement of C_p by these thermometry errors depends on the temperature gradient in the thermocouple in the contaminated region. Of course, this gradient will depend on the method and experimental apparatus employed.

In conclusion, pulse calorimetry employing thermocouple thermometry should not be used if contamination of the thermocouple is possible.

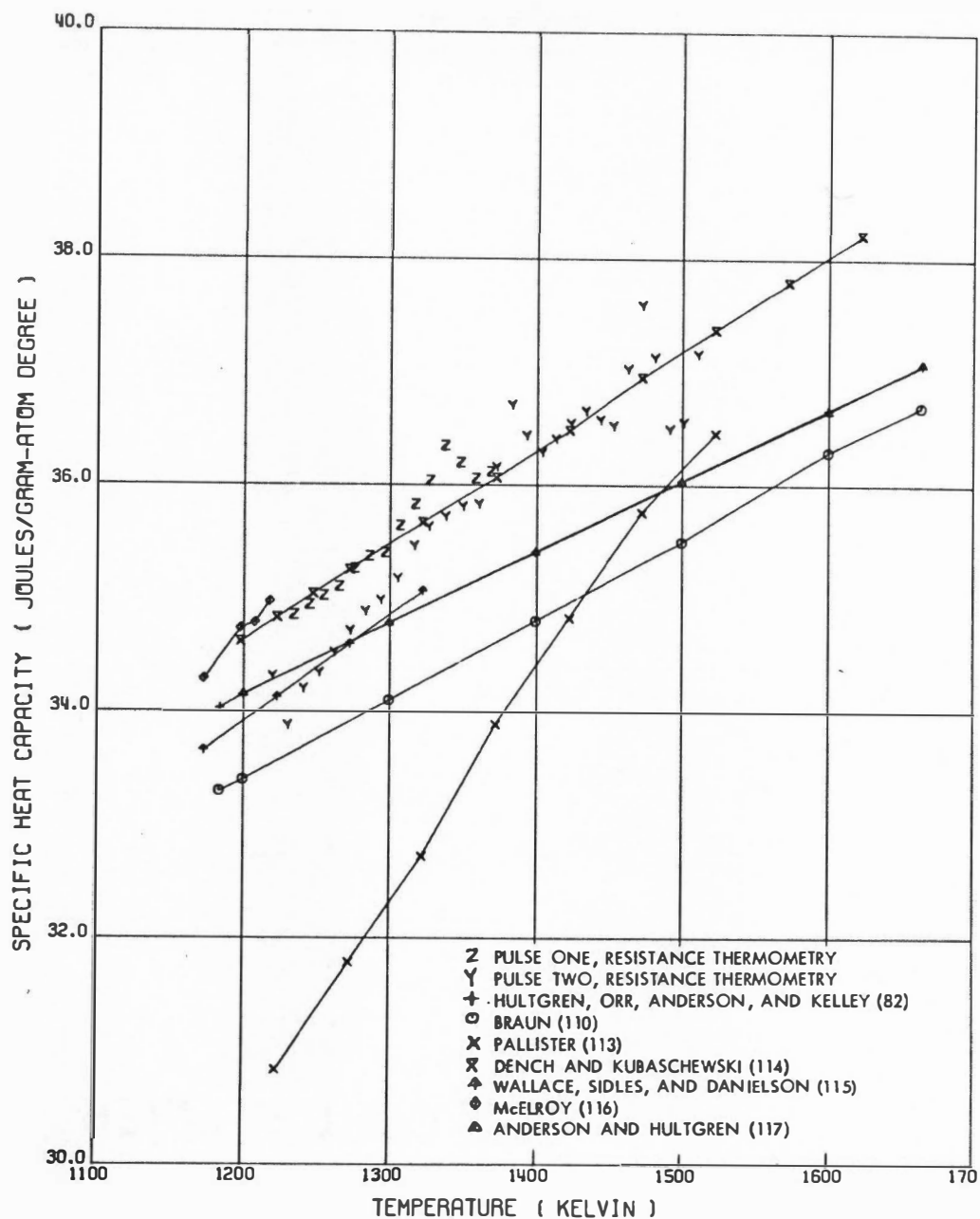


Figure 32. Measurements of the C_p of γ -Iron. Note the excellent agreement of pulse one with the C_p values of Dench and Kubaschewski. Numbers in parentheses in legend are reference numbers.

Repeat measurements at low temperatures reveal whether contamination of the thermocouple occurred at higher temperatures.

Preliminary Comments on the Calculation of C_{vm} of Nickel and Iron

Solution of Equation (12), page 8, for the magnetic specific heat capacity yields

$$C_{vm} = C_p - C_{vh} - C_{va} - C_{ve} - C_d - C_{vw} \quad (105)$$

In order to calculate C_{vm} from the measured values of C_p , each of the other terms on the right-hand side of Equation (105) must be evaluated. The theoretical expressions for these contributions have been discussed in detail in Chapter I. It was noted that these expressions are subject to many qualifications; in the present treatment, the following postulates were used in their evaluation:

1. The harmonic contribution C_{vh} is precisely given by the Debye model when an appropriate choice is made for the characteristic Debye temperature θ_d .
2. The anharmonic contribution C_{va} is linear in temperature; and the magnitude of the constant of proportionality B , as well as its sign, must be determined experimentally.
3. The electronic contribution C_{ve} is given by the sum of a term linear in temperature and another cubic in temperature, $\gamma T + AT^3$. The constant γ is the temperature coefficient of C_p determined near liquid helium temperatures and the constant A also must be found experimentally.

4. The dilation contribution C_d is given by the Nernst-Lindemann approximation.
5. The contribution C_{vw} due to the atomic rearrangement of the atoms of the solid is assumed to be negligible.

Some justification for these assumptions is given for the case of nickel and then extended without further proof to iron.

Using the symbology of Chapter I, define C_x by the expression

$$C_x = C_p - C_{vh} - C_d - \gamma T = C_p - 3R F_d(T/\theta_d) - \gamma_{nl}(C_p)^2 T - \gamma T. \quad (106)$$

The quantity C_x is a convenient tool in the evaluation of C_{vm} because it does not contain second-order terms - namely C_{va} and the AT^3 term of C_{ve} . Also, C_x is approximately equal to C_{vm} near T_c and below 300 K. This definition has three parameters - θ_d , γ_{nl} , and γ - whose values must be selected to evaluate C_x . The constants γ and γ_{nl} are temperature independent, but the Debye temperature θ_d is not. However, use of a temperature dependent θ_d in the Debye theory of specific heat capacity is contradictory to its basic premise; that is, the existence of a single characteristic temperature or cut-off frequency for the harmonic oscillations of the normal modes of the atoms of a solid. Consequently, the value of θ_d chosen should be one which is applicable in the temperature range of interest. This is impossible in the evaluation of C_{vm} of nickel and iron because the temperature range necessary is too broad for a single θ_d . Its selection must then be based on the temperature range where it is most important.

Below about 100 K, the value of C_x (or C_{vm}) for nickel and iron is small. Between 100 K and temperatures of about $0.7 \theta_d$ (≈ 300 K), the

value of C_x (or C_{vm}) is controlled largely by the value of $F_d(T/\theta_d)$, which is a rapidly varying function of temperature. At temperatures in excess of $0.7 \theta_d$, $F_d(T/\theta_d)$ varies slowly with temperature and the value of C_x is not significantly affected by the choice of θ_d . Hence, the important temperature range is, in the opinion of this author, between 100 K and about 300 K. This opinion was not shared by the various other investigators who have presented calculations of C_{vm} of iron and nickel in the open literature. They chose a θ_d evaluated either at liquid helium temperatures or between 20 K and 50 K. Some consequences of these choices are presented below for nickel.

Calculation of C_{vm} of Nickel

In the following calculation of C_{vm} of nickel, the compilation of Hultgren, Orr, Anderson, and Kelley⁸² was used for C_p values below room temperature. Above room temperature, the data employed were obtained in this investigation. These data are presented in Figure 18, page 102, and in Figure 31, page 122. The latter data were obtained using resistance thermometry and were normalized to agree with the former in their region of overlap. (The lowest temperature point of the latter was brought into coincidence and the remainder were corrected a proportionate amount.) These data are listed in Table XXIII in the Appendix.

The value of γ employed, 7.028×10^{-3} joules/gram-atom K^2 , was that calculated by Dixon, Hoare, Holden, and Moody³³ from their C_p measurements from 1 K to 4 K. Use of their γ value was based on the excellent agreement between the γ values of Dixon, Hoare, and Holden³⁴ on disordered Ni_3Fe and those obtained by J. O. Scarbrough of the Oak Ridge

National Laboratory for use in this work. The value of γ_{nl} , 2.624×10^{-6} gram-atom/joule, was selected from the compilation of Gschneidner.¹¹⁸

C_x of Nickel. Reconsider the quantity C_x . In Figure 33(a), C_x is evaluated using the values of γ and γ_{nl} described above and a θ_d of 471 K, which was obtained from the low-temperature C_p measurements of Dixon, Hoare, Holden, and Moody.³³ This θ_d is in good agreement with the value of 477 K found by Alers¹¹⁹ using low temperature elastic constant measurements. In Figure 33(b), a θ_d of 390 K was used to calculate C_x , but γ and γ_{nl} were not changed. This Debye temperature was calculated by Hofmann, Paskin, Tauer, and Weiss⁶² from the C_p data of Busey and Giauque¹²⁰ between 20 and 50 K. Rayne and Kemp¹²¹ also obtained a θ_d of 390 K from their C_p measurements between 1.2 and 4.2 K.

Above 600 K, the values of C_x obtained using a θ_d of 390 or 471 K are essentially the same. However, below 200 K, the results are strikingly different. With θ_d equal to 471 K, C_x demonstrates a maximum near 100 K which cannot be explained theoretically; that is, near 100 K, C_x is equal to C_{vm} , which is monotonically approaching zero. On the other hand, a θ_d of 390 K yields a C_x which goes rapidly to zero between 300 and 200 K. Theoretically, C_x should become zero only at zero kelvin. Hence, the behavior of C_x below 300 K is not acceptable with θ_d 's of 471 or 390 K.

Simerská¹²² measured the Debye temperature of nickel between 300 and 900 K using an x-ray diffraction technique. His results indicate that θ_d decreases slowly with increasing temperature from a value of

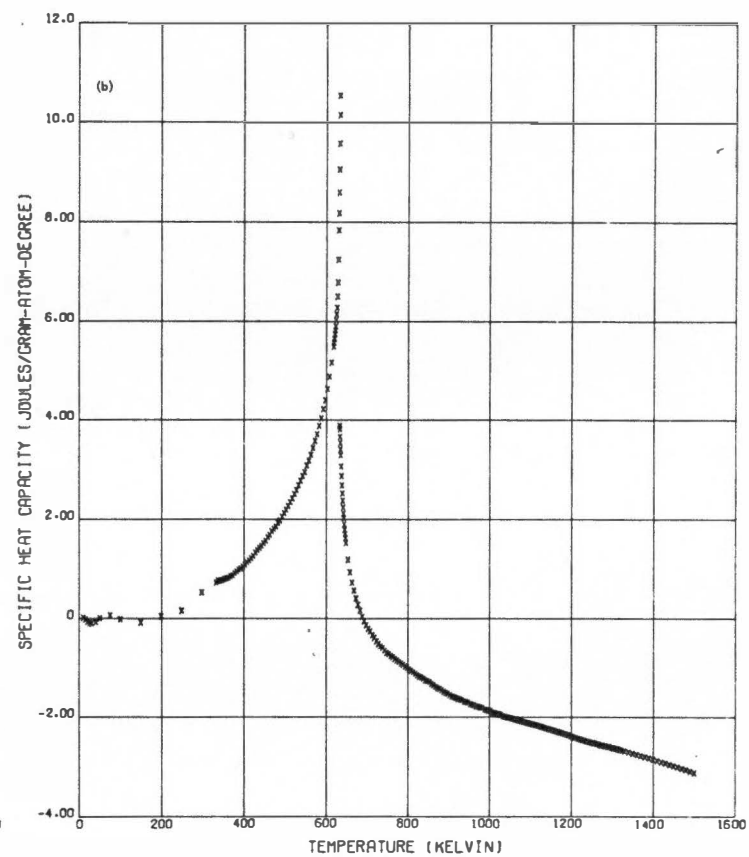
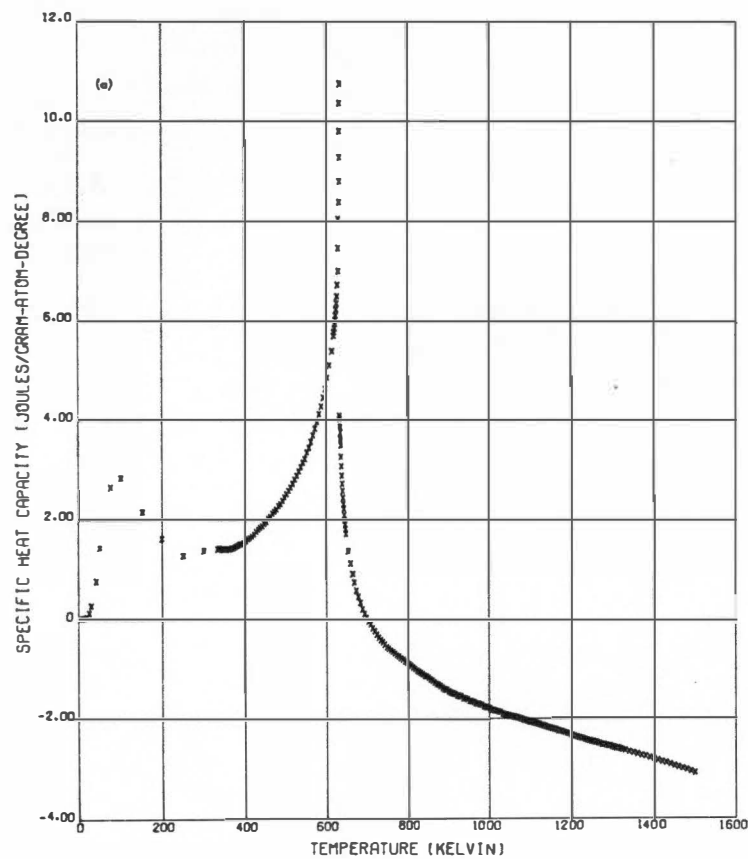


Figure 33. Temperature Dependence of C_x of Nickel Calculated with a γ of 7.028×10^{-3} joules/gram-atom K^2 and a γ_{nl} of 2.624×10^{-6} gram-atom/joule. (a) θ_d equals 471 K, (b) θ_d equals 390 K.

410 K at 300 K to a value of about 360 K at 900 K. Consequently, if one assumes that the temperature dependence of θ_d of nickel below 300 K is similar to that of silver shown in Figure 1(c), page 17, then θ_d of nickel between 100 and 300 K should lie between 390 and 410 K from Simerská's measurements and the calculations of Hofmann, Paskin, Tauer, and Weiss.⁶²

The $C_x:T$ relationship obtained using θ_d 's of 410 and 400 K is shown in Figure 34(a) and 34(b), respectively. A small maximum appears in both these plots at 100 K; however, the maximum obtained using a θ_d of 400 K is not as pronounced. Note also that C_x at 200 K is not zero for either case. It is the author's opinion that a θ_d of 400 K is the "best" value for nickel based on this method of analysis.

C_d of Nickel. The values of C_x of Figures 33 and 34 were calculated using the Nernst-Lindemann approximation [Equation (20), page 9] for the dilation contribution C_d . This approximation was employed because measurements of the thermal expansion and compressibility of nickel requisite to a precise calculation of C_d by Equation (14), page 8, have not been made at high temperatures. However, since the Nernst-Lindemann approximation is empirical, the values of C_d obtained using it were compared to the more theoretically sound Grüneisen approximation [Equation (18), page 9], which only requires values of the thermal expansion coefficient α_ℓ as a function of temperature.

Values of α_ℓ of nickel were calculated by two methods. For temperatures between 300 and 760 K, the differential thermal expansion data of Nix and MacNair,⁹ which were normalized to the length of the specimen at room temperature, were fitted by the method of least-squares to a second

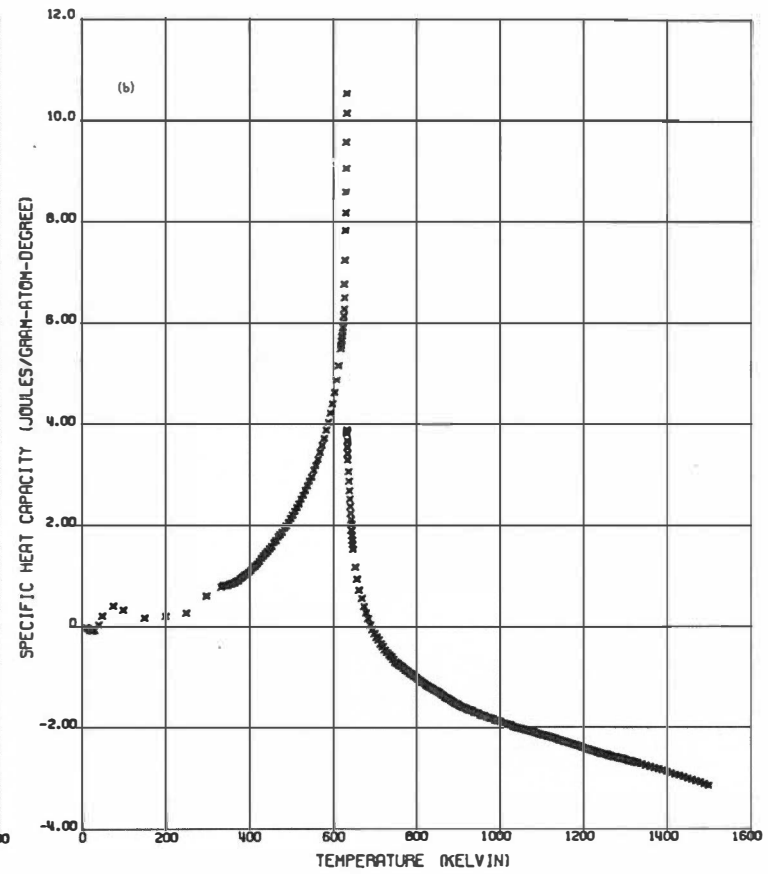
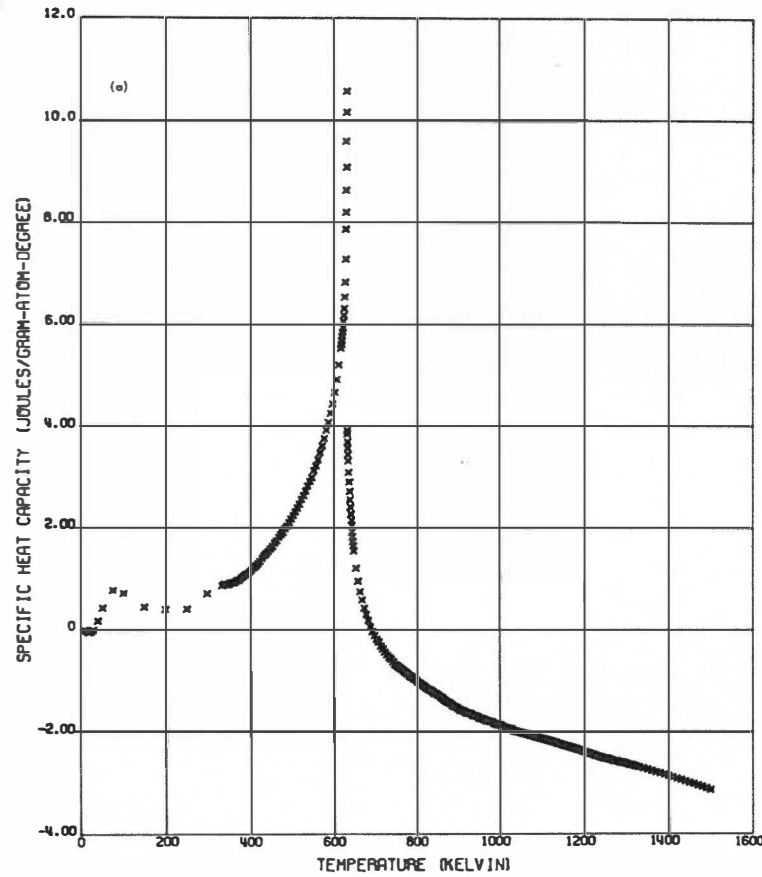


Figure 34. Plot of the Temperature Dependence of C_x of Nickel Calculated with a γ of 7.028×10^{-3} joules/gra -ato K^2 and a γ_{nl} of 2.624×10^{-6} gram-atom/joule. (a) θ_d equals 410 K, (b) θ_d equals 400 K.

order polynomial in temperature in intervals of about 50 degrees. Thus, α_ℓ was the first temperature derivative of the functions obtained from these fits. For temperatures below 300 K and above 760 K, Grüneisen's² theory for thermal expansion was used to obtain α_ℓ . After substitution of the appropriate constants given by Nix and MacNair⁹ for nickel, Grüneisen's² expression for α_ℓ at a temperature T is

$$\alpha_\ell(T) = 5.55 \times 10^{-7} C_{vh} / (1 - 6.32 \times 10^{-6} E)^2, \quad (107)$$

where

$$E = \int_0^T C_{vh} dT. \quad (108)$$

In Equations (107) and (108), the Debye theory with a θ_d of 410 K was used by Nix and MacNair to evaluate C_{vh} .

In Figure 35, values of C_d calculated using Grüneisen's approximation are shown as a solid line ($\gamma_g = 1.88$)¹¹⁸ and those of the Nernst-Lindemann approximation are shown as points ($\gamma_{n\ell} = 2.624 \times 10^{-6}$ gram-atom/joule).¹¹⁸ Below 600 K, the two approximations are in agreement to better than 4%, except near 450 K where an 8% deviation occurs because of the erratic behavior of the expansion data of Nix and MacNair near this temperature. Between 600 K and the Curie temperature of 633 K, the Grüneisen C_d diverges from the Nernst-Lindemann value and is 18.3% lower just below T_c . This difference was attributed to inaccuracies of the expansion data of Nix and MacNair in this temperature region. For example, the value of α_ℓ calculated at T_c was $17.7 \times 10^{-6} K^{-1}$, whereas Kirby's¹²³ compilation predicts a value of $19.5 \times 10^{-6} K^{-1}$ near T_c . This 10% higher value of α_ℓ would reflect an equivalent increase in C_d when used in the Grüneisen approximation for C_d .

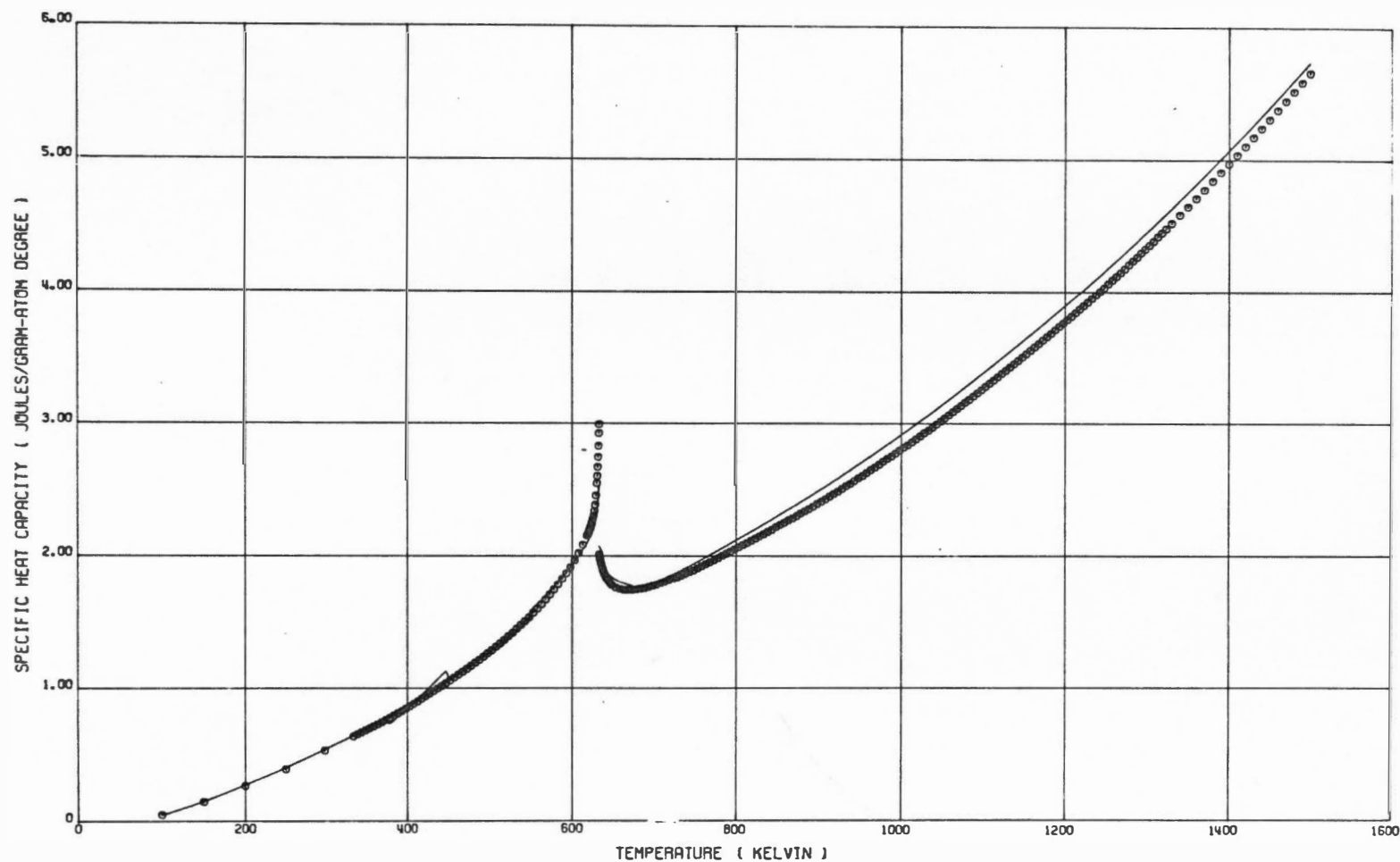


Figure 35. Calculated Values of the Dilation Contribution C_d of Nickel as a Function of Temperature. Grüneisen's approximation for C_d is shown as a solid line for a γ_g of 1.88. The Nernst-Lindemann approximation is shown as points for a γ_{nl} of 2.624×10^{-6} gram-atom/joule.

Above the Curie temperature, the agreement between the two approximations is excellent. However, there is a consistent difference of about 3.8% for temperatures at which Grüneisen's theory was used to determine α_l (above 760 K). This discrepancy could be attributed to the inadequacy of this theory.

The overall good agreement between these two methods for calculating C_d is construed as a validification of the Nernst-Lindemann empirical approximation for nickel.

C_{vm} of Nickel. From Equation (105), page 126, Equation (106), page 127, and the five postulates listed at the beginning of this section, the following expression for C_x can be obtained

$$C_x = C_{vm} + C_{va} + AT^3 = C_{vm} + BT + AT^3. \quad (109)$$

Thus, in order to evaluate C_{vm} , values of the constants A and B must be determined. Suppose, as has been done by most other investigators, that the anharmonic contribution C_{va} is negligible; that is, B is very small. Also, assume that at 1500 K, C_{vm} is negligible. (This is a reasonable assumption since 1500 K is about 900 degrees above the Curie temperature. The various theories also predict this to be the case.) Then the value of A can be found from the known value of C_x [Figure 34(b), page 132] at 1500 K and is -9.3×10^{-10} joules/gram-atom K^4 . Using this value of A, C_{vm} can be calculated as a function of temperature and is depicted in Figure 36. The resulting values of C_{vm} are negative between 715 and 1500 K with a minimum value of -0.96 joules/gram-atom degree at 990 K.

Since a negative value of C_{vm} is totally unrealistic, the assumption that C_{va} is negligible must be incorrect and/or the calculated value of

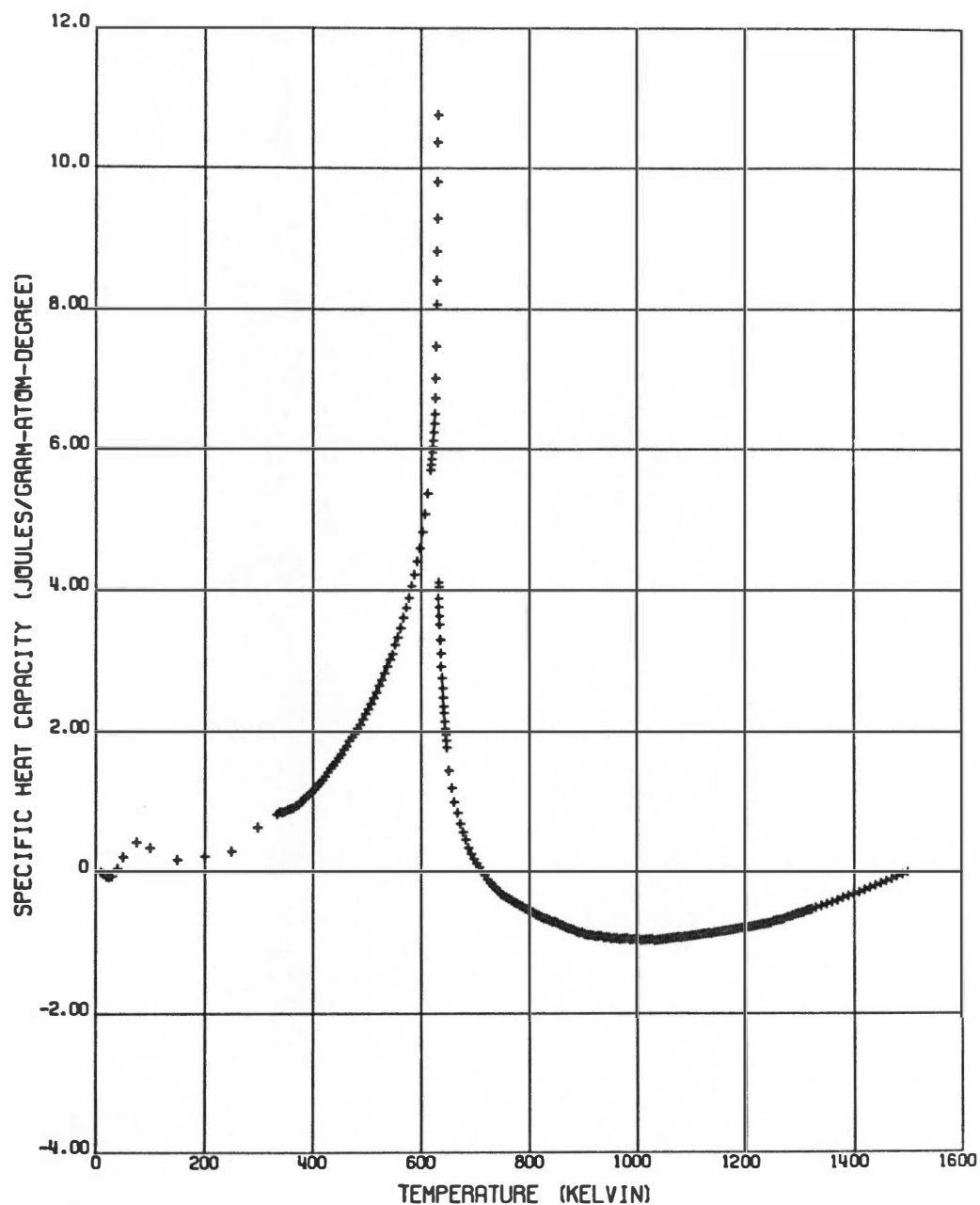


Figure 36. Temperature Dependence of C_{vm} of Nickel Calculated Assuming that the Anharmonic Contribution C_{va} is Negligible. Note that this assumption yields negative values of C_{vm} between 715 and 1500 K.

A must be erroneous. Consider the latter case. The free electron theory [Equation (44), page 22] yields a value of -1.696×10^{-9} joules/gram-atom K^4 for A, which is about a factor of two higher than the calculated value. Use of this value would give a negative C_{vm} near 1000 K but a positive value at 1500 K, which is also unrealistic. Any lower value than the one calculated above would yield a C_{vm} which is negative from 1500 K to temperatures below 715 K. Consequently, the assumption that C_{va} is negligible must be incorrect. Hence, A and B are nonzero.

In order to calculate A and B of Equation (109), C_{vm} was assumed negligible above 1400 K; and eleven C_x values between 1400 and 1500 K were fit to the function $AT^3 + BT$ by the method of least squares. This yielded a value of A of $-1.48 (\pm 0.06) \times 10^{-10}$ joules/gram-atom K^4 and a value of B of $-1.76 (\pm 0.01) \times 10^{-3}$ joules/gram-atom K^2 .

How reasonable are these results? First, note that A is negative and one order of magnitude smaller than that predicted by the free electron model. This value of A produces only a 5% change in C_{ve} at 1500 K from that predicted by the low-temperature approximation of γT . However, the negative sign for A is in agreement with the theory of Shimizu, Takahashi, and Katsuki,²⁸ which was discussed in Chapter I.

The theory of Keller and Wallace²² [Equation (40), page 21] yields a value of B for nickel of -4.42×10^{-3} joules/gram-atom K^2 for a θ_d of 400 K. Although the computed value of B is 60% less than this, such agreement is felt to be excellent, considering the assumptions and calculations made to arrive at this value of B.

In Figure 37, the temperature dependence of C_{vm} as well as the other contributions to the total specific heat capacity of nickel are shown. These were obtained using the parameters described above and the C_x values of Figure 34(b), page 132. Figure 38 is an expanded plot of the contributions showing only C_{ve} , C_d , C_{vm} , and C_{va} . Note that C_{vm} is negligibly small above 1030 K, which is in agreement with the assumption used to calculate the constants A and B. Further discussion of these results is deferred until after the following section.

Calculation of C_{vm} of Iron

In the following calculation of C_{vm} of iron, the compilation of Hultgren, Orr, Anderson, and Kelley⁸² was used for C_p values below room temperature. Above this temperature but in the α -stable region, the results of this investigation shown in Figure 19, page 103, were employed. Because of the excellent agreement between the C_p results of Dench and Kubaschewski¹¹⁴ and those of this investigation on γ -iron [Figure 32, page 125], the values they calculated for the C_p of α -iron in the γ -stable region were utilized.

As for nickel, the value of γ employed, 4.741×10^{-3} joules/gram-atom K^2 , was that calculated by Dixon, Hoare, Holden, and Moody³³ from their C_p measurements from 1 to 4 K. The value of γ_{nl} , 2.349×10^{-6} gram-atom/joule, was selected from the compilation of Gschneidner.¹¹⁸

C_x of Iron. In Figure 39, C_x of iron is evaluated using the values of γ and γ_{nl} described above and a θ_d of 440 K. This Debye temperature is in close agreement with that of Hofmann, Paskin, Tauer, and Weiss⁶² who calculated a value of 432 K from the C_p data of Kelley¹²⁴ between

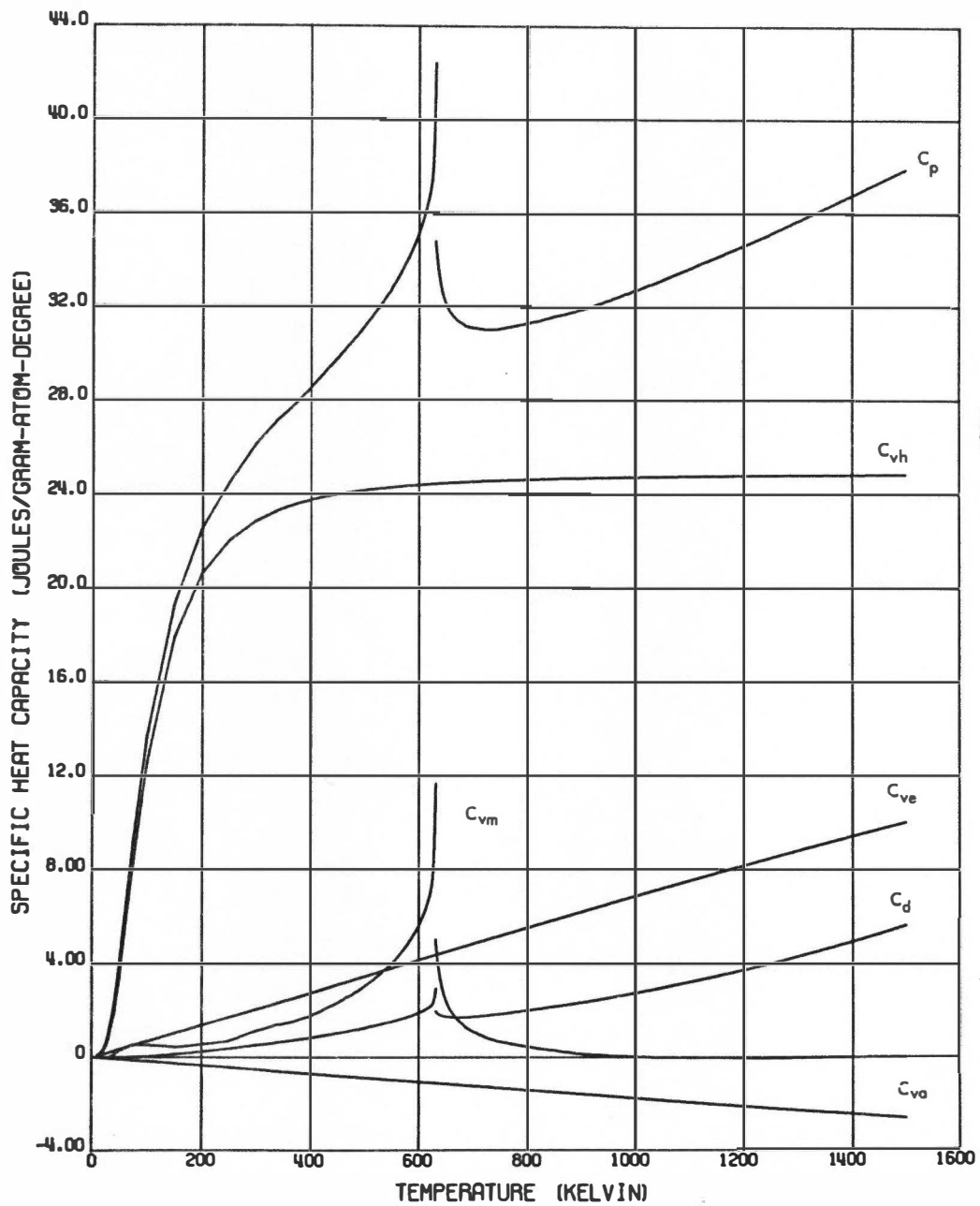


Figure 37. Contributions to the Specific Heat Capacity of Nickel as a Function of Temperature. ($\theta_d = 400$ K, $\gamma = 7.028 \times 10^{-3}$ joules/gram-atom K^2 , $\gamma_{nl} = 2.624 \times 10^{-6}$ gram-atom/joule, $A = -1.48 \times 10^{-10}$ joules/gram-atom K^4 , and $B = -1.76 \times 10^{-3}$ joules/gram atom K^2 .)

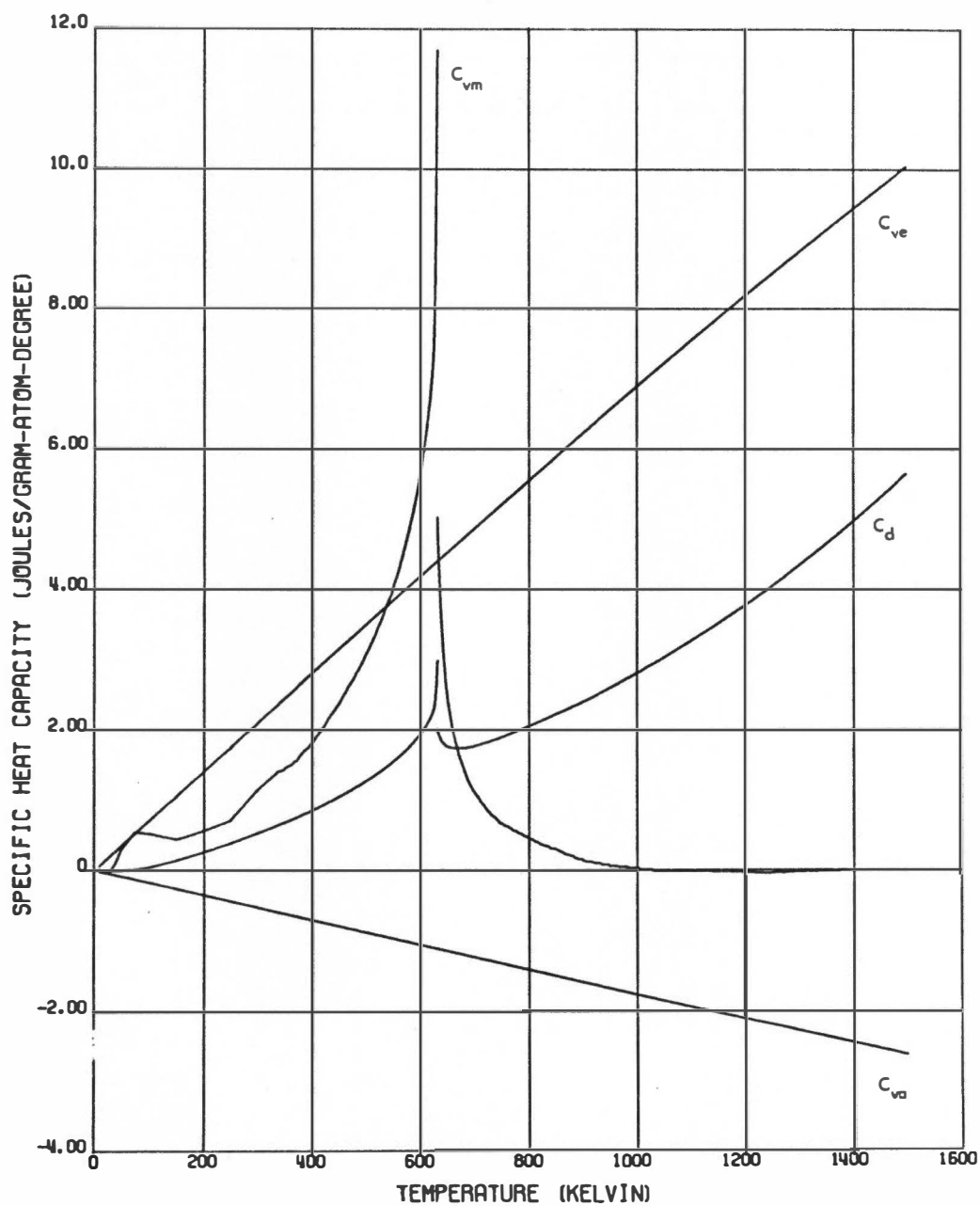


Figure 38. Expanded Plot of Figure 37 Showing the Contributions to the Specific Heat Capacity of Nickel as a Function of Temperature. Only C_{ve} , C_d , C_{vm} , and C_{va} are shown.

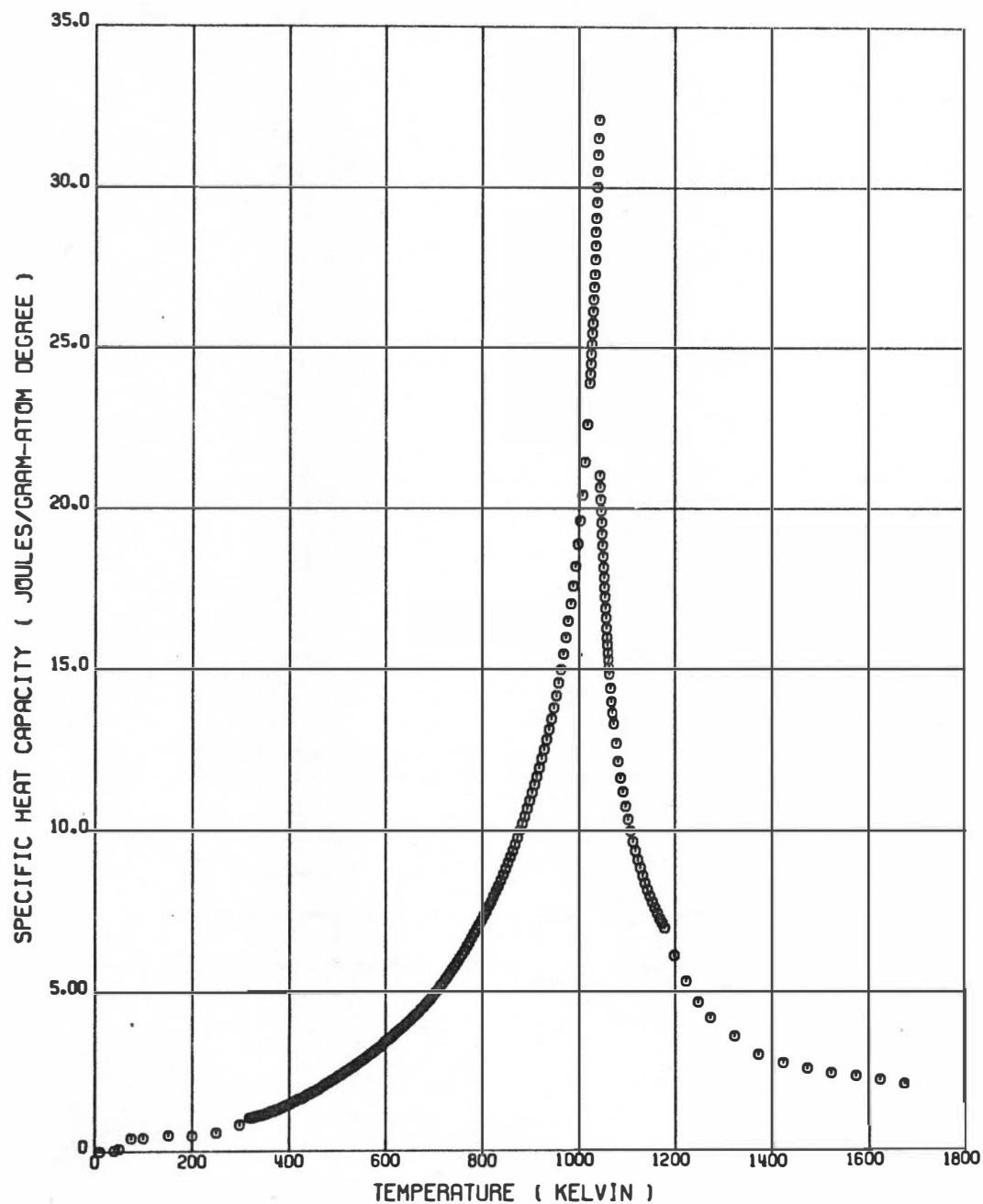


Figure 39. Temperature Dependence of C_x of Iron Calculated with a γ of 4.741×10^{-3} joules/gram-atom K^2 , and γ_{nl} of 2.349×10^{-6} gram-atom/joule, and a θ_d of 440 K.

50 and 100 K. It is below the θ_d of Dixon, Hoare, Holden, and Moody³³ who obtained 473 K from their C_p measurements between 1 and 4 K and is also below the value of 478.1 K obtained by Alers¹¹⁹ from low-temperature elastic constant measurements.

Comparing Figures 39 and 34(b), page 132, it is seen that C_x of iron is a factor of three larger than that of nickel at their Curie temperature and that C_x of iron is positive at all temperatures. The large positive value (2.6 joules/gram-atom degree) of C_x of iron at 1670 K results in the use of a different approach in the evaluation of C_{vm} of iron.

C_{vm} of Iron. If the anharmonic C_{va} and magnetic C_{vm} contributions to the C_p of iron are assumed to be negligible at 1670 K, the constant A is equal to $C_x/(1670)^3$ by Equation (109), page 135; that is, 4.42×10^{-10} joules/gram-atom K^4 . This value of A is an order of magnitude greater than the value of -3.88×10^{-11} joules/gram-atom K^4 predicted by the free-electron theory and of opposite sign. However, a positive A is predicted by the theory of Shimizu, Takahashi, and Katsuki.²⁸

The assumption that C_{vm} is negligible at 1670 K is not supported by the theories discussed in Chapter I, which predict values of C_{vm} ranging from 1 to 2 joules/gram-atom degree near this temperature. A nonzero C_{vm} at this high temperature increases the complexity in the evaluation of A and B in Equation (109) and hence in the evaluation of C_{vm} at all temperatures. Also, a nonzero value for B follows from the results on nickel.

Consider Figure 40 in which C_x of iron is plotted versus $\log_{10}|T - T_c|$ for temperatures above the Curie temperature. The straight line in this figure was obtained by fitting the twenty-one C_x values

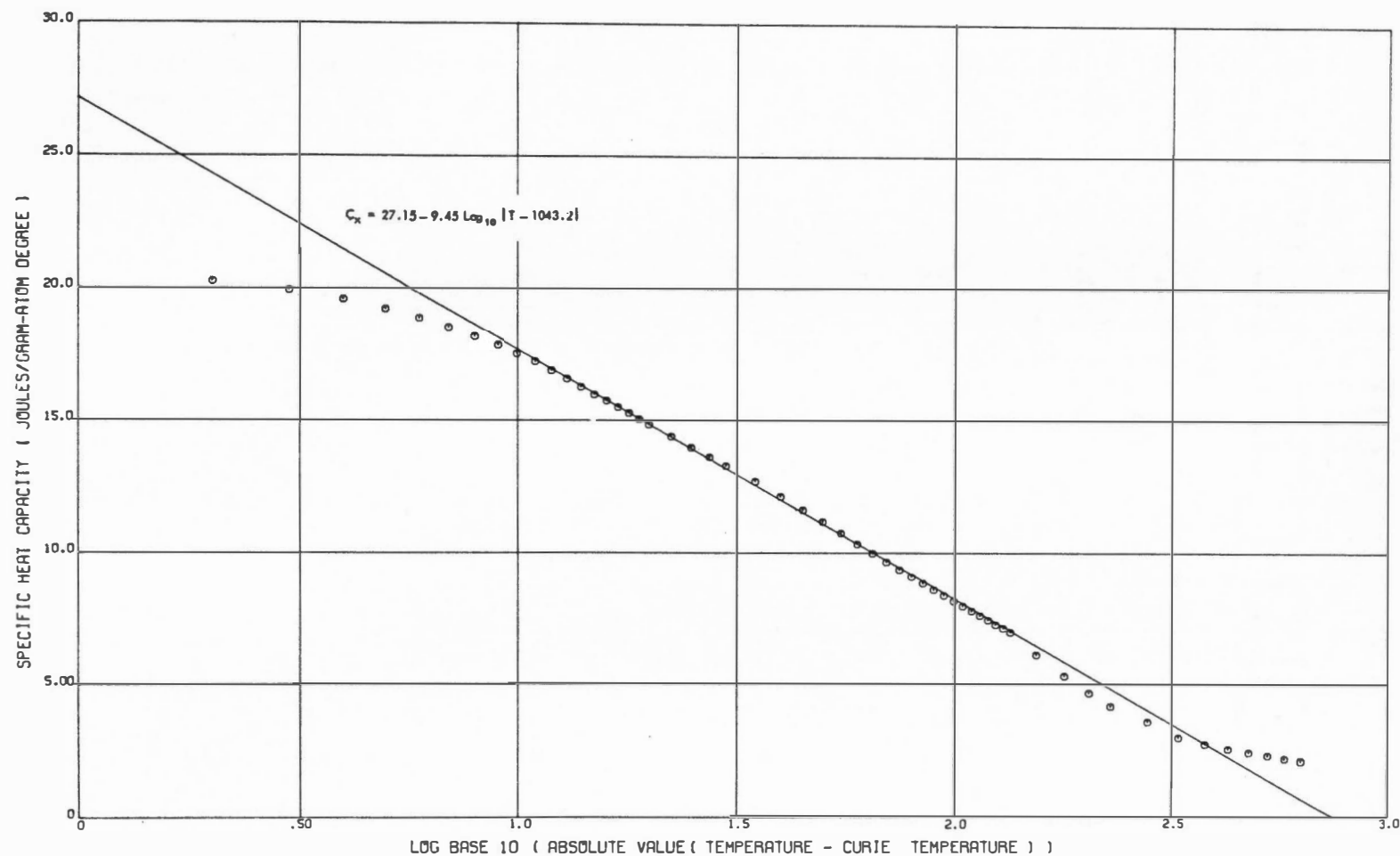


Figure 40. Plot of C_x of Iron as a Function of $\log_{10} |T - T_c|$ for Temperatures above the Curie Temperature of 1043.2 K. The straight line was obtained by fitting C_x to the function $a + b \log_{10} |T - T_c|$ between 1057 and 1123 K.

between 1057 and 1123 K to the function $a + b \log_{10}|T - 1043.2|$ by use of the method of least-squares. In this temperature region, C_{vm} is approximately equal to C_x . Hence, by assuming that C_{vm} is linear in $\log_{10}|T - T_c|$, approximate values of C_{vm} were calculated between 1250 and 1625 K by extrapolation of this straight line. Subsequently, these values of C_{vm} were subtracted from C_x and the difference $(C_x - C_{vm})$ was fit by the method of least-squares to the function $BT + AT^3$ between 1250 and 1625 K. The values of A and B obtained from this fit were used to calculate C_{vm} at all temperatures.

Because of the approximations involved, an iteration of this procedure was performed. That is, the C_{vm} (instead of C_x) values between 1057 and 1123 K were fit to the function $a + b \log_{10}|T - T_c|$ and the resulting values of a and b were used to calculate C_{vm} between 1250 and 1625 K. These C_{vm} values were subtracted from C_x and new values of A and B and then C_{vm} were calculated.

Table VI lists the values of a, b, A and B obtained from each iteration. Little change in a and b is noted between the results of the two iterations, but B decreased by a factor of two and A by a factor of six. A third iteration was performed but the standard deviation of A was larger than its magnitude and the value of 2.1×10^{-10} was within one standard deviation of the third value.

The positive sign for A is in agreement with the theory of Shimizu, Takahashi, and Katsuki.²⁸ As for nickel, the overall contribution of the AT^3 term to C_{ve} is small. Also, the results on iron and nickel suggest that the density of electron states increase with temperature for iron but decreases for nickel.

TABLE VI
VALUE OF THE CONSTANTS a , b , A , AND B OBTAINED FROM THE
TWO ITERATIONS DURING CALCULATION OF C_{vm} OF IRON*

Quantity	Iteration 1	Iteration 2
a	27.15 (± 0.09)	28.5 (± 0.1)
b	-9.45 (± 0.07)	-9.60 (± 0.07)
A	$1.23 (\pm 0.05) \times 10^{-9}$	$2.1 (\pm 0.4) \times 10^{-10}$
B	$-2.5 (\pm 0.1) \times 10^{-3}$	$-1.13 (\pm 0.09) \times 10^{-3}$

*Units of constants are consistent with specific heat capacity units of joules/gram-atom degree.

From data in the literature and a θ_d of 440 K, a value of -2.91×10^{-3} joules/gram-atom degree was calculated for B from the theory of Keller and Wallace.²² As for nickel, the experimental value of B is 60% less than the theoretical. This suggests that the geometric constants calculated by Keller and Wallace may be too high by a factor of two or three.

In Figure 41, the temperature dependence of C_{vm} as well as the other contributions to the total specific heat capacity of iron are shown. These values were obtained using the parameters described above. Figure 42 is an expanded plot of the contributions. Note that C_{vm} of iron is not zero even at 1673 K.

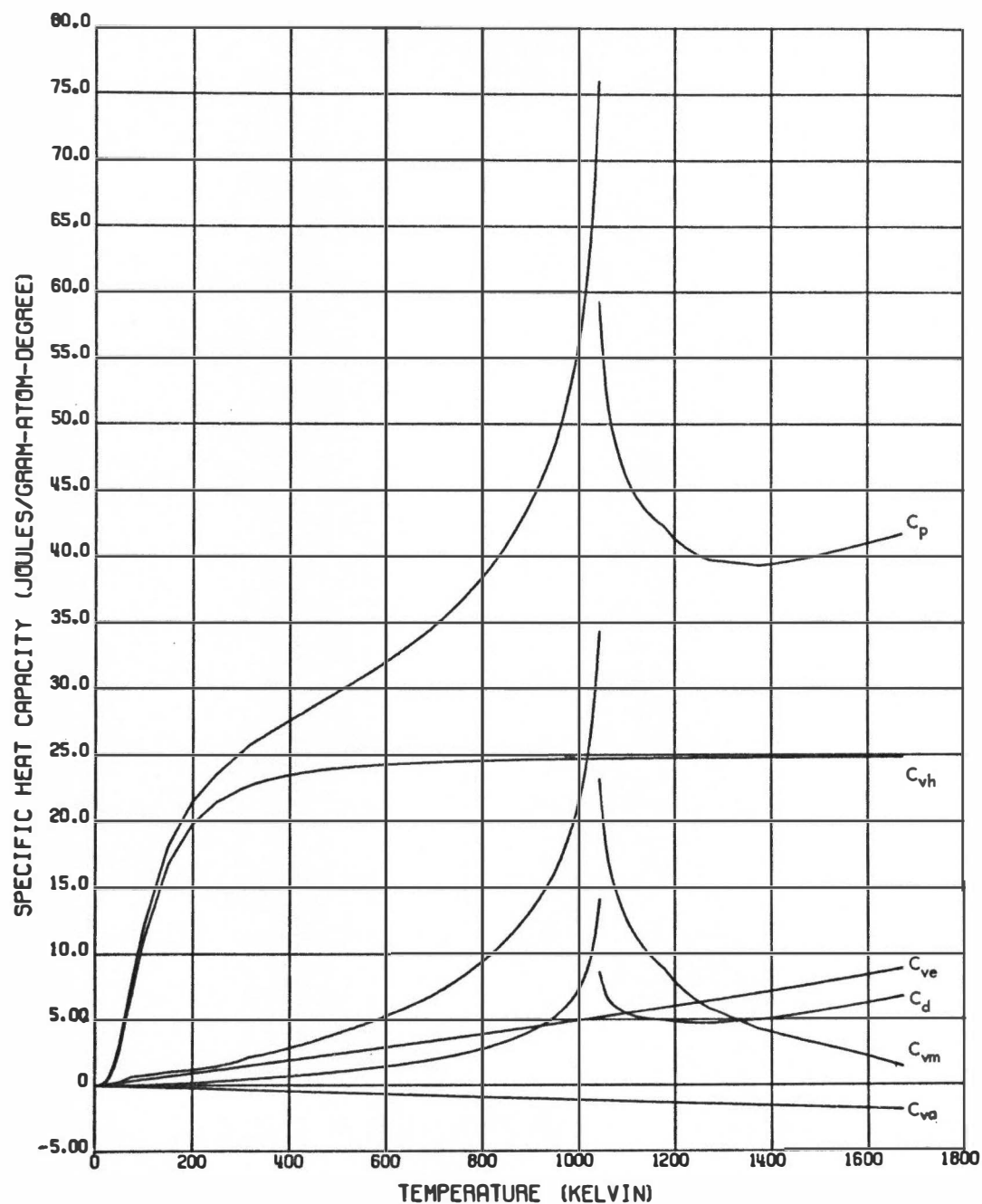


Figure 41. Contributions to the Specific Heat Capacity of Iron as a Function of Temperature. ($\theta_d = 440$ K, $\gamma = 4.741 \times 10^{-3}$ joules/gram-atom K², $\gamma_{nl} = 2.349 \times 10^{-6}$ gram-atom/joule, $A = 2.1 \times 10^{-10}$ joules/gram-atom K⁴, and $B = -1.13 \times 10^{-3}$ joules/gram-atom K².)

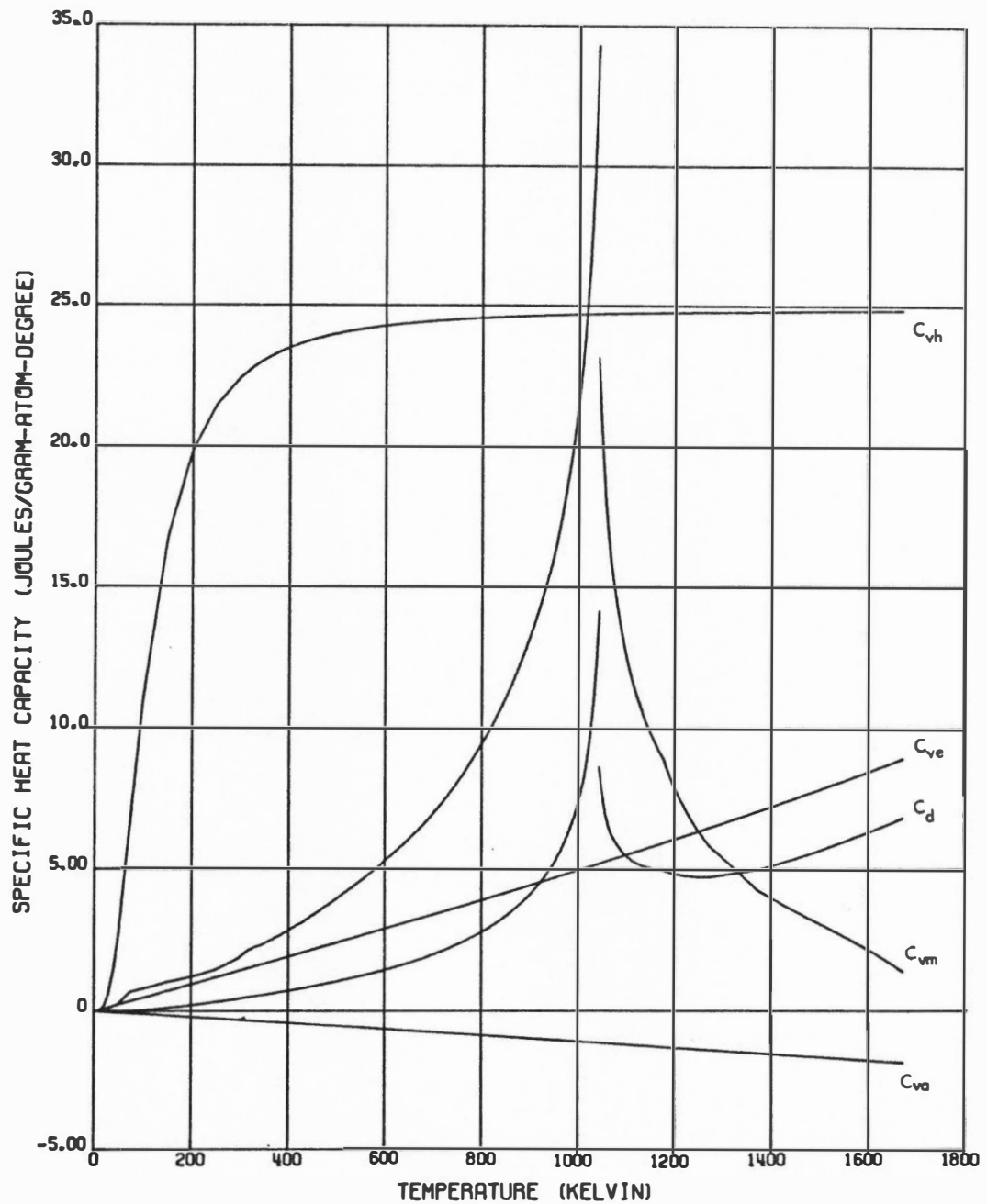


Figure 42. Expanded Plot of Figure 41 Showing the Contributions to the Specific Heat Capacity of Iron as a Function of Temperature.

Discussion of the C_{vm} Values of Nickel and Iron

The calculated values of C_{vm} of iron and nickel are presented in Figure 43 and listed in Tables XXIV and XXV in the Appendix. The data shown below 300 K were obtained by drawing a smooth curve through the C_{vm} results presented in Figure 37, page 139, and Figure 42. This procedure was employed to remove the oscillations caused by the inadequacy of the Debye theory to represent C_{vh} in this temperature region.

For sake of comparison, the results of Braun¹¹⁰ and Krauss and Warncke⁶⁴ for nickel and those of Braun¹¹⁰ for iron are also presented in Figure 43. (Results of other investigations discussed in Chapter I were not included because they were not presented in tabular form, and the inaccuracies introduced in taking values from the plots given in these works negate the usefulness of such a procedure.) In general, the C_{vm} results of this investigation are higher than those of the other investigations. Below 500 K, the higher values are caused by a number of factors which include the use of a Debye temperature for nickel and iron which was about ten degrees above that of other investigations and also the selection of lower values of γ . In addition, the present analysis includes a negative anharmonic contribution which would tend to raise the C_{vm} results at all temperatures. At higher temperatures, the C_p data used in the other investigations were in general lower. This is particularly true of Braun's iron C_p data which is 2% lower at 750 K and 5% lower at temperatures above 1100 K.

The question is now raised, "Can these differences in the reported C_{vm} values be explained by the errors introduced during the calculation

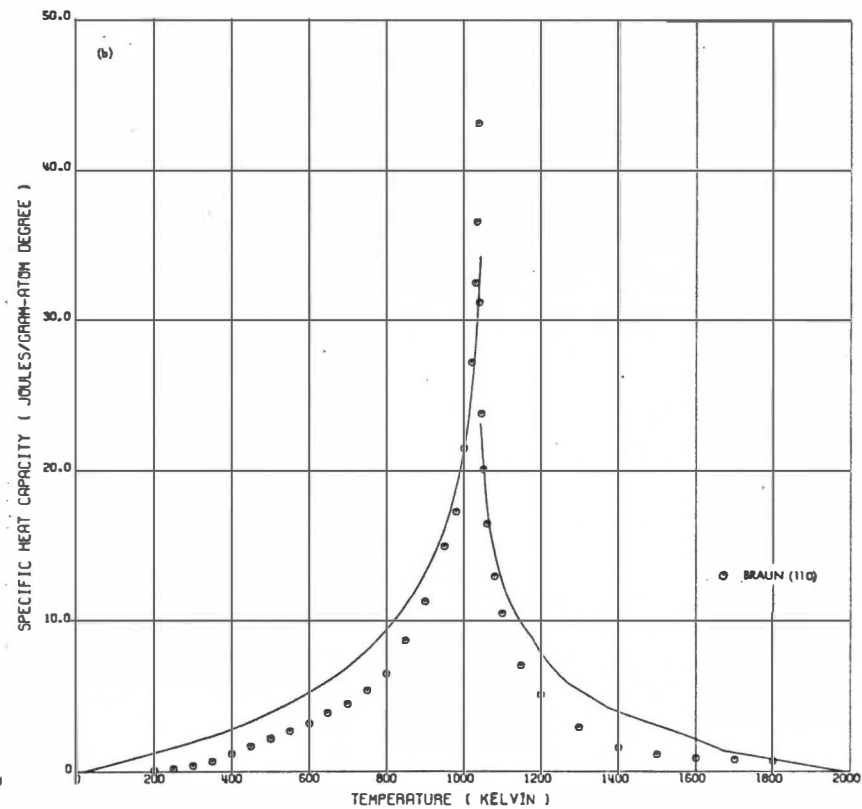
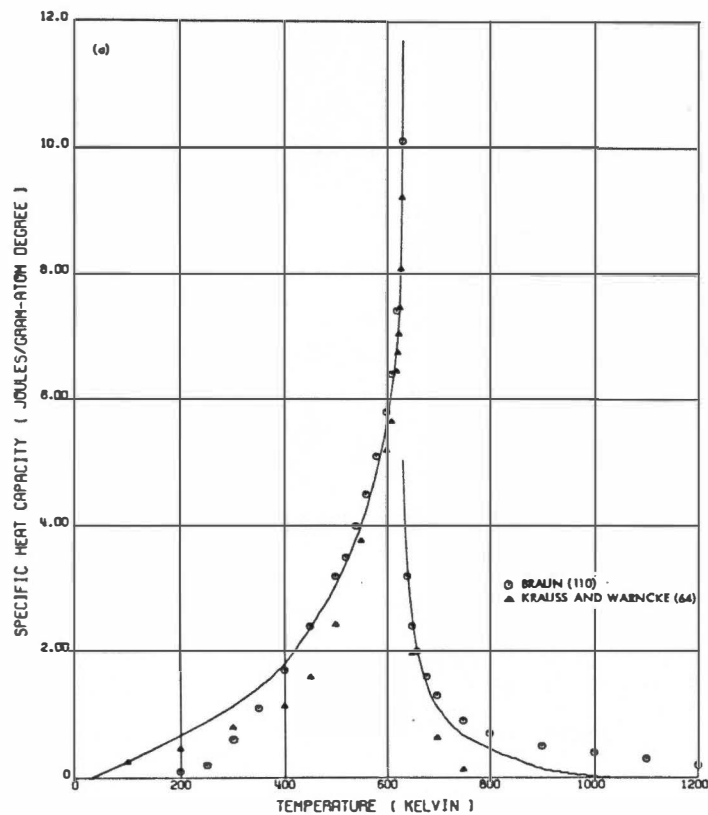


Figure 43. Comparison of the Calculated Values of C_{vm} of Nickel and Iron with Those of Other Investigations. (a) Nickel; (b) iron. Numbers in parentheses are reference numbers. Note the discontinuities of 11.13 and 6.66 joules/gram-atom degree in the C_{vm} of nickel and iron, respectively.

of C_{vm} , or are some of the analyses incorrect?" This is a very difficult question to answer because the theories in themselves are approximate at best. However, for pedagogic reasons, consider the following.

Assume that the C_p values are in error by $\pm 1\%$, the values of γ are in error by $\pm 5\%$, the Debye temperatures are off by ± 10 degrees, and the values of γ_{nl} , A , and B are in error by $\pm 10\%$. Errors due to temperature measurements and due to inaccuracies of the theories per se are not considered. (Part of the errors in the constants may be considered due to errors in the theories.) The resulting errors in C_{vm} of iron at 400 K, 1030 K, and 1200 K are given in Table VII. Near the Curie temperature the error in the calculation of C_{vm} is smaller than at lower or higher temperatures where the absolute value of C_{vm} is smaller. The errors reported in the last line of Table VII are the maximum possible error for the assumptions made. Obviously, some of the errors will compensate each other, resulting in a lower overall error. Hence, selection of an error of $\pm 15\%$ in the calculation of C_{vm} is conservative for the assumptions made. Thus, to within the errors of calculation, the sets of data presented in Figure 43 must be considered essentially in agreement.

The Curie Transformation - A Critical Phenomenon. As discussed in Chapter I, the Curie transformation may be considered as a type of critical phenomenon. As such, C_{vm} would be linear in $\log|T - T_c|$ and have the same slope but different intercept for temperatures above and below the Curie temperature T_c . To test this hypothesis, the C_{vm} of nickel and iron were plotted versus $\log_{10}|T - T_c|$ with the results as shown in Figures 44 and 45. Obviously, the expected relationship does not hold for values of $|T - T_c|$ less than ten.

TABLE VII

ERRORS IN THE CALCULATED VALUES OF C_{vm} OF IRON INTRODUCED BY ERRORS
IN CALCULATING THE VALUES OF THE OTHER CONTRIBUTIONS TO C_p

Contribution	Error Assumed	Absolute Value of Error (joules/gram-atom degree)		
		(400 K)	(1030 K)	(1200 K)
C_p	$\pm 1\%$	± 0.28	± 0.66	± 0.41
$C_d \begin{cases} \gamma_{nl} \\ C_p \end{cases}$	$\pm 10\%$	± 0.07	± 1.07	± 0.48
	$\pm 1\%$	± 0.01	± 0.21	± 0.10
$C_{ve} \begin{cases} \gamma \\ A \end{cases}$	$\pm 5\%$	± 0.10	± 0.24	± 0.28
	$\pm 10\%$		± 0.02	± 0.04
C_{va}	$\pm 10\%$	± 0.07	± 0.12	± 0.13
C_{vh}	± 10 degrees	± 0.47		
Total error		± 1.00	± 2.32	± 1.44
Value of C_{vm} (joules/gram-atom degree)		2.86	28.27	9.04
Maximum error in C_{vm}		$\pm 35.0\%$	$\pm 8.2\%$	$\pm 15.9\%$

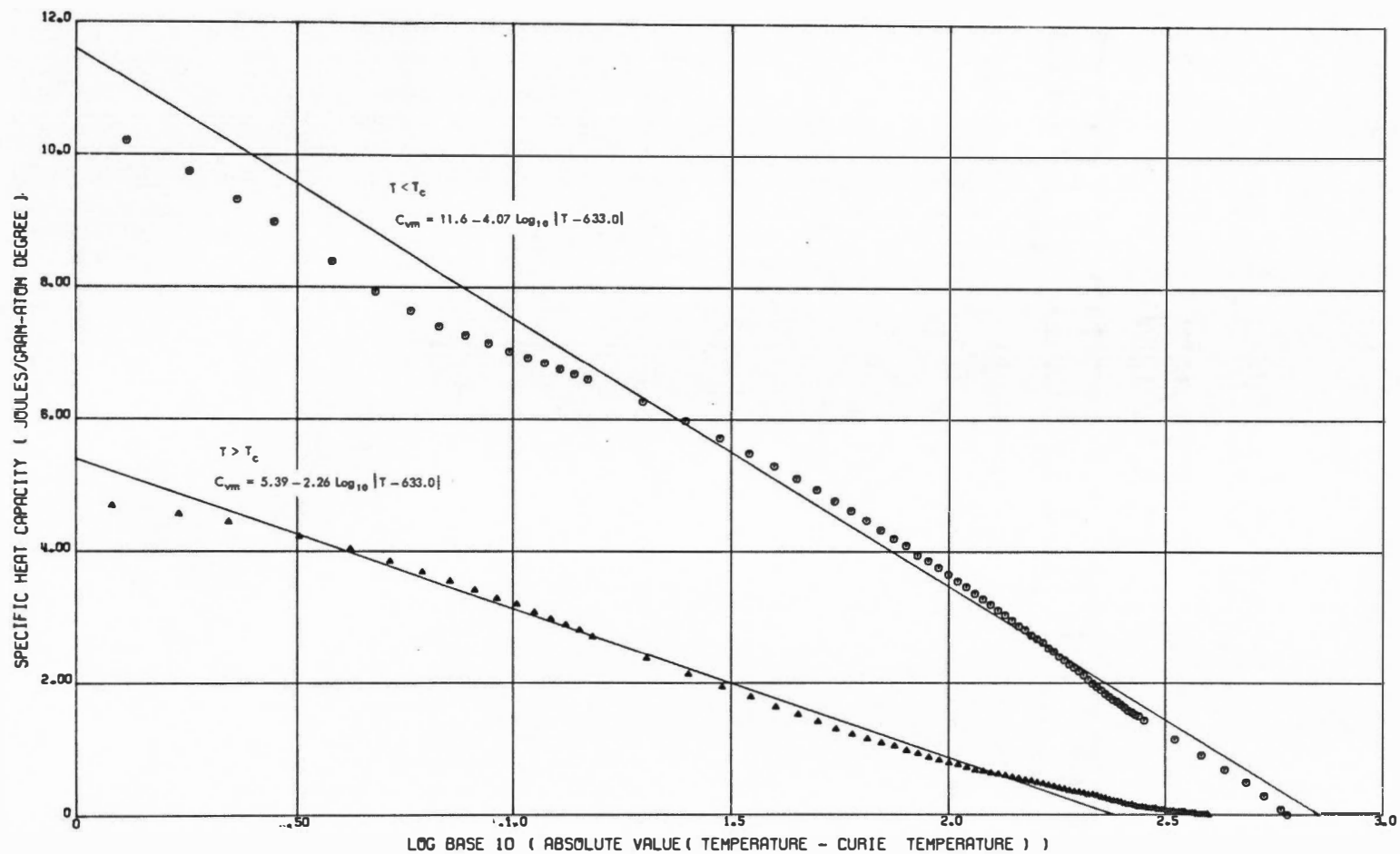


Figure 44. Plot of C_{vm} of Nickel as a Function of $\log_{10} |T - T_c|$ for Temperatures Above and Below the Curie Temperature of 633.0 K. The straight lines were obtained by fitting the data between 358 and 622 K and between 637 and 833 K.

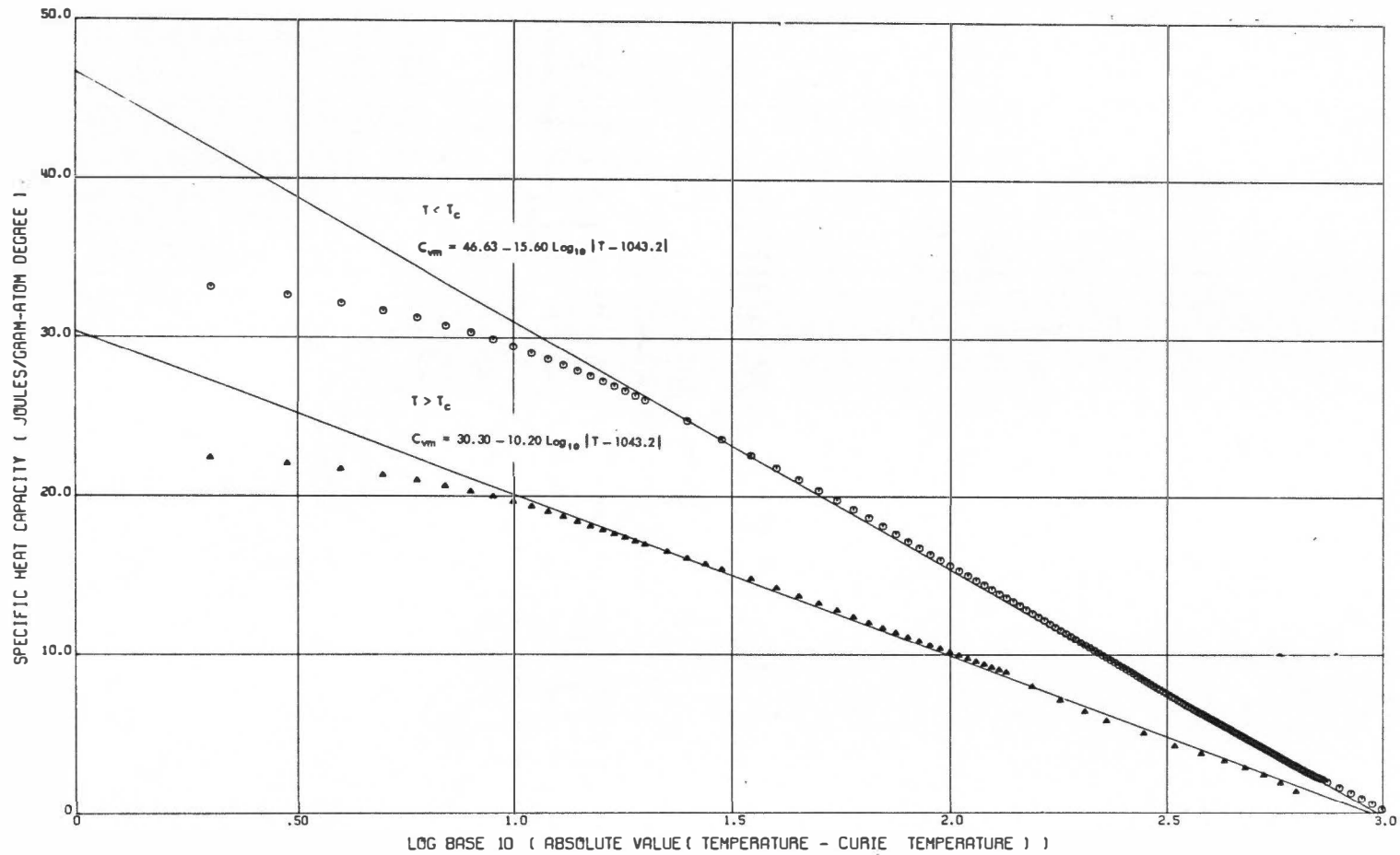


Figure 45. Plot of C_{vm} of Iron as a Function of $\log_{10} |T - T_c|$ for Temperatures Above and Below the Curie Temperature of 1043.2 K. The straight lines were obtained by fitting the data between 318 and 1028 K and between 1053 and 1673 K.

For temperatures which differ from T_c by more than ten degrees, there appears to be some adherence to the expected linear relationship. However, the slopes for data above and below T_c are not parallel. To investigate this further, the data for both iron and nickel were fit by the method of least-squares to the function $a + b \log_{10}|T - T_c|$. The values obtained for a and b and the temperature intervals employed are given in Table VIII. The resulting functions are plotted in Figures 44 and 45, and the data appear to vary periodically rather than randomly about the curve, suggesting that the assumed functional form is incorrect. However, it must be remembered that the C_{vm} data are the results of the subtraction of five temperature dependent functions from measured C_p data. Precise agreement should not be expected. Hence, the results of Figures 44 and 45, although not confirming the hypothesis, do not contradict it emphatically.

ΔC_{vm} , U_{vm} , and S_{vm} of Nickel and Iron

A straightforward method of comparing C_{vm} values between theories and/or experimental calculations is to use the C_{vm} data to compute the total magnetic energy U_{vm} and entropy S_{vm} by the appropriate integration of the $C_{vm}:T$ relationship. [See Equations (62) and (63), page 36.] These integrations were performed by the Simpson Rule, and the results are listed in Table IX. Since the value of the discontinuity ΔC_{vm} of C_{vm} at the Curie temperature is also related to the theories used to predict U_{vm} and S_{vm} , the ΔC_{vm} values are listed in Table IX and are discussed in conjunction with the U_{vm} and S_{vm} results.

TABLE VIII

RESULTS OF FITTING THE C_{vm} OF NICKEL AND IRON TO THE FUNCTION
 $a + b \log_{10}|T - T_c|$ ABOVE AND BELOW THE CURIE TEMPERATURE T_c *

	Nickel ($T_c = 633$ K)		Iron ($T_c = 1043.2$ K)	
	$T < T_c$	$T > T_c$	$T < T_c$	$T > T_c$
a	11.6 (± 0.1)	5.39 (± 0.05)	46.63 (± 0.07)	30.3 (± 0.1)
b	-4.07 (± 0.06)	-2.26 (± 0.03)	-15.60 (± 0.03)	-10.20 (± 0.07)
Variance	0.033	0.009	0.024	0.060
Temperature interval	358 K to 622 K	637 K to 833 K	318 K to 1028 K	1053 K to 1673 K
Number of points	57	49	147	48

*Units of constants are consistent with specific heat capacity units of joules/gram-atom degree.

The U_{vm} and S_{vm} values from theory and other experimental calculations from the literature were listed in Table III, page 45, for nickel and Table IV, page 47, for iron, and the theoretical values of ΔC_{vm} were presented in Table I, page 35. Tables X and XI contain the comparisons of the contents of these three tables with that of Table IX.

The general impression given by the differences listed in Tables X and XI is that the agreement between the results of this experiment and those of the theories and other experiments of the literature could be at best termed "fair." However, considering that all the experimental values

TABLE IX

MAGNETIC ENERGY U_{vm} , ENTROPY S_{vm} , AND DISCONTINUITY ΔC_{vm} OF C_{vm}
AT T_c OF NICKEL AND IRON FROM THIS INVESTIGATION

Quantity	Units	Iron	Nickel
U_{vm}	Joules/gram-atom	10600(± 1600)	1420(± 210)
S_{vm}	Joules/gram-atom degree	13.3(± 2.0)	3.20(± 0.48)
ΔC_{vm}	Joules/gram-atom degree	11.13	6.66
$\Delta C_{vm}/nk^*$		1.22 [†]	1.34 [‡]

*The quantity n is the effective number of magnetic atoms per gram-atom.

[†]For iron atoms of spin one per atom, n equals 1.1 magnetic atoms per atom.

[‡]For nickel atoms of spin one-half per atom, n equals 0.6 magnetic atoms per atom.

have error bands of ± 10 to $\pm 20\%$ and that the theories are only approximate, the quality of the agreement is good. For example, Table XI shows that the results for nickel agree to within the combined $\pm 15\%$ error bands of any two experimentally based determinations. The agreement for iron is not as good; but, considering the difficulties introduced by the α - γ transformation and a 400 degree higher Curie temperature than nickel, the iron results are acceptable with the possible exception of the values of Lytton.⁶⁶

TABLE X

COMPARISON OF THE RESULTS OF THIS INVESTIGATION FOR NICKEL AND IRON WITH THEORETICAL VALUES IN THE OPEN LITERATURE

Theory	Reference Numbers*	Percent Difference [†]					
		Nickel			Iron		
		ΔC_{vm}	U_{vm}	S_{vm}	ΔC_{vm}	U_{vm}	S_{vm}
Bethe-Peierls-Weiss	44				+179	-17	
Ising	44,53	+22	+56			-8	
Constant coupling	41,42	-4	+34		+44	-17	
Molecular field	35	+12			+64		
Heisenberg	62		+10	+8		-33	-24

*See page 214.

[†]Percent difference = 100 (Theory - This Investigation)/(This Investigation).

TABLE XI

COMPARISON OF RESULTS OF THIS INVESTIGATION FOR NICKEL AND IRON WITH LITERATURE VALUES CALCULATED FROM EXPERIMENTAL DATA

Experiment	Reference Numbers*	Percent Difference [†]			
		Nickel		Iron	
		U_{vm}	S_{vm}	U_{vm}	S_{vm}
Hofman, Paskin, Tauer, and Weiss	62	+20	+6	-24	-32
Lytton	66	-10	+21	-62	-56
Braun and Kohlhaas	8	+23		-17	
Pawel and Stansbury	61	-18	-21		
Grew	65		+5		

*See page 214.

[†]Percent difference = 100 (Experiment - This Investigation)/(This Investigation).

None of the theories appear to be universally applicable to the results on nickel and iron. For example, though the constant coupling approximation is in excellent agreement with the ΔC_{vm} results on nickel and the U_{vm} results on iron, the ΔC_{vm} of iron and U_{vm} values of nickel are too high to be attributed solely to calculation errors of the experimental results. Thus, these comparisons tend to question the validity of applying these localized electron models to metals such as nickel and iron which have highly itinerant electrons. However, the overall "best" model appears to be the Heisenberg approximation.

Brief Summary of Results on Nickel and Iron

Calculations of the magnetic contribution to the specific heat capacities of iron and nickel are plagued with uncertainties. Lacking thermal expansion and compressibility data to high temperatures, the Nernst-Lindemann approximation was used for the dilation correction. Also, a first approximation was used for the electronic contribution in the absence of the knowledge of the electron density of states as a function of temperature and energy. Similarly, the phonon spectrum is unknown for these metals as a function of temperature. Consequently, the phonon contribution was approximated by the Debye theory for the harmonic normal modes of oscillation and by a simplified theory for the anharmonic oscillations. Finally, the results of these calculations for the magnetic contribution were compared with models based on localized electrons. (The more appropriate itinerant electron models do not exist at present.) Nonetheless, the agreement with the Heisenberg approximation for U_{vm} and S_{vm} is satisfactory and with the constant coupling

approximation for ΔC_{vm} and U_{vm} is fair. Also, although the various experimental calculations appearing in the literature were performed under different sets of assumptions, the agreement of these calculations with those herein is within the calculation errors.

Table XII summarizes the parameters used to obtain the results on nickel and iron listed in Table XIII.

TABLE XII
SUMMARY OF PARAMETERS USED TO CALCULATE CONTRIBUTIONS
TO C_p OF NICKEL AND IRON

Quantities	Units	Reference*	Contribution	Nickel	Iron
γ_{nl}	Gram-atom/joule	118	C_d	2.624×10^{-6}	2.349×10^{-6}
γ	Joules/gram-atom	33	C_{ve}	7.028×10^{-3}	4.741×10^{-3}
θ_d	Kelvin	†	C_{vh}	400	440

* See page 214.

† Obtained from consideration of shape of C_x curve between 100 K and 200 K when θ_d was varied about values which appeared in the literature.

TABLE XIII

SUMMARY OF RESULTS ON NICKEL AND IRON

Quantities	Units	Contribution	Nickel	Iron
B	Joules/gram-atom K ²	C _v	$-1.76(\pm 0.01) \times 10^{-3}$	$-1.13(\pm 0.09) \times 10^{-3}$
A	Joules/gram-atom K ⁴	C _{ve}	$-1.48(\pm 0.06) \times 10^{-10}$	$2.1(\pm 0.4) \times 10^{-10}$
ΔC_{vm}	Joules/gram-atom K		6.66	11.13
$\Delta C_{vm}/nk$			1.34	1.22
U _{vm}	Joules/gram-atom		1420(±210)	10600(±1600)
S _{vm}	Joules/gram-atom K		3.20(±0.48)	13.3(±2.0)

Specific Heat Capacity of Ni₃Fe

The specific heat capacity of Ni₃Fe is a function of the prior heat treatment of the alloy as well as temperature. In addition, the measurements of this investigation revealed that the C_p of Ni₃Fe between 750 and 1050 K was dependent on the heating rate. In this temperature range, the heating rates employed varied from 20 to 60 degrees/second and changed considerably during each pulse because the specimens were heated directly by passing a current through them and because large quantities of heat were absorbed during configurational and magnetic disordering of the alloy occurring during heating. Thus, in order to eliminate verbiage, the pulses employed are described as either Class I or Class II. In essence, these two classes differed by about a factor of two in heating rate at a given temperature because Class I pulses utilized specimen currents which were nominally 100 amperes whereas the Class II pulses were nominally 150 amperes.

All C_p measurements on Ni₃Fe, other than those at liquid helium temperatures, were performed in Pulse Calorimeter I, and all heat treatments of the specimens were performed in situ. Hence, measured differences in the high temperature C_p values cannot be attributed to experimental errors caused by specimen dimension measurements or thermocouple placement. Also, all heat treatments were performed below 900 K, which greatly reduced the possibility of thermocouple contamination noted during the C_p measurements on nickel and iron above 1200 K.

Ten different heat treatments were performed on the Ni₃Fe specimen in Pulse Calorimeter I. These states of order have been cataloged as

shown in Table XIV and are referred where possible to the electrical resistivity of the state at 748 K — the approximate temperature at which the electrical resistivity differences were maximum and at which the ρ values were independent of heating rate. Of the ten states, four were ordered locally and the other six had varying degrees of long-range order. Note that the order state numbers assigned to the treatments yielding some long-range order do not refer to the degree of order but rather to the chronological sequence of the treatment. The type pulse and the temperature interval encompassed during the C_p measurements are also listed in Table XIV for each treatment. The specific heat, the electrical resistivity, and the temperature-rate-of-change of the electrical resistivity of these states as a function of temperature are listed in Tables XXVII to XXXVII in the Appendix.

In the remaining sections of this chapter, the specific heat capacity measurements of Ni_3Fe outlined above are presented and then discussed with regard to the contributions to C_p . First, however, the auxiliary electrical resistivity measurements on this alloy are described.

Auxiliary Electrical Resistivity Measurements on Ni_3Fe . Auxiliary measurements of the electrical resistivity ρ of the Ni_3Fe alloy as a function of the state of order were performed in several apparatuses described in Chapter II. These measurements were used as a monitor of the state of order of the specimen during C_p measurements and consisted essentially of eight series of experiments.

TABLE XIV

STATES OF ORDER AND DISORDER OF THE Ni_3Fe SPECIMEN FOR
WHICH C_p MEASUREMENTS WERE MADE IN PULSE CALORIMETER I

Heat Treatment	Electrical Resistivity at 748 K (Ohm-cm) $\times 10^{-6}$	Type Order	Class Pulse	Temperature Interval of Measurement (Kelvin)
Vacuum-Quench A*	65.03	Local	I	308-1423
Vacuum-Quench B*	64.74	Local	II	748-1048
Annealed at 848 K for one hour	†	Local	I	848-973
Annealed at 879 K for one hour	†	Local	I	879-973
Annealed below 770 K for four days (Order-State I)	59.42	Long	I	303-993
Annealed below 770 K for sixteen days (Order-State II)	53.53	Long	I	423-1023
Annealed below 770 K for eight days (Order-State III)	56.13	Long	II	683-1083
Annealed below 770 K for seventeen days (Order-State IV)	52.28	Long	II	673-1093
Annealed below 770 K for three days (Order-State V)	60.82	Long	II	638-1063
Annealed below 770 K for sixty-three days (Order-State VI)	50.90	Long	II	393-1073

*Quenching rate at 773 K was 0.7 degree/second.

†Estimated to be approximately 65×10^{-6} ohm-cm.

The first series involved taking ρ data as the alloy was cooled slowly from 1362 to 767 K. This cooling was performed in steps, and sufficient time was allowed at each intervening temperature to ensure that the state of order was the equilibrium state. For example, cooling from 900 to 775 K progressed over a period of thirty days and from 775 to 767 K over a period of four days. During this sequence of experiments, no perceptible change (0.1%) in the electrical resistivity occurred during the 24-hour period following a 4-hour soak at a given temperature. However, at 767 K, which is several degrees below the order-disorder equilibrium temperature, the first exception was caused by the formation of long-range order, which has a very long relaxation time.

The second through the seventh series of experiments were performed on the alloy possessing varying degrees of long-range order and consisted of holding at temperatures of 767, 755, 735, 713, 645, and 602 K until no perceptible change in ρ occurred over a 24-hour period. After each soak, the specimen was cooled rapidly to room temperature with short pauses at intervening temperatures to take ρ data. Subsequently, the specimen was heated back to the temperature from which it was cooled and the resistivity checked to ensure that no changes had occurred during cooling. Then the specimen was cooled to the next lower temperature and the sequence repeated. The pertinent data of these heat treatments are given in Table XV. It is noted that no significant change occurred after the anneal at 602 K, so that the data taken after the 645 K anneal are presumed to be a very close approximation to the equilibrium long-range ordered state at lower temperatures.

TABLE XV

HEAT TREATMENTS GIVEN THE Ni_3Fe SPECIMEN DURING FORMATION
OF LONG-RANGE ORDER BELOW THE CRITICAL TEMPERATURE
DURING AUXILIARY RESISTIVITY MEASUREMENTS

Soak Temperature (Kelvin)	Days at Temperature	Electrical Resistivity (Ohm-cm) $\times 10^{-6}$		
		At Start	At End	Change
767	47	67.00	57.66	9.34 (13.9%)
755	28	55.71	54.35	1.36 (2.4%)
735	19	51.27	49.98	1.29 (2.5%)
713	25	46.88	45.75	1.13 (2.4%)
673*	28	40.79	40.21	0.58 (1.4%)
645	12	36.83	36.78	0.05 (0.13%)
602	21	32.21	32.19	0.02 (0.06%)

*No measurements of ρ made after this heat treatment because of experimental difficulties. There should be little difference between these and those taken after the 645 K soak.

The eighth and last series of measurements were performed after the specimen had been quenched from 1400 K into ice water. These measurements consisted of heating the sample, with intermittent stops for ρ data acquisition, until the resistivity was found to decrease as a function of time at temperature. The temperature at which this change was encountered was 589 K.

Results of the auxiliary measurements are shown in Figure 46. In Table XVI, they are correlated with the heat treatments given the C_p

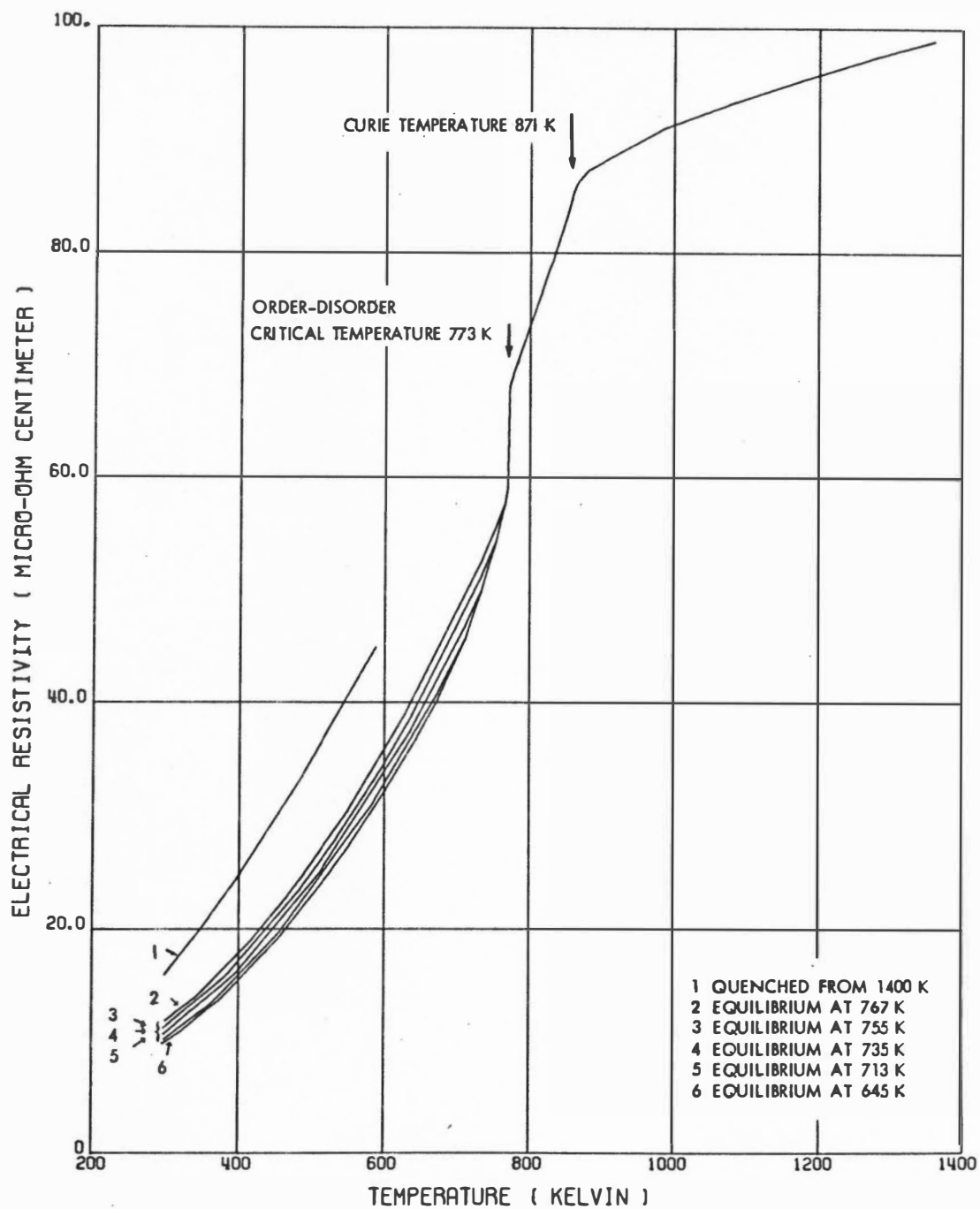


Figure 46. Electrical Resistivity Measurements on the Ni_3Fe Alloy as a Function of Its State of Order and Temperature.

TABLE XVI

CORRELATION OF THE HEAT TREATMENTS GIVEN THE C_p SPECIMENS
WITH THE AUXILIARY ELECTRICAL RESISTIVITY MEASUREMENTS
AND AN ESTIMATE OF THE LONG-RANGE ORDER PARAMETER S
FOR EACH STATE

Heat Treatment of C_p Specimen	Estimated Equilibrium Temperature of State* (Kelvin)	Estimate of Long-Range Order Parameter S
Order-State VI	714.0	0.96
Order-State IV	743.0	0.92
Order-State II	757.5	0.88
Order-State III	772.5	0.78
Order-State I	773.0	0.66
Order-State V	773.2	0.60
Vacuum-Quench B	783	0.0
Vacuum-Quench A	800	0.0
848 K anneal	848	0.0
879 K anneal	879	0.0

*Temperature of intersection of electrical resistivity of state with the equilibrium electrical resistivity curve.

specimen in Table XIV, page 163. Table XVI also contains an estimate of the long-range order parameter S for each state of order used in the C_p experiments based on the assumption that the water-quenched alloy had no long-range order and that the 602 K anneal produced perfect long-range order. This was accomplished assuming that $\Delta\rho$ was proportional to $(1 - S^2)$, as suggested by Beal's⁹⁰ theory given in Equation (74) on page 56.

In closing this section, it is noted that thermoelectric power measurements were also performed during the course of the auxiliary electrical resistivity measurements. However, no use of these data is made in this work, but the general effect of ordering is to raise the absolute thermoelectric power of Ni_3Fe . These and the auxiliary ρ data are listed in Tables XXXVIII to XLIV in the Appendix.

Low-Temperature Measurements of C_p of Ni_3Fe . Measurements of the C_p of Ni_3Fe between 1.2 and 4.4 K were performed by Mr. J. O. Scarbrough of the Metals and Ceramics Division of the Oak Ridge National Laboratory for use herein and are listed in Table XXVI in the Appendix. These measurements were acquired in a low-temperature adiabatic calorimeter described briefly in Chapter II and in more detail in Reference 100.

In Figure 47, the results obtained on an ordered and disordered specimen are plotted in the normal manner for low-temperature C_p data, namely C_p/T versus T^2 . The disordered specimen was produced by quenching the specimen into ice water from 1400 K, and the ordered state by annealing for one week at 753, 733, 723, and 683 K in succession. Electrical resistivity measurements indicated that this state of

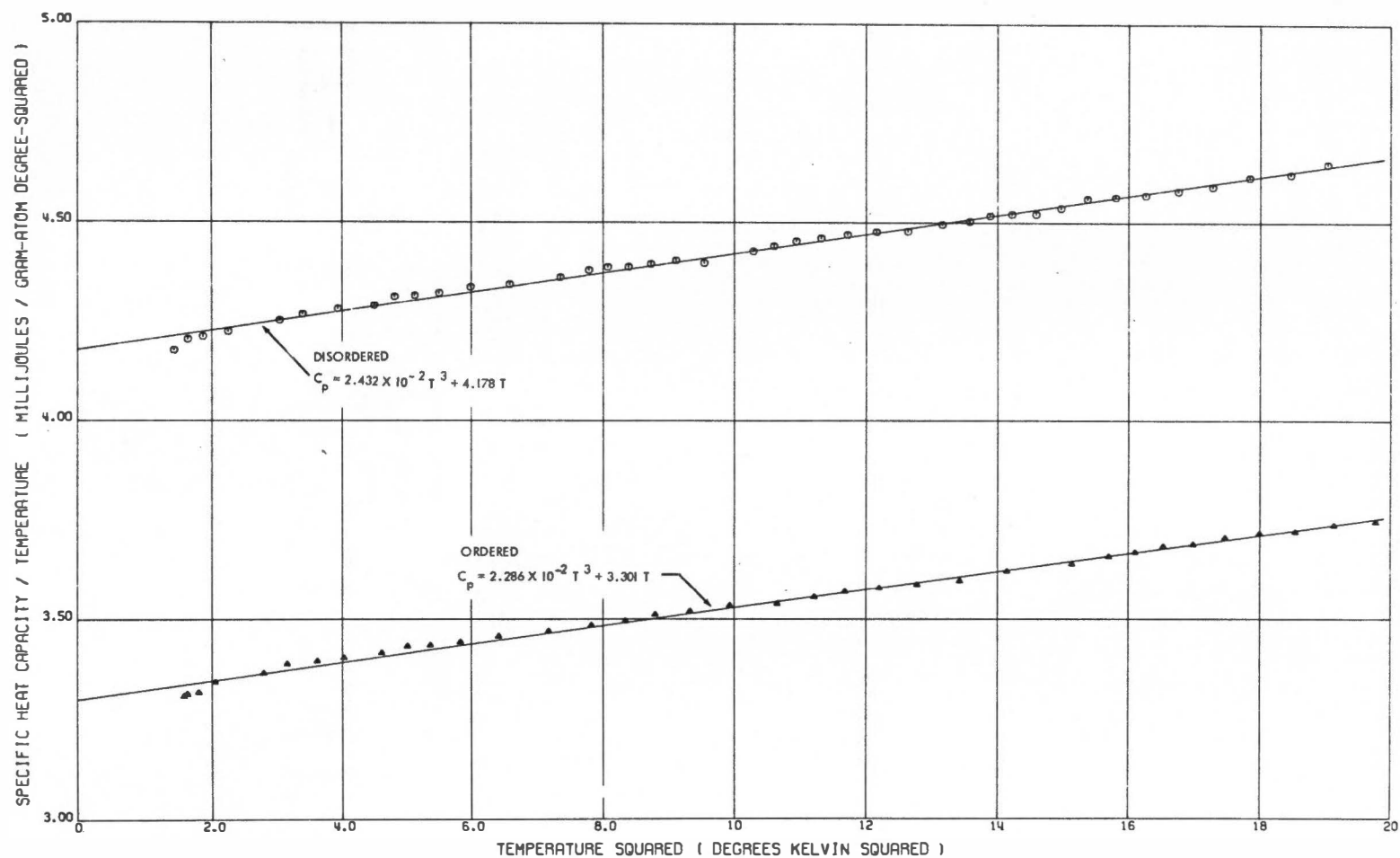


Figure 47. Low-Temperature C_p of Ordered and Disordered Ni_3Fe Plotted as C_p/T Versus T^2 . Disorder produced by quenching specimen from 1400 K into ice water. Order produced by successive one-week anneals at 753, 733, 723, and 683 K. Curves obtained by fitting the data using method of least squares.

order corresponded to an equilibrium temperature of 745 K and a long-range order parameter of 0.91. Annealing the alloy in this manner lowered the C_p by about 21% near 1.2 K and 20% near 4.2 K. Theoretical justifications for these changes are given after the discussion of the high-temperature C_p results.

C_p Measurements of Ni_3Fe below 750 K. Below 750 K, the C_p measurements obtained were independent of the 5 to 20 degrees/second heating rates employed. This does not imply that the C_p of Ni_3Fe below 750 K is independent of all experimental heating rate. For instance, the results of Leech and Sykes⁷¹ presented in Figure 7 (page 50) indicate anomalies at 650 K which were not noted in this investigation and are due to their much slower heating rate of 0.03 degree/second.

In Figure 48, the $C_p:T$ relationships for Order-States I, II, and VI and for Vacuum-Quench A are shown between 300 and 760 K. Order-States III, IV, and V are not included because their $C_p:T$ relationships were quite similar to Order-States II, VI, and I, respectively. In general, these results are analogous to those of Figure 47 in which the specific heat capacity was noted to decrease with increasing configurational order. However, the maximum percentage decrease is only 5.7% at 750 K, which is much less than the 20% difference noted at 4.2 K. Nonetheless, the theoretical justifications for these changes are the same and are considered later.

C_p Measurements of Ni_3Fe above 750 K. For temperatures between 750 and 1050 K, the $C_p:T$ relationships for all states, whether of long-range or of local order, were found to be a function of the experimental

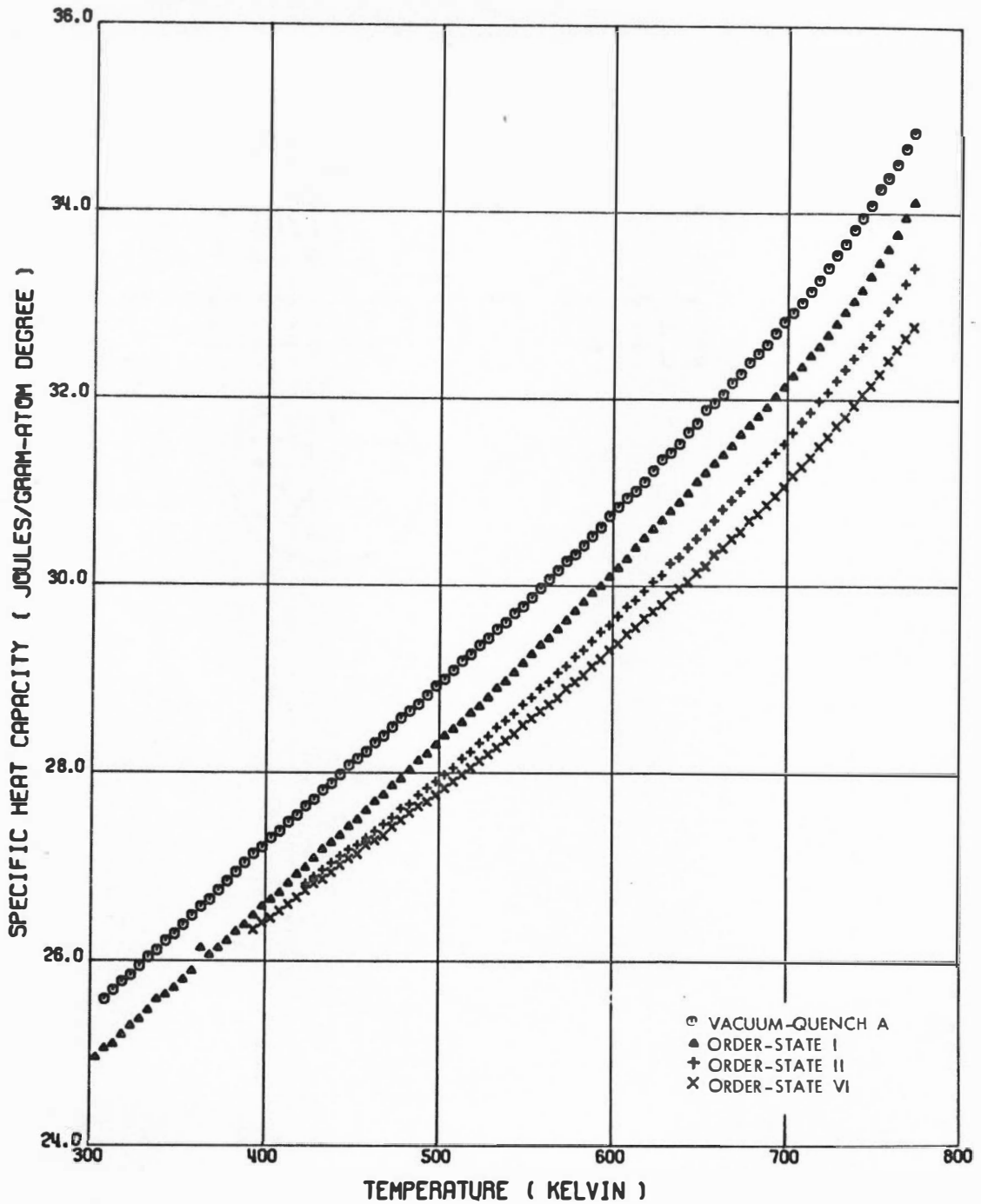


Figure 48. The Specific Heat Capacity as a Function of Temperature for Order-States I, II, and VI and for Vacuum-Quench A of the Ni_3Fe Specimen in Temperature Range where Results were Independent of Heating Rate.

heating rate. This is understandable because the configurational order-disorder critical temperature for this alloy is about 773 K. Also to be considered is the presence of the magnetic disordering phenomenon, which has a Curie temperature of about 871 K for a disordered or locally ordered configurational structure.

Between 750 K and the critical temperature of 773 K, the effects of the heating rate are quite subtle and were less than 0.5%, which was barely discernible. As the temperature was increased above 773 K, the heating rate effects became more pronounced, as demonstrated by the following four examples.

The $C_p:T$ relationships obtained for the four locally ordered states of the Ni_3Fe specimen listed in Table XIV, page 163, are given in Figure 49. All but the Vacuum-Quench B results were obtained with a Class I heating rate, and all but the 879 K anneal state were pulsed from below the Curie temperature of about 871 K. The $C_p:T$ relationships for those states pulsed from below 871 K demonstrate two peaks. The lower temperature but higher peak is associated with the Curie transformation; the higher temperature peak between 900 and 950 K is associated with the destruction of local configurational order. The latter assertion is based on noting that the peak for the 879 K anneal is lower than that of the second peak of the 848 K anneal, which had a larger amount of local order. Also note that the second peak of the Vacuum-Quench B data occurs at a temperature 40 degrees above that of the Vacuum-Quench A data, which were taken with a slower heating rate. Hence, the higher rate forced the energy absorption to occur at a higher temperature.

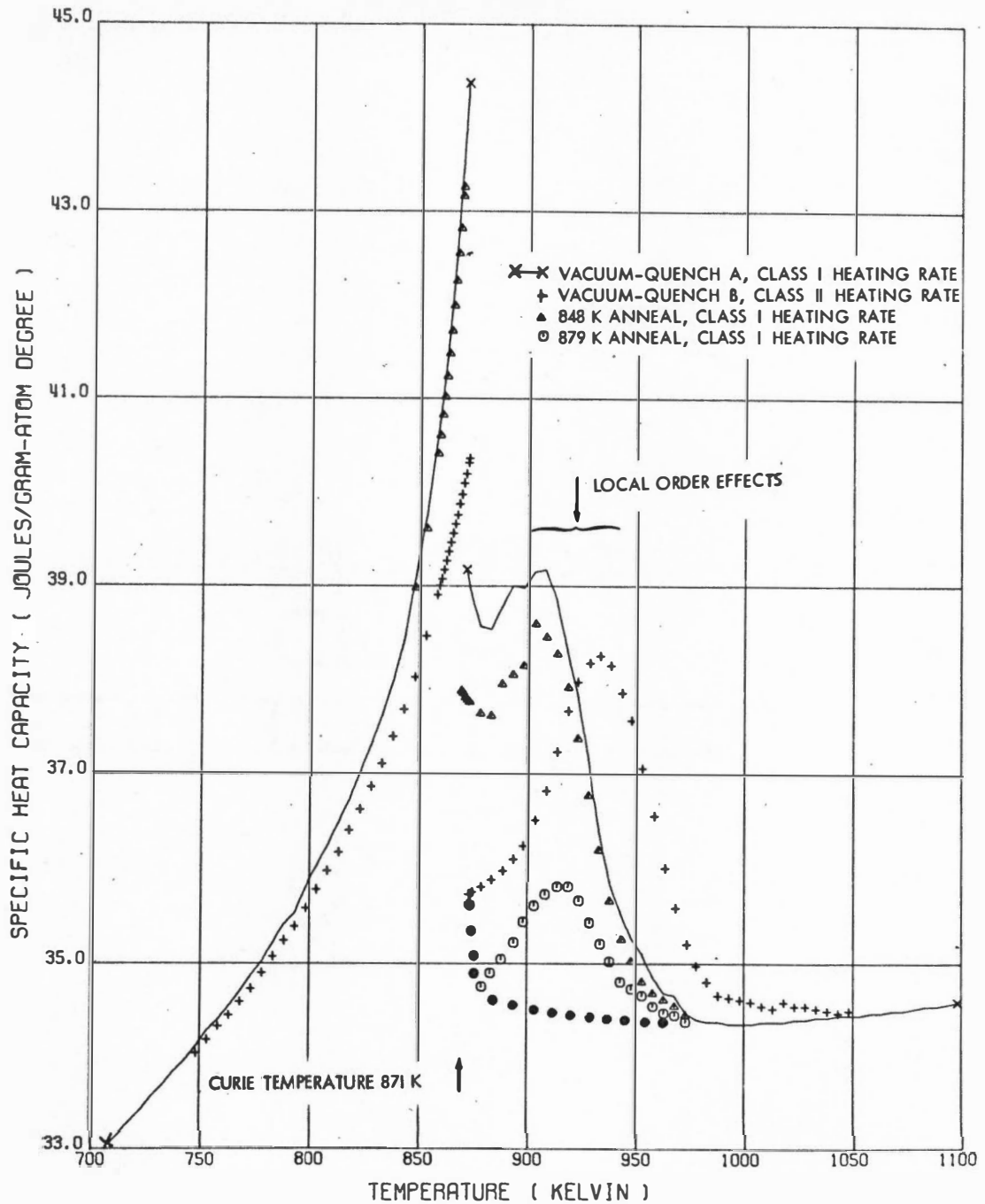


Figure 49. The Specific Heat Capacity as a Function of Temperature for Four Locally Ordered States of Ni_3Fe Showing the Effects of Heating Rate.

This is precisely the effect to be expected from a rate process such as atomic disordering. On the other hand, the heating rate did not affect the temperature at which the Curie transformation occurred because the kinetics of this process are extremely rapid.⁹⁶ Differences in the peak heights at T_c are due to the heating rate effects on the destruction of local order, not on the Curie transformation. This can be seen by comparing the differences in the peak heights of the 848 K anneal state and those of Vacuum-Anneal A state, both of which were obtained with a Class I heating rate.

Figure 50 presents a slightly different picture than Figure 49 because both states possess long-range configurational order. Order-State I had an estimated S of 0.66, and the data on this state were obtained with a Class I heating rate. The S for Order-State V was 0.60, and these C_p data resulted from a Class II heating rate. Note that the Curie temperature for Order-State I was about 890 K, which is 19 degrees above that of the locally ordered or equilibrium state. Order-State V had a Curie temperature of 905 K, some 34 degrees above the equilibrium state. These differences in T_c are a ramification of the interactions between the two cooperative phenomena — long-range magnetic order of the electrons and long-range configurational order of the atoms of the alloy. Also, the differences in T_c are only indirectly dependent on the heating rate; that is, the heating rate is not forcing the Curie transformation to higher temperatures. What happened was the faster heating rate used with Order-State V was capable of preserving the metastable ordered state to higher temperatures, and the higher the state of order, the higher the Curie temperature.

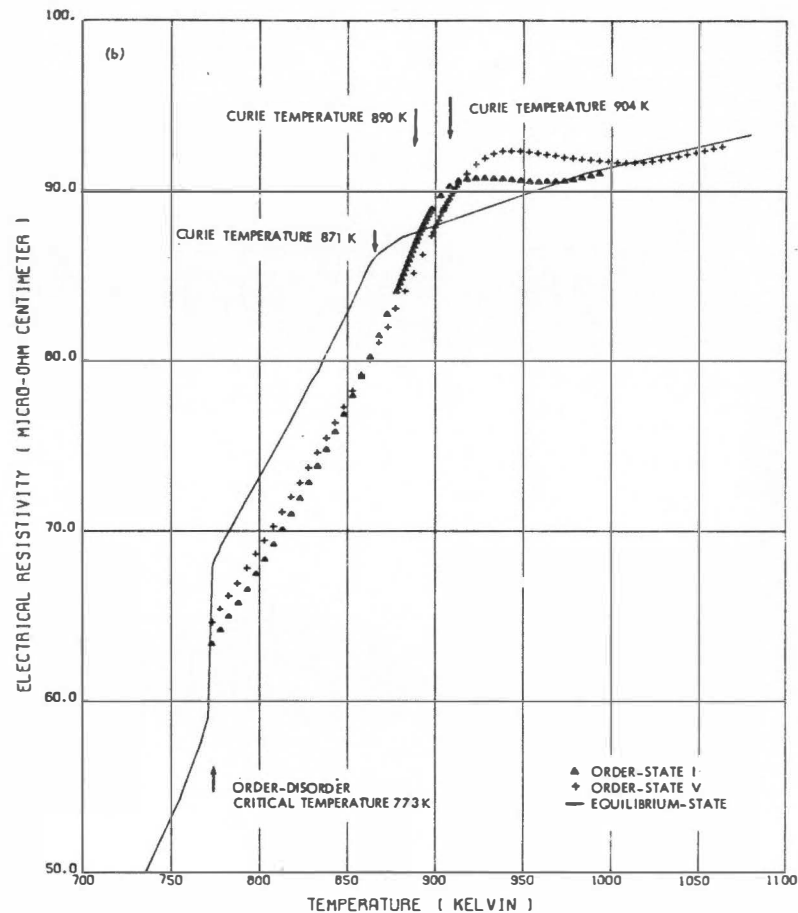
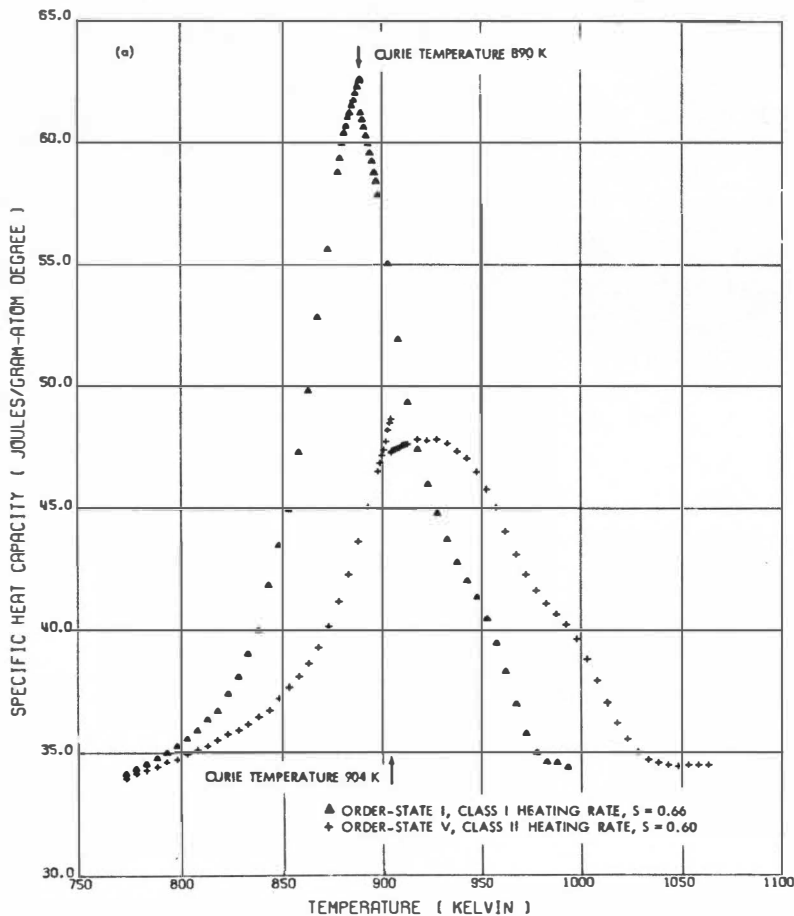


Figure 50. The Specific Heat Capacity and Electrical Resistivity of Ni_3Fe as a Function of Temperature for States Having Long-Range Order Parameters of 0.66 (Order-State I) and 0.60 (Order-State V), Showing the Effects of Heating Rate. (a) Specific heat, (b) electrical resistivity plus Equilibrium-State curve.

To demonstrate this point, consider the electrical resistivity ρ curves shown in Figure 50(b). Initially, the ρ of Order-State I was lower than that of Order-State V since the Order-State I was more highly ordered. However, at about 860 K the ρ of Order-State V crosses over and becomes lower than Order-State I, indicating that above 860 K the S of the latter state is lower. Thus, during heating below T_c , the configurational order of Order-State I was being destroyed, which accounts for the extremely large peak near T_c for this state and the absence of a second peak at higher temperatures. On the other hand, the question is raised, "Was order being destroyed during heating of Order-State V?" "Probably so," is the answer. However, note that instead of having the usual magnetic tail in the $C_p:T$ relationship above T_c , a very extended peak occurs for Order-State V. This anomaly is due to the very rapid destruction of the long-range order above 900 K.

Note the shape of the $C_p:T$ relationship of States I and V at T_c . Immediately below T_c the curvature is negative instead of positive and above T_c the curvature is positive instead of negative, when compared with similar regions of the $C_p:T$ curves for iron, nickel, and the disordered structures of Ni_3Fe . In order to explain these discrepancies it is hypothesized that the state of order is not uniform throughout the specimen. Consequently, the specimen had not one but a large number of Curie temperatures, each dependent on the state of order in a given region of the specimen. Precisely the same condition would be expected for a two-phase material undergoing a Curie transformation in

coincidence with a transformation back to one of its two phases. For example, a 5% nickel-95% iron alloy near 1040 K would yield this type $C_p:T$ relationship (see Figure 5, page 41).

The third example concerns Figure 51 in which the $C_p:T$ relationship is demonstrated for the more highly ordered states of Order-States II and III ($S = 0.88$ and $S = 0.78$, respectively). Again the Curie temperatures are raised. A T_c of 919 K was found for Order-State II and 920 K was found for Order-State III. The close proximity of these T_c 's is adequately explained by the superposition of the two ρ curves at T_c [Figure 51(b)]. This indicates that the "average" state of order was the same for both at T_c . The differences in the maxima in C_p at T_c are due to the differences in the heating rates, which allowed more configurational energy to be absorbed during the slower heating.

The second peaks in the $C_p:T$ relationship are prevalent for both states in Figure 51, and their maxima coincide in temperature with the temperature at which $d\rho/dT$ are a minima. This, plus the shape of the $\rho:T$ curve, is asserted to be the proof that the first peak is associated with the Curie phenomenon and the second peak is associated with configurational disordering. Also, note that the second peak for the faster heating rate occurred at a higher temperature, which is further evidence that an atomic-diffusion-controlled rate-process is occurring.

In comparing the results of the last two figures for the data taken with Class II heating rates, one finds that the second peak occurred at about 930 K for Order-State V ($S = 0.6$) and at about 980 K for Order-State III ($S = 0.78$). Hence the higher the order, the higher

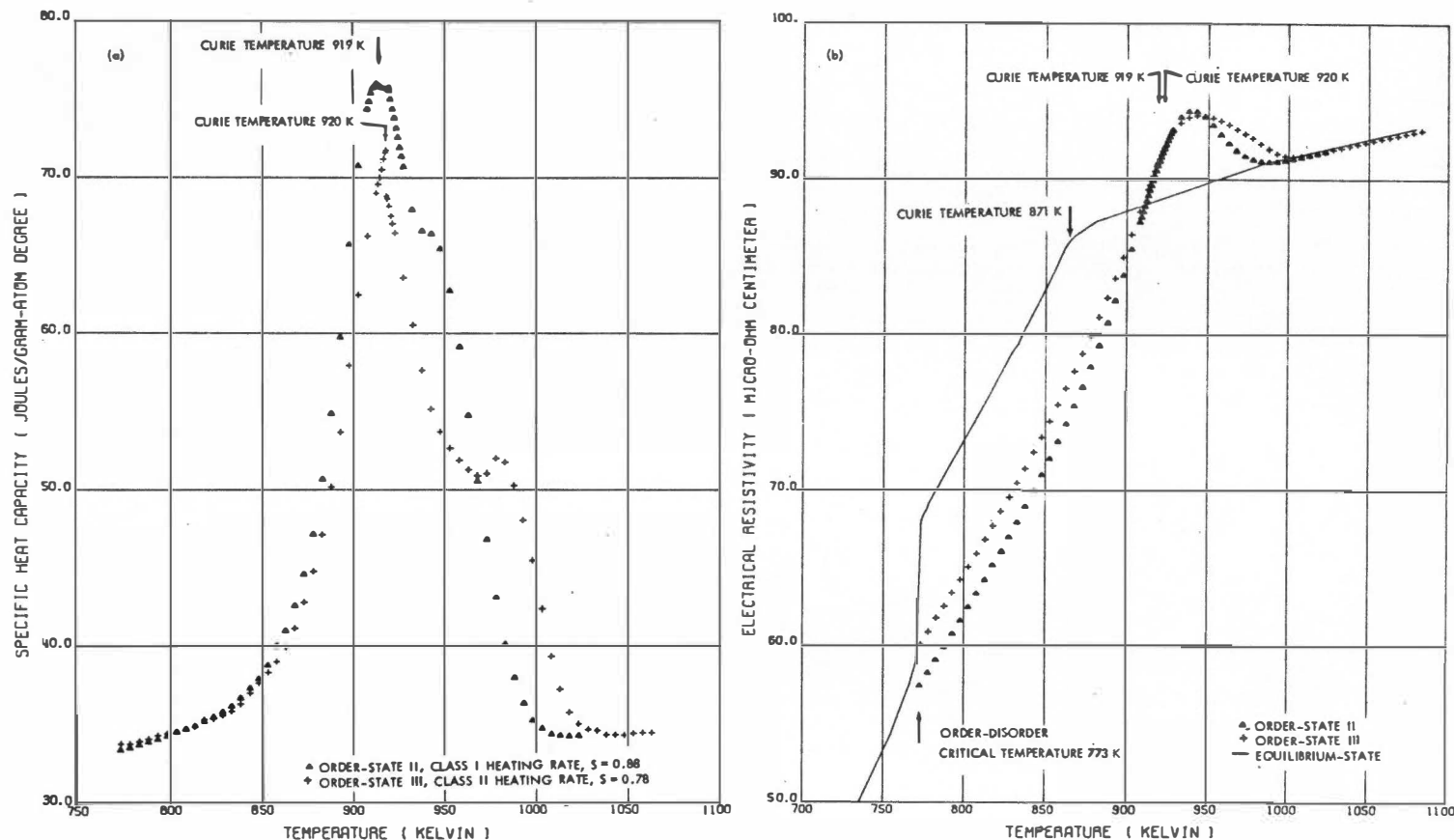


Figure 51. The Specific Heat Capacity and Electrical Resistivity of Ni_3Fe as a Function of Temperature for States Having Long-Range Order Parameters of 0.88 (Order-State II) and 0.78 (Order-State III), Showing the Effects of Heating Rate. (a) Specific heat, (b) electrical resistivity plus Equilibrium-State curve.

the temperature of the maximum rate of destruction of order. This is as though the higher order state is impeding its own destruction. The last example is further proof of this observation and is that of Figure 52. This figure depicts the $C_p:T$ and $\rho:T$ curves for Order-State VI ($S = 0.92$) in which the second peak occurred at 1005 K.

Figure 52 also demonstrates some of the points mentioned previously; for example, the shape of the $C_p:T$ curve near T_c . Also note the striking similarity between the $\rho:T$ relationships for Order-State VI and the Equilibrium-State curve, particularly in regard to the inflection at T_c .

In recapitulation, it was observed that increasing the state of order of Ni_3Fe decreases its C_p below 750 K. Above 750 K, the $C_p:T$ relationship measured was a function of the heating rate and the state of order. An increase in the state of order raised the Curie temperature of the metastable ordered states of Ni_3Fe . Also, the disordering temperature was higher for the higher heating rates and higher amounts of order. Unfortunately, the heating rates available were not sufficient to completely preserve the ordered state until the Curie transformation was complete, thereby eliminating the possibility of acquiring the magnetic specific heat capacity for the ordered state.

Interpretation of Low-Temperature C_p Measurements on Ni_3Fe

At liquid helium temperatures, the anharmonic and dilation contributions to the specific heat capacity of a solid are negligible. Consequently, the expression for C_p is

$$C_p = C_{vh} + C_{ve} + C_{vm} = \beta T^3 + \gamma T + \alpha T^{3/2} . \quad (110)$$

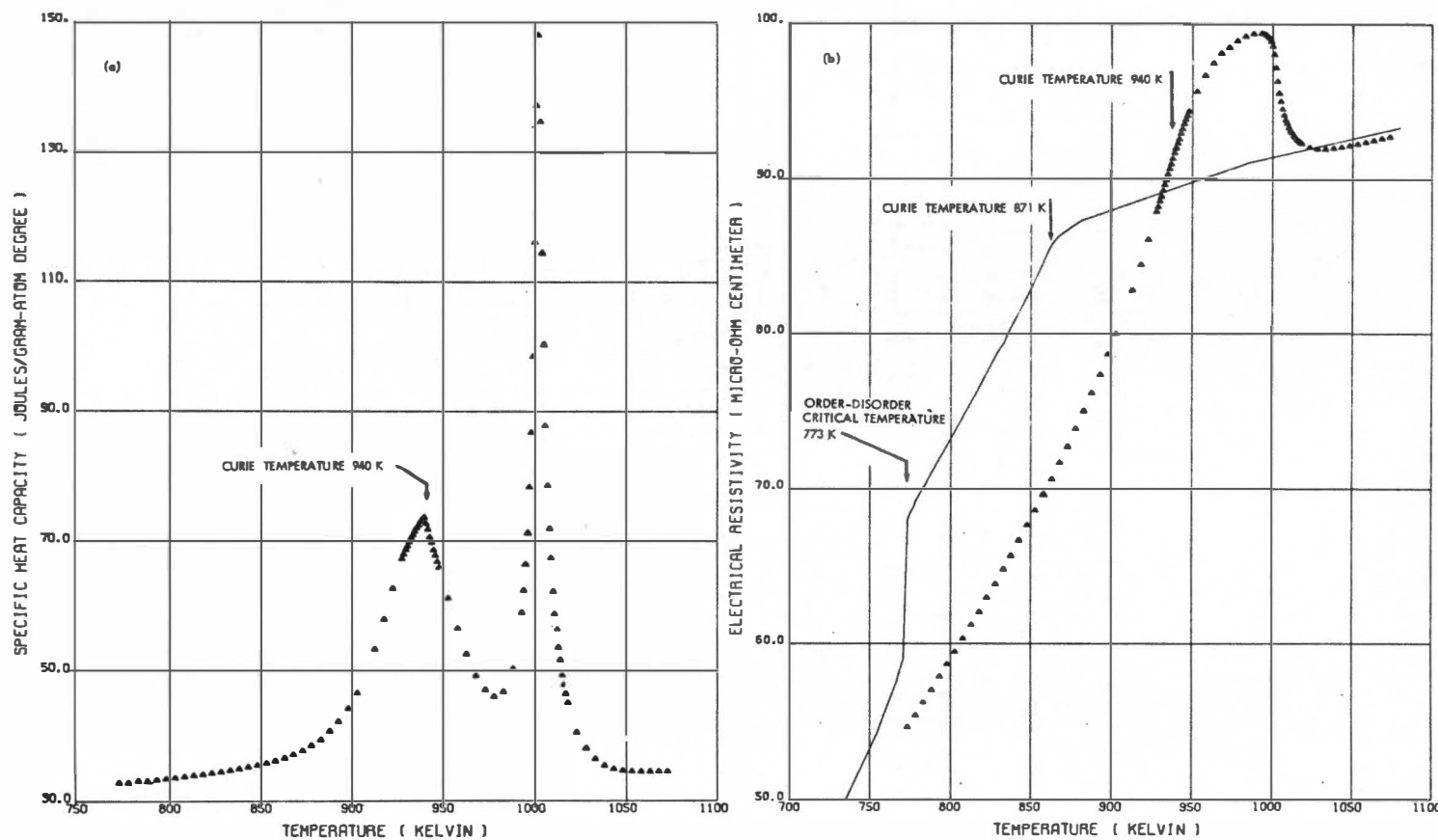


Figure 52. The Specific Heat Capacity and Electrical Resistivity as a Function of Temperature for a Highly Ordered State. (Order-State VI, $S = 0.96$). (a) Specific heat, (b) electrical resistivity plus Equilibrium-State curve.

In this equation, the low-temperature approximations for C_{vh} and C_{ve} were used, and the spin-wave theory was employed for C_{vm} [Equation (34), page 15; Equation (47), page 25; and Equation (51), page 28]. Assuming the spin-wave contribution to be negligible one finds from Equation (110) that C_p/T is linear in T^2 , that is

$$C_p = \beta T^3 + \gamma T. \quad (111)$$

Figure 47, page 169, depicts the low-temperature C_p measurements on ordered and disordered Ni_3Fe in which the data are plotted as C_p/T versus T^2 . The lines shown in this figure were obtained by fitting the data to Equation (111) by the method of least-squares, and the parameters for these fits are shown in Table XVII. These results indicate that the temperature coefficient γ of the electronic contribution C_{ve} is reduced by 21% upon ordering and the temperature coefficient β of the harmonic contribution C_{vh} is decreased by 6.4%. Such changes are justifiable theoretically, since a lowering of γ is reflected in a lowering of the density of states of the electrons near the Fermi energy because of the increase in the periodicity of the lattice upon ordering. Also, since the lattice contracts upon ordering, the cut-off frequency or θ_d increases, yielding a lower β .

Note that the four lowest temperature points for the ordered and disordered alloy in Figure 47 are below the fitted line. Since this indicates a periodic rather than random deviation from the $\beta T^3 + \gamma T$ relationship, Equation (110) was employed to fit the data. Use of the spin-wave term changed the β values substantially, but made only minor changes in the γ values. For example, γ of the ordered state decreased only 3.5%, but β decreased 21% (θ_d increased 7.8%).

TABLE XVII

LEAST-SQUARES PARAMETERS FROM FITS OF LOW-TEMPERATURE
 C_p DATA ON ORDERED AND DISORDERED Ni_3Fe

Equation of Fit	α ($\frac{\text{Millijoules-}}{\text{gram-atom K}^{5/2}}$) $\times 10^{-2}$	γ ($\frac{\text{Millijoules-}}{\text{gram-atom K}^2}$)	β ($\frac{\text{Millijoules-}}{\text{gram-atom K}^4}$) $\times 10^{-2}$	θ_d (Kelvin)	Number of Points
<u>Ordered*</u>					
111		3.301(± 0.010)	2.286(± 0.084)	439.7(± 8.4)	36
110	9.55(± 2.01)	3.187(± 0.024)	1.80(± 0.11)	476.6(± 9.4)	36
110	7.86(± 2.09)	3.209(± 0.025)	1.87(± 0.11)	470.2(± 8.9)	35 [†]
110	9.66(± 2.11)	3.186(± 0.025)	1.79(± 0.11)	477.2(± 9.4)	35 [‡]
<u>Disordered*</u>					
111		4.178(± 0.009)	2.432(± 0.083)	430.8(± 4.9)	41
110	10.44(± 1.81)	4.053(± 0.022)	1.888(± 0.097)	468.8(± 7.8)	41
110	7.44(± 1.82)	4.088(± 0.022)	2.008(± 0.094)	459.3(± 7.0)	40 [†]
110	11.61(± 1.75)	4.041(± 0.021)	1.810(± 0.095)	475.4(± 8.0)	40 [‡]

*Terms in parentheses are standard deviations of parameters.

[†]Lowest temperature data point left out of fit.

[‡]Highest temperature data point left out of fit.

The question now arises, "Which fit is the more exact?" To answer this question, the difference between the data and the fitted functions was plotted versus temperature for both the ordered and disordered cases, as shown in Figures 53 and 54. Although the variations are small, there is a definite periodicity for both functions on both alloy states. However, the differences are smaller for the fit which includes the spin-wave $\alpha T^{3/2}$ term.

One further investigation was conducted on the three term fit which consisted of systematically leaving out of the fit points from the low- or high-temperature end of the data. After the four low-temperature points were dropped from the fit, the value of α became negative and the standard deviation of α was twice its absolute value. However, leaving out an equal number of points on the high-temperature end was less influential. The parameters after leaving out the lowest and highest temperature points are included in Table XVII to illustrate this effect.

Obviously, therefore, neither the two nor three term equation is the precise representation of these data, but the three term is better if sufficient data near 1 K are included in the fit.

Dixon, Hoare, and Holden³⁴ investigated the specific heat capacity of disordered nickel-rich nickel-iron alloys between 1.2 and 4.4 K. By linearly interpolating their results between a 81.1% nickel and a 68.7% nickel alloy, their Debye temperature for Ni_3Fe was 475.7 K, which is within one standard deviation of the results shown in Table XVII for the three term fit. Similarly, their γ value is 4.163 millijoules/gram-atom K^2 , which is 2.7% higher. Some of this difference is due to the linear

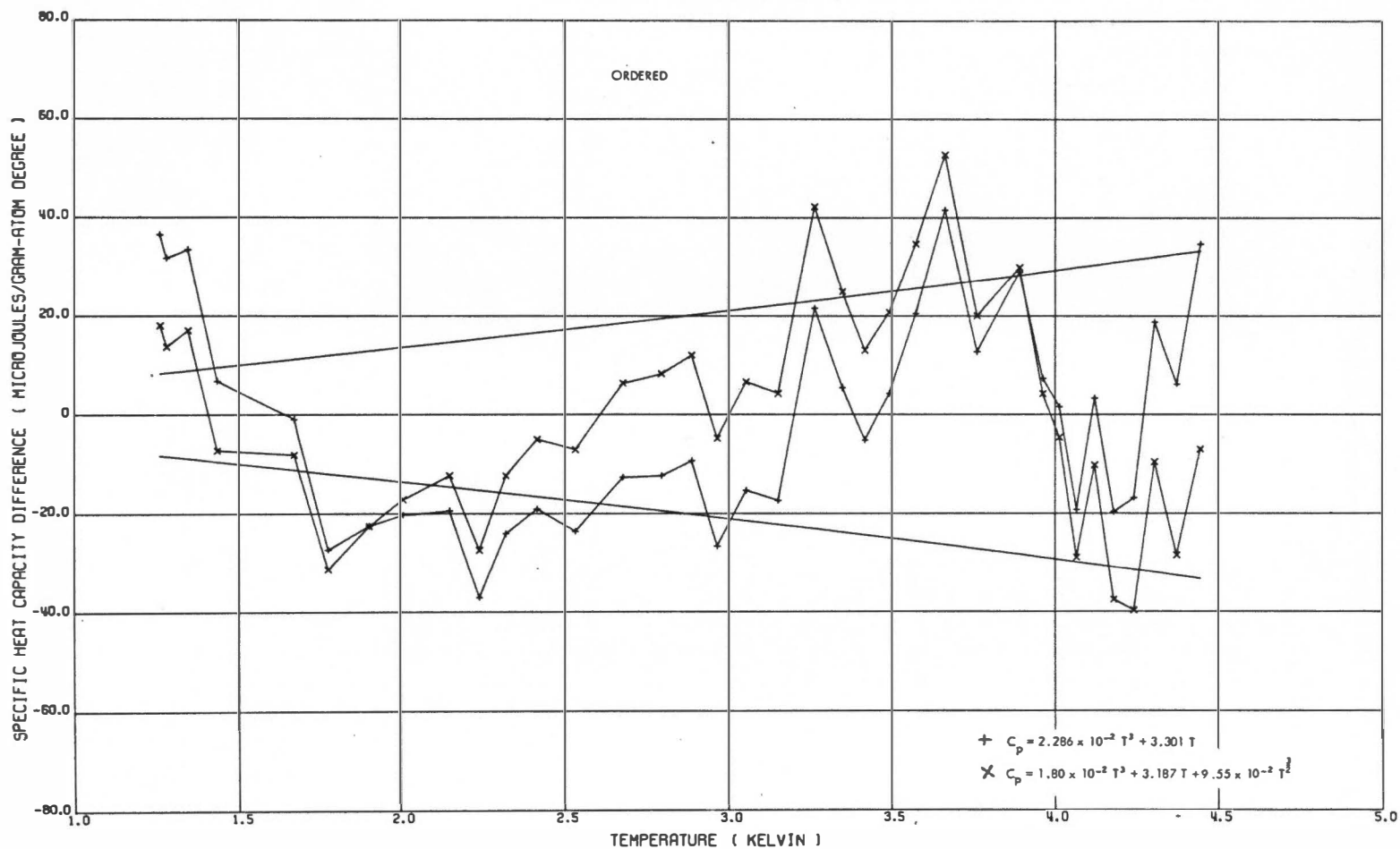


Figure 53. Specific Heat Capacity Calculated from Two-Term and Three-Term Least-Squares Functions Minus the Experimental Values for Ordered Ni_3Fe Alloy between 1.2 and 4.4 K. The solid curves represent $\pm 0.2\%$ deviations from the experimental values.

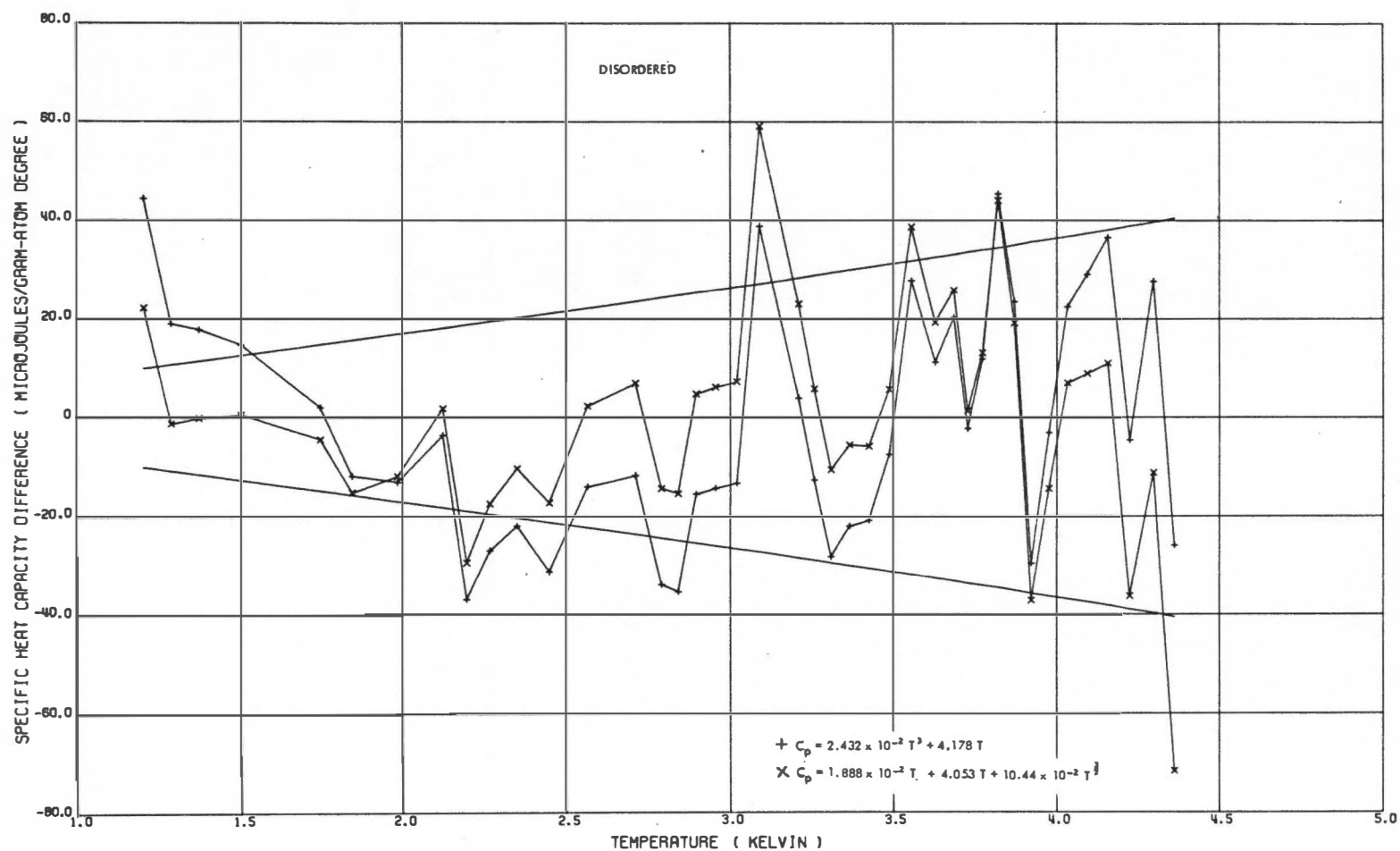


Figure 54. Specific Heat Capacity Calculated from Two-Term and Three-Term Least-Squares Functions Minus the Experimental Values for Disordered Ni_3Fe Alloy between 1.2 and 4.4 K. The solid curves represent $\pm 0.2\%$ deviations from the experimental values.

interpolation. Had a quadratic interpolation been used, the results would have been closer. Lastly, their value for α of 9.32×10^{-2} millijoules/gram-atom $K^{5/2}$ differs by about one-half of a standard deviation from the value of this investigation.

Bower, Claridge, and Tsong³² calculated the Debye temperature from elastic constant measurements of the same alloys used by Dixon, Hoare, and Holden.³⁴ Then they fit $C_p - \beta T$ to the function $\gamma T + \alpha T^{3/2}$, using the β 's calculated from their Debye temperature determinations. Their θ_d of 457.6 K is 1.5 standard deviations lower than that in Table XVII, and their γ value of 4.206 millijoules/gram-atom K^2 is within 3.8%. However, the α value derived from this procedure was 5.53×10^{-2} millijoules/gram-atom $K^{5/2}$, which is strikingly different from the value of this investigation. Note, however, that considerably better agreement in α and θ_d is obtained when the lowest temperature point was dropped from the fit. This may indicate that this value is erroneous or may be simply fortuitous.

From these comparisons, the results of the three term fit appear most meaningful for the disordered state. Since no measurements exist in the literature for the ordered state, the three term fit must be assumed "best" for this state.

Calculation of C_{vm} of Disordered Ni_3Fe

In order to calculate the C_{vm} of the disordered state of Ni_3Fe , the contributions to C_p due to the destruction of local order were subtracted first. This was done by assuming that below T_c , the data of Vacuum-Anneal B — acquired with a Class II heating rate — did not include a

contribution due to configurational disordering. From Figure 49, page 173, it is apparent that this assumption is not valid above T_c . Therefore, it was assumed that the lowest temperature data point above T_c for Vacuum-Anneal B and for the 879 K anneal were free of ordering effects as well as all of the latter data above 960 K. Thus, in the temperature interval between 879 and 960 K, no useful C_p values existed. However, if the $C_p:T$ relationship in the absence of disordering is assumed to demonstrate the magnetic tail observed in iron and nickel, extrapolation in this temperature interval is relatively free of errors because the $C_p:T$ curve is almost parallel to the temperature axis. Using this assumption, a curve was drawn by hand between the data points at 871 and 879 K and those above 960 K and is the dotted line in Figure 49.

C_x of Disordered Ni_3Fe . The $C_x:T$ curve shown in Figure 55 was acquired using the $C_p:T$ relationship constructed as described in the above section. The shape of this curve is quite similar to that shown in Figure 39, page 141, for the C_x of iron, implying that the above assumptions used to establish C_p of the disordered state were realistic.

Recall that three parameters are required to find C_x - namely γ , γ_{nl} , and θ_d . The γ value used is that determined from the low-temperature C_p measurements on the quenched Ni_3Fe specimen and is 4.053×10^{-3} joules/gram-atom degree. Since a search of the literature failed to find a value for the compressibility of disordered Ni_3Fe , the γ_{nl} value was calculated by assuming a linear relationship between that of nickel and iron. This should be a relatively good approximation because γ_{nl} of iron and nickel differ only by 10%, which is very close to the total uncertainties in these quantities. Lastly, θ_d was selected

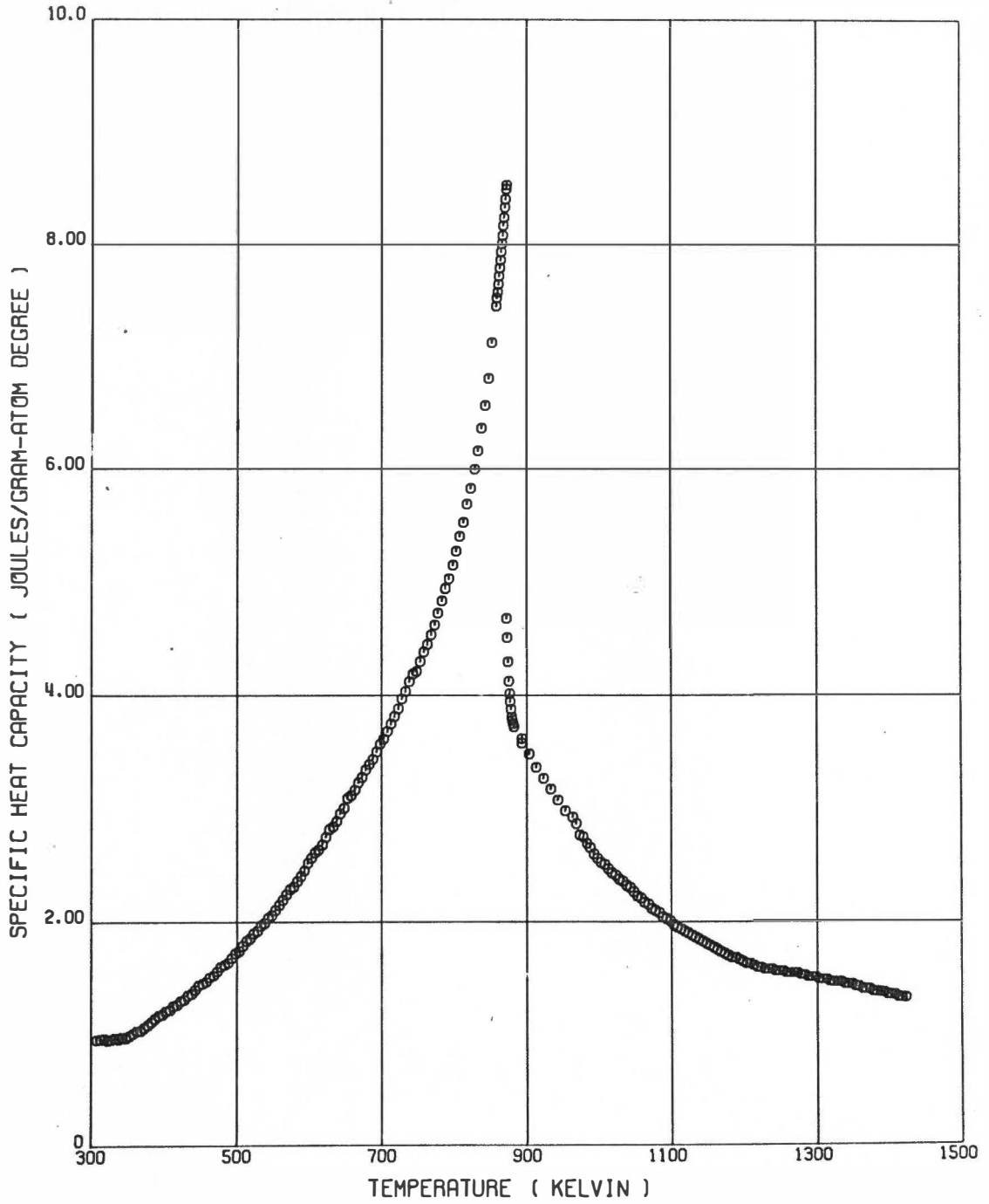


Figure 55. Temperature Dependence of C_x of Disordered Ni_3Fe Calculated with a γ of 4.053×10^{-3} joules/gram-atom K^2 , a γ_{nl} of 2.56×10^{-6} gram-atom/joule, and a θ_d of 410 K.

on the basis of the following suppositions. First, it was noted that between 1.2 and 4.4 K the θ_d of 468 K found for the disordered state of Ni_3Fe at liquid helium temperatures was within 10 degrees of that of nickel³³ (471 K) and iron³³ (473 K). Secondly, the results of Dixon, Hoare, and Holden³⁴ indicate that the θ_d of nickel-iron alloys is almost independent of composition for alloys containing more than 65% nickel. Thirdly, it was assumed that the temperature dependence of θ_d of disordered Ni_3Fe was approximately that of nickel. With these three observations and a $C_x:T$ versus θ_d analysis similar to that for nickel, a θ_d of 410 K was selected for use in the analysis for C_{vm} .

C_{vm} of Disordered Ni_3Fe . As for iron, C_x of Ni_3Fe is positive at temperatures well above the Curie temperature. This cannot be construed as a ramification of configurational disordering because these data were acquired with a Class I heating rate and are about 600 degrees above the equilibrium order-disorder temperature. Hence, the positive value of C_x must be attributed to the sum of its contributions, $C_{vm} + BT + AT^3$.

The method of finding B and A that was used for iron cannot be employed for two reasons. First, C_x for temperatures from T_c to temperatures 100 degrees above T_c is not even approximately equal to C_{vm} . Secondly, and most important, these data were those obtained from the extrapolation procedure necessary to eliminate the local ordering effects. Therefore, the extrapolation of the C_x versus $\log|T - T_c|$ relationship used in the case of iron could not be employed.

At this point two further assumptions were made. First, it was assumed that at 1423 K (the highest C_p data point) C_{vm} was negligibly

small. Then the theory of Keller and Wallace²² was used to calculate B. Based on the results for nickel and iron, this value of B was reduced by 60% and along with the C_x value at 1423 K was used to calculate A. Such a procedure yielded a B of -1.67×10^{-3} joules/gram-atom K^2 and an A of 1.282×10^{-4} joules/gram-atom K^4 . This value of A is about a factor of five larger than that of iron and of opposite sign to that of nickel. Such a large value for A increases C_{ve} at 1000 K by 32% over that of a simple γT contribution.

Figure 56 shows the final results of the analysis of the contributions to the C_p of disordered Ni_3Fe . In Figure 57, all contributions except C_{vh} are shown on an expanded plot. Note that all results are for temperatures above 300 K, which is the lower temperature limit of the present calorimeters. In order to calculate U_{vm} and S_{vm} , C_{vm} values are needed between 0 and 300 K. Consequently, these results were extrapolated by hand to lower temperatures. The final results for C_{vm} of the disordered alloy are shown in Figure 58 and are listed in Table XLV in the Appendix.

ΔC_{vm} , U_{vm} , and S_{vm} of Disordered Ni_3Fe

Table XVIII contains a summary of results on the disordered state of Ni_3Fe and includes values calculated for ΔC_{vm} , $\Delta C_{vm}/nk$, U_{vm} , and S_{vm} . Crangle and Hallam's⁸⁶ value of 1.1 Bohm-magnetons/atom for disordered Ni_3Fe was used to calculate nk together with the assumption that the spin per atom for disordered Ni_3Fe is one.

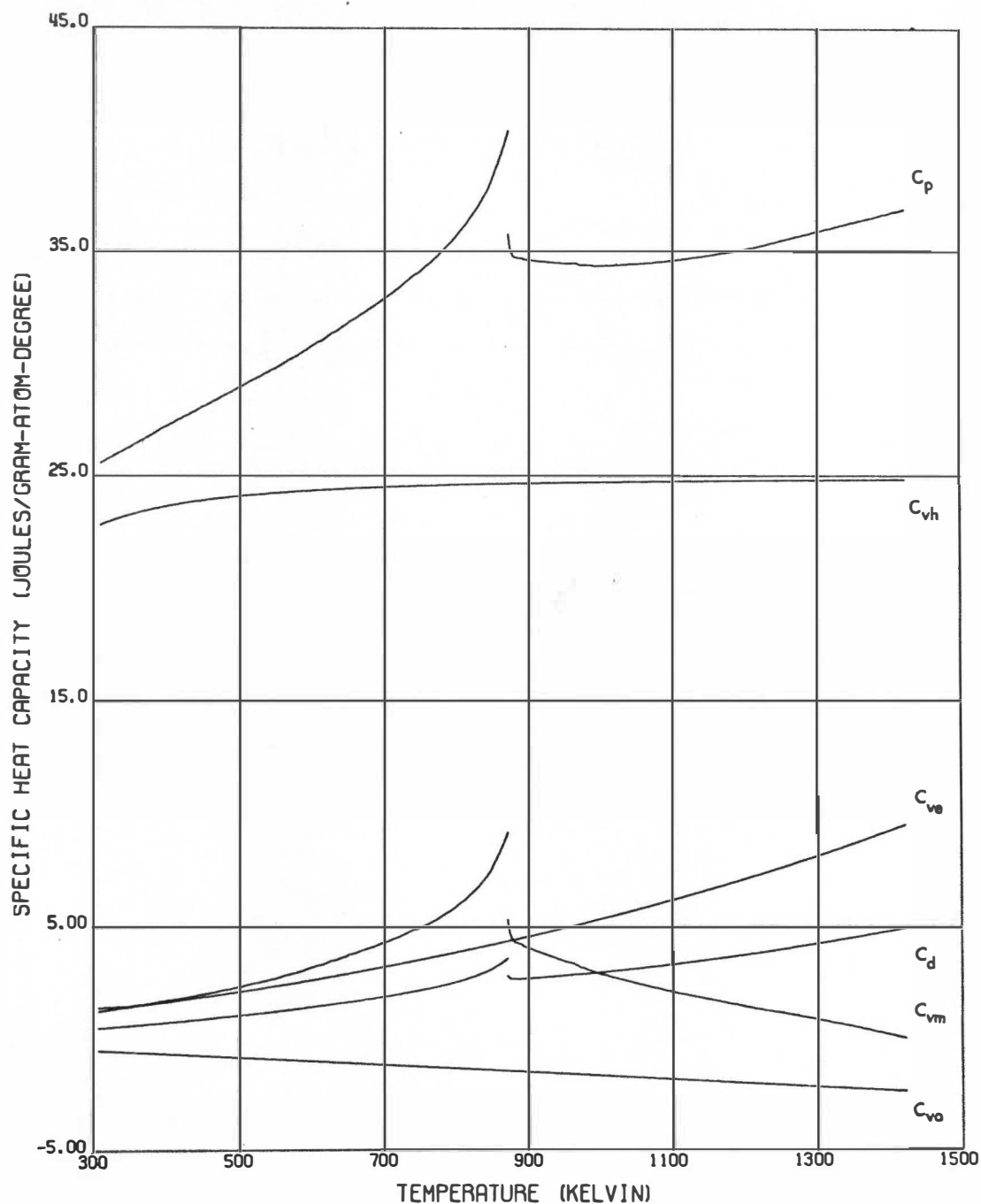


Figure 56. Contributions to the Specific Heat Capacity of Disordered Ni₃Fe as a Function of Temperature. ($\theta_d = 410$ K, $\gamma = 4.053 \times 10^{-3}$ joules/gram-atom K², $\gamma_{nl} = 2.56 \times 10^{-6}$ gram-atom/joule, $A = 1.282 \times 10^{-9}$ joules/gram-atom K⁴, and $B = -1.67 \times 10^{-3}$ joules/gram-atom K².)

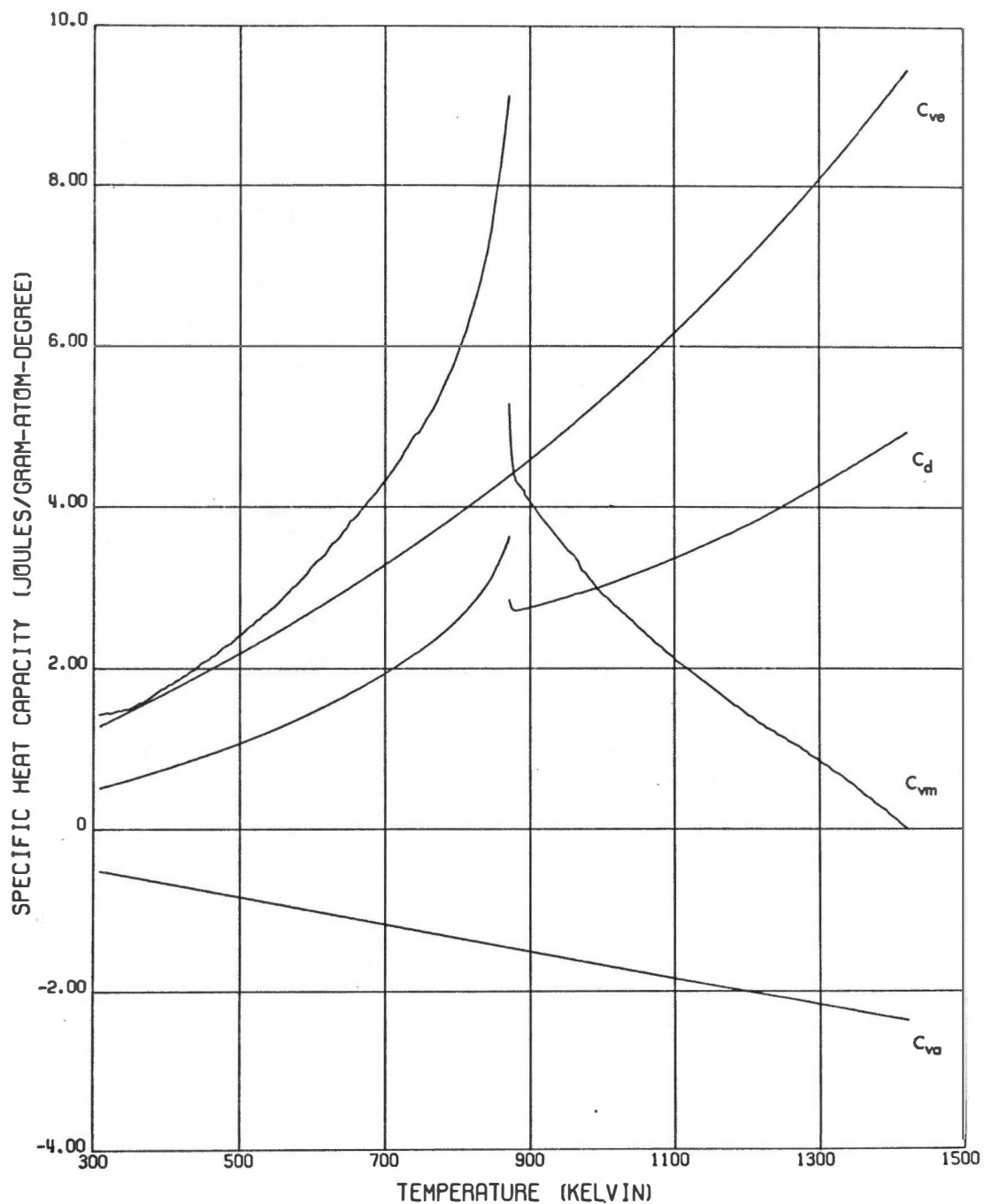


Figure 57. Expanded Plot of Figure 56 Showing the Contributions to the Specific Heat Capacity of Disordered Ni_3Fe as a Function of Temperature. Only C_{ve} , C_d , C_{vm} , and C_{va} are shown.

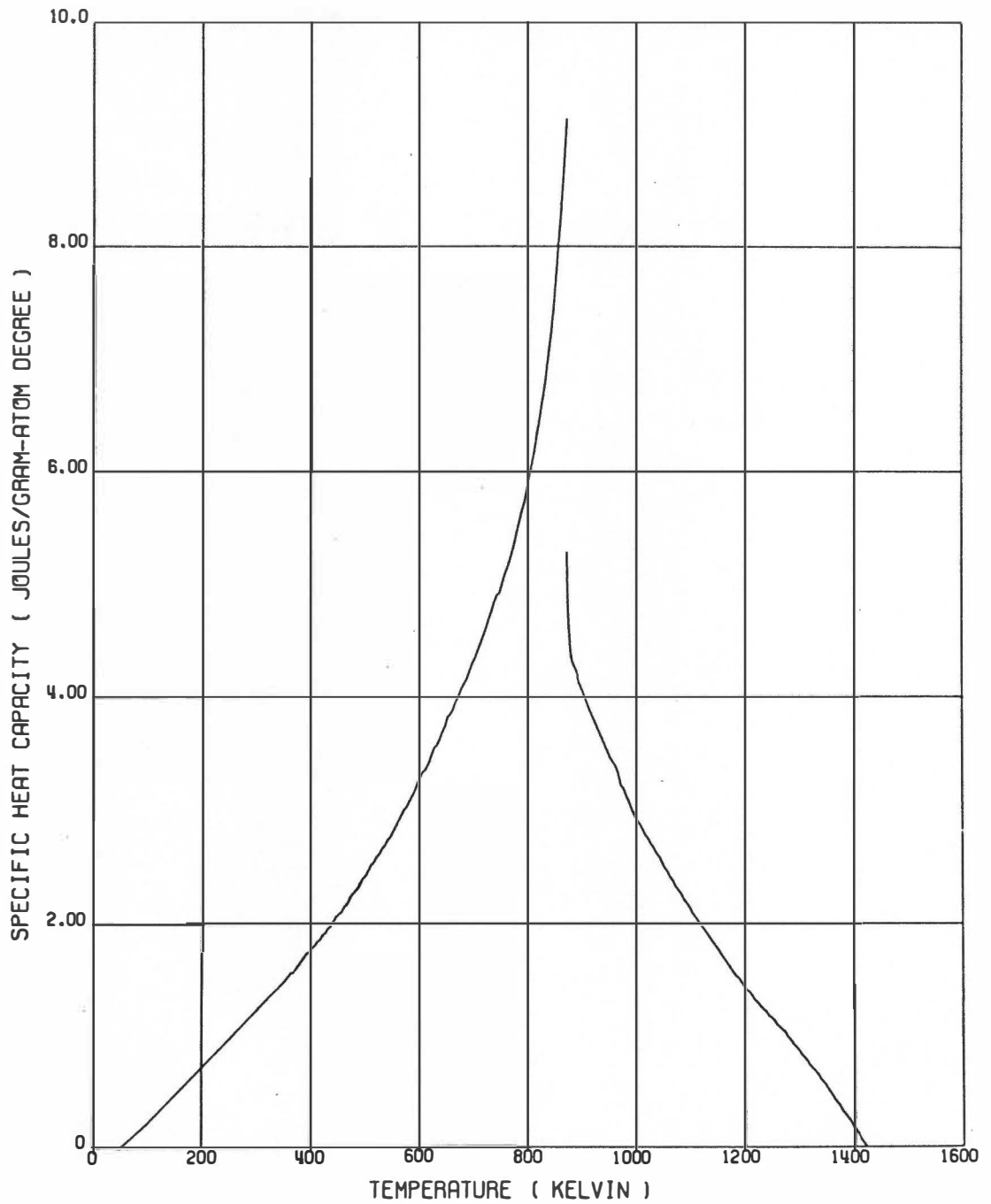


Figure 58. Temperature Dependence of C_{vm} of Disordered Ni_3Fe Calculated from Experimental C_p Values.

TABLE XVIII
SUMMARY OF RESULTS ON DISORDERED Ni_3Fe ALLOY

Quantities	Units	Contribution	Value
γ_{nl}	Gram-atom/joule	C_d	2.56×10^{-6}
γ	Joules/gram-atom	C_{ve}	4.053×10^{-3}
θ_d	Kelvin	C_{vh}	410
B	Joules/gram-atom K^2	C_v	-1.67×10^{-3}
A	Joules/gram-atom K^4	C_{ve}	1.282×10^{-9}
ΔC_{vm}	Joules/gram-atom K		3.85
$\Delta C_{vm}/nk^*$			0.84
U_{vm}	Joules/gram-atom		3249.4
S_{vm}	Joules/gram-atom K		5.05

*Here n is taken to be 0.55 magnetic atoms per atom with a spin of one per atom.

Since the theoretical values of ΔC_{vm} , U_{vm} , and S_{vm} are directly proportional to n, values of these quantities for disordered Ni_3Fe of spin one were calculated from those of iron listed in Table IV, page 47. These theoretical values are compared with the experimental results as shown in Table XIX. As in the case of iron and nickel, the agreement with theory is qualitatively good. In particular, as for iron and nickel, the Heisenberg theory appears best, and the theoretical results are higher than the experimental. Also, the values of $\Delta C_{vm}/nk$ are in poor agreement with theory. This may be caused by the masking effects of the destruction of local order.

TABLE XIX
COMPARISON OF THE EXPERIMENTAL RESULTS FOR DISORDERED
Ni₃Fe WITH THOSE PREDICTED FROM THEORY

Theory	Reference*	Theoretical			Percent Difference†		
		U_{vm} ($\frac{\text{Joules}}{\text{gram-atom}}$)	S_{vm} ($\frac{\text{Joules}}{\text{gram-atom K}}$)	$\Delta C_{vm}/nk$	U_{vm}	S_{vm}	$\Delta C_{vm}/nk$
Bethe-Peierls-Weiss	44	4422		3.40	36		304
Ising	44, 53	4888			50		
Constant coupling	41, 42	4435		1.76	37		208
Molecular field	35			2.0			237
Heisenberg	62	3535	5.02		9	-0.6	

*See page 214.

†Percent difference = $100 (\text{Theory} - \text{This Investigation}) / (\text{This Investigation})$.

Calculation of C_{vm} , ΔC_{vm} , U_{vm} , and S_{vm} of Ordered Ni_3Fe

In the calculations of C_{vm} of nickel, iron, and disordered Ni_3Fe , the data above the Curie temperature were used extensively to find values for A and B in the expression for C_{vm} given by Equation (109), page 135. Unfortunately, the data on the ordered states of Ni_3Fe in this temperature range include configurational disordering effects which cannot be separated accurately enough to warrant this calculation. Thus, a suggested future experiment is to redesign the pulse calorimeter so that 200 to 300 ampere pulses might be employed, thereby allowing more rapid heating. Then it might be possible to retain the order to high enough temperatures so that the heat effects of the Curie transformation could be separated adequately from the disordering effects.

Energy of Transformation U_{Od} of Ni_3Fe

By definition, the change in enthalpy dH of a closed system at constant pressure is equal to the heat absorbed by the system δq . Also by definition, the heat absorbed at constant pressure δq is equal to the product $C_p dT$ for an infinitesimal change in temperature dT . (Note that C_p as used in the following discussion is the C_p of the system undergoing the temperature change and includes first-order transformation contributions.) For any process, either reversible or irreversible, dH is equal to $C_p dT$. Hence, the change in enthalpy ΔH_{2-1} in going from temperature T_1 to T_2 is

$$\Delta H_{2-1} = H_2 - H_1 = \int_{T_1}^{T_2} C_p dT \quad . \quad (112)$$

Let T_1 be the equilibrium temperature for the order-disorder transformation and T_2 be a higher temperature. Thus, from the C_p : T relationship in Figure 56, page 191, ΔH_{2-1} of taking completely disordered Ni_3Fe from T_1 to T_2 can be calculated at any temperature up to the maximum temperature of these data. Similarly, from the C_p data in Figure 51, page 178, ΔH_{2-1} of taking Ni_3Fe in Order-State II at T_1 and transforming it to completely disordered Ni_3Fe at T_2 can be calculated when T_2 is greater than the temperature at which all order has been destroyed (1020 K for Order-State II).

Using the nomenclature that $[X]_d$ and $[X]_o$ are values of the property X of the disordered state and of Order-State II, respectively, the change in enthalpy ΔH_e at the equilibrium order-disorder temperature T_e of transforming Ni_3Fe in Order-State II to completely disordered Ni_3Fe at T_e is

$$\Delta H_e = [H_{T_e}]_d - [H_{T_e}]_o = \left\{ [H_T]_d + \int_T^{T_e} [C_p]_d dT' \right\} - \left\{ [H_T]_d + \int_T^{T_e} [C_p]_o dT' \right\}, \quad (113)$$

or

$$\Delta H_e = \int_{T_e}^T \left\{ [C_p]_o - [C_p]_d \right\} dT'. \quad (114)$$

Note that $[C_p]_o$ is the measured C_p : T relationship for Order-State II which is shown in Figure 51, page 178.

Equation (114) was employed to calculate ΔH_e for Order-States I to VI and these values are listed in Table XX. Often, the ΔH_e of transforming

TABLE XX

ORDER-DISORDER ENTHALPIES ΔH_e FOR ORDER-STATES I TO VI

Order State	Long-Range Order Parameter	ΔH_e (Joules/gram-atom)
VI	0.96	3268
IV	0.92	3000
II	0.88	2930
III	0.78	2650
IV	0.66	1679
V	0.60	1286

completely ordered Ni_3Fe ($S = 1.0$) to completely disordered Ni_3Fe ($S = 0.0$) is quoted in the literature for both experimental and theoretical determinations. For this reason, the ΔH_e values of the six ordered states were plotted versus the square of estimated long-range order parameter, and ΔH_e for S equal to one was found to be 3680 (± 140) joules/gram-atom by extrapolation. This plot is shown in Figure 59.

Iida⁷⁶⁻⁷⁸ reported a ΔH_e for the destruction of perfect order of 3716 joules/gram-atom, which is well within the experimental error of the value reported herein. Leech and Sykes⁷¹ measurements yielded a value of 3350 joules/gram-atom for a sample which probably was not completely ordered. A similar qualification must be placed on Kaya's⁷² value of 3034 joules/gram-atom. However, these two experimental values are only 9.2 and 17.5% below the extrapolated value found herein and are within the experimental error of the value for Order-State VI, which was 3268 joules/gram-atom.

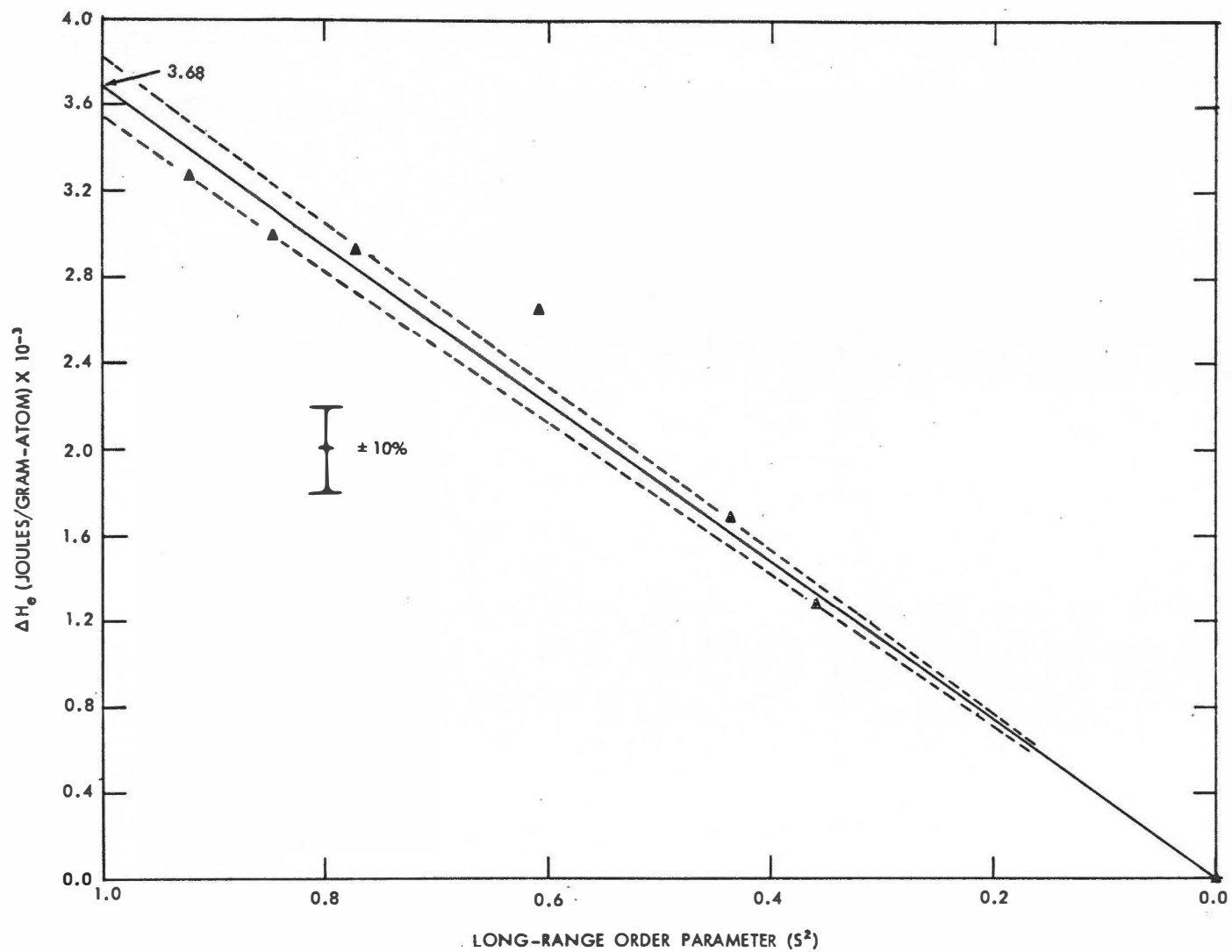


Figure 59. Enthalpy ΔH_e of the Order-Disorder Transformation as a Function of the Square of the Long-Range Order Parameter. Solid straight line shows extrapolation to complete order. Dashed lines are estimated maximum and minimum extrapolations.

During the order-disorder transformation of Ni_3Fe , the specimen undergoes a volume change of the order of 0.2%. The energy associated with this change is very small. Consequently, the change in enthalpy at constant pressure is slightly smaller than the change in energy U_{od} . Hence, the value of U_{od} is approximately 3680 joules/gram-atom.

Entropy of Transformation S_{od} of Ni_3Fe

By definition, the change in entropy dS of a closed system undergoing a reversible process at constant pressure is equal to $\delta q_r/T$, where δq_r is the reversible heat absorbed by the system from its surroundings. Denbigh¹²⁵ points out that for a system undergoing an irreversible process (such as the transformation of the ordered Ni_3Fe states to disordered Ni_3Fe during pulse heating measurements of C_p), the heat absorbed will be less than that of the reversible path. Therefore, since the heat absorbed δq is given by $C_p dT$, δq_r is greater than $C_p dT$.

In a manner analogous to the derivation of Equation (114), page 197, for ΔH_e , the following inequality can be found for the entropy change S_{od} during an order to disorder transformation at T_e

$$S_{\text{od}} > \int_{T_e}^T \left\{ \left[C_p \right]_o - \left[C_p \right]_d \right\} d \ln T' . \quad (115)$$

Thus, integration of the data of the various ordered states would yield only a lower limit for the value of the entropy of disordering.

For pedagogic reasons, these integrations were performed and a value of 3.43 joules/gram-atom degree was found for the lower limit of S_{od} when completely ordered Ni_3Fe transforms to ordered Ni_3Fe at T_e .

If it is assumed that the difference in the Gibbs free energy ΔG is small between the completely ordered state and the equilibrium ordered state at T_e , the entropy change S_{od} would be $\Delta H_e/T_e$. From the measured value of ΔH_e and an assumed T_e of 773 K, a value of 4.76 joules/gram-atom degree was calculated for S_{od} , which is 28% greater than the above value.

The value calculated from this line of reasoning forms a better lower bound for S_{od} because the change in the Gibbs free energy ΔG_{od} for the completely ordered to disordered transformation, though small, is less than zero. By definition, ΔG_{od} is

$$\Delta G_{od} = \Delta H_e - T_e S_{od} , \quad (116)$$

which yields

$$S_{od} = (\Delta H_e - \Delta G_{od})/T_e > \Delta H_e/T_e . \quad (117)$$

Due to the slow heating rate employed by Leech and Sykes,⁷¹ the order-disorder transformation occurred almost under equilibrium conditions during their C_p measurements (see Figure 7, page 50). Therefore, the value that they obtained from Equation (115) should also form a good estimate for S_{od} . Their value is 4.78 joules/gram-atom degree, which is within 0.4% of the value obtained using Equation (117).

CHAPTER IV

SUMMARY AND RECOMMENDATIONS

Summary of Chapter I

The specific heat capacity at constant volume C_v of a solid was assumed to be separable into five contributions resulting from changes in energy of the phonons and electrons of the solid. Since the specific heat capacity at constant pressure C_p was measured, it was first necessary to compute C_v by subtraction of the dilation contribution C_d from C_p . Because the precise thermodynamic expression for C_d involved properties whose values were not known at high temperatures for the materials of interest — nickel, iron, and the alloy Ni_3Fe — the approximations of Grüneisen² and Nernst and Lindemann³ were presented and their validity discussed. The other five contributions were for a solid at constant volume.

As is traditional, the phonon contribution was separated into two components. The first and largest, designated C_{vh} , was that due to the harmonic oscillations of the normal modes of the atoms of a solid; that is, that due to the square of the displacement in the expression for the potential energy of the oscillators. The other component C_{va} was due to all higher order terms — cubic, quartic, ... — of the potential energy of the oscillators and is normally referred to as the anharmonic contribution. Debye's¹⁴ theory for C_{vh} was outlined and the various qualifications reported in the literature were reviewed. It was noted that this contribution is dominant at room temperature and

above. Although the theoretical expressions for C_{va} agreed in magnitude, there existed a discrepancy as to its sign. Keller and Wallace's²² theoretical approach yielded a negative sign, while that of Foreman²¹ was positive.

The contribution due to the energy changes of the electrons was assumed separable into a contribution C_{ve} due to the change in their energy distribution and a contribution C_{vm} due to changes in the magnetic coupling of the spins of the electrons. Stoner's²⁵ free-electron expression for C_{ve} was given and amended by the experimental and theoretical observations of Shimizu, Takahashi, and Katsuki.²⁸ Although the electrons of nickel, iron, and the alloy Ni_3Fe are itinerant, the literature search revealed only localized electron models for C_{vm} . These included the Bethe-Peierls and Ising models of Weiss,⁴⁴ the constant coupling model results given by Wagner,⁴¹ and the molecular field theory approach as outlined by Morrish.³⁵ Results of these theories for the total energy U_{vm} and entropy S_{vm} of the transformation from complete magnetic order at zero kelvin to complete magnetic disorder at very high temperature were outlined as a straightforward method of comparing theoretical and/or experimental calculations of C_{vm} . Since the Curie transformations are second-order, the expressions of these theories were presented for the discontinuity ΔC_{vm} in C_{vm} at the Curie temperature T_c .

The fifth contribution to C_v , which was assumed negligible for iron and nickel, was that due to rearrangement of atoms C_{vw} . However, a large C_{vw} is observed during the order-disorder transformation in Ni_3Fe . Since the order-disorder transformation does not occur under equilibrium

conditions during experimental measurements of C_p of Ni_3Fe , the theoretical expressions for C_{vw} were not reviewed. As for nickel and iron, theory and/or experiment are usually compared by calculating the total energy U_{od} and entropy S_{od} of the order-disorder transformation.

The existing knowledge of the contributions to the specific heat capacity of nickel, iron, and Ni_3Fe was reviewed. This included tabulation of values of ΔC_{vm} , U_{vm} , and S_{vm} for nickel and iron and values of U_{od} and S_{od} for Ni_3Fe which had appeared in the literature. Use of the electrical resistivity as a monitor of the state of order of Ni_3Fe was outlined.

The pitfalls in adiabatic and pulse calorimetric measurements of C_p near the Curie transformation of ferromagnets were discussed in general terms. Lastly, the goals of this thesis were listed.

Summary of Chapter II

Six apparatuses were used in this investigation to measure the specific heat capacity, electrical resistivity, and thermoelectric power of the materials of interest. Only the salient features of five of these were listed, as they had been described previously in the literature. However, since the principal interest was the specific heat capacity measurements and since it had been developed during the course of this research, Pulse-Calorimeter II was described in detail. This included a description of the equipment, of the circuitry, of the data acquisition procedure, of the data reduction and calculation techniques, and of the accuracies of the measurements. Primary attributes of this

method were the accurate and simultaneous measurement of the specific heat capacity ($\pm 1.05\%$) and electrical resistivity ($\pm 0.48\%$) at temperature intervals of 0.2 degree while the specimen was heated from 100 to 600 degrees above its initial temperature at rates of 5 to 60 degrees/second.

All specimens utilized in this research were in the form of rods (0.3-cm nominal diameter) and were prepared by melting, casting, and swaging of stock materials. Chemical analysis of the stock and the final heat-treated specimens revealed a minimum amount of contamination during fabrication. Final purities were: nickel 99.89%, iron 99.79%, and Ni₃Fe alloy 99.87%. The alloy composition was 74.77 atomic percent nickel and 25.23 atomic percent iron. Photomicrographs of the specimens revealed a small amount of second phase, probably an oxide, which was most predominant in the iron specimen but present in the others also. Ratios of the resistance of the specimen at room temperature to that at 4.2 K confirmed the results of the chemical analyses. No voids were present in the specimens.

Summary of Chapter III

Nickel and Iron. Experimental measurements of the specific heat capacity C_p of nickel and iron were presented and compared with literature values. Two regions of significant disagreement were evident - in the vicinity of the Curie transformations and at high temperatures. Both of these discrepancies were attributed to experimental errors.

First, the effects of temperature gradients in the specimen on measured values of C_p near the Curie temperature T_c were discussed

qualitatively. These effects were shown to be similar to: (a) adiabatic calorimetric measurements which span T_c ; (b) pulse calorimetric measurements in which an erroneous T_c is selected during data treatment; and (c) measurements by either method in which an improper functional form for the time-temperature relationship is used when dT/dt is calculated near T_c . The last two experimental difficulties were demonstrated quantitatively using a pulse through T_c of nickel. These results established the validity of the qualitative arguments, were adequate proof that the difference in C_p measurements near T_c were due to improper experimental methods and procedures, and demonstrated that the Curie transformation was second-order by virtue of a finite but discontinuous C_p at T_c .

Above 1200 K, accurate C_p measurements become increasingly difficult. One of the main problems is thermometry, and it was postulated that this was the major reason for the discrepancies among the investigations of the C_p of nickel and iron at high temperatures. Errors which resulted from the use of contaminated thermocouples during the C_p measurements on nickel and iron in this research were illustrated, and the improvement of these data after recalculation using the specimen as its own resistance thermometer was shown. It was noted that large temperature gradients are induced in the thermocouples at their junction with the specimen during pulse calorimetric measurements of C_p . These gradients produce large errors when this method is used at temperatures where the thermocouples are contaminated by their environment.

From the discussions of the contributions to the specific heat capacity of a solid, it was postulated that the C_p of nickel and iron could be written as

$$C_p = C_d + C_{vh} + C_{ve} + C_{va} + C_{vm} = \gamma_{nl}(C_p)^2T + 3RF_d(T/\theta_d) + [\gamma T + AT^3] + BT + C_{vm} \quad (118)$$

Equation (118) was used in conjunction with the C_p data to calculate the C_{vm} of nickel and iron. For convenience during these calculations, the algebraic sums $C_p - \gamma_{nl}(C_p)^2T - 3RF_d(T/\theta_d) - \gamma T$ and $AT^3 + BT + C_{vm}$, being equal, were designated C_x . To calculate C_x by the first sum, values of the Nernst-Lindemann constant γ_{nl} and of the low-temperature coefficient γ of C_{ve} were selected from the literature. Since there existed some uncertainty as to the most appropriate value of θ_d to use, C_x was calculated for several values of θ_d which had been given in the literature. At low temperatures and near T_c , C_x is approximately equal to C_{vm} . Consequently, the values of C_x between 100 and 200 K were used to select the "best" values of θ_d for nickel and iron, basing the decision on the expected shape of the $C_{vm}:T$ relationship in this temperature region.

It then was possible to determine C_{vm} from the C_x values - which were calculated using the selected values of γ_{nl} , γ and θ_d - by evaluating A and B of the second expression for C_x . This was accomplished for nickel by assuming that C_{vm} was negligibly small between 1400 and 1500 K and fitting the C_x values in this temperature interval to the function $AT^3 + BT$ by the method of least-squares. For iron, the C_x values between 1057 and 1123 K were fit by the method of least-squares to the function $a + b \log_{10}|T - T_c|$. Since C_x was approximately C_{vm} in this temperature region and since this was the expected form for

C_{vm} if the Curie transformation was a critical phenomenon, the acquired function was extrapolated to higher temperatures as a first approximation to C_{vm} . These approximate values of C_{vm} were subtracted from C_x between 1250 and 1625 K, and the difference $(C_x - C_{vm})$ was fit by the method of least-squares to the function $AT^3 + BT$. An iteration of the process was performed using C_{vm} between 1057 and 1123 K instead of C_x . These C_{vm} values were determined using A and B of the first iteration.

The resulting values of B of iron and nickel were 60% below those calculated from the theory of Keller and Wallace.²² These values were also negative, which is in agreement with their theory. The sign of the constant A for iron was positive and was negative for nickel, which is in agreement with the predictions of Shimizu, Takahashi, and Katsuki.²⁸ The magnitude of A for nickel was a factor of ten smaller than that predicted by the free electron theory, whereas that for iron is a factor of sixteen larger and of opposite sign.

The $C_{vm}:T$ relationships obtained from these calculations were within experimental error of those in the open literature for both nickel and iron. This was also true for the total magnetic energy U_{vm} and entropy S_{vm} obtained from the appropriate integrations of the $C_{vm}:T$ curves. Agreement of the theoretical calculations of U_{vm} , S_{vm} , and the discontinuity ΔC_{vm} in C_{vm} at T_c was within fair agreement with theoretical predictions, which were based on localized instead of itinerant electron models. Agreement with the Heisenberg approximation of U_{vm} and S_{vm} was rated "best."

Plots of C_{vm} versus $\log_{10} |T - T_c|$ did not yield the expected parallel curves for temperatures above and below T_c . This would be the case if the Curie transformation of iron and nickel were critical phenomena. Also, the values within 10 degrees of T_c did not fit the least-square function found from the values at temperatures more than 10 degrees from T_c . Periodic oscillations of the latter C_{vm} values about this function suggested that the presumed form was incorrect.

Ni₃Fe Alloy. The specific heat capacity of Ni₃Fe was found to be a function of the thermal history of the Ni₃Fe alloy as well as temperature. In addition, the experimental values of C_p between 750 and 1050 K were heating rate dependent. Measurements on four locally ordered and six long-range ordered states of Ni₃Fe were performed. The degree of order for these treatments was established by auxiliary electrical resistivity measurements and Beal's⁹⁰ theory for the change in electrical resistivity as a function of the long-range order parameter S. It was found that the C_p of Ni₃Fe decreased as S increased. This change amounted to 21% of C_p at 1.2 K and 5.7% of C_p at 750 K.

Due to the rapid heating rates employed, it was possible to heat the ordered structure far above its equilibrium transformation temperature of 773 K. Data acquired for the locally ordered states during pulses from below the Curie temperature of 871 K demonstrated two peaks. The lower temperature and larger peak at 871 K was associated with the Curie transformation, whereas the higher temperature peak was due to the destruction of local order. The temperature at which the latter

peak occurred was heating rate dependent because it was associated with an atomic-diffusion-controlled rate-process.

In measurements on the long-range ordered states, the second peaks were prevalent only when faster heating rates were employed because this peak was associated with the destruction of long-range configurational order, which is also a rate-controlled process. An increase in S was observed to increase the Curie temperature, being a maximum of 70 degrees for a state with an S of 0.96 at the inception of the pulse. Similarly, the temperature of the second peak increased with increasing order and occurred about 230 degrees above the equilibrium order-disorder transformation temperature.

From measurements performed near liquid helium temperatures on Ni_3Fe , the decrease of C_p with increasing S was associated with a 21% change in the temperature coefficient γ of the electronic contribution and a 6% decrease in the temperature coefficient β of the harmonic contribution C_{vh} . That is, the density of electron states was lowered upon ordering and the cut-off frequency increased. Also, these C_p data were fitted better by a three term relationship, which included the $\alpha T^{3/2}$ spin-wave contribution, than by the standard two term expression, namely $\gamma T + \beta T^3$. Values of α , β , and γ were in good agreement with those of the literature.

It was impossible to calculate C_{vm} for the ordered states of Ni_3Fe because the ordered structure could not be retained to temperatures high enough to yield meaningful values of A and B of Equation (118). However, C_{vm} of the disordered state was calculated in a manner analogous

to that for iron and nickel. First, C_x was calculated using the value of γ found from the low-temperature measurements and the value of γ_{nl} calculated from a linear interpolation of the nickel and iron values. The "best" value of θ_d was chosen as for nickel and iron. It was then assumed that C_{vm} was zero at 1423 K, the highest C_p data point. Also, Keller and Wallace's²² theory was assumed to yield a value of B , the temperature coefficient of C_{va} , that was 60% too high. From the C_x value at 1423 K and this value of B , the value of A was calculated. With these values of A and B , the $C_{vm}:T$ relationship was calculated from the $C_x:T$ relationship.

Integration of the $C_{vm}:T$ curve obtained for the disordered Ni_3Fe state yielded values of U_{vm} and S_{vm} which were in reasonable agreement with theoretical values calculated assuming that the spin per atom was one and using Crangle and Hallam's⁸⁶ value of 1.1 Bohr-magnetons/atom to calculate the number of magnetic atoms/atom. In particular, the Heisenberg approximation results were within 10%. On the other hand, the values of ΔC_{vm} were at least 200% below all theoretical predictions, indicating that the discontinuity in C_{vm} was masked by the simultaneous destruction of local order.

Appropriate integrations of the ten $C_p:T$ curves which were obtained were used in conjunction with the estimated states of order to predict a value for the energy U_{od} associated with transforming completely ordered Ni_3Fe to completely disordered Ni_3Fe at the equilibrium transformation temperature. Similarly, lower bounds were predicted for the entropy S_{od} of this transformation. Exact values of the entropy

could not be found since the transformations took place in an irreversible manner. Literature values of U_{od} were in excellent agreement with the result obtained herein. The higher estimated value of S_{od} was in excellent agreement with that of the only available literature source.

Recommendations

As for most other investigations, this work has suggested a number of additional experiments and interpretative work which should be performed. While not attempting to be complete, the following list indicates some of these recommendations:

1. Measurements of C_p of nickel and iron, as well as other ferromagnetic materials, should be made within one degree of the Curie temperature on specimens with extremely small internal temperature gradients. This would yield more accurate values of ΔC_{vm} .

2. Measurements on iron in the γ and δ stable regions using the specimen as its own resistance thermometer are suggested. This involves obtaining accurate resistivity data on the iron specimen from auxiliary measurements. Similar C_p measurements are in order for nickel and Ni_3Fe above 1200 K. (Also, measurements above 1200 K on all solids should, in general, be made by resistance thermometry.)

3. The measurement technique should be extended below room temperature to at least the boiling point of nitrogen, but preferably to 20 or 30 K. This would allow measurements of C_p in a temperature range where few data are available and in which the $C_p:T$ relationship is varying rapidly. This temperature region provides useful data for interpretative work on the components of C_p .

4. Use of faster heating rates is recommended during repeat measurements of the C_p of ordered Ni_3Fe . This would maintain the ordered structure to temperatures above which the Curie transformation is complete and would allow calculation of C_{vm} , U_{vm} , and S_{vm} as a function of the state of order.

5. Use of slower heating rates is needed during remeasurements of the C_p of ordered Ni_3Fe near the equilibrium order-disorder transformation temperature. This would allow the transformation to occur under nearly reversible conditions, which would provide data for a better estimate of S_{od} .

6. Separations of the various contributions to the electrical resistivity of the materials investigated are possible. Such a treatment would possibly allow correlation of the magnetic part of the $d\rho/dT:T$ relationship with the $C_{vm}:T$ relationship.

7. Measurements of C_p of other nickel-iron alloys as a function of state of order would be informative.

8. Measurement of other thermophysical properties, such as thermal conductivity, might reveal effects to be correlated with the C_p measurements.

BIBLIOGRAPHY

BIBLIOGRAPHY

1. Pippard, A. B., Elements of Classical Thermodynamics for Advanced Students of Physics. Cambridge: University Press, 1960.
2. Grüneisen, E., "Zustand des festen Körpers," Handbuch der Physik Bd. 10, F. Henning, editor. Berlin: Springer, 1926. Pp. 1-59.
3. Nernst, W. and F. A. Lindemann, "Spezifische Wärme-Quantentheorie," Zeitschrift für Elektrochemie, 17: 817-827, 1911.
4. Blackman, M., "The Specific Heat of Solids," Handbuch der Physik Bd. 7/1, S. Flügge, editor. Berlin, Göttingen, Heidelberg; Springer, 1955. Pp. 325-382.
5. Fraser, D. B. and A.C.H. Hallett, "The Coefficient of Linear Expansion and Grüneisen γ of Cu, Ag, Au, Fe, Ni, and Al from 4°K to 300°K," Proceedings of the VIIth International Conference on Low Temperature Physics, G. M. Graham and A.C.H. Hallett, editors. Toronto: University of Toronto Press, 1961.
6. Chang, Y. A. and R. Hultgren, "The Dilation Contribution to the Heat Capacity of Copper and α -Brass at Elevated Temperatures," Journal of Physical Chemistry, 69: 4162-4165, December 1965.
7. Singh, R. P. and G. S. Verma, "Validity of Nernst-Lindemann Equation in the Range 24°-1800°C in Tungsten," Solid State Communications, 6: 113-114, January 1968.
8. Braun, M. and R. Kohlhaas, "Die spezifische Wärme von Eisen, Kobalt, und Nickel im Bereich hoher Temperaturen," Physica Status Solidi, 12: 429-444, 1965.
9. Nix, F. C. and D. MacNair, "The Thermal Expansion of Pure Metals: Copper, Gold, Aluminum, Nickel and Iron," Physical Review, 60: 597-605, October 1941.
10. Tauer, K. J. and R. J. Weiss, "An Analysis of the Specific Heat of α -Manganese and its Antiferromagnetic Structure," Journal of Physics and Chemistry of Solids, 2: 237-239, 1957.
11. Kaufman, L., E. V. Clougherty, and R. J. Weiss, "The Lattice Stability of Metals - III. Iron," Acta Metallurgica, 11: 323-335, May 1963.
12. Einstein, A., "Die Plancksche Theorie der Strahlung und die Theorie der Spezifischen Wärme," Ann. Physik, 22: 180-190, 1907.

13. De Launay, J., "The Theory of Specific Heats and Lattice Vibrations," Solid State Physics Vol. 2, F. Seitz and D. Turnbull, editors. New York and London: Academic Press, 1955.
14. Debye, P., "Zur Theorie der Spezifischen Wärmen," Annalen der Physik, 39: 789-839, 1912.
15. Stark, W. A. and R. N. Kortzeborn, A Convenient Tabulation of the Debye Energy, Heat Capacity, Free Energy, and Entropy For a Crystalline Solid. University of California Radiation Laboratory, UCRL-17225, 1966.
16. Clement, J. R., "Atomic Heat of Indium Below 20°K," Physical Review, 92: 258-267, October 1953.
17. Born, M. and T. von Kármán, "Über Schwingungen in Raumgittern," Physikalische Zeitschrift, 8: 297-309, 1912.
18. Fine, P. C., "The Normal Modes of Vibration of a Body-Centered Cubic Lattice," Physical Review, 56: 355-359, August 1939.
19. Leighton, R. B., "The Vibrational Spectrum and Specific Heat of a Face-Centered Cubic Crystal," Reviews of Modern Physics, 20: 165-174, January 1948.
20. Hultgren, R., Specific Heat of Metals and Alloys. Air Force Office of Scientific Research, AFOSR-TN60-527, 1960.
21. Foreman, J. E., "Anharmonic Specific Heat of Solids," Proceedings of the Physical Society, 79: 1124-1141, 1962.
22. Keller, J. M. and D. C. Wallace, "Anharmonic Contributions to Specific Heat," Physical Review, 126: 1275-1282, May 1962.
23. Mott, N. F. and H. Jones, The Theory of the Properties of Metals and Alloys. New York: Dover, 1936.
24. Mott, N. F., "Electrons in Transition Metals," Advances in Physics Vol. 13, B. R. Coles, editor. London: Taylor and Francis, 1964.
25. Stoner, E. C., "Collective Electron Ferromagnetism II. Energy and Specific Heat," Proceedings of the Royal Society (London) Series A, 169: 339-371, 1939.
26. Stoner, E. C., "The Magnetic Susceptibility and Electronic Specific Heat of Transition Metals in Relation to their Electronic Structure," Acta Metallurgica, 2: 259-273, 1954.

27. Seitz, F., The Modern Theory of Solids. New York and London: McGraw-Hill, 1940.
28. Shimizu, M., T. Takahashi, and A. Katsuki, "Calculations of Electronic Specific Heat and Paramagnetic Susceptibility of Chromium," Journal of the Physical Society of Japan, 17: 1740-1746, November 1962.
29. Miller, A. P. and B. N. Brockhouse, "Anomalous Behavior of the Lattice Vibrations and the Electronic Specific Heat of Palladium," Physical Review, 20: 798-801, April 1968.
30. Gersdorf, R., "Ferromagnetic Properties of Fe and Ni in Relation to Their Band Structure," Journal de Physique et le Radium, 23: 726-729, October 1962.
31. Heisenberg, W., "Theory of Ferromagnetism," Zeitschrift für Physik, 49: 619-636, 1928.
32. Bower, D. I., E. Claridge, and I.S.T. Tsong, "Low Temperature Elastic Constants and Specific Heats of F.C.C. Nickel-Iron Alloys," Physica Status Solidi, 29: 617-625, 1968.
33. Dixon, M., F. E. Hoare, T. M. Holden, and D. E. Moody, "The Low Temperature Specific Heats of Some Pure Metals (Cu, Ag, Pt, Al, Ni, Fe, Co)," Proceedings of the Royal Society (London) Series A, 285: 561-580, May 1965.
34. Dixon, M., F. E. Hoare, and T. M. Holden, "The Low-Temperature Specific Heats of Some Nickel-based Iron and Copper Alloys," Proceedings of the Royal Society (London) Series A, 303: 339-354, 1968.
35. Morrish, A. H., The Physical Principles of Magnetism. New York: Wiley, 1965.
36. Ising, E., "A Contribution to the Theory of Ferromagnetism," Zeitschrift für Physik, 31: 253-258, 1925.
37. Newell, G. F. and E. W. Montroll, "On the Theory of the Ising Model of Ferromagnetism," Reviews of Modern Physics, 25: 353-389, April 1953.
38. Wannier, G. H., "The Statistical Problem in Cooperative Phenomena," Reviews of Modern Physics, 17: 50-60, January 1945.
39. Domb, C., "On the Theory of Cooperative Phenomena in Crystals," Advances in Physics Vol. 9, B. H. Flowers, editor. London: Taylor and Francis, 1960. Pp. 150-361.

40. Kasteleijn, P. W. and J. Van Kranendonk, "Constant Coupling Approximation for Heisenberg Ferromagnetism," Physica, 22: 317-337, 1956.
41. Wagner, D., "Thermodynamische Eigenschaften am Curiepunkt," Physica, 29: 803-812, 1963.
42. Ballensiefen, G. and D. Wagner, "Specific Heat In Constant-Coupling Approximation," Physica, 30: 1543-1544, 1964.
43. Smart, J. S., "Magnetic Short Range Order and Specific Heat in Ferromagnets and Antiferromagnets," Journal of Physics and Chemistry of Solids, 20: 41-49, 1961.
44. Weiss, P. R., "The Application of the Bethe-Peierls Method to Ferromagnetism," Physical Review, 74: 1493-1504, October 1948.
45. Mattis, D. C., The Theory of Magnetism. New York, Evanston, and London: Harper and Row, 1965.
46. Voronel, A. V., Y. R. Chaskin, V. A. Popov, and V. G. Simkin, "Measurement of the Specific Heat C_V of Oxygen Near the Critical Point," Journal Experimental Theoretical Physics (U.S.S.R.), 45: 828-830, September 1963.
47. Bagatskii, M. I., A. V. Voronel, and V. G. Gusak, "Measurement of the Specific Heat C_V of Argon in the Immediate Vicinity of the Critical Point," Journal Experimental Theoretical Physics (U.S.S.R.), 43: 728-729, August 1962.
48. Landau, L. and E. Lifshitz, Statistical Physics, translated from Russian by D. Shoenberg. Oxford: Clarendon Press, 1938.
49. Miedema, A. R., R. F. Wielinga, and W. J. Huiskamp, "Experimental Study of the Specific Heat Singularity of a B.C.C. Heisenberg Ferromagnet and Two Ising Antiferromagnets," Physics Letters, 17: 87-89, July 1965.
50. Voronel, A. V., S. R. Garber, A. P. Simkina, and I. A. Charkina, "Specific Heat of Gd Near the Curie Point," Journal Experimental Theoretical Physics (U.S.S.R.), 49: 429-432, August 1965.
51. Kraftmakher, Y. A., "Thermal Capacity of Nickel Near the Curie Point," Soviet-Physics Solid State, 8: 1048-1049, October 1966.
52. Kraftmakher, Y. A., "Specific Heat of Iron Near the Curie Point," Soviet Physics-Solid State, 7: 2040-2041, February 1966.

53. Brown, H. A. and J. M. Luttinger, "Ferromagnetic and Antiferromagnetic Curie Temperatures," Physical Review, 100: 685-692, October 1955.
54. Krivoglaz, M. A. and A. A. Smirnov, The Theory of Order-Disorder In Alloys. New York: American Elsevier, 1965.
55. Green, H. S. and C. A. Hurst, Order-Disorder Phenomena, London, New York, Sydney: Interscience, 1964.
56. Shewmon, P. G., Diffusion in Solids. New York: McGraw-Hill, 1963.
57. Muto, T., and Y. Takagi, "The Theory of Order-Disorder Transitions in Alloys," Solid State Physics Vol. 1, F. Seitz and D. Turnbull, editors. New York and London: Academic Press, 1955.
58. Guttman, L., "Order-Disorder Phenomena in Metals," Solid State Physics Vol. 3, F. Seitz and D. Turnbull, editors. New York and London: Academic Press, 1956.
59. Hansen, M., Constitution of Binary Alloys. New York: McGraw-Hill, 1958.
60. Touloukian, Y. S., (editor), Thermophysical Properties Research Center Data Book, Vol. 1. Lafayette, Indiana: Purdue Research Foundation, 1963.
61. Pawel, R. E. and E. E. Stansbury, "Specific Heat Contributions of the Ferromagnetic Transition in Nickel and Nickel-Copper Alloys," Journal of Physics and Chemistry of Solids, 26: 757-765, 1965.
62. Hofmann, J. A., A. Paskin, K. J. Tauer, and R. J. Weiss, "Analysis of Ferromagnetic and Antiferromagnetic Second-Order Transitions," Journal of Physics and Chemistry of Solids, 1: 45-60, 1956.
63. Lapp, E., "Étude de la Chaleur Spécifique Vraie du Nickel," Annales de Physique, 12: 442-521, 1929.
64. Krauss, F. and H. Warncke, "Die Spezifische Wärme von Nickel zwischen 180 und 1160°," Zeitschrift für Metallkunde, 46: 61-69, 1955.
65. Grew, K. E., "The Specific Heat of Nickel and of Some Nickel-Copper Alloys," Proceedings of the Royal Society (London) Series A, 145: 509-522, 1934.

66. Lytton, J. L., "Influence of Ferromagnetic Elastic Modulus Relaxation on the Determination of Magnetic Specific Heat of Fe, Ni, and Co," Journal of Applied Physics, 35: 2397-2406, August 1964.
67. Darken, L. S., and R. P. Smith, "Thermodynamic Function of Iron," Industrial and Engineering Chemistry, 43: 1815-1820, August 1951.
68. Weiss, R. J., and K. J. Tauer, "Components of the Thermodynamic Functions of Iron," Physical Review, 102: 1490-1495, June 1956.
69. Stoner, E. C., Magnetism and Matter. London: Methuen, 1934.
70. Kaya, S., and M. Nakayama, "Die Überstrukturbildung in den Eisen-Nickel-Kobalt-Legierungen und das Perminvarproblem," Zeitschrift für Physik, 112: 420-429, 1939.
71. Leech, P., and C. Sykes, "The Evidence for a Superlattice in the Nickel-Iron Alloy Ni_3Fe ," Philosophical Magazine, Series 7, 27: 742-753, 1939.
72. Kaya, S., "Die Überstrukturbildung in den Nickel-Eisen Legierungen und das Permalloyproblem," Journal of the Faculty of Science, Hokkaido Imperial University, 2: 29-53, 1938.
73. Zuithoff, A. J., "The Exact Measurement of the Specific Heats of Solid Substances at High Temperatures. XII The Specific Heats of Iron-Nickel-Alloys of Various Compositions between 100° and 1400°C," Recueil des Travaux Chimiques des Pays-bas, 131-160, 1940.
74. Keesom, W. H., and B. Kurrelmeyer, "Specific Heats of Nickel with Copper and with Iron From 1.2 to 29°K," Physica, 7: 1003-1024, December 1940.
75. Gupta, K. P., C. H. Cheng, and P. A. Beck, "Low Temperature Specific Heat of F.C.C. Alloys of 3-d Transition Elements," Journal of Physics and Chemistry of Solids, 25: 73-83, 1964.
76. Iida, S., "Formation Energy of Superlattice for Ni_3Fe , I Co-Operative Formation of Superlattice at the Critical Temperature," Journal of the Physical Society of Japan, 7: 373-379, July-August 1952.
77. Iida, S., "Formation Energy of Superlattice in $\text{Ni}_3\text{Fe(II)}$. Kinetics of the Superlattice in the Stage of Local Ordering," Journal of the Physical Society of Japan, 9: 346-354, May-June 1954.

78. Iida, S., "Formation Energy of Superlattice in $\text{Ni}_3\text{Fe(III)}$. Kinetics of the Superlattice at the Formation Stage with Long Range Order," Journal of the Physical Society of Japan, 10: 9-22, January 1955.
79. Bowen, D. B., "The Debye Temperature of AuCu_3 as a Function of Long-Range Order Parameter," Acta Metallurgica, 2: 573-575, July 1954.
80. Rayne, J. A., "Heat Capacity of Cu_3Au below 4.2°K ," Physical Review, 108: 649-651, November 1957.
81. Martin, D. L., "Effect of Ordering on the Specific Heat of Cu_3Au below 3°K ," Canadian Journal of Physics, 46: 923-927, 1968.
82. Hultgren, R., R. L. Orr, T. D. Anderson, and K. K. Kelley, Selected Values of Thermodynamic Properties of Metals and Alloys. New York and London: Wiley, 1963.
83. Collins, M. F., R. V. Jones, and R. D. Lowde, "On the Magnetic Moments and the Degree of Order in Iron-Nickel Alloys," Journal of the Physical Society of Japan, Supplement B-III, 17: 19-26, 1962.
84. Wakelin, R. J., and E. L. Yates, "A Study of the Order-Disorder Transformation in Iron-Nickel Alloys in the Region FeNi_3 ," Proceedings of the Physical Society (London) Series B, 66: 221-240, 1953.
85. Taoka, T., and T. Ohtsuka, "The Magnetic Properties and Their Temperature Dependence of Ferromagnetic Alloys with an Order-Disorder Transformation. I. Ni_3Fe ," Journal of the Physical Society of Japan, 9: 712-722, September-October 1954.
86. Crangle, J. and G. C. Hallam, "The Magnetization of Face-Centered Cubic and Body-Centered Cubic Iron and Nickel Alloys," Proceedings of the Royal Society (London) Series A, 272: 119-132, 1963.
87. Grabbe, E. M., "Ferromagnetic Anisotropy, Magnetization at Saturation, and Superstructure in Ni_3Fe and Nearby Compositions," Physical Review, 57: 728-734, April 1940.
88. Weiss, R. J., Solid State Physics for Metallurgists. Reading, Massachusetts; Palo Alto, London: Addison-Wesley, 1963.
89. Meaden, G. T., Electrical Resistance of Metals. New York: Plenum, 1965.

90. Beal, M. T., "On the Electrical Resistivity of Alloys of the Type Cu_3Au as a Function of Order," Journal of Physics and Chemistry of Solids, 18: 156-161, 1961.
91. Craig, P. P., W. I. Goldberg, T. A. Kitchens, and J. I. Budnick, "Transport Properties at Critical Points: The Resistivity of Nickel," Physical Review Letters, 19: 1334-1337, December 1967.
92. Kraftmakher, Y. A., "Electrical Conductivity of Nickel Close to the Curie Point," Soviet Physics-Solid State, 9: 1199-1200, November 1967.
93. Kraftmakher, Y. A., and T. Y. Romashina, "Electrical Conductivity of Iron Near the Curie Point," Soviet Physics-Solid State, 9: 1459-1460, December 1967.
94. Fisher, M. E., and J. S. Langer, "Resistive Anomalies at Magnetic Critical Points," Physical Review Letters, 20: 665-668, March 1968.
95. Moore, J. P., W. Fulkerson, and D. L. McElroy, "Thermal Conductivity, Electrical Resistivity, and Seebeck Coefficient of Uranium Mononitride," submitted to Journal of the American Ceramic Society.
96. Kollie, T. G., "The Development of a Pulse Heating Calorimetric Technique for Measuring the Specific Heat of Electrical Conductors and its Application to Pure Iron from 100 to 1400°C," M.S. Thesis, the University of Tennessee, 1965. (Oak Ridge National Laboratory, ORNL-TM-1187.)
97. Fulkerson, W., J. P. Moore, and D. L. McElroy, "Comparison of the Thermal Conductivity, Electrical Resistivity, and Seebeck Coefficient of a High-Purity Iron and an Armco Iron to 1000°C," Journal of Applied Physics, 37: 2639-2653, June 1966.
98. Moore, J. P., D. L. McElroy, and R. S. Graves, "Thermal Conductivity and Electrical Resistivity of High-Purity Copper From 78 to 400°K," Canadian Journal of Physics, 45: 3849-3865, 1967.
99. Cusack, N. and P. Kendall, "The Absolute Scale of Thermoelectric Power at High Temperature," Proceedings of the Physical Society, 72: 898-901, 1958.

100. Kneip, G. D., J. O. Betterton, and J. O. Scarbrough, "Low-Temperature Specific Heats of Titanium, Zirconium, and Hafnium," Physical Review, 130: 1687-1692, June 1963.
101. Kollie, T. G., "Specific Heat Determinations by Pulse Calorimetry Utilizing a Digital Voltmeter for Data Acquisition," Review of Scientific Instruments, 38: 1452-1463, October 1967.
102. Kollie, T. G., Pulse Calorimetry Using a Digital Voltmeter for Transient Data Acquisition, Oak Ridge National Laboratory, ORNL-4380, 1969.
103. Kollie, T. G., D. L. McElroy, and C. R. Brooks, Convolute Method of Smoothing or Calculating the Time-Derivatives of a Signal Recorded in Digital Form at Equal Time Intervals, Oak Ridge National Laboratory, ORNL-TM-2517, 1969.
104. Flynn, D. R., National Bureau of Standards, private communication to W. Fulkerson, Oak Ridge National Laboratory, April 10, 1963.
105. Simpson, R. L., Oak Ridge National Laboratory, private communication to T. G. Kollie, Oak Ridge National Laboratory, March 20, 1969.
106. Adams, R. K. and E. G. Davisson, "Smooth Thermocouples Tables of Extended Significance ($^{\circ}\text{C}$)," Oak Ridge National Laboratory, ORNL-3649 (Volume 2, Section 2.1), 1965.
107. Viting, L. M., "Investigation of the Iron-Nickel-Cobalt System in the Region of the Metallic Compounds Ni_3Fe and FeCo ," Journal of Inorganic Chemistry (USSR), 2: 367-374, 1957.
108. Powell, R. W., R. P. Tye, and M. J. Hickman, "The Thermal Conductivity of Nickel," International Journal of Heat and Mass Transfer, 8: 679-688, 1965.
109. Lyman, T. (editor), Metals Handbook. Novelty, Ohio: American Society for Metals, 1961.
110. Braun, M., "Über die spezifische Wärme von Eisen, Kobalt und Nickel im Bereich hoher Temperaturen," Ph.D. Thesis, The University of Köln, 1964.
111. Pawel, R. E., "The Application of Dynamic Adiabatic Calorimetry to the Copper-Nickel System From 50 to 620°C ," Ph.D. Dissertation, The University of Tennessee, 1956.
112. Wright, J. W., "A New Adiabatic Calorimeter for Specific Heat Determinations From 100° to 800°C ," M.S. Thesis, The University of Tennessee, 1964.

113. Pallister, P. R., "The Specific Heat and Resistivity of High-Purity Iron up to 1250°C," Journal of the Iron and Steel Institute, 161: 87-90, February 1949.
114. Dench, W. A. and O. Kubaschewski, "Heat Capacity of Iron at 800° to 1420°C," Journal of the Iron and Steel Institute, 201: 140-143, February 1963.
115. Wallace, D. C., P. H. Sidles, and G. C. Danielson, "Specific Heat of High Purity Iron by a Pulse Heating Method," Journal of Applied Physics, 31: 168-176, January 1960.
116. McElroy, D. L., "Calorimetry of High Purity Iron and Steels," Ph.D. Dissertation, The University of Tennessee, 1957.
117. Anderson, P. D. and R. Hultgren, "The Thermodynamics of Solid Iron at Elevated Temperatures," Transactions of the Metallurgical Society of AIME, 224: 842-845, August 1962.
118. Gschneidner, K. A., "Physical Properties and Interrelationships of Metallic and Semimetallic Elements," Solid State Physics Vol. 16, F. Seitz and D. Turnbull, editors. New York and London: Academic Press, 1964. Pp. 275-426.
119. Alers, G. A., "Use of Sound Velocity Measurements in Determining the Debye Temperature of Solids," Physical Acoustics Vol. 3, Part B, Mason, W. P., editor. New York and London: Academic Press, 1965. Pp. 1-42.
120. Busey, R. H. and W. F. Giaque, "The Heat Capacity of Nickel from 15 to 300°K. Entropy and Free Energy Functions," Journal of the American Chemical Society, 74: 3157-3158, 1952.
121. Rayne, J. A. and W.R.G. Kemp, "The Heat Capacities of Chromium and Nickel," Philosophical Magazine, 1: 918-925, 1956.
122. Simerská, M., "The Temperature Dependence of the Characteristic Temperature of Nickel," Czechoslovakian Journal of Physics, 12: 858-859, 1962.
123. Kirby, R. K., National Bureau of Standards, private communication to C. R. Brooks, University of Tennessee, June 10, 1969.
124. Kelley, K. K., "The Specific Heat of Pure Iron at Low Temperatures," Journal of Chemical Physics, 11: 16-18, 1943.
125. Denbigh, K., Principles of Chemical Equilibrium. Cambridge: University Press, 1961.

APPENDIX

TABLE XXI

SPECIFIC HEAT CAPACITY, ELECTRICAL RESISTIVITY, AND TEMPERATURE DERIVATIVE
OF ELECTRICAL RESISTIVITY OF NICKEL FROM 333 K TO 1323 K

TEMPERATURE	SPECIFIC HEAT CAPACITY	ELECTRICAL RESISTIVITY	TEMPERATURE DERIVATIVE OF RESISTIVITY	TEMPERATURE	SPECIFIC HEAT CAPACITY	ELECTRICAL RESISTIVITY	TEMPERATURE DERIVATIVE OF RESISTIVITY
(KELVIN)	(JOULES/GRAM-ATOM DEGREE)	(OHM-CM) 10 E-6	(OHM/DEGREE) 10 E-6	(KELVIN)	(JOULES/GRAM-ATOM DEGREE)	(OHM-CM) 10 E-6	(OHM/DEGREE) 10 E-6
333.2	27.00	8.79	0.0434	583.2	34.13	24.11	0.0874
338.2	27.13	9.01	0.0440	588.2	34.37	24.55	0.0893
343.2	27.22	9.23	0.0445	593.2	34.64	25.01	0.0915
348.2	27.32	9.47	0.0451	598.2	34.91	25.47	0.0938
353.2	27.44	9.69	0.0457	603.2	35.23	25.95	0.0964
358.2	27.54	9.92	0.0462	608.2	35.58	26.44	0.0994
363.2	27.64	10.14	0.0468	613.2	35.97	26.96	0.1028
368.2	27.76	10.37	0.0474	618.2	36.41	27.51	0.1073
373.2	27.86	10.62	0.0479	619.2	36.51	27.60	0.1083
378.2	27.99	10.85	0.0485	620.2	36.61	27.71	0.1095
383.2	28.11	11.10	0.0491	621.2	36.73	27.81	0.1107
388.2	28.23	11.34	0.0497	622.2	36.83	27.93	0.1121
393.2	28.33	11.59	0.0503	623.2	36.95	28.05	0.1137
398.2	28.45	11.85	0.0510	624.2	37.10	28.16	0.1156
403.2	28.57	12.11	0.0516	625.2	37.25	28.27	0.1177
408.2	28.70	12.38	0.0522	626.2	37.42	28.39	0.1202
413.2	28.82	12.63	0.0528	627.2	37.69	28.51	0.1237
418.2	28.94	12.90	0.0535	628.2	38.03	28.63	0.1269
423.2	29.07	13.18	0.0542	629.2	38.57	28.76	0.1310
428.2	29.21	13.45	0.0549	630.2	39.26	28.89	0.1354
433.2	29.34	13.74	0.0556	630.7	39.66	28.96	0.1376
438.2	29.46	14.03	0.0563	631.2	40.15	29.02	0.1400
443.2	29.58	14.32	0.0571	631.7	40.69	29.08	0.1420
448.2	29.71	14.60	0.0578	632.2	41.33	29.14	0.1446
453.2	29.83	14.89	0.0586	632.7	41.97	29.18	0.1480
458.2	29.98	15.19	0.0594	633.0	42.43	29.21	0.1494
463.2	30.10	15.50	0.0603	633.0	34.79	29.21	0.0822
468.2	30.25	15.80	0.0612	633.2	34.72	29.23	0.0806
473.2	30.37	16.10	0.0622	633.7	34.55	29.28	0.0779
478.2	30.49	16.41	0.0630	634.2	34.42	29.31	0.0752
483.2	30.64	16.72	0.0639	634.7	34.28	29.35	0.0725
488.2	30.76	17.04	0.0648	635.2	34.15	29.39	0.0705
493.2	30.91	17.36	0.0658	636.2	33.91	29.46	0.0675
498.2	31.06	17.69	0.0667	637.2	33.71	29.52	0.0652
503.2	31.20	18.02	0.0676	638.2	33.51	29.59	0.0631
508.2	31.35	18.35	0.0686	639.2	33.34	29.65	0.0615
513.2	31.50	18.68	0.0695	640.2	33.19	29.72	0.0594
518.2	31.65	19.02	0.0705	641.2	33.05	29.77	0.0585
523.2	31.82	19.38	0.0715	642.2	32.92	29.83	0.0572
528.2	31.97	19.74	0.0725	643.2	32.83	29.89	0.0562
533.2	32.14	20.10	0.0735	644.2	32.70	29.94	0.0552
538.2	32.31	20.47	0.0746	645.2	32.60	30.00	0.0543
543.2	32.48	20.85	0.0758	646.2	32.51	30.05	0.0536
548.2	32.63	21.23	0.0770	647.2	32.43	30.10	0.0527
553.2	32.85	21.62	0.0783	648.2	32.33	30.17	0.0520
558.2	33.02	22.01	0.0795	653.2	32.01	30.41	0.0488
563.2	33.22	22.42	0.0809	658.2	31.79	30.64	0.0463
568.2	33.44	22.83	0.0824	663.2	31.62	30.87	0.0443
573.2	33.66	23.25	0.0840	668.2	31.50	31.08	0.0424
578.2	33.88	23.67	0.0856	673.2	31.38	31.29	0.0417

TABLE XXI (continued)

TEMPERATURE	SPECIFIC HEAT CAPACITY	ELECTRICAL RESISTIVITY	TEMPERATURE DERIVATIVE OF RESISTIVITY	TEMPERATURE	SPECIFIC HEAT CAPACITY	ELECTRICAL RESISTIVITY	TEMPERATURE DERIVATIVE OF RESISTIVITY
(KELVIN)	(JOULES/GRAM -ATOM DEGREE)	(OHM-CM) 10 E-6	(OHM/DEGREE) 10 E-6	(KELVIN)	(JOULES/GRAM -ATOM DEGREE)	(OHM-CM) 10 E-6	(OHM/DEGREE) 10 E-6
678.2	31.37	31.49	0.0477	928.2	32.09	39.67	0.0284
683.2	31.23	31.69	0.0397	933.2	32.14	39.82	0.0284
688.2	31.15	31.89	0.0390	938.2	32.16	39.96	0.0283
693.2	31.11	32.08	0.0384	943.2	32.21	40.10	0.0283
698.2	31.08	32.28	0.0378	948.2	32.26	40.24	0.0282
703.2	31.06	32.47	0.0373	953.2	32.28	40.38	0.0281
708.2	31.06	32.66	0.0367	958.2	32.33	40.52	0.0281
713.2	31.03	32.84	0.0363	963.2	32.38	40.66	0.0280
718.2	31.03	33.02	0.0360	968.2	32.41	40.80	0.0280
723.2	31.01	33.20	0.0356	973.2	32.46	40.94	0.0279
728.2	31.01	33.38	0.0353	978.2	32.51	41.08	0.0279
733.2	31.01	33.55	0.0349	983.2	32.56	41.22	0.0278
738.2	31.03	33.73	0.0346	988.2	32.58	41.36	0.0277
743.2	31.03	33.90	0.0343	993.2	32.63	41.49	0.0276
748.2	31.03	34.07	0.0340	998.2	32.68	41.63	0.0276
753.2	31.06	34.23	0.0338	1003.2	32.73	41.77	0.0275
758.2	31.08	34.40	0.0334	1008.2	32.75	41.91	0.0274
763.2	31.11	34.56	0.0332	1013.2	32.80	42.04	0.0274
768.2	31.13	34.73	0.0330	1018.2	32.85	42.18	0.0274
773.2	31.15	34.89	0.0328	1023.2	32.90	42.32	0.0273
778.2	31.18	35.06	0.0326	1028.2	32.95	42.45	0.0272
783.2	31.20	35.22	0.0324	1033.2	32.97	42.58	0.0272
788.2	31.23	35.38	0.0322	1038.2	33.02	42.72	0.0271
793.2	31.25	35.54	0.0320	1043.2	33.07	42.85	0.0271
798.2	31.28	35.70	0.0318	1048.2	33.12	42.99	0.0270
803.2	31.30	35.86	0.0317	1053.2	33.17	43.12	0.0269
808.2	31.33	36.02	0.0315	1058.2	33.22	43.25	0.0269
813.2	31.35	36.17	0.0313	1063.2	33.27	43.38	0.0268
818.2	31.38	36.33	0.0312	1068.2	33.32	43.52	0.0268
823.2	31.40	36.48	0.0310	1073.2	33.37	43.65	0.0267
828.2	31.43	36.64	0.0308	1078.2	33.42	43.78	0.0266
833.2	31.47	36.78	0.0306	1083.2	33.46	43.92	0.0266
838.2	31.50	36.94	0.0304	1088.2	33.51	44.05	0.0265
843.2	31.52	37.09	0.0303	1093.2	33.56	44.19	0.0264
848.2	31.57	37.26	0.0301	1098.2	33.61	44.32	0.0264
853.2	31.60	37.43	0.0300	1103.2	33.66	44.45	0.0263
858.2	31.62	37.58	0.0299	1108.2	33.71	44.58	0.0262
863.2	31.65	37.74	0.0298	1113.2	33.76	44.71	0.0262
868.2	31.67	37.89	0.0296	1118.2	33.81	44.84	0.0261
873.2	31.70	38.05	0.0295	1123.2	33.86	44.97	0.0261
878.2	31.74	38.21	0.0294	1128.2	33.91	45.10	0.0260
883.2	31.77	38.36	0.0293	1133.2	33.96	45.23	0.0260
888.2	31.79	38.51	0.0292	1138.2	34.00	45.36	0.0259
893.2	31.82	38.66	0.0291	1143.2	34.05	45.49	0.0259
898.2	31.87	38.80	0.0290	1148.2	34.10	45.62	0.0258
903.2	31.89	38.95	0.0289	1153.2	34.15	45.76	0.0258
908.2	31.92	39.09	0.0288	1158.2	34.20	45.88	0.0258
913.2	31.97	39.24	0.0287	1163.2	34.25	46.01	0.0257
918.2	32.01	39.39	0.0286	1168.2	34.30	46.14	0.0257
923.2	32.04	39.53	0.0285	1173.2	34.35	46.27	0.0257

TABLE XXI (continued)

TEMPERATURE	SPECIFIC HEAT CAPACITY	ELECTRICAL RESISTIVITY	TEMPERATURE DERIVATIVE OF RESISTIVITY	TEMPERATURE	SPECIFIC HEAT CAPACITY	ELECTRICAL RESISTIVITY	TEMPERATURE DERIVATIVE OF RESISTIVITY
(KELVIN)	(JOULES/GRAM -ATOM DEGREE)	(OHM-CM) 10 E-6	(OHM/DEGREE) 10 E-6	(KELVIN)	(JOULES/GRAM -ATOM DEGREE)	(OHM-CM) 10 E-6	(OHM/DEGREE) 10 E-6
1178.2	34.40	46.40	0.0256	1253.2	35.16	48.29	0.0252
1183.2	34.45	46.53	0.0256	1258.2	35.21	48.42	0.0251
1188.2	34.50	46.65	0.0256	1263.2	35.26	48.55	0.0251
1193.2	34.55	46.78	0.0256	1268.2	35.31	48.67	0.0250
1198.2	34.59	46.92	0.0255	1273.2	35.36	48.79	0.0250
1203.2	34.64	47.04	0.0255	1278.2	35.43	48.92	0.0250
1208.2	34.69	47.17	0.0254	1283.2	35.48	49.04	0.0249
1213.2	34.74	47.29	0.0254	1288.2	35.53	49.17	0.0249
1218.2	34.79	47.42	0.0254	1293.2	35.60	49.29	0.0249
1223.2	34.84	47.55	0.0253	1298.2	35.65	49.42	0.0248
1228.2	34.89	47.67	0.0253	1303.2	35.70	49.55	0.0248
1233.2	34.94	47.79	0.0253	1308.2	35.75	49.66	0.0248
1238.2	34.99	47.92	0.0252	1313.2	35.82	49.79	0.0247
1243.2	35.04	48.05	0.0252	1318.2	35.87	49.91	0.0247
1248.2	35.09	48.18	0.0252	1323.2	35.92	50.03	0.0247

TABLE XXII

SPECIFIC HEAT CAPACITY, ELECTRICAL RESISTIVITY, AND TEMPERATURE DERIVATIVE
OF ELECTRICAL RESISTIVITY OF IRON FROM 318 K TO 1178 K

TEMPERATURE (KELVIN)	SPECIFIC HEAT CAPACITY (JOULES/GRAM -ATOM DEGREE)	ELECTRICAL RESISTIVITY (OHM-CM) 10 E-6	TEMPERATURE DERIVATIVE OF RESISTIVITY (OHM/DEGREE) 10 E-6	TEMPERATURE (KELVIN)	SPECIFIC HEAT CAPACITY (JOULES/GRAM -ATOM DEGREE)	ELECTRICAL RESISTIVITY (OHM-CM) 10 E-6	TEMPERATURE DERIVATIVE OF RESISTIVITY (OHM/DEGREE) 10 E-6
318.2	25.76	11.53	0.0562	568.2	31.23	30.57	0.0977
323.2	25.87	11.81	0.0567	573.2	31.34	31.06	0.0986
328.2	25.99	12.11	0.0573	578.2	31.46	31.54	0.0999
333.2	26.11	12.40	0.0579	583.2	31.58	32.03	0.1005
338.2	26.22	12.69	0.0585	588.2	31.69	32.53	0.1015
343.2	26.32	12.98	0.0592	593.2	31.81	33.05	0.1025
348.2	26.43	13.28	0.0599	598.2	31.93	33.56	0.1035
353.2	26.55	13.58	0.0605	603.2	32.07	34.08	0.1044
358.2	26.67	13.89	0.0613	608.2	32.18	34.61	0.1054
363.2	26.79	14.20	0.0620	613.2	32.30	35.13	0.1063
368.2	26.88	14.51	0.0628	618.2	32.44	35.66	0.1073
373.2	27.00	14.84	0.0635	623.2	32.56	36.19	0.1082
378.2	27.09	15.16	0.0643	628.2	32.68	36.74	0.1092
383.2	27.21	15.48	0.0651	633.2	32.82	37.28	0.1102
388.2	27.32	15.80	0.0659	638.2	32.93	37.84	0.1111
393.2	27.44	16.14	0.0667	643.2	33.07	38.38	0.1121
398.2	27.53	16.48	0.0675	648.2	33.19	38.93	0.1131
403.2	27.65	16.81	0.0683	653.2	33.33	39.49	0.1141
408.2	27.77	17.15	0.0691	658.2	33.47	40.06	0.1150
413.2	27.86	17.50	0.0699	663.2	33.61	40.64	0.1160
418.2	27.98	17.86	0.0707	668.2	33.73	41.21	0.1169
423.2	28.07	18.22	0.0716	673.2	33.89	41.79	0.1179
428.2	28.16	18.58	0.0724	678.2	34.01	42.37	0.1189
433.2	28.28	18.95	0.0733	683.2	34.17	42.99	0.1199
438.2	28.40	19.33	0.0741	688.2	34.31	43.60	0.1209
443.2	28.49	19.69	0.0750	693.2	34.45	44.19	0.1218
448.2	28.61	20.08	0.0759	698.2	34.62	44.79	0.1227
453.2	28.70	20.47	0.0767	703.2	34.78	45.39	0.1237
458.2	28.82	20.85	0.0777	708.2	34.92	46.04	0.1247
463.2	28.91	21.24	0.0785	713.2	35.11	46.65	0.1256
468.2	29.03	21.63	0.0796	718.2	35.25	47.29	0.1266
473.2	29.15	22.03	0.0803	723.2	35.43	47.91	0.1275
478.2	29.26	22.44	0.0813	728.2	35.63	48.55	0.1285
483.2	29.36	22.85	0.0820	733.2	35.76	49.20	0.1295
488.2	29.47	23.27	0.0829	738.2	35.95	49.84	0.1303
493.2	29.57	23.69	0.0839	743.2	36.11	50.49	0.1313
498.2	29.68	24.20	0.0848	748.2	36.30	51.14	0.1323
503.2	29.80	24.54	0.0857	753.2	36.49	51.82	0.1333
508.2	29.89	24.97	0.0866	758.2	36.67	52.48	0.1343
513.2	30.01	25.40	0.0875	763.2	36.86	53.15	0.1353
518.2	30.13	25.87	0.0884	768.2	37.07	53.83	0.1363
523.2	30.22	26.31	0.0893	773.2	37.26	54.49	0.1373
528.2	30.34	26.78	0.0902	778.2	37.47	55.20	0.1383
533.2	30.43	27.24	0.0911	783.2	37.68	55.88	0.1393
538.2	30.55	27.71	0.0920	788.2	37.89	56.57	0.1403
543.2	30.67	28.17	0.0930	793.2	38.10	57.29	0.1413
548.2	30.78	28.65	0.0939	798.2	38.31	57.99	0.1423
553.2	30.88	29.11	0.0949	803.2	38.54	58.70	0.1433
558.2	30.99	29.60	0.0959	808.2	38.75	59.49	0.1443
563.2	31.11	30.09	0.0967	813.2	38.99	60.20	0.1453

TABLE XXII (continued)

TEMPERATURE (KELVIN)	SPECIFIC HEAT CAPACITY (JOULES/GRAM -ATON DEGREE)	ELECTRICAL RESISTIVITY (OHM-CM) 10 E-6	TEMPERATURE DERIVATIVE OF RESISTIVITY (OHM/DEGREE) 10 E-6	TEMPERATURE (KELVIN)	SPECIFIC HEAT CAPACITY (JOULES/GRAM -ATON DEGREE)	ELECTRICAL RESISTIVITY (OHM-CM) 10 E-6	TEMPERATURE DERIVATIVE OF RESISTIVITY (OHM/DEGREE) 10 E-6
818.2	39.20	60.93	0.1465	1032.2	67.55	98.88	0.2550
823.2	39.45	61.63	0.1475	1033.2	68.20	99.18	0.2576
828.2	39.69	62.36	0.1487	1034.2	68.90	99.40	0.2604
833.2	39.94	63.12	0.1499	1035.2	69.58	99.68	0.2640
838.2	40.20	63.86	0.1510	1036.2	70.28	99.92	0.2670
843.2	40.46	64.62	0.1521	1037.2	70.98	100.20	0.2708
848.2	40.74	65.59	0.1533	1038.2	71.73	100.44	0.2742
853.2	41.02	66.16	0.1545	1039.2	72.50	100.76	0.2780
858.2	41.30	66.98	0.1556	1040.2	73.32	101.04	0.2824
863.2	41.58	67.63	0.1578	1041.2	74.14	101.28	0.2860
868.2	41.88	68.51	0.1581	1042.2	75.00	101.56	0.2904
873.2	42.19	69.29	0.1593	1043.2	75.94	101.80	0.2952
878.2	42.52	70.07	0.1605	1043.2	59.30	101.80	0.1640
883.2	42.84	70.89	0.1617	1044.2	58.81	101.96	0.1610
888.2	43.17	71.68	0.1630	1045.2	58.29	102.12	0.1578
893.2	43.52	72.60	0.1642	1046.2	57.82	102.26	0.1542
898.2	43.89	73.44	0.1655	1047.2	57.33	102.42	0.1510
903.2	44.25	74.24	0.1669	1048.2	56.84	102.56	0.1480
908.2	44.62	75.05	0.1683	1049.2	56.38	102.70	0.1450
913.2	44.99	75.88	0.1698	1050.2	55.91	102.84	0.1418
918.2	45.39	75.70	0.1712	1051.2	55.46	102.96	0.1386
923.2	45.81	77.53	0.1726	1052.2	55.04	103.12	0.1360
928.2	46.23	78.32	0.1741	1053.2	54.62	103.24	0.1328
933.2	46.68	79.18	0.1757	1054.2	54.23	103.36	0.1302
938.2	47.14	80.04	0.1772	1055.2	53.78	103.50	0.1275
943.2	47.61	80.89	0.1789	1056.2	53.38	103.64	0.1252
948.2	48.12	81.77	0.1805	1057.2	52.96	103.76	0.1230
953.2	48.66	82.68	0.1823	1058.2	52.59	103.89	0.1207
958.2	49.25	83.60	0.1841	1059.2	52.29	104.00	0.1198
963.2	49.85	84.50	0.1857	1060.2	51.98	104.12	0.1166
968.2	50.53	85.43	0.1877	1061.2	51.70	104.22	0.1148
973.2	51.26	86.42	0.1900	1062.2	51.40	104.34	0.1128
978.2	52.03	87.38	0.1925	1063.2	51.14	104.47	0.1112
983.2	52.80	88.36	0.1952	1065.7	50.58	104.74	0.1072
988.2	53.64	89.30	0.1983	1068.2	50.06	105.00	0.1036
993.2	54.55	90.32	0.2018	1070.7	49.62	105.26	0.1004
998.2	55.56	91.37	0.2055	1073.2	49.22	105.49	0.0978
1003.2	56.63	92.38	0.2101	1078.2	48.50	105.96	0.0925
1008.2	57.82	93.38	0.2153	1083.2	47.82	106.41	0.0860
1013.2	59.32	94.46	0.2213	1088.2	47.21	106.84	0.0839
1018.2	61.05	95.67	0.2279	1093.2	46.70	107.24	0.0801
1023.2	62.99	96.72	0.2364	1098.2	46.19	107.63	0.0767
1024.2	63.41	96.92	0.2376	1103.2	45.72	108.02	0.0735
1025.2	63.88	97.16	0.2396	1108.2	45.32	108.38	0.0707
1026.2	64.35	97.40	0.2414	1113.2	44.95	108.72	0.0682
1027.2	64.81	97.64	0.2434	1118.2	44.64	109.05	0.0658
1028.2	65.33	97.92	0.2456	1123.2	44.34	109.38	0.0635
1029.2	65.82	98.14	0.2476	1128.2	44.08	109.69	0.0614
1030.2	66.38	98.38	0.2500	1133.2	43.82	109.99	0.0594
1031.2	66.96	98.62	0.2524	1138.2	43.59	110.29	0.0575

TABLE XXII (continued)

TEMPERATURE	SPECIFIC HEAT CAPACITY	ELECTRICAL RESISTIVITY	TEMPERATURE DERIVATIVE OF RESISTIVITY	TEMPERATURE	SPECIFIC HEAT CAPACITY	ELECTRICAL RESISTIVITY	TEMPERATURE DERIVATIVE OF RESISTIVITY
(KELVIN)	(JOULES/GRAM -ATOM DEGREE)	(OHM-CM) 10 F-6	(OHM/DEGREE) 10 E-6	(KELVIN)	(JOULES/GRAM -ATOM DEGREE)	(OHM-CM) 10 F-6	(OHM/DEGREE) 10 F-6
1143.2	43.38	110.57	0.0558	1163.2	42.68	111.65	0.0503
1148.2	43.19	110.85	0.0542	1168.2	42.52	111.91	0.0493
1153.2	43.01	111.12	0.0528	1173.2	42.40	112.17	0.0483
1158.2	42.84	111.39	0.0515	1178.2	42.26	112.41	0.0475

TABLE XXIII

SPECIFIC HEAT CAPACITY OF NICKEL FROM 1330 K TO 1500 K*

Temperature (Kelvin)	Specific Heat Capacity (Joules/gram- atom degree)	Temperature (Kelvin)	Specific Heat Capacity (Joules/gram- atom degree)
1330	36.00	1420	37.00
1340	36.11	1430	37.12
1350	36.22	1440	37.23
1360	36.33	1450	37.34
1370	36.44	1460	37.46
1380	36.56	1470	37.57
1390	36.67	1480	37.69
1400	36.78	1490	37.80
1410	36.89	1500	37.91

*Calculated using specimen as its own resistance thermometer. Adjusted to agree with thermocouple thermometry data of Figure 18, page 102, in region of overlap. Estimated accuracy of this data is $\pm 2\%$.

TABLE XXIV

MAGNETIC SPECIFIC HEAT CAPACITY C_{vm} OF NICKEL
FROM 30 K TO 1030 K

Temperature (Kelvin)	C_{vm} (Joules/gram- atom degree)	Temperature (Kelvin)	C_{vm} (Joules/gram- atom degree)
30.0	0.00*	633.0	11.69
50.0	0.08*	633.0	5.03
100.0	0.27*	633.2	4.97
150.0	0.47*	635.2	4.44
200.0	0.68*	637.2	4.04
250.0	0.90*	639.2	3.69
300.0	1.14*	641.2	3.41
350.0	1.43	643.2	3.20
403.2	1.84	653.2	2.37
453.2	2.40	663.2	1.94
503.2	3.11	673.2	1.63
553.2	4.09	683.2	1.41
593.2	5.30	693.2	1.22
603.2	5.72	703.2	1.08
613.2	6.27	753.2	0.66
623.2	7.04	803.2	0.45
628.2	7.93	853.2	0.29
629.2	8.39	903.2	0.13
630.2	8.98	953.2	0.06
631.2	9.74	1003.2	0.03
632.2	10.73	1030.0	0.0

*Obtained from smoothed curve drawn through data.

TABLE XXV

MAGNETIC SPECIFIC HEAT CAPACITY C_{vm} OF IRON FROM 15 K TO 1673.2 K

Temperature (Kelvin)	C_{vm} (Joules/gram- atom degree)	Temperature (Kelvin)	C_{vm} (Joules/gram- atom degree)
15.0	0.0*	1028.2	27.59
50.0	0.24*	1033.2	29.45
100.0	0.58*	1038.2	31.69
150.0	0.92*	1043.2	34.29
200.0	1.27*	1043.2	23.16
250.0	1.62*	1048.2	21.33
300.0	1.99*	1053.2	19.65
353.2	2.40	1058.2	18.10
403.2	2.86	1063.2	16.96
453.2	3.38	1068.2	16.09
503.2	3.99	1073.2	15.40
553.2	4.61	1083.2	14.22
603.2	5.33	1093.2	13.26
653.2	6.11	1103.2	12.39
703.2	7.04	1123.2	11.10
753.2	8.16	1143.2	10.14
803.2	9.52	1163.2	9.37
853.2	11.19	1198.2	7.98
873.2	11.98	1123.2	7.11
893.2	12.88	1273.2	5.81
913.2	13.88	1323.2	5.03
933.2	15.02	1373.2	4.24
953.2	16.37	1423.2	3.75
973.2	18.15	1473.2	3.29
983.2	19.20	1523.2	2.86
993.2	20.39	1573.2	2.41
1003.2	21.79	1623.2	1.91
1013.2	23.60	1673.2	1.38
1023.2	26.05		

*Obtained from smoothed curve drawn through data.

TABLE XXVI

LOW-TEMPERATURE SPECIFIC HEAT CAPACITY DATA OF Ni_3Fe

Ordered		Disordered	
Temperature (Kelvin)	Specific Heat Capacity (Millijoules/gram- atom degree)	Temperature (Kelvin)	Specific Heat Capacity (Millijoules/gram- atom degree)
1.2585	4.1635	1.2011	5.0165
1.2780	4.2348	1.2841	5.3978
1.3430	4.4553	1.3698	5.7685
1.4330	4.7910	1.5002	6.3355
1.6708	5.6231	1.7448	7.4174
1.7755	6.0164	1.8439	7.8690
1.9026	6.4606	1.9859	8.5012
2.0089	6.8372	2.1227	9.1059
2.1493	7.3415	2.1956	9.4686
2.2400	7.6885	2.2671	9.7828
2.3210	7.9718	2.3500	10.1569
2.4168	8.3199	2.4489	10.6210
2.5338	8.7599	2.5660	11.1463
2.6786	9.2944	2.7121	11.8293
2.7971	9.7462	2.7910	12.2243
2.8885	10.0956	2.8422	12.4692
2.9666	10.4166	2.8970	12.7118
3.0548	10.7513	2.9556	12.9921
3.1530	11.1424	3.0204	13.3040
3.2653	11.5535	3.0908	13.5939
3.3501	11.9132	3.2093	14.2099
3.4189	12.2050	3.2579	14.4661
3.4938	12.5042	3.3091	14.7357
3.5752	12.8264	3.3655	15.0116
3.6645	13.1804	3.4248	15.3075
3.7621	13.6237	3.4879	15.6129
3.8918	14.1659	3.5555	15.9217
3.9634	14.4997	3.6280	16.3094
4.0135	14.7255	3.6851	16.5946
4.0665	14.9806	3.7276	16.8373
4.1221	15.2055	3.7727	17.0574
4.1799	15.4876	3.8204	17.2738
4.2421	15.7658	3.8701	17.5566
4.3059	16.0207	3.9217	17.8828
4.3740	16.3461	3.9765	18.1472
4.4462	16.6522	4.0334	18.4265
		4.0938	18.7450
		4.1571	19.0806
		4.2242	19.4880
		4.2977	19.8597
		4.3625	20.2727

TABLE XXVII

SPECIFIC HEAT CAPACITY, ELECTRICAL RESISTIVITY, AND TEMPERATURE DERIVATIVE
OF ELECTRICAL RESISTIVITY OF VACUUM-QUENCHED Ni_3Fe IN TEMPERATURE REGIONS
WHERE RESULTS WERE INDEPENDENT OF HEATING RATES USED IN THIS WORK

TEMPERATURE (KELVIN)	SPECIFIC HEAT CAPACITY (JOULES/GRAM -ATON DEGREE)	ELECTRICAL RESISTIVITY (OHM-CM) 10 E-6	TEMPERATURE DERIVATIVE OF RESISTIVITY (OHM/DEGREE) 10 E-6	TEMPERATURE (KELVIN)	SPECIFIC HEAT CAPACITY (JOULES/GRAM -ATON DEGREE)	ELECTRICAL RESISTIVITY (OHM-CM) 10 E-6	TEMPERATURE DERIVATIVE OF RESISTIVITY (OHM/DEGREE) 10 E-6
308.2	25.58	15.92	0.0742	558.2	29.97	40.02	0.1160
313.2	25.68	16.30	0.0767	563.2	30.07	40.60	0.1166
318.2	25.78	16.69	0.0778	568.2	30.17	41.18	0.1173
323.2	25.85	17.08	0.0787	573.2	30.27	41.74	0.1183
328.2	25.95	17.48	0.0801	578.2	30.34	42.34	0.1189
333.2	26.04	17.88	0.0802	583.2	30.44	42.93	0.1195
338.2	26.12	18.28	0.0813	588.2	30.53	43.53	0.1205
343.2	26.21	18.70	0.0824	593.2	30.63	44.14	0.1215
348.2	26.29	19.11	0.0833	598.2	30.75	44.75	0.1220
353.2	26.38	19.53	0.0842	603.2	30.85	45.36	0.1228
358.2	26.48	19.95	0.0850	608.2	30.95	45.97	0.1234
363.2	26.58	20.38	0.0858	613.2	31.02	46.60	0.1244
368.2	26.65	20.81	0.0865	618.2	31.12	47.22	0.1254
373.2	26.75	21.24	0.0879	623.2	31.24	47.85	0.1262
378.2	26.84	21.69	0.0883	628.2	31.36	48.47	0.1270
383.2	26.94	22.13	0.0894	633.2	31.43	49.12	0.1278
388.2	27.04	22.58	0.0906	638.2	31.53	49.76	0.1288
393.2	27.13	23.03	0.0911	643.2	31.65	50.40	0.1295
398.2	27.21	23.49	0.0916	648.2	31.75	51.06	0.1305
403.2	27.30	23.95	0.0928	653.2	31.89	51.72	0.1314
408.2	27.38	24.42	0.0935	658.2	31.96	52.37	0.1321
413.2	27.47	24.89	0.0942	663.2	32.06	53.03	0.1329
418.2	27.55	25.36	0.0949	668.2	32.18	53.69	0.1339
423.2	27.64	25.84	0.0958	673.2	32.28	54.36	0.1347
428.2	27.72	26.30	0.0964	678.2	32.40	55.04	0.1359
433.2	27.81	26.78	0.0970	683.2	32.50	55.72	0.1368
438.2	27.89	27.27	0.0979	688.2	32.60	56.41	0.1378
443.2	27.98	27.76	0.0988	693.2	32.72	57.09	0.1386
448.2	28.08	28.25	0.0993	698.2	32.84	57.80	0.1397
453.2	28.15	28.73	0.1000	703.2	32.94	58.48	0.1408
458.2	28.23	29.23	0.1009	708.2	33.06	59.21	0.1417
463.2	28.32	29.74	0.1014	713.2	33.18	59.90	0.1427
468.2	28.40	30.25	0.1021	718.2	33.30	60.63	0.1436
473.2	28.49	30.76	0.1028	723.2	33.42	61.34	0.1444
478.2	28.59	31.27	0.1035	728.2	33.57	62.07	0.1458
483.2	28.66	31.80	0.1043	733.2	33.69	62.80	0.1467
488.2	28.74	32.32	0.1054	738.2	33.83	63.55	0.1477
493.2	28.83	32.84	0.1060	743.2	33.96	64.28	0.1488
498.2	28.93	33.38	0.1065	748.2	34.10	65.03	0.1500
503.2	29.00	33.91	0.1075	1048.2	34.44	92.37	0.0226
508.2	29.10	34.45	0.1084	1053.2	34.44	92.49	0.0225
513.2	29.20	35.00	0.1088	1058.2	34.46	92.59	0.0223
518.2	29.27	35.54	0.1097	1063.2	34.46	92.71	0.0221
523.2	29.37	36.10	0.1104	1068.2	34.49	92.82	0.0221
528.2	29.44	36.65	0.1110	1073.2	34.49	92.93	0.0222
533.2	29.54	37.20	0.1119	1078.2	34.51	93.04	0.0219
538.2	29.61	37.76	0.1127	1083.2	34.54	93.15	0.0218
543.2	29.71	38.33	0.1135	1088.2	34.54	93.26	0.0218
548.2	29.74	38.86	0.1142	1093.2	34.56	93.36	0.0217
553.2	29.88	39.44	0.1152	1098.2	34.59	93.47	0.0217

TABLE XXVII (continued)

TEMPERATURE	SPECIFIC HEAT CAPACITY	ELECTRICAL RESISTIVITY	TEMPERATURE DERIVATIVE OF RESISTIVITY	TEMPERATURE	SPECIFIC HEAT CAPACITY	ELECTRICAL RESISTIVITY	TEMPERATURE DERIVATIVE OF RESISTIVITY
(KELVIN)	(JOULES/GRAM-ATOM DEGREE)	(OHM-CM) 10 E-6	(OHM/DEGREE) 10 E-6	(KELVIN)	(JOULES/GRAM-ATOM DEGREE)	(OHM-CM) 10 E-6	(OHM/DEGREE) 10 E-6
1103.2	34.59	93.59	0.0216	1268.2	35.61	97.08	0.0214
1108.2	34.61	93.69	0.0216	1273.2	35.65	97.18	0.0211
1113.2	34.63	93.80	0.0216	1278.2	35.68	97.29	0.0207
1118.2	34.66	93.90	0.0216	1283.2	35.73	97.39	0.0205
1123.2	34.68	94.02	0.0216	1288.2	35.75	97.48	0.0205
1128.2	34.71	94.13	0.0214	1293.2	35.80	97.60	0.0205
1133.2	34.73	94.23	0.0213	1298.2	35.85	97.70	0.0206
1138.2	34.76	94.33	0.0213	1303.2	35.87	97.79	0.0209
1143.2	34.78	94.44	0.0211	1308.2	35.92	97.90	0.0209
1148.2	34.81	94.55	0.0212	1313.2	35.97	98.02	0.0208
1153.2	34.83	94.65	0.0212	1318.2	35.99	98.11	0.0207
1158.2	34.85	94.76	0.0214	1323.2	36.04	98.21	0.0207
1163.2	34.88	94.87	0.0213	1328.2	36.09	98.31	0.0208
1168.2	34.90	94.98	0.0215	1333.2	36.14	98.43	0.0209
1173.2	34.93	95.07	0.0211	1338.2	36.16	98.53	0.0208
1178.2	34.95	95.19	0.0210	1343.2	36.21	98.64	0.0209
1183.2	34.97	95.28	0.0212	1348.2	36.26	98.74	0.0208
1188.2	35.02	95.39	0.0210	1353.2	36.29	98.84	0.0209
1193.2	35.05	95.50	0.0212	1358.2	36.33	98.94	0.0210
1198.2	35.07	95.61	0.0210	1363.2	36.36	99.05	0.0211
1203.2	35.10	95.71	0.0209	1368.2	36.41	99.16	0.0209
1208.2	35.14	95.82	0.0208	1373.2	36.46	99.25	0.0207
1213.2	35.17	95.92	0.0209	1378.2	36.48	99.37	0.0206
1218.2	35.19	96.02	0.0210	1383.2	36.53	99.47	0.0206
1223.2	35.24	96.12	0.0211	1388.2	36.58	99.56	0.0207
1228.2	35.27	96.23	0.0210	1393.2	36.62	99.68	0.0208
1233.2	35.31	96.33	0.0210	1398.2	36.65	99.80	0.0207
1238.2	35.36	96.44	0.0209	1403.2	36.70	99.88	0.0207
1243.2	35.39	96.54	0.0209	1408.2	36.75	99.98	0.0209
1248.2	35.44	96.64	0.0210	1413.2	36.77	100.09	0.0212
1253.2	35.48	96.76	0.0211	1418.2	36.82	100.20	0.0210
1258.2	35.51	96.85	0.0212	1423.2	36.87	100.29	0.0207
1263.2	35.56	96.97	0.0213				

TABLE XXVIII

SPECIFIC HEAT CAPACITY, ELECTRICAL RESISTIVITY, AND TEMPERATURE DERIVATIVE
OF ELECTRICAL RESISTIVITY OF VACUUM-QUENCHED Ni_3Fe PULSED FROM BELOW THE
ORDER-DISORDER CRITICAL TEMPERATURE WITH CLASS I HEATING RATE IN
TEMPERATURE REGION WHERE RESULTS WERE HEATING RATE DEPENDENT

TEMPERATURE	SPECIFIC HEAT CAPACITY	ELECTRICAL RESISTIVITY	TEMPERATURE DERIVATIVE OF RESISTIVITY	TEMPERATURE	SPECIFIC HEAT CAPACITY	ELECTRICAL RESISTIVITY	TEMPERATURE DERIVATIVE OF RESISTIVITY
(KELVIN)	(JOULES/GRAM -ATOM DEGREE)	(OHM-CM) 10 E-6	(OHM/DEGREE) 10 E-6	(KELVIN)	(JOULES/GRAM -ATOM DEGREE)	(OHM-CM) 10 E-6	(OHM/DEGREE) 10 E-6
753.2	34.27	65.78	0.1513	872.2	39.10	86.45	0.1252
758.2	34.39	66.55	0.1518	873.2	38.98	86.56	0.1200
763.2	34.54	67.31	0.1526	878.2	38.57	87.10	0.0972
768.2	34.71	68.06	0.1538	883.2	38.54	87.53	0.0796
773.2	34.88	68.84	0.1554	888.2	38.79	87.89	0.0657
778.2	35.02	69.63	0.1571	893.2	39.00	88.19	0.0545
783.2	35.22	70.42	0.1586	898.2	38.98	88.43	0.0448
788.2	35.41	71.21	0.1594	903.2	39.15	88.63	0.0377
793.2	35.53	72.00	0.1605	908.2	39.17	88.81	0.0316
798.2	35.80	72.82	0.1620	913.2	38.86	88.96	0.0279
803.2	36.02	73.61	0.1638	918.2	38.32	89.09	0.0259
808.2	36.24	74.44	0.1654	923.2	37.84	89.21	0.0252
813.2	36.48	75.29	0.1671	928.2	37.16	89.34	0.0256
818.2	36.72	76.11	0.1692	933.2	36.41	89.47	0.0260
823.2	37.01	76.98	0.1713	938.2	35.85	89.60	0.0271
828.2	37.30	77.83	0.1737	943.2	35.53	89.74	0.0277
833.2	37.62	78.70	0.1765	948.2	35.27	89.88	0.0278
838.2	37.98	79.61	0.1799	953.2	35.10	90.02	0.0278
843.2	38.42	80.51	0.1837	958.2	34.85	90.15	0.0274
848.2	39.08	81.46	0.1887	963.2	34.68	90.30	0.0270
853.2	39.73	82.40	0.1951	968.2	34.66	90.43	0.0265
858.2	40.58	83.40	0.2040	973.2	34.46	90.57	0.0260
859.2	40.78	83.61	0.2061	978.2	34.39	90.70	0.0257
860.2	40.97	83.81	0.2081	983.2	34.37	90.82	0.0254
861.2	41.19	84.02	0.2110	988.2	34.37	90.95	0.0250
862.2	41.41	84.24	0.2138	993.2	34.34	91.07	0.0247
863.2	41.65	84.43	0.2165	998.2	34.34	91.20	0.0246
864.2	41.92	84.66	0.2201	1003.2	34.34	91.32	0.0246
865.2	42.18	84.89	0.2234	1008.2	34.37	91.44	0.0240
866.2	42.47	85.09	0.2269	1013.2	34.37	91.57	0.0237
867.2	42.79	85.32	0.2306	1018.2	34.37	91.68	0.0237
868.2	43.13	85.57	0.2347	1023.2	34.39	91.80	0.0235
869.2	43.45	85.81	0.2385	1028.2	34.39	91.92	0.0230
870.2	43.81	86.05	0.2430	1033.2	34.42	92.03	0.0229
871.2	44.17	86.30	0.2477	1038.2	34.42	92.14	0.0229
871.6	44.37	86.40	0.2493	1043.2	34.44	92.26	0.0228
871.6	39.17	86.40	0.1288				

TABLE XXIX

SPECIFIC HEAT CAPACITY, ELECTRICAL RESISTIVITY, AND TEMPERATURE DERIVATIVE
OF ELECTRICAL RESISTIVITY OF Ni_3Fe PULSED FROM 75 DEGREES ABOVE THE
ORDER-DISORDER CRITICAL TEMPERATURE WITH CLASS I HEATING RATE

TEMPERATURE	SPECIFIC HEAT CAPACITY	ELECTRICAL RESISTIVITY	TEMPERATURE DERIVATIVE OF RESISTIVITY	TEMPERATURE	SPECIFIC HEAT CAPACITY	ELECTRICAL RESISTIVITY	TEMPERATURE DERIVATIVE OF RESISTIVITY
(KELVIN)	(JOULES/GRAM -ATOM DEGREE)	(OHM-CM) 10 E-6	(OHM/DEGREE) 10 E-6	(KELVIN)	(JOULES/GRAM -ATOM DEGREE)	(OHM-CM) 10 E-6	(OHM/DEGREE) 10 E-6
848.2	38.98	81.91	0.1899	878.2	37.64	87.27	0.0876
853.2	39.61	82.90	0.1968	883.2	37.62	87.67	0.0726
858.2	40.41	83.91	0.2064	888.2	37.96	88.00	0.0636
859.2	40.61	84.11	0.2091	893.2	38.06	88.30	0.0512
860.2	40.82	84.31	0.2118	898.2	38.15	88.51	0.0412
861.2	41.02	84.51	0.2144	903.2	38.59	88.71	0.0352
862.2	41.24	84.73	0.2176	908.2	38.45	88.87	0.0303
863.2	41.48	84.96	0.2213	913.2	38.28	89.00	0.0268
864.2	41.72	85.18	0.2245	918.2	37.91	89.13	0.0247
865.2	41.99	85.40	0.2278	923.2	37.38	89.26	0.0240
866.2	42.26	85.65	0.2318	928.2	36.77	89.37	0.0244
867.2	42.55	85.87	0.2359	933.2	36.19	89.50	0.0256
868.2	42.81	86.08	0.2400	938.2	35.65	89.63	0.0263
869.2	43.15	86.30	0.2444	943.2	35.24	89.76	0.0268
869.5	43.25	86.38	0.2456	948.2	35.02	89.89	0.0273
869.5	37.89	86.38	0.1279	953.2	34.80	90.03	0.0275
870.2	37.86	86.45	0.1177	958.2	34.68	90.17	0.0272
871.2	37.81	86.55	0.1133	963.2	34.61	90.31	0.0268
872.2	37.79	86.67	0.1093	968.2	34.54	90.44	0.0263
873.2	37.77	86.78	0.1053	973.2	34.44	90.57	0.0259

TABLE XXX

SPECIFIC HEAT CAPACITY, ELECTRICAL RESISTIVITY, AND TEMPERATURE DERIVATIVE
OF ELECTRICAL RESISTIVITY OF Ni_3Fe PULSED FROM 106 DEGREES ABOVE THE
ORDER-DISORDER CRITICAL TEMPERATURE WITH CLASS I HEATING RATE

TEMPERATURE	SPECIFIC HEAT CAPACITY	ELECTRICAL RESISTIVITY	TEMPERATURE DERIVATIVE OF RESISTIVITY	TEMPERATURE	SPECIFIC HEAT CAPACITY	ELECTRICAL RESISTIVITY	TEMPERATURE DERIVATIVE OF RESISTIVITY
(KELVIN)	(JOULES/GRAM -ATOM DEGREE)	(OHM-CM) 10 E-6	(OHM/DEGREE) 10 E-6	(KELVIN)	(JOULES/GRAM -ATOM DEGREE)	(OHM-CM) 10 E-6	(OHM/DEGREE) 10 E-6
879.2	34.76	87.10	0.0683	928.2	35.41	89.30	0.0374
883.2	34.90	87.35	0.0644	933.2	35.19	89.45	0.0295
888.2	35.05	87.66	0.0595	938.2	35.02	89.60	0.0290
893.2	35.22	87.94	0.0540	943.2	34.80	89.75	0.0285
898.2	35.44	88.20	0.0487	948.2	34.73	89.89	0.0281
903.2	35.61	88.42	0.0436	953.2	34.66	90.02	0.0276
908.2	35.73	88.63	0.0392	958.2	34.54	90.17	0.0272
913.2	35.90	88.82	0.0357	963.2	34.46	90.30	0.0268
918.2	35.87	88.99	0.0333	968.2	34.44	90.43	0.0265
923.2	35.65	89.14	0.0316	973.2	34.37	90.56	0.0260

TABLE XXXI

SPECIFIC HEAT CAPACITY, ELECTRICAL RESISTIVITY, AND TEMPERATURE DERIVATIVE OF ELECTRICAL RESISTIVITY OF VACUUM-QUENCHED Ni_3Fe PULSED FROM BELOW THE ORDER-DISORDER CRITICAL TEMPERATURE WITH CLASS II HEATING RATE IN TEMPERATURE REGION WHEN RESULTS WERE HEATING RATE DEPENDENT

TEMPERATURE (KELVIN)	SPECIFIC HEAT CAPACITY (JOULES/GRAM -ATOM DEGREE)	ELECTRICAL RESISTIVITY (OHM-CM) 10 E-6	TEMPERATURE DERIVATIVE OF RESISTIVITY (OHM/DEGREE) 10 E-6	TEMPERATURE (KELVIN)	SPECIFIC HEAT CAPACITY (JOULES/GRAM -ATOM DEGREE)	ELECTRICAL RESISTIVITY (OHM-CM) 10 E-6	TEMPERATURE DERIVATIVE OF RESISTIVITY (OHM/DEGREE) 10 E-6
748.2	34.03	64.74	0.1495	872.6	35.73	85.85	0.1200
753.2	34.17	65.44	0.1500	873.2	35.73	85.95	0.1187
758.2	34.32	66.24	0.1499	874.2	35.75	86.09	0.1163
763.2	34.44	66.94	0.1504	878.2	35.80	86.60	0.1072
768.2	34.59	67.73	0.1524	883.2	35.87	87.12	0.0968
773.2	34.73	68.44	0.1548	888.2	35.97	87.58	0.0840
778.2	34.91	69.27	0.1570	893.2	36.09	87.93	0.0752
783.2	35.07	70.08	0.1576	898.2	36.24	88.28	0.0664
788.2	35.24	70.83	0.1573	903.2	36.50	88.57	0.0590
793.2	35.39	71.61	0.1588	908.2	36.82	88.89	0.0518
798.2	35.58	72.45	0.1605	913.2	37.23	89.14	0.0451
803.2	35.78	73.25	0.1620	918.2	37.67	89.26	0.0384
808.2	35.97	74.11	0.1635	923.2	37.98	89.48	0.0330
813.2	36.16	74.89	0.1643	928.2	38.18	89.66	0.0288
818.2	36.41	75.69	0.1657	933.2	38.25	89.77	0.0238
823.2	36.62	76.57	0.1682	938.2	38.15	89.86	0.0195
828.2	36.87	77.34	0.1711	943.2	37.86	90.01	0.0173
833.2	37.11	78.20	0.1749	948.2	37.57	90.05	0.0176
838.2	37.41	79.10	0.1776	953.2	37.06	90.10	0.0190
843.2	37.69	80.01	0.1796	958.2	36.55	90.18	0.0204
848.2	38.03	80.95	0.1830	963.2	35.99	90.40	0.0204
853.2	38.47	81.81	0.1883	968.2	35.58	90.45	0.0201
858.2	38.91	82.76	0.1949	973.2	35.19	90.52	0.0213
859.2	39.00	83.00	0.1964	978.2	34.97	90.60	0.0233
860.2	39.08	83.20	0.1980	983.2	34.80	90.70	0.0250
861.2	39.17	83.40	0.1995	988.2	34.66	90.93	0.0259
862.2	39.27	83.60	0.2011	993.2	34.63	91.07	0.0251
863.2	39.37	83.80	0.2028	998.2	34.61	91.11	0.0233
864.2	39.46	84.01	0.2044	1003.2	34.59	91.24	0.0229
865.2	39.56	84.23	0.2063	1008.2	34.54	91.39	0.0239
866.2	39.66	84.44	0.2080	1013.2	34.51	91.48	0.0244
867.2	39.76	84.63	0.2098	1018.2	34.59	91.61	0.0243
868.2	39.88	84.85	0.2118	1023.2	34.54	91.72	0.0241
869.2	39.97	85.07	0.2138	1028.2	34.54	91.88	0.0235
870.2	40.10	85.30	0.2159	1033.2	34.51	91.96	0.0229
871.2	40.19	85.53	0.2178	1038.2	34.49	92.09	0.0227
872.2	40.31	85.77	0.2199	1043.2	34.46	92.20	0.0229
872.6	40.36	85.85	0.2207	1048.2	34.49	92.31	0.0229

TABLE XXXII

SPECIFIC HEAT CAPACITY, ELECTRICAL RESISTIVITY, AND TEMPERATURE DERIVATIVE OF ELECTRICAL RESISTIVITY OF Ni_3Fe IN ORDER-STATE I PULSED FROM BELOW THE ORDER-DISORDER CRITICAL TEMPERATURE WITH CLASS I HEATING RATE

TEMPERATURE (KELVIN)	SPECIFIC HEAT CAPACITY (JOULES/GRAM -ATOM DEGREE)	ELECTRICAL RESISTIVITY (OHM-CM) 10 E-6	TEMPERATURE DERIVATIVE OF RESISTIVITY (OHM/DEGREE) 10 E-6	TEMPERATURE (KELVIN)	SPECIFIC HEAT CAPACITY (JOULES/GRAM -ATOM DEGREE)	ELECTRICAL RESISTIVITY (OHM-CM) 10 E-6	TEMPERATURE DERIVATIVE OF RESISTIVITY (OHM/DEGREE) 10 E-6
373.2	24.95	13.20	0.0983	553.2	29.27	34.18	0.1760
378.2	25.05	13.50	0.0616	558.2	29.37	34.71	0.1078
313.2	25.10	13.81	0.0629	563.2	29.44	35.25	0.1086
318.2	25.19	14.13	0.0634	568.2	29.54	35.80	0.1090
323.2	25.29	14.45	0.0646	573.2	29.63	36.34	0.1101
328.2	25.36	14.78	0.0659	578.2	29.73	36.90	0.1110
333.2	25.46	15.11	0.0666	583.2	29.83	37.45	0.1123
338.2	25.58	15.45	0.0677	588.2	29.93	38.02	0.1133
343.2	25.63	15.79	0.0684	593.2	30.00	38.59	0.1147
348.2	25.70	16.13	0.0695	598.2	30.10	39.17	0.1155
353.2	25.80	16.44	0.0702	603.2	30.19	39.75	0.1165
358.2	25.90	16.83	0.0713	608.2	30.29	40.33	0.1180
363.2	26.14	17.19	0.0720	613.2	30.41	40.92	0.1186
368.2	26.07	17.55	0.0729	618.2	30.51	41.51	0.1197
373.2	26.14	17.92	0.0736	623.2	30.61	42.12	0.1210
378.2	26.21	18.29	0.0747	628.2	30.70	42.73	0.1224
383.2	26.31	18.67	0.0755	633.2	30.80	43.34	0.1235
388.2	26.38	19.04	0.0764	638.2	30.90	43.97	0.1245
393.2	26.48	19.43	0.0776	643.2	30.99	44.59	0.1254
398.2	26.58	19.87	0.0782	648.2	31.12	45.22	0.1265
403.2	26.65	20.21	0.0791	653.2	31.21	45.85	0.1284
408.2	26.72	20.61	0.0799	658.2	31.31	46.50	0.1297
413.2	26.82	21.01	0.0810	663.2	31.41	47.15	0.1307
418.2	26.92	21.42	0.0817	668.2	31.50	47.80	0.1316
423.2	26.99	21.83	0.0829	673.2	31.63	48.46	0.1338
428.2	27.09	22.24	0.0833	678.2	31.72	49.42	0.1334
433.2	27.18	22.67	0.0846	683.2	31.82	50.08	0.1348
438.2	27.26	23.09	0.0852	688.2	31.92	50.76	0.1360
443.2	27.33	23.52	0.0862	693.2	32.04	51.45	0.1377
448.2	27.43	23.92	0.0870	698.2	32.13	52.14	0.1388
453.2	27.50	24.38	0.0879	703.2	32.26	52.84	0.1399
458.2	27.60	24.86	0.0888	708.2	32.35	53.53	0.1416
463.2	27.69	25.33	0.0897	713.2	32.47	54.25	0.1428
468.2	27.77	25.63	0.0906	718.2	32.57	54.97	0.1446
473.2	27.86	26.33	0.0915	723.2	32.69	55.70	0.1452
478.2	27.94	26.73	0.0925	728.2	32.81	56.42	0.1473
483.2	28.03	27.20	0.0936	733.2	32.94	57.16	0.1494
488.2	28.13	27.67	0.0955	738.2	33.06	57.91	0.1497
493.2	28.20	28.14	0.0943	743.2	33.18	58.66	0.1516
498.2	28.30	28.61	0.0958	748.2	33.32	59.42	0.1528
503.2	28.40	29.10	0.0969	753.2	33.47	60.20	0.1542
508.2	28.47	29.59	0.0976	758.2	33.62	60.97	0.1559
513.2	28.54	30.08	0.0982	763.2	33.79	61.75	0.1578
518.2	28.64	30.59	0.0985	768.2	33.96	62.54	0.1596
523.2	28.71	31.08	0.0981	773.2	34.13	63.35	0.1610
528.2	28.81	31.58	0.1016	778.2	34.32	64.16	0.1632
533.2	28.91	32.09	0.1025	783.2	34.54	64.97	0.1643
538.2	28.98	32.61	0.1031	788.2	34.78	65.80	0.1672
543.2	29.08	33.12	0.1043	793.2	35.00	66.63	0.1689
548.2	29.17	33.65	0.1053	798.2	35.27	67.50	0.1704

TABLE XXXII (continued)

TEMPERATURE	SPECIFIC HEAT CAPACITY	ELECTRICAL RESISTIVITY	TEMPERATURE DERIVATIVE OF RESISTIVITY	TEMPERATURE	SPECIFIC HEAT CAPACITY	ELECTRICAL RESISTIVITY	TEMPERATURE DERIVATIVE OF RESISTIVITY
(KELVIN)	(JOULES/GRAM -ATOM DEGREE)	(OHM-CM) 10 E-6	(OHM/DEGREE) 10 E-6	(KELVIN)	(JOULES/GRAM -ATOM DEGREE)	(OHM-CM) 10 E-6	(OHM/DEGREE) 10 E-6
873.2	35.56	68.35	0.1733	890.2	60.94	87.29	0.2418
874.2	35.90	69.22	0.1756	891.2	60.60	87.54	0.2338
875.2	36.33	70.10	0.1791	892.2	60.26	87.76	0.2258
876.2	36.77	71.00	0.1811	893.2	59.93	87.98	0.2175
877.2	37.40	71.93	0.1851	894.2	59.59	88.20	0.2091
878.2	38.11	72.86	0.1890	895.2	59.25	88.40	0.2011
879.2	39.03	73.81	0.1938	896.2	58.78	88.61	0.1926
880.2	40.00	74.79	0.1987	897.2	58.42	88.80	0.1845
881.2	41.07	75.81	0.2056	898.2	57.86	88.98	0.1759
882.2	42.49	76.84	0.2138	899.2	55.02	89.74	0.1323
883.2	44.55	77.94	0.2199	900.2	51.92	90.29	0.0844
884.2	47.30	79.05	0.2291	901.2	49.34	90.61	0.0438
885.2	49.80	80.23	0.2399	902.2	47.43	90.75	0.0184
886.2	52.81	81.46	0.2505	903.2	46.02	90.80	0.0074
887.2	55.63	82.75	0.2598	904.2	44.80	90.81	-0.0027
888.2	58.81	84.06	0.2702	905.2	43.74	90.79	-0.0044
889.2	59.37	84.32	0.2720	906.2	42.81	90.77	-0.0072
890.2	59.95	84.61	0.2740	907.2	42.04	90.73	-0.0092
891.2	60.36	84.87	0.2751	908.2	41.36	90.68	-0.0095
892.2	60.65	85.15	0.2756	909.2	40.46	90.63	-0.0094
893.2	61.04	85.44	0.2764	910.2	39.46	90.60	-0.0078
894.2	61.24	85.70	0.2772	911.2	38.32	90.57	-0.0039
895.2	61.53	85.98	0.2770	912.2	36.96	90.56	0.0036
896.2	61.75	86.24	0.2764	913.2	35.78	90.59	0.0111
897.2	62.04	86.51	0.2757	914.2	34.97	90.66	0.0178
898.2	62.30	86.77	0.2751	915.2	34.59	90.78	0.0228
899.2	62.55	87.04	0.2744	916.2	34.56	90.89	0.0240
900.2	62.62	87.09	0.2743	917.2	34.37	91.01	0.0247
901.2	61.24	87.09	0.2489				

TABLE XXXIII

SPECIFIC HEAT CAPACITY, ELECTRICAL RESISTIVITY, AND TEMPERATURE DERIVATIVE OF ELECTRICAL RESISTIVITY OF Ni_3Fe IN ORDER-STATE II PULSED FROM BELOW THE ORDER-DISORDER CRITICAL TEMPERATURE WITH CLASS I HEATING RATE

TEMPERATURE (KELVIN)	SPECIFIC HEAT CAPACITY (JOULES/GRAM -ATOM DEGREE)	ELECTRICAL RESISTIVITY (OHM-CM) 10 E-6	TEMPERATURE DERIVATIVE OF RESISTIVITY (OHM/DEGREE) 10 E-6	TEMPERATURE (KELVIN)	SPECIFIC HEAT CAPACITY (JOULES/GRAM -ATOM DEGREE)	ELECTRICAL RESISTIVITY (OHM-CM) 10 E-6	TEMPERATURE DERIVATIVE OF RESISTIVITY (OHM/DEGREE) 10 E-6
423.2	26.82	18.87	0.0728	673.2	31.02	43.09	0.1253
428.2	26.89	19.24	0.0738	678.2	31.14	43.84	0.1269
433.2	26.97	19.61	0.0746	683.2	31.24	44.47	0.1288
438.2	27.04	19.98	0.0754	688.2	31.33	45.12	0.1300
443.2	27.11	20.36	0.0763	693.2	31.43	45.78	0.1313
448.2	27.18	20.74	0.0769	698.2	31.53	46.43	0.1332
453.2	27.23	21.13	0.0777	703.2	31.65	47.10	0.1351
458.2	27.30	21.52	0.0787	708.2	31.77	47.79	0.1362
463.2	27.38	21.92	0.0797	713.2	31.87	48.47	0.1382
468.2	27.45	22.32	0.0804	718.2	31.99	49.18	0.1402
473.2	27.52	22.72	0.0813	723.2	32.09	49.88	0.1416
478.2	27.62	23.13	0.0821	728.2	32.21	50.59	0.1434
483.2	27.67	23.55	0.0829	733.2	32.33	51.32	0.1451
488.2	27.77	23.96	0.0839	738.2	32.45	52.04	0.1470
493.2	27.84	24.39	0.0847	743.2	32.57	52.79	0.1488
498.2	27.91	24.81	0.0858	748.2	32.69	53.53	0.1511
503.2	27.98	25.24	0.0866	753.2	32.81	54.28	0.1525
508.2	28.06	25.67	0.0874	758.2	32.96	55.06	0.1548
513.2	28.15	26.12	0.0888	763.2	33.11	55.83	0.1565
518.2	28.23	26.57	0.0895	768.2	33.25	56.63	0.1589
523.2	28.32	27.01	0.0901	773.2	33.42	57.41	0.1613
528.2	28.40	27.47	0.0913	778.2	33.57	58.24	0.1632
533.2	28.49	27.93	0.0921	783.2	33.74	59.06	0.1655
538.2	28.57	28.39	0.0933	788.2	33.91	59.89	0.1676
543.2	28.64	28.85	0.0943	793.2	34.08	60.74	0.1703
548.2	28.74	29.33	0.0951	798.2	34.27	61.59	0.1728
553.2	28.81	29.81	0.0961	803.2	34.49	62.46	0.1748
558.2	28.91	30.29	0.0972	808.2	34.68	63.35	0.1778
563.2	28.98	30.78	0.0984	813.2	34.93	64.23	0.1807
568.2	29.08	31.27	0.0993	818.2	35.17	65.16	0.1834
573.2	29.15	31.77	0.1003	823.2	35.46	66.08	0.1871
578.2	29.25	32.28	0.1011	828.2	35.78	67.02	0.1905
583.2	29.32	32.78	0.1022	833.2	36.14	67.98	0.1938
588.2	29.42	33.29	0.1034	838.2	36.67	68.97	0.1981
593.2	29.51	33.82	0.1045	843.2	37.28	69.97	0.2030
598.2	29.59	34.34	0.1055	848.2	37.91	71.00	0.2076
603.2	29.68	34.87	0.1068	853.2	38.79	72.04	0.2133
608.2	29.78	35.42	0.1084	858.2	40.02	73.14	0.2207
613.2	29.85	35.96	0.1095	863.2	40.97	74.25	0.2286
618.2	29.95	36.51	0.1103	868.2	42.55	75.41	0.2381
623.2	30.05	37.06	0.1114	873.2	44.59	76.62	0.2496
628.2	30.12	37.62	0.1130	878.2	47.16	77.90	0.2622
633.2	30.24	38.19	0.1143	883.2	50.68	79.25	0.2782
638.2	30.31	38.87	0.1161	888.2	54.83	80.69	0.2951
643.2	30.41	39.45	0.1171	893.2	59.76	82.21	0.3137
648.2	30.51	40.04	0.1185	898.2	65.73	83.84	0.3327
653.2	30.61	40.64	0.1197	903.2	70.75	85.53	0.3443
658.2	30.70	41.24	0.1210	908.2	74.32	87.27	0.3429
663.2	30.82	41.85	0.1228	909.2	74.80	87.59	0.3418
668.2	30.97	42.46	0.1240	910.2	75.36	87.93	0.3406

TABLE XXXIII (continued)

TEMPERATURE	SPECIFIC HEAT CAPACITY	ELECTRICAL RESISTIVITY	TEMPERATURE DERIVATIVE OF RESISTIVITY	TEMPERATURE	SPECIFIC HEAT CAPACITY	ELECTRICAL RESISTIVITY	TEMPERATURE DERIVATIVE OF RESISTIVITY
(KELVIN)	(JOULES/GRAM -ATOM DEGREE)	(OHM-CM) 10 E-6	(OHM/DEGREE) 10 E-6	(KELVIN)	(JOULES/GRAM -ATOM DEGREE)	(OHM-CM) 10 E-6	(OHM/DEGREE) 10 E-6
911.2	75.68	88.28	0.3382	933.2	67.89	93.97	0.1169
912.2	75.75	88.62	0.3344	938.2	66.58	94.34	0.0307
913.2	75.94	88.97	0.3311	943.2	66.38	94.31	-0.0393
914.2	75.87	89.30	0.3264	948.2	65.43	93.97	-0.0898
915.2	75.77	89.60	0.3217	953.2	62.72	93.45	-0.1142
916.2	75.68	89.93	0.3163	958.2	59.08	92.86	-0.1147
917.2	75.68	90.23	0.3118	963.2	54.71	92.31	-0.1009
918.2	75.63	90.55	0.3065	968.2	50.56	91.85	-0.0899
919.2	75.60	90.87	0.3013	973.2	46.77	91.50	-0.0585
920.2	75.70	91.15	0.2969	978.2	43.06	91.26	-0.0352
920.3	75.70	91.19	0.2965	983.2	40.07	91.14	-0.0153
920.3	75.51	91.19	0.2991	988.2	37.91	91.10	-0.0035
921.2	74.97	91.43	0.2896	993.2	36.26	91.13	0.0100
922.2	74.34	91.71	0.2782	998.2	35.22	91.20	0.0166
923.2	73.71	91.98	0.2666	1003.2	34.66	91.30	0.0206
924.2	73.08	92.24	0.2548	1008.2	34.34	91.40	0.0227
925.2	72.50	92.50	0.2426	1013.2	34.25	91.52	0.0234
926.2	71.91	92.74	0.2297	1018.2	34.22	91.64	0.0234
927.2	71.33	92.95	0.2167	1023.2	34.25	91.76	0.0233
928.2	70.68	93.17	0.2013				

TABLE XXXIV

SPECIFIC HEAT CAPACITY, ELECTRICAL RESISTIVITY, AND TEMPERATURE DERIVATIVE OF ELECTRICAL RESISTIVITY OF Ni_3Fe IN ORDER-STATE III PULSED FROM BELOW THE ORDER-DISORDER CRITICAL TEMPERATURE WITH CLASS II HEATING RATE

TEMPERATURE (KELVIN)	SPECIFIC HEAT CAPACITY (JOULES/GRAM -ATOM DEGREE)	ELECTRICAL RESISTIVITY (OHM-CM) 10 E-6	TEMPERATURE DERIVATIVE OF RESISTIVITY (OHM/DEGREE) 10 E-6	TEMPERATURE (KELVIN)	SPECIFIC HEAT CAPACITY (JOULES/GRAM -ATOM DEGREE)	ELECTRICAL RESISTIVITY (OHM-CM) 10 E-6	TEMPERATURE DERIVATIVE OF RESISTIVITY (OHM/DEGREE) 10 E-6
583.2	31.77	46.87	0.1328	913.2	68.98	89.40	0.2903
588.2	31.96	47.52	0.1343	914.2	69.58	89.69	0.2893
693.2	31.75	48.18	0.1354	915.2	70.00	89.98	0.2873
698.2	32.06	48.91	0.1373	916.2	70.56	90.25	0.2859
703.2	32.39	49.56	0.1379	917.2	71.19	90.59	0.2839
708.2	31.96	50.27	0.1393	918.2	71.63	90.86	0.2816
713.2	32.16	50.96	0.1408	918.7	71.75	90.97	0.2806
718.2	32.47	51.66	0.1429	918.7	68.78	91.00	0.2814
723.2	32.35	52.38	0.1446	919.2	68.61	91.11	0.2754
728.2	32.67	53.12	0.1463	920.2	68.15	91.32	0.2631
733.2	32.79	53.86	0.1482	921.2	67.57	91.59	0.2483
738.2	33.33	54.59	0.1522	922.2	67.06	91.84	0.2341
743.2	32.81	55.37	0.1515	923.2	66.45	92.07	0.2196
748.2	33.33	56.13	0.1527	928.2	63.61	93.32	0.1546
753.2	33.78	56.90	0.1546	933.2	60.51	93.63	0.0955
758.2	33.13	57.65	0.1563	938.2	57.60	93.98	0.0455
763.2	33.47	58.45	0.1584	943.2	55.12	94.09	0.0095
768.2	33.66	59.23	0.1633	948.2	53.71	94.35	-0.0152
773.2	33.79	60.07	0.1628	953.2	52.67	93.94	-0.0311
778.2	33.79	60.88	0.1643	958.2	51.87	93.73	-0.0428
783.2	33.96	61.72	0.1659	963.2	51.28	93.51	-0.0510
788.2	34.13	62.50	0.1682	968.2	50.92	93.22	-0.0564
793.2	34.32	63.37	0.1709	973.2	51.07	92.94	-0.0616
798.2	34.46	64.27	0.1726	978.2	51.99	92.61	-0.0659
803.2	34.54	65.10	0.1732	983.2	51.75	92.26	-0.0660
808.2	34.73	65.95	0.1748	988.2	50.29	91.96	-0.0577
813.2	34.88	66.83	0.1773	993.2	48.01	91.66	-0.0405
818.2	35.31	67.72	0.1803	998.2	45.48	91.52	-0.0194
823.2	35.34	68.64	0.1826	1003.2	42.35	91.47	-0.0021
828.2	35.53	69.56	0.1853	1008.2	39.32	91.51	0.0105
833.2	35.82	70.52	0.1880	1013.2	37.16	91.58	0.0173
838.2	36.31	71.42	0.1914	1018.2	35.73	91.68	0.0212
843.2	36.99	72.42	0.1963	1023.2	35.00	91.79	0.0230
848.2	37.67	73.42	0.2009	1028.2	34.68	91.92	0.0237
853.2	38.32	74.44	0.2052	1033.2	34.59	92.03	0.0236
858.2	39.33	75.49	0.2098	1038.2	34.29	92.16	0.0232
863.2	39.95	76.53	0.2151	1043.2	34.34	92.26	0.0229
868.2	41.16	77.61	0.2217	1048.2	34.29	92.38	0.0226
873.2	42.79	78.75	0.2288	1053.2	34.37	92.49	0.0225
878.2	44.87	79.89	0.2370	1058.2	34.39	92.61	0.0223
883.2	47.11	81.11	0.2455	1063.2	34.46	92.71	0.0222
888.2	50.22	82.39	0.2554	1068.2	35.68	92.83	0.0221
893.2	53.66	83.66	0.2671	1073.2	36.14	92.94	0.0220
898.2	57.96	85.03	0.2802	1078.2	35.19	93.04	0.0219
903.2	62.47	86.49	0.2912	1083.2	34.56	93.16	0.0218
908.2	66.28	87.97	0.2951				

TABLE XXXV

SPECIFIC HEAT CAPACITY, ELECTRICAL RESISTIVITY, AND TEMPERATURE DERIVATIVE OF ELECTRICAL RESISTIVITY OF Ni_3Fe IN ORDER-STATE IV PULSED FROM BELOW THE ORDER-DISORDER CRITICAL TEMPERATURE WITH CLASS II HEATING RATE

TEMPERATURE (KELVIN)	SPECIFIC HEAT CAPACITY (JOULES/GRAM -ATOM DEGREE)	ELECTRICAL RESISTIVITY (OHM-CM) 10 E-6	TEMPERATURE DERIVATIVE OF RESISTIVITY (OHM/DEGREE) 10 E-6	TEMPERATURE (KELVIN)	SPECIFIC HEAT CAPACITY (JOULES/GRAM -ATOM DEGREE)	ELECTRICAL RESISTIVITY (OHM-CM) 10 E-6	TEMPERATURE DERIVATIVE OF RESISTIVITY (OHM/DEGREE) 10 E-6
573.2	30.44	42.94	0.1206	934.2	72.72	93.57	0.3062
579.2	30.53	43.14	0.1226	935.2	73.32	90.84	0.3052
583.2	30.63	43.76	0.1242	936.2	74.00	91.18	0.3038
588.2	30.73	44.38	0.1253	937.2	74.68	91.44	0.3033
593.2	30.82	44.98	0.1266	938.2	75.41	91.76	0.3024
598.2	30.92	45.61	0.1287	939.2	76.19	92.38	0.3017
723.2	31.72	46.24	0.1296	943.2	76.99	92.42	0.3013
728.2	31.14	46.92	0.1308	945.2	77.13	92.45	0.3012
713.2	31.24	47.59	0.1321	940.5	68.86	92.45	0.2948
718.2	31.33	48.23	0.1343	941.2	68.44	92.56	0.2886
723.2	31.46	48.89	0.1359	942.2	67.72	92.85	0.2750
728.2	31.55	49.66	0.1377	943.2	66.94	93.10	0.2616
733.2	31.67	50.34	0.1394	944.2	66.16	93.34	0.2484
738.2	31.79	50.91	0.1409	945.2	65.36	93.59	0.2354
743.2	31.92	51.59	0.1433	946.2	64.51	93.85	0.2227
748.2	32.01	52.28	0.1437	947.2	63.69	94.07	0.2102
753.2	32.13	53.00	0.1469	948.2	62.93	94.29	0.1983
758.2	32.26	53.72	0.1493	953.2	59.10	95.12	0.1461
763.2	32.38	54.45	0.1502	958.2	54.90	95.75	0.0961
768.2	32.52	55.22	0.1521	963.2	51.82	96.12	0.0586
773.2	32.64	56.00	0.1534	968.2	49.85	96.32	0.0334
778.2	32.77	56.79	0.1553	973.2	48.69	96.47	0.0140
783.2	32.91	57.55	0.1580	978.2	48.33	96.48	-0.0003
788.2	33.06	58.34	0.1603	983.2	48.98	96.40	-0.0122
793.2	33.27	59.17	0.1629	988.2	51.55	96.36	-0.0311
798.2	33.35	59.98	0.1659	990.7	53.93	96.29	-0.0468
803.2	33.49	60.84	0.1676	993.2	57.69	96.15	-0.0706
808.2	33.66	61.64	0.1692	995.7	63.15	95.94	-0.1059
813.2	33.83	62.52	0.1709	998.2	70.99	95.57	-0.1603
818.2	34.07	63.36	0.1733	1000.7	79.73	95.10	-0.2309
823.2	34.23	64.23	0.1763	1033.2	83.42	94.37	-0.2798
828.2	34.39	65.11	0.1792	1005.7	76.62	93.58	-0.2575
833.2	34.61	66.02	0.1827	1008.2	65.70	92.98	-0.1965
838.2	34.85	66.93	0.1851	1010.7	57.13	92.52	-0.1424
843.2	35.12	67.89	0.1877	1013.2	51.04	92.17	-0.1014
848.2	35.41	68.82	0.1916	1018.2	42.96	91.83	-0.0442
853.2	35.68	69.77	0.1952	1023.2	38.74	91.76	-0.0134
858.2	36.16	70.77	0.1991	1028.2	36.38	91.75	0.0046
863.2	36.75	71.80	0.2035	1033.2	35.22	91.78	0.0148
868.2	37.47	72.83	0.2094	1038.2	34.73	91.94	0.0206
873.2	38.28	73.86	0.2156	1043.2	34.59	92.01	0.0233
878.2	39.42	75.01	0.2227	1048.2	34.63	92.16	0.0241
883.2	40.61	76.12	0.2290	1053.2	34.63	92.27	0.0238
888.2	42.18	77.28	0.2371	1058.2	34.61	92.41	0.0232
893.2	44.17	78.47	0.2478	1063.2	34.56	92.51	0.0227
898.2	46.92	79.75	0.2620	1068.2	34.54	92.62	0.0224
903.2	50.29	81.07	0.2753	1073.2	34.54	92.75	0.0223
908.2	53.76	82.48	0.2862	1078.2	34.51	93.07	0.0220
913.2	57.86	83.95	0.3003	1083.2	34.49	93.19	0.0220
918.2	62.72	85.50	0.3126	1088.2	34.59	92.85	0.0224
923.2	67.09	87.11	0.3185	1093.2	34.56	92.96	0.0223
928.2	69.66	88.74	0.3164				
933.2	72.18	90.24	0.3084				

TABLE XXXVI

SPECIFIC HEAT CAPACITY, ELECTRICAL RESISTIVITY, AND TEMPERATURE DERIVATIVE OF ELECTRICAL RESISTIVITY OF Ni_3Fe IN ORDER-STATE V PULSED FROM BELOW THE ORDER-DISORDER CRITICAL TEMPERATURE WITH CLASS II HEATING RATE

TEMPERATURE (KELVIN)	SPECIFIC HEAT CAPACITY (JOULES/GRAM -ATOM DEGREE)	ELECTRICAL RESISTIVITY (OHM-CM) 10 E-6	TEMPERATURE DERIVATIVE OF RESISTIVITY (OHM/DEGREE) 10 E-6	TEMPERATURE (KELVIN)	SPECIFIC HEAT CAPACITY (JOULES/GRAM -ATOM DEGREE)	ELECTRICAL RESISTIVITY (OHM-CM) 10 E-6	TEMPERATURE DERIVATIVE OF RESISTIVITY (OHM/DEGREE) 10 E-6
638.2	31.16	45.68	0.1256	888.2	43.69	85.21	0.2162
643.2	31.16	46.34	0.1261	893.2	45.07	86.30	0.2214
648.2	31.24	46.97	0.1273	898.2	46.53	87.40	0.2265
653.2	31.26	47.59	0.1282	899.2	46.87	87.64	0.2276
658.2	31.33	48.24	0.1291	900.2	47.18	87.90	0.2287
663.2	31.43	48.90	0.1300	901.2	47.40	88.07	0.2294
668.2	31.55	49.56	0.1314	902.2	47.74	88.31	0.2305
673.2	31.63	50.19	0.1326	903.2	48.20	88.57	0.2322
678.2	31.72	50.88	0.1335	904.2	48.49	88.82	0.2329
683.2	31.82	51.54	0.1344	904.9	48.66	88.89	0.2336
688.2	31.94	52.25	0.1358	904.9	47.28	88.99	0.2061
693.2	32.06	52.93	0.1373	905.2	47.35	89.05	0.2038
698.2	32.13	53.62	0.1382	906.2	47.40	89.20	0.1987
703.2	32.26	54.27	0.1394	907.2	47.43	89.41	0.1908
708.2	32.33	54.98	0.1404	908.2	47.45	89.55	0.1855
713.2	32.45	55.70	0.1414	909.2	47.47	89.77	0.1777
718.2	32.60	56.39	0.1428	910.2	47.57	89.95	0.1701
723.2	32.72	57.12	0.1439	911.2	47.60	90.08	0.1650
728.2	32.84	57.84	0.1454	912.2	47.62	90.27	0.1574
733.2	32.91	58.55	0.1465	913.2	47.64	90.44	0.1499
738.2	33.06	59.33	0.1477	918.2	47.81	91.08	0.1192
743.2	33.18	60.07	0.1488	923.2	47.79	91.59	0.0888
748.2	33.32	60.82	0.1502	928.2	47.86	91.95	0.0632
753.2	33.49	61.58	0.1518	933.2	47.69	92.23	0.0388
758.2	33.62	62.30	0.1531	938.2	47.35	92.36	0.0190
763.2	33.74	63.09	0.1545	943.2	47.06	92.37	0.0048
768.2	33.86	63.88	0.1557	948.2	46.50	92.36	-0.0050
773.2	33.93	64.63	0.1566	953.2	45.82	92.31	-0.0107
778.2	34.15	65.45	0.1583	958.2	45.05	92.25	-0.0144
783.2	34.29	66.22	0.1598	963.2	44.08	92.16	-0.0162
788.2	34.44	67.00	0.1614	968.2	43.13	92.09	-0.0158
793.2	34.63	67.86	0.1631	973.2	42.33	91.99	-0.0143
798.2	34.73	68.68	0.1643	978.2	41.62	91.94	-0.0122
803.2	34.95	69.48	0.1660	983.2	41.12	91.88	-0.0106
808.2	35.12	70.30	0.1675	988.2	40.68	91.84	-0.0099
813.2	35.29	71.15	0.1688	993.2	40.24	91.79	-0.0095
818.2	35.53	72.02	0.1707	998.2	39.63	91.74	-0.0083
823.2	35.75	72.86	0.1727	1003.2	38.81	91.69	-0.0056
828.2	35.95	73.74	0.1746	1008.2	37.96	91.66	-0.0016
833.2	36.19	74.63	0.1765	1013.2	37.04	91.66	0.0034
838.2	36.48	75.48	0.1784	1018.2	36.19	91.69	0.0087
843.2	36.77	76.36	0.1800	1023.2	35.53	91.75	0.0135
848.2	37.23	77.30	0.1831	1028.2	35.02	91.84	0.0174
853.2	37.69	78.25	0.1864	1033.2	34.73	91.94	0.0199
858.2	38.13	79.19	0.1896	1038.2	34.56	92.05	0.0215
863.2	38.66	80.07	0.1926	1043.2	34.51	92.17	0.0225
868.2	39.32	81.06	0.1962	1048.2	34.44	92.27	0.0228
873.2	40.17	82.04	0.2006	1053.2	34.49	92.39	0.0229
878.2	41.21	83.11	0.2056	1058.2	34.51	92.51	0.0226
883.2	42.33	84.12	0.2107	1063.2	34.49	92.62	0.0225

TABLE XXXVII

SPECIFIC HEAT CAPACITY, ELECTRICAL RESISTIVITY, AND TEMPERATURE DERIVATIVE OF ELECTRICAL RESISTIVITY OF Ni_3Fe IN ORDER-STATE VI PULSED FROM BELOW THE ORDER-DISORDER CRITICAL TEMPERATURE WITH CLASS II HEATING RATE

TEMPERATURE (KELVIN)	SPECIFIC HEAT CAPACITY (JOULES/GRAM -ATOM DEGREE)	ELECTRICAL RESISTIVITY (OHM-CM) 10 E-6	TEMPERATURE DERIVATIVE OF RESISTIVITY (OHM/DEGREE) 10 E-6	TEMPERATURE (KELVIN)	SPECIFIC HEAT CAPACITY (JOULES/GRAM -ATOM DEGREE)	ELECTRICAL RESISTIVITY (OHM-CM) 10 E-6	TEMPERATURE DERIVATIVE OF RESISTIVITY (OHM/DEGREE) 10 E-6
393.2	26.33	15.78	0.0647	643.2	30.05	37.43	0.1122
398.2	24.41	16.11	0.0656	648.2	30.14	38.01	0.1135
403.2	26.46	16.44	0.0664	653.2	30.22	38.58	0.1148
408.2	26.53	16.77	0.0671	658.2	30.34	39.16	0.1162
413.2	26.60	17.11	0.0680	663.2	30.41	39.73	0.1175
418.2	26.67	17.45	0.0689	668.2	30.51	40.31	0.1189
423.2	26.75	17.80	0.0697	673.2	30.58	40.99	0.1207
428.2	26.82	18.15	0.0706	678.2	30.70	41.58	0.1221
433.2	26.87	18.50	0.0714	683.2	30.78	42.21	0.1235
438.2	26.94	18.86	0.0720	688.2	30.87	42.82	0.1252
443.2	27.01	19.23	0.0729	693.2	30.97	43.46	0.1266
448.2	27.09	19.59	0.0737	698.2	31.07	44.07	0.1280
453.2	27.13	19.96	0.0745	703.2	31.19	44.73	0.1296
458.2	27.23	20.33	0.0754	708.2	31.29	45.37	0.1311
463.2	27.28	20.71	0.0762	713.2	31.38	46.03	0.1328
468.2	27.33	21.09	0.0771	718.2	31.50	46.71	0.1344
473.2	27.43	21.49	0.0778	723.2	31.60	47.39	0.1360
478.2	27.50	21.87	0.0787	728.2	31.72	48.06	0.1377
483.2	27.57	22.27	0.0798	733.2	31.82	48.74	0.1395
488.2	27.64	22.67	0.0807	738.2	31.94	49.44	0.1411
493.2	27.69	23.17	0.0814	743.2	32.06	50.16	0.1432
498.2	27.77	23.49	0.0822	748.2	32.16	50.90	0.1449
503.2	27.84	23.90	0.0831	753.2	32.28	51.60	0.1471
508.2	27.91	24.32	0.0840	758.2	32.43	52.37	0.1491
513.2	27.98	24.74	0.0851	763.2	32.55	53.11	0.1510
518.2	28.06	25.17	0.0859	768.2	32.67	53.87	0.1530
523.2	28.13	25.60	0.0867	773.2	32.79	54.64	0.1552
528.2	28.20	26.04	0.0876	778.2	32.94	55.39	0.1572
533.2	28.28	26.48	0.0885	783.2	33.08	56.21	0.1595
538.2	28.35	26.92	0.0894	788.2	33.20	56.99	0.1619
543.2	28.42	27.37	0.0904	793.2	33.35	57.85	0.1644
548.2	28.52	27.82	0.0913	798.2	33.49	58.67	0.1667
553.2	28.59	28.29	0.0923	803.2	33.64	59.46	0.1697
558.2	28.66	28.75	0.0933	808.2	33.81	60.32	0.1713
563.2	28.74	29.22	0.0943	813.2	33.98	61.22	0.1739
568.2	28.81	29.68	0.0952	818.2	34.15	62.06	0.1765
573.2	28.91	30.16	0.0962	823.2	34.34	62.99	0.1796
578.2	28.98	30.65	0.0971	828.2	34.54	63.88	0.1824
583.2	29.05	31.13	0.0981	833.2	34.78	64.80	0.1854
588.2	29.15	31.63	0.0993	838.2	35.00	65.73	0.1888
593.2	29.22	32.13	0.1005	843.2	35.27	66.69	0.1920
598.2	29.32	32.62	0.1015	848.2	35.56	67.67	0.1956
603.2	29.39	33.14	0.1026	853.2	35.85	68.61	0.1991
608.2	29.49	33.66	0.1037	858.2	36.21	69.64	0.2036
613.2	29.56	34.10	0.1049	863.2	36.60	70.62	0.2079
618.2	29.66	34.72	0.1061	868.2	37.13	71.70	0.2131
623.2	29.73	35.24	0.1073	873.2	37.77	72.73	0.2185
628.2	29.80	35.79	0.1087	878.2	38.42	73.86	0.2242
633.2	29.90	36.33	0.1098	883.2	39.46	75.01	0.2316
638.2	29.97	36.88	0.1112	888.2	40.65	76.19	0.2396

TABLE XXXVII (continued)

TEMPERATURE	SPECIFIC HEAT CAPACITY	ELECTRICAL RESISTIVITY	TEMPERATURE DERIVATIVE OF RESISTIVITY	TEMPERATURE	SPECIFIC HEAT CAPACITY	ELECTRICAL RESISTIVITY	TEMPERATURE DERIVATIVE OF RESISTIVITY
(KELVIN)	(JOULES/GRAM -ATOM DEGREE)	(OHM-CM) 10 E-6	(OHM/DEGREE) 10 E-6	(KELVIN)	(JOULES/GRAM -ATOM DEGREE)	(OHM-CM) 10 E-6	(OHM/DEGREE) 10 E-6
893.2	42.21	77.38	0.2496	994.2	62.30	99.33	-0.0349
898.2	44.22	78.68	0.2615	995.2	66.45	99.30	-0.0549
903.2	46.62	80.00	0.2744	996.2	71.24	99.26	-0.0772
913.2	53.37	82.86	0.3045	997.2	78.32	99.15	-0.1115
918.2	58.08	84.50	0.3225	998.2	86.77	99.04	-0.1599
923.2	62.79	86.10	0.3374	999.2	98.47	98.84	-0.2311
928.2	67.30	87.90	0.3457	1000.2	116.14	98.52	-0.3548
929.2	68.01	88.21	0.3464	1001.2	137.20	97.99	-0.5388
930.2	68.71	88.59	0.3462	1002.2	147.98	97.13	-0.7077
931.2	69.25	88.89	0.3457	1003.2	134.66	96.25	-0.6785
932.2	69.88	89.26	0.3450	1004.2	114.49	95.50	-0.5634
933.2	70.48	89.64	0.3440	1005.2	100.29	94.98	-0.4720
934.2	70.97	89.94	0.3432	1006.2	87.69	94.48	-0.3970
935.2	71.53	90.31	0.3419	1007.2	78.54	94.10	-0.3233
936.2	72.06	90.66	0.3405	1008.2	71.94	93.78	-0.2763
937.2	72.45	90.96	0.3391	1009.2	67.38	93.56	-0.2432
938.2	73.01	91.31	0.3377	1010.2	62.23	93.29	-0.2058
939.2	73.42	91.67	0.3356	1011.2	58.76	93.09	-0.1798
940.2	73.69	91.95	0.3335	1012.2	56.36	92.96	-0.1619
940.2	73.69	92.02	0.3398	1013.2	53.52	92.79	-0.1403
941.2	72.67	92.30	0.3372	1014.2	51.65	92.68	-0.1257
942.2	71.79	92.58	0.3218	1015.2	49.29	92.54	-0.1078
943.2	70.58	92.93	0.3178	1016.2	47.81	92.45	-0.0959
944.2	69.75	93.21	0.3028	1017.2	46.41	92.35	-0.0846
945.2	68.61	93.54	0.2923	1018.2	45.12	92.29	-0.0744
946.2	67.76	93.81	0.2843	1023.2	40.56	92.03	-0.0367
947.2	66.82	94.08	0.2759	1028.2	38.06	91.93	-0.0146
948.2	65.90	94.34	0.2677	1033.2	36.41	91.91	0.0007
953.2	61.19	95.60	0.2265	1038.2	35.41	91.97	0.0108
958.2	56.53	96.65	0.1838	1043.2	34.88	92.05	0.0165
963.2	52.50	97.47	0.1422	1048.2	34.66	92.14	0.0198
968.2	49.20	98.10	0.1072	1053.2	34.54	92.25	0.0216
973.2	47.01	98.50	0.0812	1058.2	34.51	92.36	0.0223
978.2	46.09	98.90	0.0610	1063.2	34.51	92.48	0.0226
983.2	46.82	99.16	0.0431	1068.2	34.56	92.60	0.0226
988.2	50.29	99.32	0.0199	1073.2	34.56	92.71	0.0224
993.2	58.93	99.35	-0.0194				

TABLE XXXVIII

ELECTRICAL RESISTIVITY OF Ni_3Fe IN EQUILIBRIUM STATE
FROM 4.2 K TO 1361.8 K

Temperature (Kelvin)	Electrical Resistivity (Ohm-cm $\times 10^{+6}$)	Temperature (Kelvin)	Electrical Resistivity (Ohm-cm $\times 10^{+6}$)
4.2	2.81	777.7	68.92
80.0	3.37	778.2	69.15
100.0	3.70	782.0	69.86
120.0	4.10	785.0	70.38
140.0	4.52	790.8	71.47
160.0	5.01	796.5	72.53
180.0	5.54	807.3	74.47
200.0	6.12	817.2	76.35
220.0	6.76	829.8	78.83
240.0	7.46	833.2	79.35
260.0	8.22	833.7	79.41
280.0	9.07	835.7	79.93
300.0	9.98	840.5	80.89
320.0	10.95	846.5	82.10
340.0	11.99	851.6	83.14
360.0	13.10	858.1	84.61
380.0	14.27	859.4	84.94
400.0	15.53	862.0	85.54
458.4	19.49	862.7	85.69
463.9	19.95	863.4	85.79
527.8	25.19	864.4	85.95
552.7	27.39	865.4	86.08
602.0	32.19	867.5	86.32
645.2	36.78	870.0	86.54
674.2	40.21	881.7	87.39
713.2	45.75	975.9	90.56
735.2	49.98	985.4	91.09
755.2	54.35	1079.9	93.34
767.2	57.65	1159.0	94.67
771.2	58.31	1178.5	95.44
773.9	68.09	1279.1	97.46
775.3	68.45	1361.8	98.93

TABLE XXXIX

THERMOELECTRIC POWER OF Ni_3Fe IN EQUILIBRIUM STATE
FROM 80 K TO 1362 K

Temperature (Kelvin)	Thermoelectric Power (Microvolts/degree)	Temperature (Kelvin)	Thermoelectric Power (Microvolts/degree)
80.0	-7.90	320.0	-30.75
100.0	-9.65	340.0	-30.50
120.0	-12.15	360.0	-29.95
140.0	-15.10	380.0	-29.10
160.0	-18.05	400.0	-28.00
180.0	-20.90	462.7	-23.71
200.0	-23.40	562.6	-17.62
220.0	-25.60	646.2	-11.60
240.0	-27.55	833.3	-2.73
260.0	-29.05	975.6	6.42
280.0	-30.00	1158.6	7.41
300.0	-30.55	1362.0	7.04

TABLE XL

ELECTRICAL RESISTIVITY AND THERMOELECTRIC POWER OF Ni_3Fe
IN STATE AT EQUILIBRIUM AT 767 K

Temperature (Kelvin)	Electrical Resistivity ($\text{Ohm-cm} \times 10^{-6}$)	Temperature (Kelvin)	Thermoelectric Power (Microvolts/degree)
300.3	11.85	337.9	-33.64
344.8	14.20	460.7	-29.59
419.8	19.20	547.6	-24.29
467.4	22.95	632.1	-18.72
487.6	24.70	767.1	-8.08
550.2	30.43		
629.7	38.95		
735.7	52.67		
755.2	55.71		

TABLE XLI

ELECTRICAL RESISTIVITY AND THERMOELECTRIC POWER OF Ni_3Fe
IN STATE AT EQUILIBRIUM AT 755 K

Temperature (Kelvin)	Electrical Resistivity ($\text{Ohm-cm} \times 10^{+6}$)	Temperature (Kelvin)	Thermoelectric Power ($\text{Ohm-cm} \times 10^{+6}$)
297.4	11.20	479.1	-27.09
386.6	16.17	600.5	-19.20
484.8	23.54	753.8	-8.21
533.9	27.90		
599.8	34.46		
638.0	38.71		
735.2	51.27		

TABLE XLII

ELECTRICAL RESISTIVITY AND THERMOELECTRIC POWER OF Ni_3Fe
IN STATE AT EQUILIBRIUM AT 735 K

Temperature (Kelvin)	Electrical Resistivity ($\text{Ohm-cm} \times 10^{+6}$)	Temperature (Kelvin)	Thermoelectric Power ($\text{Ohm-cm} \times 10^{+6}$)
297.9	10.64	375.2	-29.97
398.6	16.29	500.9	-23.76
513.3	25.13	616.6	-16.42
637.0	37.46	736.0	-8.18
712.8	46.83		

TABLE XLIII

ELECTRICAL RESISTIVITY AND THERMOELECTRIC POWER OF Ni_3Fe
IN STATE AT EQUILIBRIUM AT 713 K

Temperature (Kelvin)	Electrical Resistivity ($\text{Ohm-cm} \times 10^{+6}$)	Temperature (Kelvin)	Thermoelectric Power (Microvolts/degree)
298.7	10.21	363.5	-29.73
361.6	13.36	447.4	-25.59
457.3	19.85	591.6	-15.87
585.2	31.11	715.1	-7.67
674.1	40.78		

TABLE XLIV

ELECTRICAL RESISTIVITY AND THERMOELECTRIC POWER OF Ni_3Fe
QUENCHED FROM 1400 K

Temperature (Kelvin)	Electrical Resistivity ($\text{Ohm-cm} \times 10^{+6}$)	Thermoelectric Power (Microvolts/degree)
86.2	5.02	-12.64
92.1	5.35	-13.48
109.6	5.86	-16.47
129.9	6.54	-20.04
153.1	7.45	-23.93
174.3	8.39	-27.16
193.6	9.34	-29.85
212.6	10.36	-32.17
232.9	11.56	-34.28
255.3	13.08	-36.08
282.6	14.97	-37.69
301.7	16.33	-38.44
321.2	17.86	-38.90
341.7	19.49	-38.98
357.7	20.92	-38.81
372.9	22.25	-38.51
392.2	24.00	-37.90
406.7	25.37	-37.36
487.2	33.52	
488.5		-33.42
589.1	44.96	
591.3		-26.80

TABLE XLV

MAGNETIC SPECIFIC HEAT CAPACITY C_{vm} OF DISORDERED Ni_3Fe
FROM 50 K TO 1423 K

Temperature (Kelvin)	C_{vm} (Joules/gram- atom degree)	Temperature (Kelvin)	C_{vm} (Joules/gram- atom degree)
50.0	0.00	853.2	7.76
100.0	0.22	858.2	8.07
150.0	0.47	863.2	8.41
200.0	0.72	868.2	8.78
250.0	0.97	872.6	9.13
300.0	1.23	872.6	5.28
350.0	1.49	877.2	4.55
403.2	1.79	882.2	4.32
453.2	2.09	893.2	4.19
503.2	2.43	903.2	4.04
553.2	2.81	923.2	3.80
603.2	3.29	943.2	3.57
653.2	3.82	963.2	3.38
703.2	4.34	983.2	3.11
723.2	4.60	1003.2	2.90
743.2	4.90	1053.2	2.49
763.2	5.15	1103.2	2.09
783.2	5.53	1153.2	1.76
803.2	5.95	1203.2	1.41
813.2	6.19	1253.2	1.14
823.2	6.49	1303.2	0.83
833.2	6.81	1353.2	0.50
843.2	7.21	1403.2	0.15
848.2	7.44	1423.2	0.00

VITA

The author was born in New Orleans, Louisiana, on April 18, 1937. He is the only child of James Milner and Thelma Accardo McCandlish. He completed his first four years of grammar school in New Orleans. After his father's death in 1947, his mother married Paul Casper Kollie and moved to Atlanta, Georgia. The author was legally adopted by Paul Kollie in 1948 at which time he assumed the surname Kollie. After completing his primary and secondary education in Atlanta, the author entered the Georgia Institute of Technology in September of 1955. In August of 1958, he married Mary Rita Hamby. Upon receiving his Bachelor of Ceramic Engineering (with highest honor) in June of 1959, the author was employed by the Metals and Ceramics Division of the Oak Ridge National Laboratory in Oak Ridge, Tennessee. In July of 1959, he was called to active duty as a second lieutenant in the United States Army Reserve and trained recruits at Fort Benning, Georgia. Returning to the Oak Ridge National Laboratory in January of 1960, he joined the Thermophysical Properties Group of the Metals and Ceramics Division. The author began his postgraduate studies on a part-time basis in September of 1960 at the Oak Ridge School of Reactor Technology from which he received a certificate in June of 1962. In September of 1962, he began his studies in the Oak Ridge Resident Graduate Program of the University of Tennessee and received the degree of Master of Science in Metallurgical Engineering in August of 1965. In September of 1967, the author, through the educational assistance program of the Oak Ridge National Laboratory, was relieved of his duties in the Metals and Ceramics Division and allowed to attend the University of

Tennessee (Knoxville) as a full-time student. In August of 1969, the author received the degree of Doctor of Philosophy in Metallurgical Engineering. The author and his wife have three children - Angela, age 9, Thomas, Jr., age 7, and Theresa, age 4.